

ANALYSIS OF SPHINGOLIPIDS FROM
BIOLOGICAL SOURCES USING ON-LINE
HIGH PERFORMANCE LIQUID
CHROMATOGRAPHY WITH DETECTION
BY ATMOSPHERIC PRESSURE CHEMICAL
IONIZATION AND ELECTROSPRAY
IONIZATION MASS SPECTROMETRY

RICHARD H. PERRY

**ANALYSIS OF SPHINGOLIPIDS FROM BIOLOGICAL
SOURCES USING ON-LINE HIGH PERFORMANCE
LIQUID CHROMATOGRAPHY WITH DETECTION BY
ATMOSPHERIC PRESSURE CHEMICAL IONIZATION
AND ELECTROSPRAY IONIZATION MASS
SPECTROMETRY**

by

Richard H. Perry

A Thesis Submitted to the Faculty of

The Charles E. Schmidt College of Science

In Partial Fulfillment of the Requirements for the Degree of

Master of Science

Florida Atlantic University

Boca Raton, Florida

December 2004

Copyright Richard H. Perry 2004

**ANALYSIS OF SPHINGOLIPIDS FROM BIOLOGICAL SOURCES USING ON-
LINE HIGH PERFORMANCE LIQUID CHROMATOGRAPHY WITH
DETECTION BY ATMOSPHERIC PRESSURE CHEMICAL IONIZATION AND
ELECTROSPRAY IONIZATION MASS SPECTROMETRY**

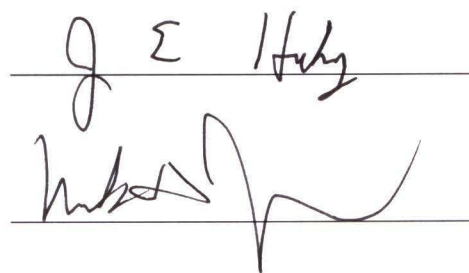
by


Richard H. Perry

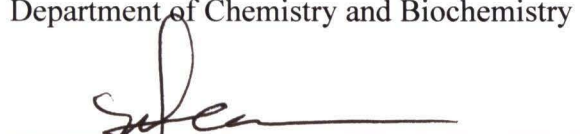
This thesis was prepared under the direction of the candidate's thesis advisor, Dr. William Craig Byrdwell, Department of Chemistry and Biochemistry, and has been approved by the members of his supervisory committee. It was submitted to the faculty of The Charles E. Schmidt College of Science and was accepted in partial fulfillment of the requirements for the degree of Master of Science.

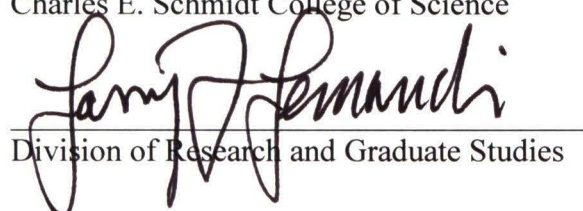
SUPERVISORY COMMITTEE

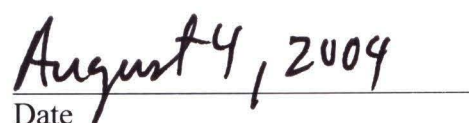

Thesis Advisor




Chairman
Department of Chemistry and Biochemistry


Dean
Charles E. Schmidt College of Science


Division of Research and Graduate Studies


Date

ACKNOWLEDGEMENTS

First, and foremost, I especially wish to thank Mr. David W. Lowe, the former Associate Vice President of University Advancement at Florida Atlantic University, for his constant support and encouragement. His modesty and kindness inspired me to be the best that I can be, and I am grateful to have had the opportunity to meet him. I would also like to acknowledge the members of the University Advancement team who cheered from sidelines when I succeeded, and shouted encouraging words when I failed. They provided me with a lifetime of hilarious and loving memories. I will miss them all, but they will never be forgotten.

Sincere appreciation is expressed to Drs. Salvatore Lepore, Mark Jackson, Patricia Snyder and Jerome Haky for taking time out of their hectic days to help me make important decisions regarding my future career in chemistry. Time is a precious commodity that can never be regained once it has passed, and whether I had occupied one second, five minutes or one hour of their time, I am grateful for such a priceless and considerate gift. I would also like to acknowledge my mentor, Dr. William Craig Byrdwell, for introducing me to the world of mass spectrometry, and for providing me with the tools that are essential to be successful in this exciting field.

I would also like to extend a general thank you to all my friends and colleagues who have inspired, encouraged, aided and supported my academic advancement. But most of all, I must thank my biggest fan, closest friend and greatest unconditional supporter, Anita Khoram. Her opinions, insights, words of encouragement and chastising fulminations were all geared towards my success. I am thankful to have had such a competent and genuine copilot on this academic adventure. '*Tashakhur*'

And last but not least, I must thank my parents for a gift of immeasurable value. My parents were not scientists. But, by introducing me to skepticism, rationalism and wonder, they instilled in me the respect for the thought processes that are essential to appreciate the scientific method. As Carl Sagan pointed out in *The Demon-Haunted World*, “Science is not just a body of knowledge; it is a way of thinking.” And that was my parent’s gift to me. I now realize that the greatest lessons that I have learnt were not from my high school or university professors, but from my parents, people who did not know anything about science, but who understood the value and dependability of reason.

ABSTRACT

Author: Richard H. Perry

Title: Analysis of Sphingolipids from Biological Sources Using On-Line High Performance Liquid Chromatography with Detection by Atmospheric Pressure Chemical Ionization and Electrospray Ionization Mass Spectrometry

Institution: Florida Atlantic University

Thesis Advisor: Dr. William Craig Byrdwell

Degree: Master of Science

Year: 2004

Sphingolipids (SPLs) are important structural components of membranes in some types of cells and are involved in numerous signaling processes. Sphingomyelin (SPM) and dihydrosphingomyelin (DHS) are the two major SPLs in membranes. Very little is known about the molecular species and role of DHS in biological systems. In this work, we employed high performance liquid chromatography with detection by atmospheric pressure chemical ionization and electrospray ionization (ESI) mass spectrometry to elucidate the SPL composition in biological extracts. No common dietary source of DHS is known to exist. A novel analytical method developed to analyze complex SPL mixtures was used to show that bovine milk contained substantial amounts of DHS. Also, the human lens is the only known system in which DHS is the most abundant SPL. The molecular species of DHS in cataractous lenses has never been reported. It was shown that there was a preference for monounsaturated species of DHS and SPM in all ages and in cataractous lenses. It was also discovered that SPLs were the primary PLs remaining in cataractous lenses. Finally, the formation of sodium adducts and dimers in the ESI source of the ion trap mass spectrometer prevented the accurate quantitative analysis of PLs. A new method was developed to eliminate these undesirable ions.

To the world

TABLE OF CONTENTS

List of Tables.....	xii
List of Figures.....	xvi
List of Schemes.....	xxiii

CHAPTERS

I. INTRODUCTION.....	1
I. The Importance of Lipids.....	1
II. The Structures of Glycerophospholipids and Sphingolipids.....	7
III. The Importance of Sphingomyelin and Dihydrosphingomyelin.....	12
III.A. MEMBRANE STRUCTURE.....	13
III.B. CELL SIGNALING.....	15
1. Dihydroceramide in Cellular Signaling Processes.....	23
IV. The Mass Spectrometric Analysis of Sphingolipids from Biological Sources.....	24
IV.A. CHANGES IN THE COMPOSITION OF THE MOLECULAR SPECIES OF DIHYDROSPHINGOMYELIN AND SPHINGOMYELIN IN HUMAN EYE LENS MEMBRANES, WITH AGE AND THE ONSET OF CATARACTS.....	26
IV.B. THE COMPOSITION OF BOVINE MILK.....	28
IV.C. SOLVING THE SODIUM ADDUCT AND DIMER PROBLEM.....	32
V. Summary.....	33
II. EXPERIMENTAL.....	34
I. Liquid Chromatography/Mass Spectrometry.....	34

I.A.	MATERIALS.....	34
I.B.	LIQUID CHROMATOGRAPHY.....	35
	1. Sphingomyelin Extracts.....	36
	2. Human Eye Lenses.....	38
	3. Elimination of Dimers and Sodium Adducts.....	39
I.C.	MASS SPECTROMETRY.....	44
	1. Sphingomyelin Extracts.....	44
	<i>1.1. Atmospheric Pressure Chemical Ionization.....</i>	<i>44</i>
	<i>1.2. Electrospray Ionization.....</i>	<i>45</i>
	2. Human Eye Lenses.....	46
	3. Elimination of Dimers and Sodium Adducts.....	46
II.	³¹ P Nuclear Magnetic Resonance.....	49
II.A.	MATERIALS.....	49
II.B.	³¹ P NMR.....	49
III.	RESULTS AND DISCUSSION.....	50
I.	Commercially Available Sphingomyelin Standards.....	50
I.A.	LIQUID CHROMATOGRAPHY/MASS SPECTROMETRY.....	50
	1. Mass Spectrometry.....	50
	<i>1.1. Bovine Milk.....</i>	<i>52</i>
	<i>1.2. Bovine Brain.....</i>	<i>80</i>
	<i>1.3. Chicken Egg Yolk.....</i>	<i>84</i>
	2. Tandem Mass Spectrometry.....	89

2.1.	<i>Sphingolipids with Saturated Fatty Acid Chains (X:A/Y:0).....</i>	90
2.2.	<i>Sphingolipids that have Fatty Acids with One Double Bond (X:A/Y:1).....</i>	98
2.3.	<i>Sphingolipids that have Fatty Acids with Two Double Bonds (X:A/Y:2).....</i>	102
2.4.	<i>Hydroxy-Sphingolipids.....</i>	105
2.5	<i>Other Fragment Ions.....</i>	109
3.	<i>Quantification.....</i>	113
3.1.	<i>Quantification of X:A/Y:0 and X:A/Y:2 Sphingolipids.....</i>	114
3.2.	<i>Quantification of X:A/Y:1 Sphingolipids.....</i>	123
4.	<i>Composition of the Long-Chain Base/Fatty Acid Combinations in Bovine Milk, Bovine Brain and Chicken Egg Yolk Sphingomyelin Extracts by On-Line High Performance Liquid Chromatography with Detection by Atmospheric Pressure Chemical Ionization and Electrospray Ionization Mass Spectrometry.....</i>	131
4.1.	<i>Composition of Bovine Milk by APCI-MS.....</i>	132
4.2.	<i>Composition of Bovine Milk by ESI-MS.....</i>	134
4.3.	<i>Composition of Bovine Brain by APCI-MS.....</i>	136
4.4.	<i>Composition of Bovine Brain by ESI-MS.....</i>	138
4.5.	<i>Composition of Chicken Egg Yolk by APCI-MS.....</i>	140
4.6.	<i>Composition of Chicken Egg Yolk by ESI-MS.....</i>	142
I.C.	³¹ P NUCLEAR MAGNETIC RESONANCE.....	145
1.	Quantification by ³¹ P NMR.....	145
2.	Composition of Bovine Milk, Bovine Brain and Chicken Egg Yolk Sphingomyelin Extracts by ³¹ P Nuclear Magnetic Resonance Spectroscopy.....	147

I.E.	KARLSSON'S MISTAKES.....	148
	1. Full-scan and Tandem Mass Spectrometry.....	148
	2. The Results.....	163
I.F.	CONCLUSIONS.....	165
II.	Human Eye Lenses.....	169
II.A.	LIQUID CHROMATOGRAPHY/MASS SPECTROMETRY.....	169
	1. Mass Spectrometry.....	169
	2. Tandem Mass Spectrometry.....	171
II.B.	RESULTS.....	172
II.C.	CONCLUSIONS.....	184
	1. Methodology.....	184
	2. Biological Implications.....	185
III.	Solving the “Sodium Adduct and Dimer Problem” in ESI-MS.....	189
III.A.	MODIFIED HEATED CAPILLARY.....	189
III.B.	ETHYLENEDIAMINETETRAACETIC ACID.....	190
III.C.	18-CROWN-6 ETHER.....	192
III.D.	AMMONIUM FORMATE.....	193
III.E.	DIETHYLENETRIAMINETETRAACETIC ACID.....	193
III.F.	AMMONIUM ACETATE SOLUTIONS.....	196
III.G.	AMINO ACIDS.....	197
	1. Glutamic Acid (Glu).....	197
	2. Aspartic Acid (Asp).....	197
	3. Serine (Ser).....	198

4. Alanine (Ala).....	198
5. Glycine (Gly).....	199
III.H. CONCLUSIONS.....	202
IV. CONCLUDING REMARKS.....	211
LITERATURE CITED.....	213

LIST OF TABLES

CHAPTER II

Table 1:	Types of LC1MS1 Experiments.....	47
Table 2:	Types of LC1MS2 Experiments.....	47
Table 3:	Summary of the Unique Experiments Performed on the Commercially Available SPM Extracts.....	48

CHAPTER III

Table 1:	Calculated masses for SPMs with an 18:1 LCB.....	56
Table 2:	Calculated masses for DHSs with an 18:0 LCB.....	57
Table 3:	Short Chain (S-C) LCBs.....	58
Table 4:	Long Chain (L-C) LCBs.....	58
Table 5:	Isobaric SPM-LCB and FA fragment ions in APCI-MS.....	59
Table 6:	Isobaric DHS-LCB and FA fragment ions in APCI-MS.....	59
Table 7:	Composition of the L-C DHSs (mole%) in the SPL1 Peak of Bovine Milk.....	69
Table 8:	Composition of the Saturated LCBs (mole%) in SPL1 of Bovine Milk.....	70

Composition of the SPLs in the SPL2 Peak of Bovine Milk

Table 9:	Composition of the DHSs in SPL2.....	73
Table 10:	Percent Composition of the SPMs in SPL2.....	73
Table 11:	DHS-LCB Composition in SPL2.....	73
Table 12:	SPM-LCB Composition in SPL2.....	73
Table 13:	Percent Composition of the SPLs in SPL3 of Bovine Milk.....	74
Table 14:	Percent composition of the LCBs in SPL3 of Bovine Milk.....	75

Table 15: Composition of the L-C DHSs (mole%) in the SPL1 Peak of Bovine Brain.....	81
Table 16: Composition of the Saturated LCBs (mole%) in the SPL1 Peak of Bovine Brain.....	81
Table 17: Composition of the S-C DHSs (mole%) in the SPL2 Peak of Bovine Brain.....	82
Table 18: Composition of the L-C SPMs (mole%) in the SPL2 Peak of Bovine Brain.....	82
Table 19: Composition of the SPM-LCBs (mole%) in the SPL2 Peak of Bovine Brain.....	83
Table 20: Composition of the S-C SPMs (mole%) in the SPL3 Peak of Bovine Brain.....	83
Table 21: Composition of the LCBs (mole%) in the SPL3 Peak of Bovine Brain.....	84
Table 22: Composition of the L-C DHSs (mole%) in the SPL1 Peak of Chicken Egg Yolk.....	85
Table 23: Composition of the S-C DHSs (mole%) in the SPL2 Peak of Chicken Egg Yolk.....	86
Table 24: Composition of the DHS-LCBs (mole%) in the SPL2 Peak of Chicken Egg Yolk.....	86
Table 25: Composition of the L-C SPMs (mole%) in the SPL2 Peak of Chicken Egg Yolk.....	87
Table 26: Composition of the SPM-LCBs (mole%) in the SPL2 Peak of Chicken Egg Yolk.....	87
Table 27: Composition of the S-C SPMs (mole%) in the SPL3 Peak of Chicken Egg Yolk.....	88
Table 28: Composition of the SPM-LCBs (mole%) in the SPL3 Peak of Chicken Egg Yolk.....	88
Table 29: Calculation of the Proportioning Factors (PFs) for [21:1 SPM Cer + H] ⁺ in APCI-MS.....	128

Table 30: Calculation of the Proportioning Factors (PFs) for [21:1 SPM + H] ⁺ in ESI-MS.....	129
---	-----

Composition of Bovine Milk by APCI-MS

Table 31: Composition (mole%) of the LCB/FA Combinations.....	132
Table 32: Fatty Acid (FA) Composition.....	133
Table 33: Saturated LCB Composition.....	133
Table 34: Unsaturated LCB Composition.....	133
Table 35: Sphingolipid Composition.....	133

Composition of Bovine Milk by ESI-MS

Table 36: Composition (Mole%) of the LCB/FA Combinations.....	134
Table 37: Fatty Acid (FA) Composition.....	135
Table 38: Saturated LCB Composition.....	135
Table 39: Unsaturated LCB Composition.....	135
Table 40: Sphingolipid Composition.....	135

Composition of Bovine Brain by APCI-MS

Table 41: Composition (mole%) of the LCB/FA Combinations.....	136
Table 42: Fatty Acid (FA) Composition.....	137
Table 43: Saturated LCB Composition.....	137
Table 44: Unsaturated LCB Composition.....	137
Table 45: Sphingolipid Composition.....	137

Composition of Bovine Brain by ESI-MS

Table 46: Composition (mole%) of the LCB/FA Combinations.....	138
Table 47: Fatty Acid (FA) Composition.....	139
Table 48: Saturated LCB Composition.....	139

Table 49: Unsaturated LCB Composition.....	139
Table 50: Sphingolipid Composition.....	139
Composition of Chicken Egg Yolk by APCI-MS	
Table 51: Composition (mole%) of the LCB/FA Combinations.....	140
Table 52: Fatty Acid (FA) Composition.....	141
Table 53: Saturated LCB Composition.....	141
Table 54: Unsaturated LCB Composition.....	141
Table 55: Sphingolipid Composition.....	141
Composition of Chicken Egg Yolk by ESI-MS	
Table 56: Composition (mole%) of the LCB/FA Combinations.....	142
Table 57: Fatty Acid (FA) Composition.....	143
Table 58: Saturated LCB Composition.....	143
Table 59: Unsaturated LCB Composition.....	143
Table 60: Sphingolipid Composition.....	143
Table 61: Hydroxy-Sphingolipids Identified in Bovine Milk from APCI Tandem Mass Spectrometry.....	144
Table 62: Hydroxy-Sphingolipids Identified in Chicken Egg Yolk from APCI Tandem Mass Spectrometry.....	144
Table 63: Composition of Bovine Milk, Bovine Brain and Chicken Egg Yolk Sphingomyelin by ³¹ P NMR.....	147
Table 64: Composition of the Sphingolipids (mole%) in Young, Old and Cataractous Eye Lenses.....	177
Table 65: Composition of the SPLs (mole%) in Human Lenses by APCI-MS.....	184
Table 66: The Main Experiments Performed to Eliminate the Dimers and Sodium Adducts (DSAs).....	204

LIST OF FIGURES

CHAPTER I

Figure 1:	“The fluid mosaic model for membrane structure. The fatty acyl chains in the interior of the membrane form a fluid, hydrophobic region. Integral membrane proteins float in this sea of lipids, held by hydrophobic interactions of their nonpolar amino acid side chains with neighboring lipids. Both proteins and lipids are free to move laterally in the plane of the bilayer, but movement of either from one face to the other is restricted. The carbohydrate moieties attached to some proteins and lipids of the plasma membrane are exposed on the extracellular face of the membrane.” ²⁶	3
Figure 2:	Types of phospholipid movement in the bilayer	4
Figure 3:	“The distribution of specific erythrocyte membrane lipids between the inner and outer face is asymmetric” ²⁶	6
Figure 4:	Structures of the glycerophospholipid backbone and generic phospholipid head groups ²⁴	8
Figure 5:	Structures of common dihydrosphingomyelin (DHS), sphingomyelin (SPM) and phosphatidylcholine molecules. Sphingolipids have the general formula X:A/Y:B where X and Y are the number of carbons on the long-chain base (LCB) backbone and fatty acid (FA) chain respectively, and A and B are the number of double bonds on each respectively. So, the specific 16:0 DHS shown is 18:0/16:0. For a detailed description of these designations refer to Section I.A.1. in chapter III.	11
Figure 6:	General scheme illustrating signal transduction through the regulation of an enzyme involved in sphingolipid metabolism ²¹	17
Figure 7:	Role of ceramide in the stress response ²¹	20
Figure 8:	Hypothetical scheme showing the role of ceramide in modulating cell growth and cell senescence. The sphingomyelin cycle is highlighted. ²¹	21
Figure 9:	Scheme showing 5 examples of transmembrane signal transducers. The sphingomyelinase-linked transducer and the SPM cycle are highlighted. ²¹	22

CHAPTER II

- Figure 1:** The LC1MS1(a) LC configuration. The specific experimental parameters shown were for the APCI tandem mass spectrometric analysis of the SPM extracts (LC1MS1(a.2) in Table 1). The LC1MS2(b) configuration had the ESI source on the LCQ (instead of the APCI source shown above). [Original picture design was taken from reference 52]..... 40
- Figure 2:** The LC1MS2(a) LC configuration. The specific experimental parameters shown were for the positive full-scan mass spectrometric analysis of the SPM extracts (LC1MS2(a.1) in Table 2). [Original picture design was taken from reference 52]..... 41
- Figure 3:** The LC1MS2(b) LC configuration. The specific experimental parameters shown were for the positive full-scan mass spectrometric analysis of the SPM extracts (LC1MS2(b.1) in Table 2). [Original picture design was taken from reference 52]..... 42
- Figure 4:** The LC1MS2(c) LC configuration. The specific experimental parameters shown were for the positive full-scan mass spectrometric analysis of the SPM extracts (LC1MS2(c.1) in Table 2). [Original picture design was taken from reference 52]..... 43
- Figure 5:** Schematic of the 9 scan events used in the positive APCI tandem MS experiments for the SPM extracts. Example: Scan event 5 was the MS² of the second most abundant ion (or second most abundant ion listed in parent mass list, if one was used) in the full-scan mass spectrum from scan event 4..... 45

CHAPTER III

- Figure 1:** LC1MS2a analysis of BMS. APCI-MS and UV data obtained on the LCQ (column 1.1), and ESI-MS plus ELSD data obtained on the TSQ (column 1.2)..... 60

Figure 2:	Mass spectrometric analysis of DPPC. A) Total ion +APCI (column 2.1) and +ESI (column 2.2) chromatograms for BMS acquired on the LCQ. B) Extracted ion chromatograms of the DPPC diglyceride ion (2.1.B) and protonated molecule (2.2.B). C) APCI (2.1.C) and ESI (2.2.C) mass spectra across the corresponding DPPC peaks shown in 2.1.B and 2.1.C , respectively. These LC1MS2 runs were acquired sequentially. The LC configuration used in column 2.1 was LC1MS2a (Figure 2). The LC configuration used in column 2.2 was LC1MS2c (Figure 4).....	62
Figure 3:	Proposed molecules and fragment ions formed from DPPC under APCI-MS conditions.....	63
Figure 4:	APCI-MS extracted ion chromatograms (EICs) of the protonated ceramide ions of A) 23:0 DHS, B) 22:0 DHS, C) 21:0 DHS and D) 20:0 DHS. E) EIC showing that the ion at m/z 574.6 was the dehydrated ceramide fragment ion from 21:0 DHS. Similarly, F) showed that the ion at m/z 560.6 was [20:0 DHS Cer – H ₂ O + H] ⁺	65
Figure 5:	Extracted APCI ion chromatograms (EICs) of the protonated ceramide ion of A) 24:0 SPM, B) 23:0 SPM, C) 22:0 SPM and F) 21:0 SPM. D) EIC showing that the ion at m/z 600.6 was the dehydrated ceramide fragment ion from 23:0 SPM. Similarly, E) showed that the ion at m/z 560.6 was [22:0 SPM Cer – H ₂ O + H] ⁺	71
Figure 6:	Positive averaged ESI-MS mass spectra of bovine milk and young eye lens phospholipids, acquired on the LCQ. A) Positive spectrum across the SPL1 peak in BMS; B) positive spectrum across the SPL2 peak in BMS; C) positive spectrum across the SPL3 peak in BMS; and D) positive spectrum across the SPL2 peak in young eye lens samples.....	77
Figure 7:	Negative ion averaged ESI-MS mass spectra acquired on the LCQ, of bovine milk and young eye lens phospholipids. A) Negative spectrum across the SPL1 peak in BMS; B) negative spectrum across the SPL2 peak in BMS; C) negative spectrum across the SPL3 peak in BMS; and D) negative spectrum across the SPL2 peak in the young eye lens sample.....	79
Figure 8:	Identification of 20:0 SPM using the full-scan ESI and APCI mass spectra.....	93
Figure 9:	MS ² (A) and MS ³ (B) mass spectra of 20:0 SPM.....	95
Figure 10:	MS ² (A) and MS ³ (B) mass spectra for 22:0 SPM.....	96
Figure 11:	MS ² (A) and MS ³ (B) APCI mass spectra for 22:0 DHS.....	97

- Figure 12:** Identification of the ion at m/z 588.6 as the plus two isotope of the 22:0 SPM dehydrated ceramide fragment ion in chicken egg yolk..... 101
- Figure 13:** Mass spectrometric analysis of 21:1 SPM in bovine milk. The mass spectra (**F – H**) and late RT of the species at m/z 588.6 was $[21:1 \text{ SPM Cer} + \text{H}]^+$ and the +2 isotope of $[22:0 \text{ SPM Cer} - \text{H}_2\text{O} + \text{H}]^+$. The $[21:1(\text{L})]^+$ and $[21:1(\text{S})]^+$ ions were present at m/z 348.3 and 324.0 respectively..... 103
- Figure 14:** Mass spectrometric analysis of 22:2 SPM in chicken egg yolk. The mass spectra (**F – H**) and late RT of the species at m/z 600.6 was $[22:2 \text{ SPM Cer} + \text{H}]^+$ and $[23:0 \text{ SPM Cer} - \text{H}_2\text{O} + \text{H}]^+$ 104
- Figure 15:** **A)** EIC for $[16:0 \text{ SPM Cer} + \text{H}]^+$ showing that hydroxy-16:0 SPM (**B**) had a later RT. The MS^2 (**C**) and MS^3 (**D**) mass spectra across the shaded region in (**B**) showed the fragment ions used to identify this species. The $[16:0\text{OH}(\text{S})]^+$ and its dehydrated fragment ion at m/z 272.3 and 254.3 were present at very low abundances in the MS^2 mass spectra..... 106
- Figure 16:** Other fragment ions observed under APCI-MS conditions. These fragments were very abundant in the APCI mass spectra obtained by Karlsson *et al.*¹ However, in our experiments their abundances were much lower in comparison to the protonated ceramide ion..... 110
- Figure 17:** Extracted ion chromatograms showing the fragments from 16:0 SPM under APCI-MS conditions. $[16:0 \text{ SPM Cer} + \text{H}]^+$ and its dehydrated ceramide fragment ions were the most abundant. All the other ions were 1 to 2 orders of magnitude less in abundance. Figure 18 shows that all the fragments, except $[16:0 \text{ SPM Cer} - \text{H}_2\text{O} + \text{H}]^+$, had a very low abundances relative to the protonated ceramide ion..... 111
- Figure 18:** Mass spectra showing that the ion at m/z 626.6 was $[16:0 \text{ SPM} - \text{N}(\text{CH}_3)_3 - \text{H}_2\text{O} + \text{H}]^+$ by comparison with the MS^2 (**B**) and MS^3 (**C**) mass spectra for $[16:0 \text{ SPM Cer} + \text{H}]^+$. Both ions had the same LCB and FA fragment ions in the tandem MS data..... 112
- Figure 19:** Integration of the peaks for the protonated ceramide ion, dehydrated ceramide ion and protonated molecule of 20:0 SPM in EICs. The area and RT range over which the peak was integrated are shown..... 116
- Figure 20:** (**D**), (**E**) and (**F**) show the intensities of $[20:0(\text{L})]^+$, $[21:0(\text{L})]^+$ and $[22:0(\text{L})]^+$ in the MS^2 mass spectra for 20:0 SPM (**C**). These intensities were used to calculate the proportioning factor necessary to divide the area of the $[20:0 \text{ SPM Cer} + \text{H}]^+$ peak (**A**) among its constituent SPLs..... 117

Figure 21:	Spectrum list showing the intensities of the $[\text{FA(L)}]^+$ ions used to calculate the proportioning factors for the isobaric species $[\text{21:1 SPM Cer} + \text{H}]^+$ and the + 2 isotope of $[\text{22:0 SPM Cer} - \text{H}_2\text{O} + \text{H}]^+$. The $[\text{FA(L)}]^+$ intensities that were used are highlighted.....	127
Figure 22:	^{31}P NMR spectra of BMS, BBS and CES. The resonance signals from downfield to upfield are as follows: DHS at 0.13 δ , SPM at -0.08 δ and DPPC at -0.84 δ . Each peak is integrated and the normalized areas are shown below each peak. DPPC was used to calibrate the scale.....	146
Figure 23:	Figure 5 from Karlsson <i>et al.</i> 's paper showing the chromatographic profile of the SPLs in bovine milk.....	149
Figure 24:	Figure 6 from Karlsson <i>et al.</i> 's paper showing the ESI mass spectra across SM1, SM2 and SM3, in Figure 23.....	149
Figure 25:	Figure 7 from Karlsson <i>et al.</i> 's paper showing the APCI MS/MS of the ion at m/z 606.6. The asterisks indicated ions which were not labeled. These peaks, from left to right, were probably the $[\text{17:1 LCB} - \text{H}_2\text{O} + \text{H} + 1]^+$ at m/z 251.2 and $[\text{23:0(L)} + 1]^+$ at m/z 379.4.....	151
Figure 26:	The MS^2 (A) and MS^3 (B) of the ion at m/z 606.6 in SPL2. This figure clearly shows that this ion was the +2 isotope of $[\text{22:0 SPM Cer} + \text{H}]^+$, which proved that mass spectra in Figure 25 were incorrectly labeled by Karlsson <i>et al.</i> . The upper was the MS/MS of 606.6 in SM2 and the lower was the MS/MS of 606.6 in SM1.....	155
Figure 27:	Figure 5 from reference 4 showing the PSP MS/MS-CID spectra of protonated ceramides. The mass spectra were similar to that obtained by APCI MS^n . This data was obtained by Karlsson <i>et al.</i>	157
Figure 28:	Diagram from Karlsson <i>et al.</i> 's paper illustrating the +ESI and +APCI MS of $d\text{-18:1/18:0}$. The use of upfront CID in these experiments resulted in extensive fragmentation in the APCI source. The +ESI and +APCI m.s. acquired in our analyses are shown in Figure 29.....	158
Figure 29:	The positive ESI (A) and positive APCI (B) mass spectra of 18:0 SPM in bovine brain. Comparison with Karlsson <i>et al.</i> 's data in Figure 28 showed that there was extensive fragmentation in their data that made it difficult to decipher the mass spectra.....	159
Figure 30:	Figure 3 from Karlsson <i>et al.</i> 's paper showing the structures of the primary fragment ions observed in the APCI MS and MS/MS mass spectra.....	162

Figure 31:	Karlsson <i>et al.</i> 's final table of results showing the LCB/FA compositions of bovine milk, bovine brain and chicken egg yolk sphingomyelin extracts. The composition was denoted using asterisks to represent ambiguous quantities. Our compositions in Tables 31 to 60 significantly improve upon Karlsson <i>et al.</i> 's results.....	164
Figure 32:	A table from Karlsson <i>et al.</i> 's paper showing the LCB/FA composition of bovine milk by plasmaspray tandem mass spectrometry.....	165
Figure 33:	Positive APCI (column 33.1) and positive ESI (column 33.2) extracted ion chromatograms (A – C) of young eye lens extracts.....	170
Figure 34:	Composition of the Sphingolipids in Young Eye Lens Extract.....	178
Figure 35:	Composition of the Sphingolipids in Old Eye Lens Extract.....	179
Figure 36:	Composition of the Sphingolipids in Cataractous Lens Extract.....	180
Figure 37:	Compositions of the DHSs (mole%) in Human Lenses by APCI-MS.....	181
Figure 38:	Compositions of the SPMs (mole%) in Human Lenses by APCI-MS.....	182
Figure 39:	Composition of the PCs (mole%) in Human Lenses by APCI-MS.....	183
Figure 40:	Total ion chromatograms showing the lipids present in young (A), old (B) and cataractous (C) human eye lenses. The disappearance of the PC peak and substantial reduction in the PE plasmalogen peak in (C), implied that these PLs were degraded during the onset of cataracts.....	187
Figure 41:	Positive ESI-MS mass spectra of bovine brain total lipid extract. (A) and (B) show the mass spectra of a 'normal' analysis in which no additive was introduced into the system. (C) to (D) show the mass spectra when 40mM EDTA in MeOH @ 50µL/min was introduced into the mobile phase via a post-column tee. (C) shows the full-scan mass spectrum of the phosphatidylcholines, (D) of the short-chain sphingomyelins and (E) was an extracted <i>m/z</i> range from (D).....	194
Figure 42:	(A) The protonated H ₄ Y configuration of EDTA. (B) The cleavages that produce the primary fragment ions observed in the ESI-MS m.s.....	195
Figure 43:	The ions of the 18-Crown-6 (18C6) ether molecule (A) that were observed in the ESI mass spectra. (B) The chelation of NH ₄ ⁺ by 18C6. (C) The [18C6 + PL + Na] ⁺ complex observed in the ESI-MS m.s.....	195
Figure 44:	(A) the [H ₅ Y + H] ⁺ configuration of DTPA. (B) The cleavages that produce the primary fragment ions observed in the ESI m.s.....	196

Figure 45: “The 20 standard amino acids of proteins. They are shown with their amino and carboxylic groups ionized, as they would occur at a pH of 7.0.”²⁶ The unshaded portions are those groups unique to each amino acid. The asterisks indicate the amino acids that were tested..... 200

Figure 46: (A) and (B) are extracted ion chromatograms (EICs) showing the short-chain (S-C) and long-chain (L-C) lipids respectively, in bovine brain total lipid extract (BBTL). (C) and (D) show the positive ESI mass spectra for the S-C phosphatidylcholines (PCs) and S-C sphingomyelins (SPMs) respectively. (E) and (F) show the negative ESI mass spectra for the S-C PCs and S-C SPMs respectively. These chromatograms show that introducing 40mM glycine/1M NH₄OCOH with a pH of 8.80 into the flow stream via a post-column tee eliminated the phospholipid dimers and sodium adducts. Compare the mass spectra in this figure with those in Figure 45..... 201

LIST OF SCHEMES

CHAPTER I

- Scheme 1:** The metabolic synthesis of ceramide; the basis of sphingolipids. ²⁴ 10
- Scheme 2:** Production of various sphingolipids and signaling molecules from ceramide. The biosynthetic pathway for dihydrosphingomyelin is not known but is postulated to occur by one of the two mechanisms shown... 11
- Scheme 3:** Structural characteristics of sphingomyelins (SPMs) and dihydrosphingomyelins (DHSs) that affect the stability of cellular membranes. The larger arrows indicate that DHSs make a greater contribution (per mole) to the overall stability and fluidity of the membrane SPMs (per mole). **Abbreviations:** PTT, Phase Transition Temperature..... 16

CHAPTER III

- Scheme 1:** Organizational chart showing the subdivisions of the SPL class, and the terms used to refer to each subdivision. The general formulas and acronyms used to refer to the species at each level are also shown.....51
- Scheme 2:** Proposed fragment ions produced from the sphingolipids under APCI-MS conditions. SPMs and DHSs produced similar fragments; the latter being two mass units heavier due to the absence of the double bond on the LCB backbone. All fragment ions were observed in the MS, MS² and MS³ mass spectra, except for the [M – 212]⁺ and [LCB + H]⁺ ions, which were not present in the MS³ m.s. The 3-membered ring structures in square brackets were proposed by Karlsson *et al.*¹, but the 5-membered ring systems are believed to be more stable configurations.....54
- Scheme 3:** Proposed fragment and adduct ions produced from the phosphocholine head group under ESI-MS conditions.....55
- Scheme 4:** Proposed fragment ions formed from 18:1/16:0OH under APCI-MS conditions. Superscript 'a' is used to represent the additional hydroxyl group in the molecule. The normal –OH on the LCB is denoted by superscripted 'b'107

Scheme 5:	Fragmentation of 18:1OH/16:0 under APCI-MS conditions (pathway 1). Superscript ‘a’ is used to represent the additional hydroxyl group on the LCB Backbone. The normal –OH on the LCB is denoted by superscripted ‘b’	108
Scheme 6:	Fragmentation pathway of 18:1OH/16:0 under APCI-MS conditions (pathway 2). Superscript ‘a’ is used to represent the additional hydroxyl group on the LCB Backbone. The normal –OH on the LCB is denoted by superscripted ‘b’	109
Scheme 7:	This scheme serves a guide to aid in deciding which ions are most suitable to calculate PFs. The arrow with a cross indicates a scenario that was not observed in our analyses.....	124
Scheme 8:	The methods used to calculate the final adjusted area (FAA) for the Y:0 and Y:2 sphingolipids by APCI and ESI MS. The mole% for each SPL was calculated by dividing the FAA by the total area of the SPM or DHS populations, multiplied by 100%. Abbreviations: Superscripted ‘A’, represented “Area of”; PF1 and PF2, are the proportioning factors calculated from the MS ² m.s. of protonated ceramide and dehydrated ceramide fragment ions respectively.....	125
Scheme 9:	Scheme 9 shows the methods used to calculate the final adjusted area (FAA) for the Y:1 sphingolipids by APCI and ESI MS. The mole% for each SPL was then calculated by dividing the FAA by the total area of the SPM or DHS populations multiplied by 100%. The scheme shows the method in general terms where superscripted ‘A’ represented “Area”. PF1 and PF2 are the proportioning factors calculated from the MS ² m.s. of the protonated ceramide and dehydrated ceramide fragment ions respectively. The +1 and +2 isotope ions are represented by placing ‘(+1)’ and ‘(+2)’, respectively, after the general formula for the ion.....	130

CHAPTER I

INTRODUCTION

I. The Importance of Lipids

One of the most important structures of any eukaryotic cell is the plasma membrane, which separates the intracellular compartment from the extracellular environment. Other membranes also enclose compartments within the cell which define specific cellular organelles such as the nucleus versus the mitochondria, etc. Lipids and proteins are the two major components of all membranes, and their relative proportions vary greatly between membrane types. Glycerophospholipids (GPLs) and sphingolipids (SPLs)) are the major phospholipid (PL) components of cellular membranes.

Cellular membranes have three very important functions. First, very specific transport mechanisms operate in membranes to permit the translocation of both charged and uncharged molecules from one side of the membrane to the other. This allows the cell to regulate the concentrations of transported substances in various cellular compartments. Macromolecules, such as enzymes, do not cross the membrane unless the membrane contains a specific mechanism for the movement, or the membrane is damaged. Thus, a major function of the plasma membrane is to permit the entrance of some substances into the cell, but to exclude others. Secondly, cells communicate using multiple specific receptor sites on the membrane surface for chemical signals, such as hormones and other signaling molecules. Finally, membranes maintain the integrity of the cell or organelle, by protecting the inner components from the external environment.

All these functions are vital to the health of any cell or organelle, therefore, understanding the molecular composition of cellular membranes will provide detailed knowledge of the mechanisms involved in maintaining membrane structure, stability and fluidity, as well as signal transduction, and intra- and intercellular communication. Lipids are the primary components of cellular membranes; so, they play a major role in the biochemical reactions that determine the properties and functions of these membranes.

Lipid bilayers (Figure 1) are not static, but are fluid and allow for the rapid lateral diffusion of substances (primarily lipids and proteins) in the plane of the membrane. The fluidity of the membrane is dictated, for the most part, by the phospholipid classes present **and** the characteristics of their acyl chains (i.e. carbon chain length and degree of unsaturation).²⁴ A diagram of the common types of PL movement in the bilayer is shown in Figure 2. PLs with FA chains that contain several sites of unsaturation are more fluid than saturated chains because their *cis*- double bonds cause 'kinks' in the FA chains (almost all double bonds in biological systems are *cis*- double bonds), which prevent the PLs from forming tightly packed paracrystalline 'gel-like' arrays. Saturated PLs can pack more tightly in the bilayer, thereby decreasing its fluidity.²⁶

The packing order of the lipids in the hydrophobic core of the bilayer, in turn, affects the permeability of the membrane. A higher percentage of unsaturated FA chains results in a bilayer in which the lipids are unable to pack as tightly compared to when the FA chains are saturated (i.e. without kinks). As a result, the permeability (and fluidity) of the membrane increases with the degree of unsaturation of the FA chains present in the bilayer. In addition, it was found that in general, the lipids of more metabolically active membranes have more unsaturated FA chains.²⁵ However, a higher degree of unsaturation

also makes the bilayer more susceptible to oxidative damage, resulting in the conversion of carbon-carbon double bonds to oxygen-containing functional groups. Such chemical reactions, can significantly affect the functions, stability and permeability of the bilayer.

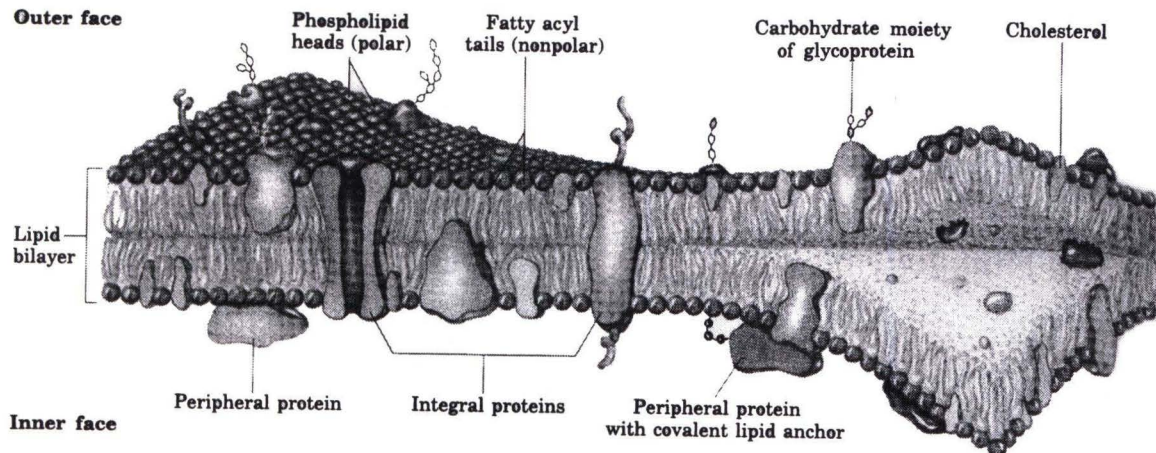


Figure 1. “The fluid mosaic model for membrane structure. The fatty acyl chains in the interior of the membrane form a fluid, hydrophobic region. Integral membrane proteins float in this sea of lipids, held by hydrophobic interactions of their nonpolar amino acid side chains with neighboring lipids. Both proteins and lipids are free to move laterally in the plane of the bilayer, but movement of either from one face to the other is restricted. The carbohydrate moieties attached to some proteins and lipids of the plasma membrane are exposed on the extracellular face of the membrane.”²⁶

The PL classes and the characteristics of their acyl chains also have a profound impact on the proteins that are associated with the membrane. Proteins that are associated with the bilayer are either located on the surface of the hydrophilic layer (peripheral proteins), or are embedded into or through the membrane bilayer (integral proteins). Peripheral proteins are weakly bound to the membrane surface (by electrostatic interactions and hydrogen bonding) and so are easily removed by treatment with salt solutions of differing ionic strengths. Membrane bound molecules, such as peripheral

proteins and glycolipids, are involved in important biological processes such as signal transduction and cellular recognition (integral proteins are also involved in these processes). Therefore, since the PL head groups (HGs) form the surface of the bilayer the composition of the PL classes that are present determines which proteins (and glycolipids) can be bound to the surface, and therefore ultimately the properties of the membrane.

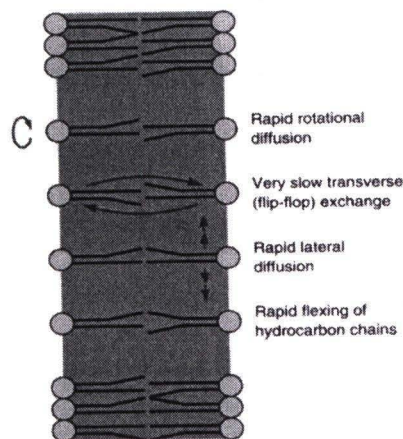


Figure 2. Types of phospholipid movement in the bilayer.

Unlike peripheral proteins, integral proteins are tightly bound to the membrane and are usually dissociated and solubilized by treatment with a detergent such sodium dodecyl sulfate. Integral proteins have a fixed orientation in the bilayer. For example, the glycoproteins of the plasma membrane are invariably situated with their sugar residues on the outer surface of the cell. Similarly, the orientation of protein ion pumps never changes, so as to ensure that they all pump in the same direction.²⁶ Many of these transmembrane proteins have hydrophobic domains that interact with the hydrophobic fatty acid chains of the PLs in the bilayer. These hydrophobic interactions maintain the disposition of the proteins in the membrane. It has been demonstrated that the

characteristics of the acyl chains neighboring integral proteins have a great impact on the proper functioning of the proteins as well as their stability in the membrane.

One of the most commonly used tools to assess the fluidity of PLs, and therefore their likely behavior in membranes, is determination of their phase transition temperatures (PTTs). PTT is the temperature at which a population of PLs change from a highly ordered 'gel phase' to the less organized 'liquid phase'. Most PLs have a phase transition temperature well below the biological range and so are fluid in biological systems. SPLs however, have a PTT in the biological range, which allows them to remain highly ordered at higher temperatures. The higher PTT of the SPLs can be correlated not only with PL class, but also with the identities and therefore characteristics of their FA chains.

The PTT depends on the class and fatty acyl chain composition of a PL in a way that is analogous to the way that the melting points of fats or oils can be directly correlated to the identities of the triacylglycerols present, and the composition of the fatty acids that make them up. Just as saturated fatty acids lead to a solid fat made from triacylglycerols, and unsaturated fats lead to a liquid oil, so, too, do more saturated fatty acids lead to a more ordered, less fluid membrane and more sites of unsaturation lead to a more fluid, less ordered environment. Also, longer fatty chains provide more order, and therefore a higher PTT, while shorter chains yield lower PTTs. SPMs have a tendency to have longer, more saturated acyl chains than glycerol-based PLs such as phosphatidylcholines (PCs), which imparts a higher degree of order to the membrane than other PLs. These observations indicate that the PL classes and the compositions of

their FA chains in cellular membranes play important roles in membrane stability, fluidity and structure.

One last point to make about membrane PLs is that there is substantial asymmetry between the inner and the outer leaflets. PC, SPM and glycolipids are located to a larger extent on the outer monolayer of the membrane. Phosphatidylethanolamine (PE) and phosphatidylserine (PS) and phosphatidylinositol (PI) partition primarily into the inner monolayer (Figure 3)²⁶ Phospholipids translocate by themselves only slowly or not at all across the plasma membrane, because there is too large an energy barrier to overcome to move the polar head group through the hydrophobic core. Instead, there is a complex lipid transport system in place, involving phospholipid transfer proteins, that maintains the asymmetry between the two monolayers.

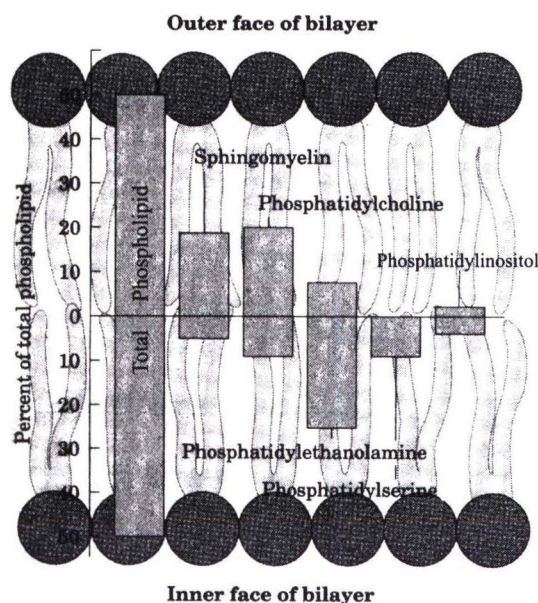


Figure 3. “The distribution of specific erythrocyte membrane lipids between the inner and outer face is asymmetric.”²⁶

From the above discussion it is seen that lipids play a major role in the structure and function of all cellular membranes. This means that lipids are essential components

in biological processes that involve molecules present in or associated with cellular membranes. Whether it is signal transduction, cellular recognition, or membrane transport, determining the PL classes that are in the membrane as well as the characteristics and composition of their FA acyl chains is necessary in order to develop a complete understanding of any of these processes. Before we look at the methods used to determine these PL compositions however, it would be beneficial to first review the structures of the two major PL components of cellular membranes.

II. The Structures of Glycerophospholipids and Sphingolipids

The major lipid components of cellular membranes are PLs, and the primary PL components are GPLs and SPLs. PLs fall into two primary categories, based on the type of backbone they possess: 1) those based on a three-carbon glycerol backbone (Figure 4); and 2) those based on a three-carbon serine backbone (Figure 5 and Scheme 1). Within each of these two categories there are several classes, based on the type of ‘polar head group’ they contain. For example, Phosphatidylcholines (PCs) contain a phosphocholine head group and Phosphatidylethanolamines (PEs) contain a phosphoethanolamine HG (Figure 4). PLs are amphipathic (having a dual nature), with two fatty chains that constitute a non-polar (hydrophobic) region, and a phosphate-containing HG that is polar (or ionic) and hydrophilic. In glycerol-based PLs, the phosphate HG is on the *sn*-3 carbon of the glycerol backbone, and two fatty chains are attached (usually by ester linkages) to the other two carbons of the backbone. These types of PLs are equivalent to a diacylglycerol with a phosphate HG on the third glycerol carbon. Therefore, these types may be referred to as diacylglycerol-containing PLs. The common GPLs are shown in Figure 4.

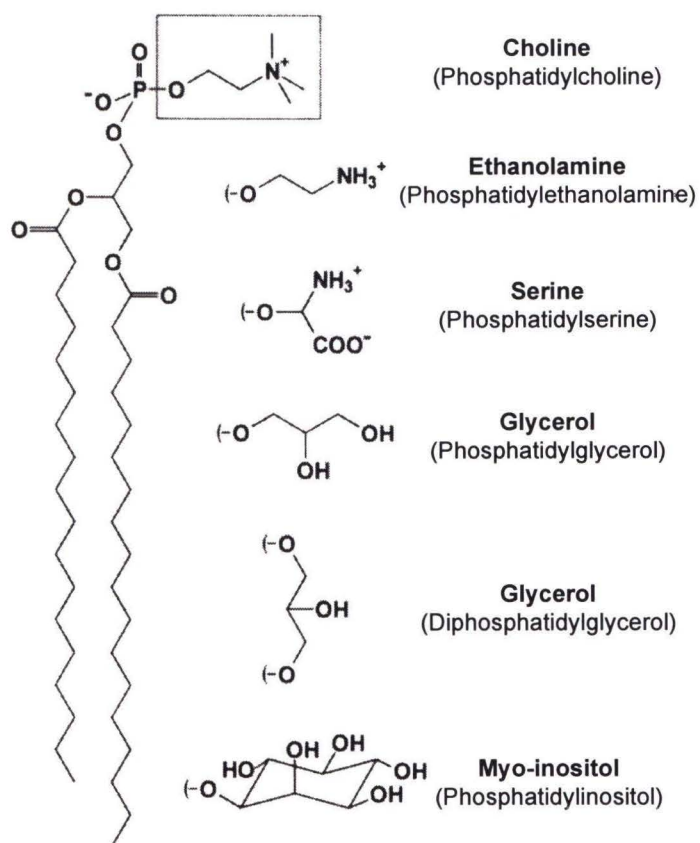


Figure 4. Structures of the glycerophospholipid backbone and generic phospholipid head groups.²⁴

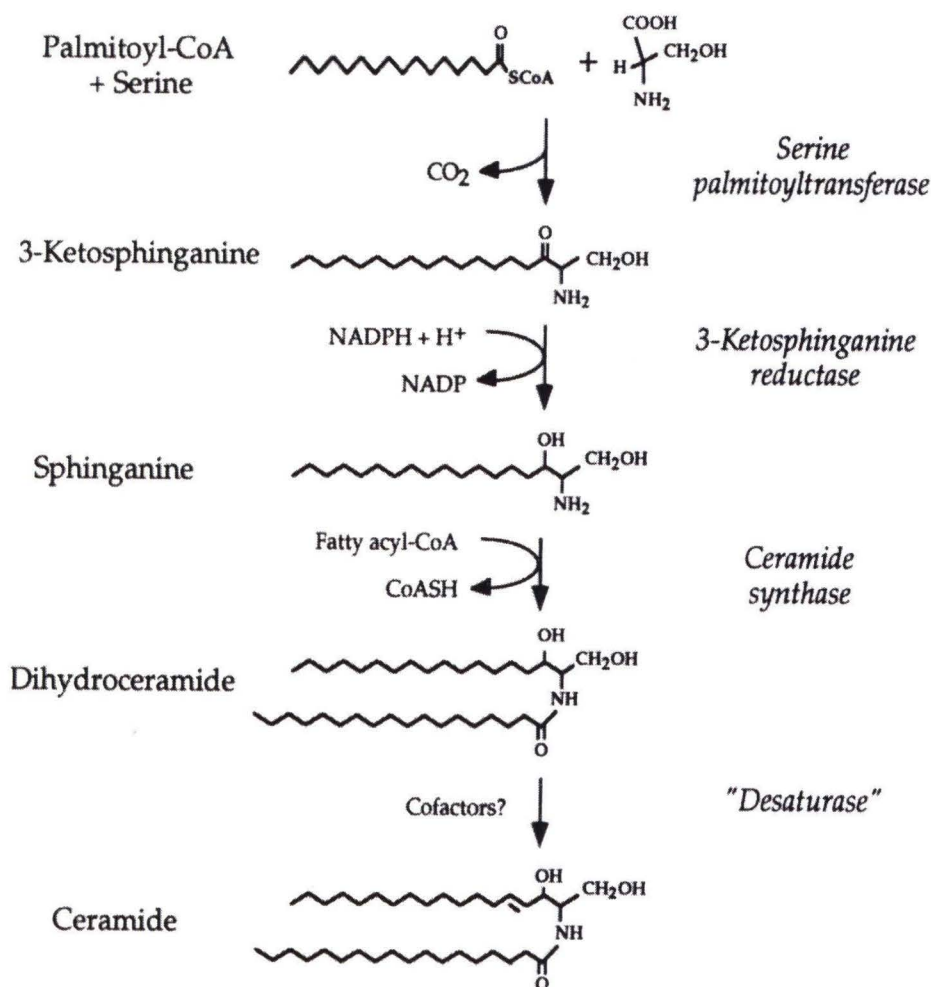
SPLs do not contain a glycerol backbone; instead they are produced from the three-carbon molecule, serine. Scheme 1 shows the biosynthetic steps leading to formation of the ceramide backbone, which is the foundation of SPLs. The synthesis begins with the condensation of serine and palmitoyl Coenzyme A to yield 3-ketodihydrosphingosine, which is then reduced to sphinganine. Sphinganine then serves as the precursor for *ceramide synthase*, which adds the FA chain to the amine, to form dihydroceramide. Finally, the 4,5-*trans* double bond is introduced into dihydroceramide by a *desaturase*, to produce ceramide. The ceramide then acts as the precursor for a variety of SPLs (such as SPM, galactosylceramide and glucosylceramide) and signaling

molecules (such as sphingosine and sphingosine-1-phosphate). Glucosylceramide serves as the precursor for the formation of glycosphingolipids and gangliosides²¹, while galactosylceramide is the precursor for sulfatides. SPM is then formed by the transfer of a phosphocholine HG from a PC to ceramide by *phosphatidylcholine:ceramide cholinephosphotransferase*, liberating a diacylglycerol in the process (Scheme 2).²² . It might be assumed that elimination of the last “*Desaturase*” step would yield dihydroceramide. Addition of the phosphocholine HG would then produce dihydrosphingomyelin (DHS). However, direct evidence for the biological synthesis of DHS is not yet available but the existence of these species has been demonstrated.^{2,3,5}

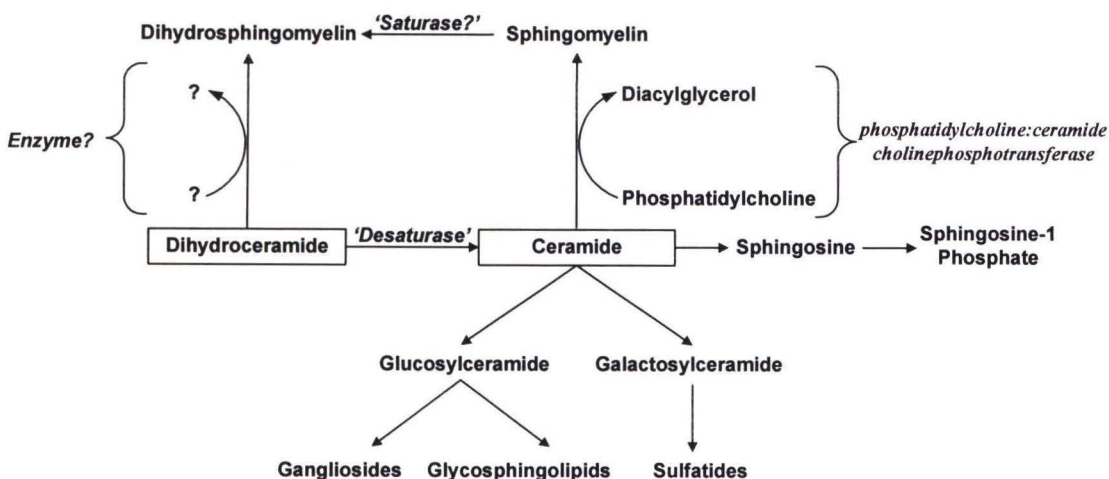
The primary PLs of interest in this work are SPM and DHS. Examples of these SPLs and 34:1-PC (POPC) are shown in Figure 5. The SPLs are composed of a phosphocholine HG, a FA chain and a long-chain base (LCB) backbone as indicated in Figure 5. So, SPMs and DHSs can be referred to using the general formula X:A/Y:B where X and Y represent the number of carbon atoms on the LCB and FA respectively, and A and B refer to the number of double bonds on each, respectively. For a further description of these terms and designation please refer to section I.A.1 of Chapter III.

The major structural difference between DHS and SPM is that the former lacks the 4,5-*trans* double bond on the ceramide (Cer) backbone. Without the double bond, the linkage to the LCB acyl chain is much more flexible. More flexibility in the backbone allows DHS to pack more tightly together, thereby imparting greater stability to the membrane. Also, since the 3-carbon backbone of the SPLs lies on the surface of the plasma membrane, the lack of the double bond on the LCB may be an important factor in the biological processes that occur at the surface. Because so little research has been done

on DHS, it is not known whether this lack of a rigid double bond is incorporated simply to render the membrane more stable and impermeable to oxidation and other degradation mechanisms, or whether it is important for signal transduction. The many unanswered questions surrounding this SPL species have made DHS and SPM the major focus of this work.



Scheme 1. The metabolic synthesis of ceramide; the basis of sphingolipids.²⁴



Scheme 2. Production of various sphingolipids and signaling molecules from ceramide. The biosynthetic pathway for dihydrosphingomyelin is not known but is postulated to occur by one of the two mechanisms shown.

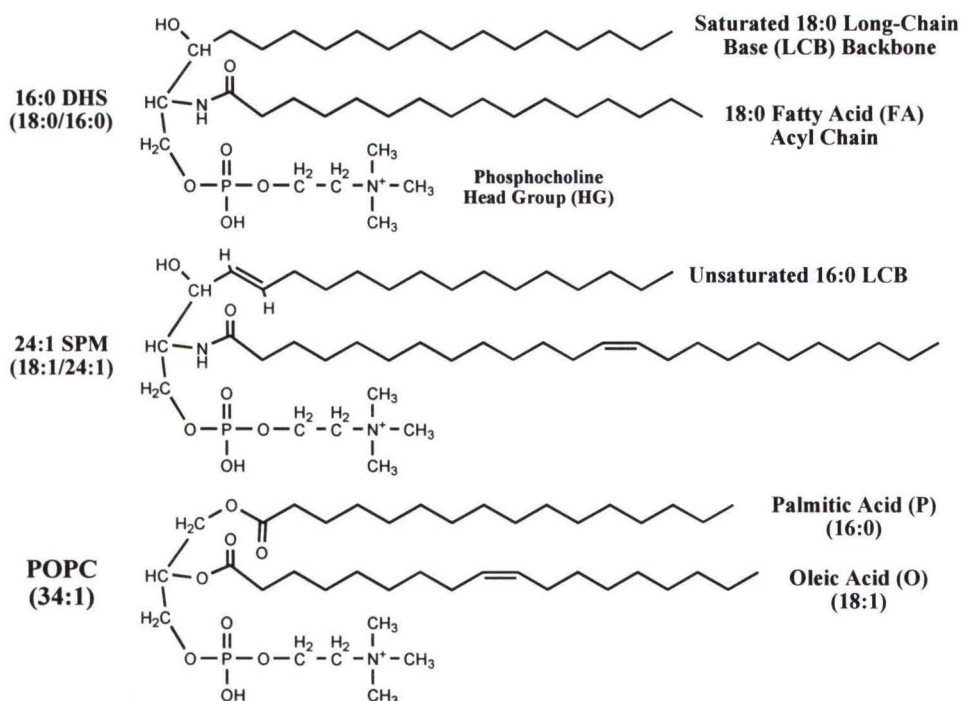


Figure 5. Structures of common dihydrosphingomyelin (DHS), sphingomyelin (SPM) and phosphatidylcholine molecules. Sphingolipids have the general formula X:A/Y:B where X and Y are the number of carbons on the long-chain base (LCB) backbone and fatty acid (FA) chain respectively, and A and B are the number of double bonds on each respectively. So, the specific 16:0 DHS shown is 18:0/16:0. For a detailed description of these designations refer to Section I.A.1. in chapter III.

III. The Importance of Sphingomyelin and

Dihydrosphingomyelin

SPLs play two important roles in cells: 1) they act as structural lipids in the bilayer and 2) they act as precursors for the production of ceramide, the active biomolecule that is associated with numerous signaling mechanisms. SPLs are found in many cellular systems and in all types of organisms. For decades, it was believed that SPLs served primarily as the building blocks of the plasma membrane bilayer. However, the discovery that sphingosine inhibits the activity and binding of protein kinase C (PKC)³⁷ in 1986 suggested that SPLs, and more specifically SPM metabolites, play an important role in signal transduction.

Then, in 1989, the Sphingomyelin Cycle was elucidated and later elaborated.^{22,38} Over the last two decades, there has been a widespread investigation of the roles of SPLs in signaling pathways associated with many natural and disease processes. The body of research has focused mostly on the biological and biochemical activities of ceramide, sphingosine, sphingosine-1-phosphate, and related SPL metabolites. A wealth of reports now unquestionably supports the hypothesis that SPLs play a role in regulating numerous cell functions and possibly mediating the effects of extracellular stimuli.

Before we can talk about the specific aims of this work is necessary to understand the roles of DHS and SPM in membrane structure and signal transduction. As will become clear, the structural characteristics of the LCBs and FAs of SPM and DHS make them unique PLs, which play important roles in many biochemical mechanisms. So, to understand these processes the compositions of the DHS and SPM FAs and LCBs in the membrane need to be determined. This is our broad goal.

III.A. MEMBRANE STRUCTURE

SPM is similar to PC in many ways (both have a phosphorylcholine HG and hydrophobic FA chains), but SPM has several structural characteristics that makes it unique. For most PLs, the two fatty acyl chains are similar in length. In SPMs however, the amide-linked fatty chain in the 2-position of the backbone is often much longer than the fatty chain attached to carbon 3. The dissimilar lengths of the acyl chains in SPMs lead to two main implications³⁹: 1) A high degree of chain length disparity. This asymmetry in the molecule is believed to lead to interdigitation of the FA chains of one side of the bilayer into the FA chains of the opposing bilayer, thereby imparting greater stability to the membrane. 2) Naturally occurring SPMs have a much higher PTT because they have longer and more saturated FA chains (in the 2-position) than other PLs. Also, the amide linkage and hydroxyl group of SPMs provide sites for hydrogen bond donation and acceptance, which increases their ability to associate into rigid lipid rafts in the plane of the membrane.^{20,40} Also, the degree of SPM chain mismatch is an important factor in determining the lateral organization of the PLs in the membrane.⁴¹ All these structural features of SPMs play important roles in maintaining the stability of cellular membranes.

Membrane rafts are localized regions of elevated cholesterol and glycosphingolipid content within cell membranes. These rafts are formed from the clustering of SPLs with cholesterol in the plane of the membrane, and it has been suggested that the propensity of SPLs for hydrogen bonding may provide them with enhanced tendencies to form these micro-domains.⁴⁰ The fatty chain length and amount of unsaturation of the SPLs has an impact on the degree to which they tend to form these micro-domains. The saturated SPLs are preferentially incorporated into raft structures.

Then, these highly saturated rafts provide greater membrane stability (decreased fluidity) and an environment to which proteins can become attached through highly saturated lipid tails covalently bound to proteins. Not only is the amount of unsaturation important, but also there is evidence to suggest that length of the fatty chain in SPM determines the degree to which micro-domains are formed. Therefore, the identities of the molecular species of SPM and DHS in cellular membrane systems are important in developing an understanding of these processes.

Kuikka *et al.*²⁰ determined the PTT of a synthetic version 16:0-DHS, the molecular species that was identified as the most abundant in human eye lenses.² They reported some interesting results: First, that “16:0-DHSM [the acronym ‘DHSM’ has the same meaning as ‘DHS’ from our work] formed crystals at lower pressure compared to 16:0-SM, and that for a bilayer system this would mean that the gel-liquid phase transition temperature of the dihydro species would be higher than that for the acyl chain-matched sphingomyelin.”²⁰ And “The crystals formed in 16:0-DHSM mono layers were much smaller in size...” They determined that the phase transition temperature for DHS occurred at 47.7°C, while the transition for SPM occurred at 41.2°C. 16:0-DHS melted at 6.5°C higher than 16:0 SPM. They also concluded that: “The lack of a *trans* double at the carbon 4 position in 16:0-DHSM results in the molecule having a higher melting temperature in bilayers, and a lower crystallization pressure in monolayers, both indicative of stronger cohesive interactions between the molecules in the model membranes.”²⁰ Borchman *et al.*⁴² also reported a phase transition temperature for DHS. Their results were from an actual human lens extract, instead of a model system. They reported a difference of 9°C between DHS and SPM. Kuikka *et al.*²⁰ also observed that

cholesterol desorption from the subphase was significantly slower from mixed mono layers containing 16:0-DHS than it was from mono layers containing only 16:0-SPM. This showed that cholesterol forms tighter associations with DHS than with SPM. Clearly the exact nature of the SPL played a key role in determining the membrane behavior of DHS. Results such as these highlight the importance of determining the exact fatty acyl chain composition of a cellular system to provide a rationale for understanding its behavior. All of these observations are summarized in Scheme 3.

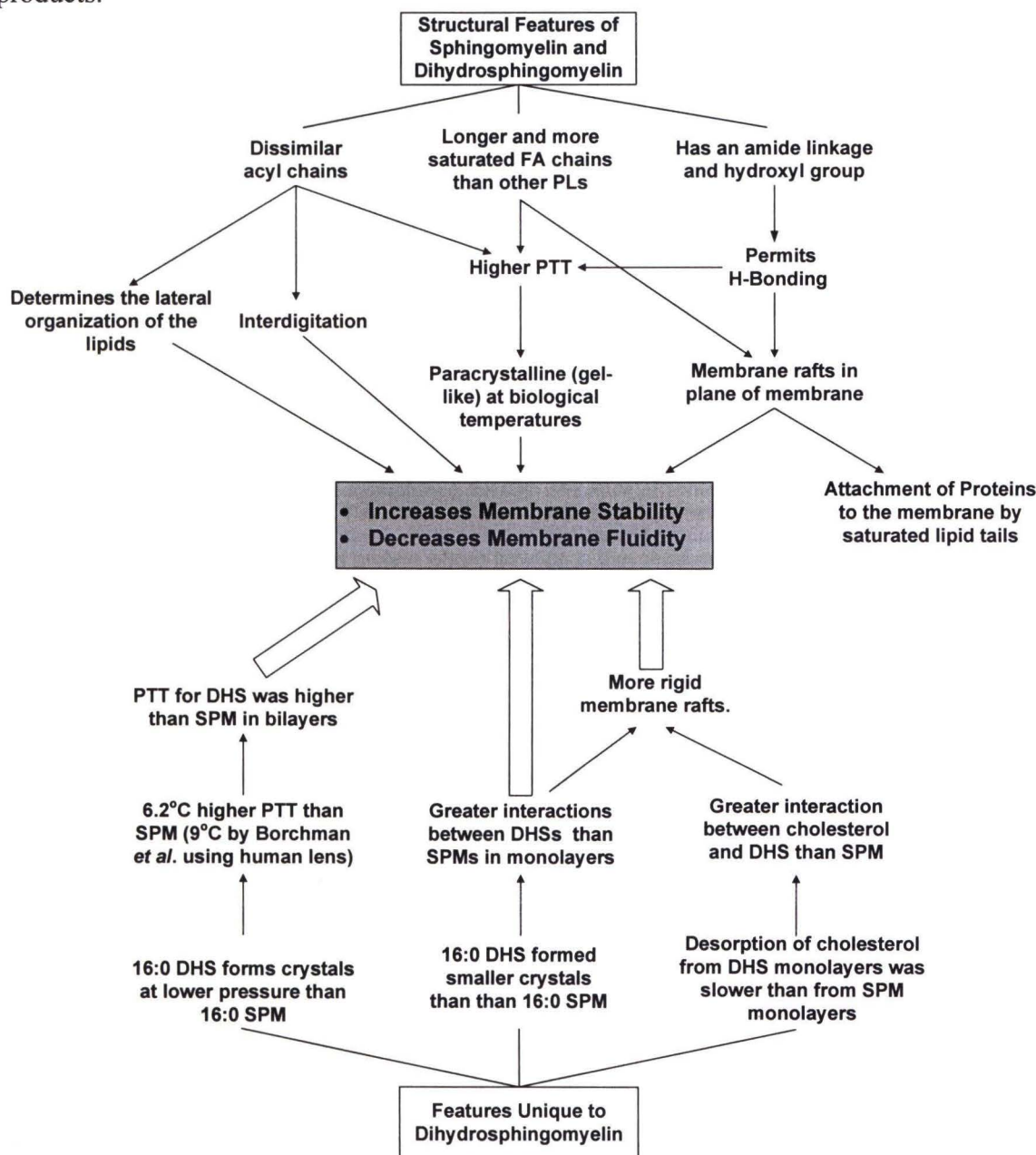
III.B. CELL SIGNALING

Y.A. Hannun in **Sphingolipid-Mediated Signal Transduction**²¹, provided a detailed description of the role of SPLs in many cell signaling pathways. He described signaling through SPLs as follows:

“In its simplest formulation (Fig. 1.1) [our Figure 6], this paradigm, as applied to signal transduction, considers each individual membrane lipid as a source of unique information encoded by the structure of the lipid. Recognition of this lipid precursor as a substrate by a specific enzyme then allows for the controlled formation of products of its metabolism. These products are then recognized by specific targets (almost invariably proteins that are capable of recognizing the specific and often subtle chemical features of these lipid-derived products). Therefore, in its simplest formulation, this paradigm requires the existence of a regulated enzyme of lipid metabolism that serves as the input point, a specific lipid substrate for this enzyme, specific products that are generated from the action of this enzyme, and specific protein targets that respond to the changing levels in these products and that constitute the output of this pathway. As such, these pathways allow for efficient signal transduction across the membrane bilayer, using the very key elements that form the structural basis of this bilayer. It is perhaps this strategic location in the plasma membrane that has rendered lipids attractive targets for information processing and signal transduction.”²¹

“For signal transduction to occur utilizing sphingolipids and their derived products..., there must be regulated metabolism of sphingolipid precursors, the generation of specific products, and the interaction of these products with specific targets (Fig. 1.1)[our Figure 6]. One may consider signal transduction in a more global sense as information processing. Processing of this information requires specificity of chemical structure at two levels: the level of the precursor sphingolipid and the level of the product. It also requires at least two regulated events: regulated enzymes that recognize the sphingolipid precursors, and targets that are regulated by the products of these

enzymatic reactions. Therefore, the basic infrastructure of signaling through lipids requires familiarity with the structures of the involved molecules, the metabolism of these molecules, the regulation of this metabolism, and the mechanism of action of these products.”²¹



Scheme 3. Structural characteristics of sphingomyelins (SPMs) and dihydrosphingomyelins (DHSs) that affect the stability of cellular membranes. The larger arrows indicate that DHSs make a greater contribution (per mole) to the overall stability and fluidity of the membrane SPMs (per mole). **Abbreviations:** PTT, Phase Transition Temperature

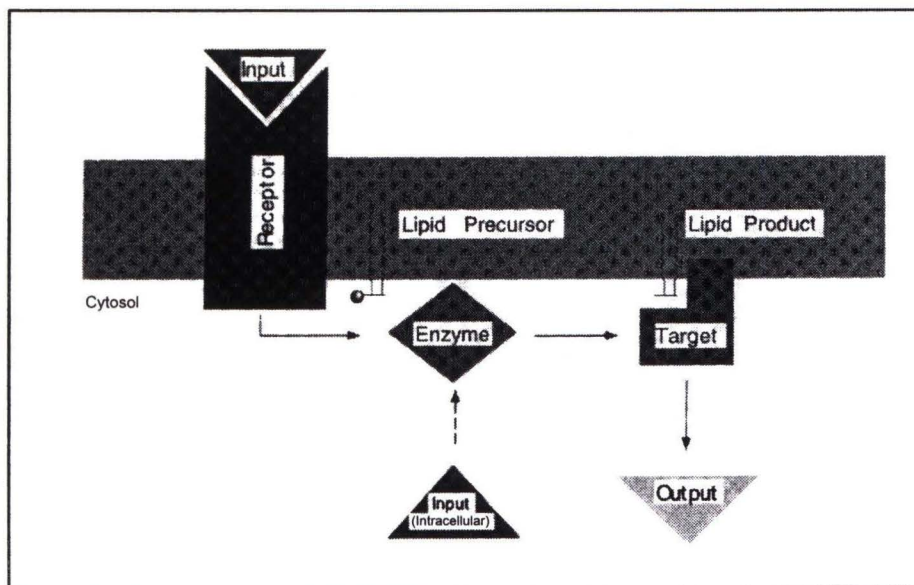


Fig. 1.1. Scheme of signaling through sphingolipids. The paradigm of signaling through sphingolipids requires the “deciphering” of an incoming signal (either from outside the cell or from within). This is accomplished through enzymes of sphingolipid metabolism that respond to these signals. The output of this signaling (or information processing) pathway requires the regulation of levels of the sphingolipid-derived product and the recognition of these changes by a target protein whose function is thus regulated by the changes in the levels of the candidate lipid mediator. This then serves as the proximal output of the system.

Figure 6. General scheme illustrating signal transduction through the regulation of an enzyme involved in sphingolipid metabolism.²¹

“The regulation of sphingolipid metabolism is probably one of the least studied areas of intermediary metabolism. However,... it is this regulated metabolism *per se* that underlies the significance of sphingolipids in signal transduction and cell regulation. According to the paradigm in Figure 1.1 [our Figure 6], in order to achieve signal transduction, an input signal must somehow result in modulation of the activity of a specific enzyme of sphingolipid metabolism. The activation of this enzyme (or, reciprocally, its inhibition) allows for regulation of the levels of precursor and product sphingolipids. This then serves as the driving force for information processing through the changes in levels of sphingolipid species and, consequently, through changes in the activity of enzymes of proteins that recognize these sphingolipids.”²¹

“It is in this aspect that the regulated metabolism of sphingolipids assumes great significance. Indeed, the existing pathways of sphingolipid metabolism already offer multiple potential sites of regulation and numerous actual or potential bioactive products. What may be even more promising is the distinct possibility that many additional pathways of sphingolipid metabolism are yet to be discovered, whose products may play additional roles in cell biology.”²¹

As previously mentioned, the idea that SPLs are directly involved in intracellular signaling pathways arose with the report in 1986 that sphingosine, a product of sphingolipid metabolism, inhibited PKC (an ubiquitous transmembrane signal transducer) activity.³⁷ Then, in 1989 Hannun and coworkers described “the sphingomyelin cycle”, which is the stimulus-regulated breakdown of SPM.²² The sphingomyelin cycle involves the binding of an extracellular ligand to its receptor, which activates a membrane-bound sphingomyelinase enzyme that cleaves the phosphorylcholine HG from SPM to yield a ceramide moiety. The ceramide moiety thus produced is the mediator of the intracellular effects of the ligand (thus SPLs are often referred to as secondary messengers).

According to Merrill and Sweeley:

“Findings over the last decade have provided evidence that sphingolipids are involved in nearly every aspect of cell regulation: i) sphingolipids serve as ligands for receptors (on neighboring cells or the extracellular matrix) and mediate changes in cell behavior in response to a cell's environment. ii) sphingolipids modulate the properties of receptors on the same cell, thereby controlling the responsiveness of the cell to external factors. iii) sphingolipid hydrolysis in response to various agonists releases second messengers (ceramide, sphingosine, and others). iv) sphingolipids are extensively involved in membrane trafficking, therefore, influence receptor internalization, sorting and recycling, as well as the movement and fusion of secretory vesicles in response to stimuli. v) sphingolipids participate in morphological changes in cells in response to factors that induce growth and differentiation, for example, by controlling cell adhesion.”²⁵

The relationship between membrane structure and function is being shown to be especially important with regard to SPLs. The cell signaling functions of SPLs have been intimately tied to their structural appearance in the form of membrane rafts.⁴³ Some reviewers say that we are in a transition from regarding these molecules as membrane constituents to regarding them as signals.⁴³ A couple of examples of signaling pathways that involve ceramide will be presented here to illustrate the importance and scope of SPL

signaling pathways. These examples are not meant to be comprehensive, but only to provide an impression of the range of systems in which sphingolipid signaling has been implicated

Figure 7 represents the production of ceramide by one of several stress inducing factors (Actinomycin D, Tumor Necrosis Factor α , and Serum deprivation). After production, the ceramide initiates signaling cascades leading to cell cycle arrest, apoptosis and inflammation. According to Dbaiibo and Hannun:

“Agents that result in the elevation of cellular ceramide levels are either inducers of apoptosis (TNF α , Fas ligand, dexamethasone), inducers of differentiation (vitamin D3, TNF α , NGF), promoters of cellular damage (chemotherapeutic agents, brefeldin A, ultraviolet light, ionizing radiation), or modulators of the inflammatory response (γ -interferon, interleukin 1, TNF α). Thus, the emerging role of ceramide in the stress response may be analogous to the role of the tumor suppressors p53 and the retinoblastoma protein which have been shown to modulate cell growth, differentiation, and apoptosis and to play a critical role in the stress response generated following genotoxic damage.”²¹

Figure 8 shows a proposed mechanism for the role of ceramide in modulating cell growth and cellular senescence (loss of function with age). See the caption for details of ceramide action. Figure 9 shows different signaling pathways initiated by 5 known classes of transmembrane signal transducers. The ceramide produced by the SPM cycle can act to produce a cellular response, or the Cer may be acted upon further (i.e. by ceramidase) to yield sphingosine or even further: N,N-dimethyl sphingosine in rat brain.²¹ Other transmembrane signaling pathways may utilize glycosphingolipids are also shown. The SPM cycle is highlighted for clarity in each figure.

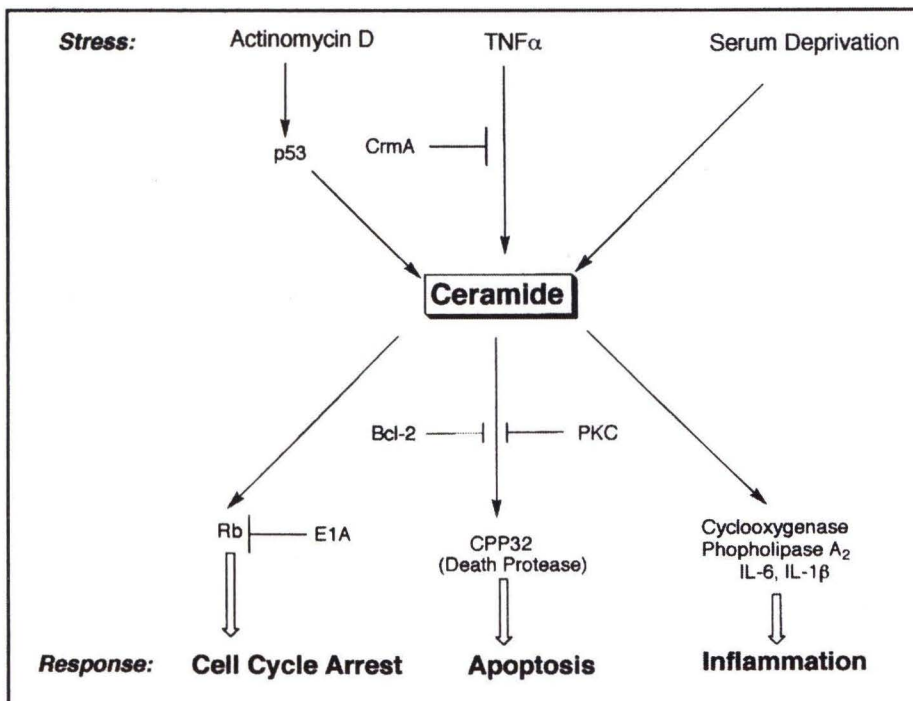


Fig. 2.2. Schematic representation for the role of ceramide in the stress response. Generation of ceramide due to the action of one of several stimuli of stress (such as TNF, chemotherapeutic and cytotoxic agents, and serum withdrawal) activates one or more pathways involved in the response to stress (such as cell cycle arrest, apoptosis, or inflammation). Modulating factors (such as PKC or Bcl-2) may influence or determine the ultimate fate of the cell.

Figure 7. Role of ceramide in the stress response.²¹

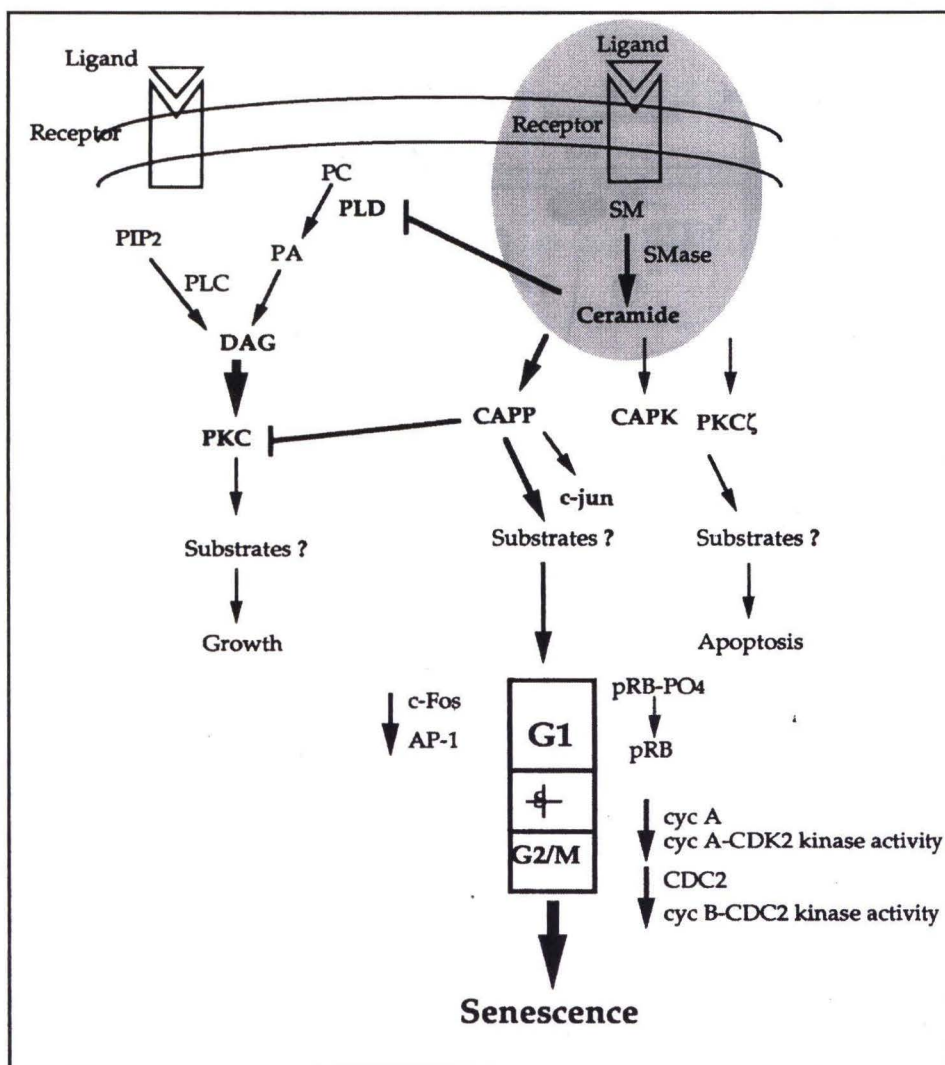


Fig. 5.1. Proposed diagrammatic scheme for ceramide signaling. Exposure to extracellular ligands or stress signals leads to hydrolysis of sphingomyelin (SM) and formation of ceramide by sphingomyelinase (SMase). Once generated, ceramide mediates growth arrest, leads to cell death and induces senescence through activation of a protein phosphatase (CAPP), a protein kinase (CAPK) and Protein Kinase C ζ (PKC ζ). In addition, ceramide induces Rb dephosphorylation, inhibits transcription factors AP-1 and c-Fos, arrests cells at G0/G1 and G2/M phases of the cell cycle, down regulates the expression of cyclin A (cyc A) and CDC2 and inhibits cyclin-dependent kinase (CDK2/CDC2) activities, mimicking cellular senescence. A number of extracellular ligands lead to the activation of phospholipase C (PLC) and phospholipase D (PLD) to generate diacylglycerol (DAG) which then activates PKC and regulates cell growth. Ceramide inhibits the PLD and PKC activities.

Figure 8. Hypothetical scheme showing the role of ceramide in modulating cell growth and cell senescence. The sphingomyelin cycle is highlighted.²¹

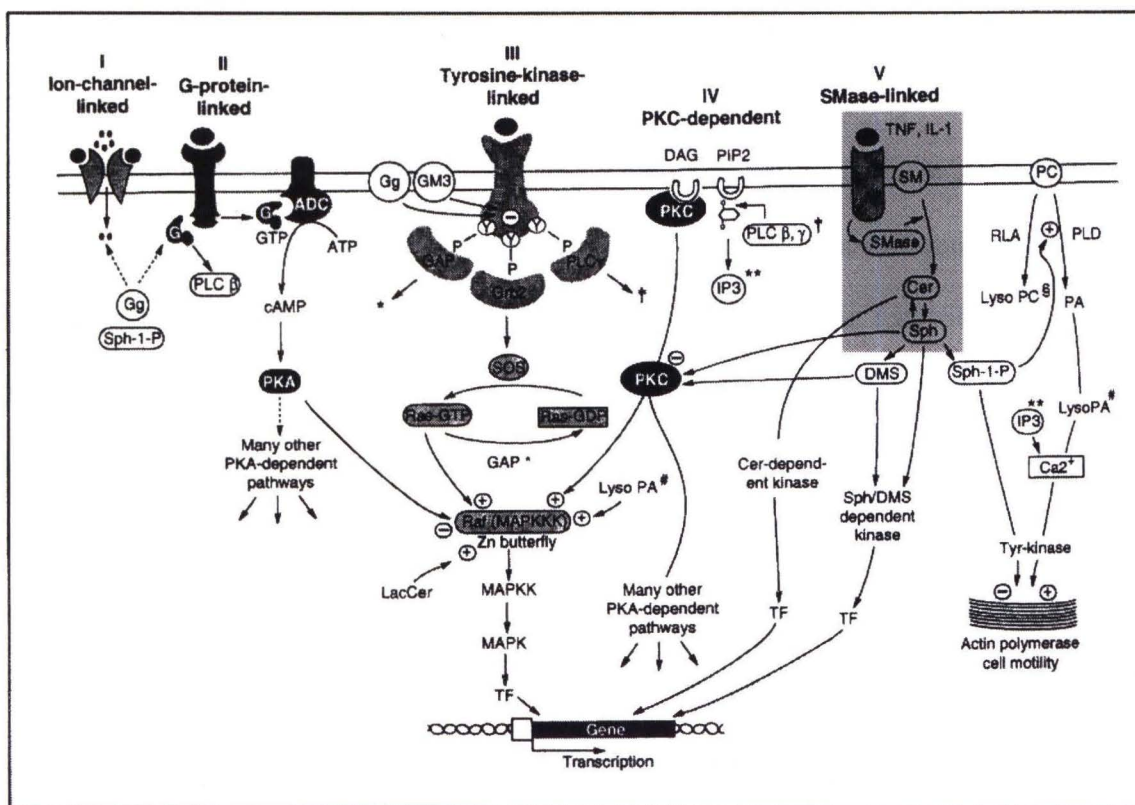


Fig. 10.3. Five classes of receptors or signal transducers which initiate transmembrane signaling. Abbreviations and conventions: Shaded and nonshaded compounds are proteins and lipids, respectively. ADC, adenyl cyclase. G, G-protein. GAP, GTP phosphatase activating protein. Gg, ganglioside. GTP, guanine triphosphate. IP₃, inositol triphosphate. PIP₂, phosphatidylinositol diphosphate. PLA, phospholipase A. PLC, phospholipase C. PLD, phospholipase D. TF, transcription factor. Zn butterfly, a symmetric, cysteine-rich domain showing lipid-binding affinity.

Five classes of receptors or transducers are involved: ion channel linked (I), G-protein linked (II), Tyr kinase linked (III), PKC-dependent (IV), and SMase linked (V). Function of classes I and II is thought to be modulated by gangliosides, but no extensive studies have been performed (see text). G-protein ("G"), activated upon GTP binding, in turn activates PLC β . On the other hand, PLC γ , which has SH domain (src homology domain 2,3), is capable of adapting to Tyr phosphate of receptor class III. Signaling through PLC is controlled by GM3 and other gangliosides. GTP-bound, activated G-protein also activates adenylate cyclase (ADC), which converts ATP to cAMP, which in turn activates PKA. Thus, many PKA-dependent pathways are opened. ADC is known to be susceptible to gangliosides,³⁹ but further extensive studies are needed. PC is converted to lyso-PC through action of PLA, and to PA by PLD. Activity of PLD is enhanced by Sph-1-P. Lyso-PC, in combination with GM3, strongly inhibits Tyr kinase linked receptor (class III). PA is converted to lyso-PA, which strongly enhances activity of Tyr kinase associated with podosomes, and also enhances actin polymerization and cell motility. PLC β , γ , activated by G-protein or Tyr kinase receptor, activates PKC via DAG formation. This event plays a crucial role in signal transduction and opens many signaling pathways. In contrast to DAG, which promotes PKC, Sph and DMS strongly inhibit PKC. PKC activity is also inhibited by various lyso-GSLs and gangliosides. Tyr kinase linked receptors (class III) are inhibited by GM3, SPG, and other gangliosides. Activation of class III receptors by binding of various signaling molecules (growth factors) results in Tyr phosphorylation at cytoplasmic sites ("P-Y"). This creates "docking sites" for binding of adapter proteins having src homology domains (SH2 and SH3), such as Grb2, phospholipase C γ , GTPase activating protein (GAP), etc. Binding of Grb2, for example, leads to activation of Sos, the GDP/GTP exchanger for Ras. This triggers a cascade of phosphorylation through Raf (MAP kinase kinase kinase), MAP kinase kinase, and finally MAPK, which phosphorylates one of the transcription factors (TF) for activation of gene transcription. One of the activated genes encodes MAPK phosphatase, which feeds back to inactivate MAPK (see Fig. 10.5). An alternative pathway leading to MAPK activation and mediated by PKC and PKA is also present. This pathway, regarded as the central event of signal transduction, is closely associated with two other well-established pathways which also depend on PKC and PKA. It has recently become clear that Raf kinase activity is stimulated by PKC^{31,32} and inhibited by PKA.^{33,34} Some types of receptors (e.g., IL-1, TNF α) show specific linkage to SMase, which induces hydrolysis of SM to give increased level of Cer. This triggers activation of Cer-dependent kinase and consequent activation of TF.^{28,101}

Figure 9. Scheme showing 5 examples of transmembrane signal transducers. The sphingomyelinase-linked transducer and the SPM cycle are highlighted.²¹

1. DIHYDROCERAMIDE IN CELLULAR SIGNALING PROCESSES

From the above discussion it was seen that ceramide plays a major role in many cellular signaling pathways. However, dihydroceramide shows little or no signaling or activation response.²¹ This implies the 4,5-*trans* double bond that differentiates ceramide from dihydroceramide is critical in the activation process. The role of ceramide and dihydroceramide⁴⁴⁻⁴⁷ in cellular signaling processes has been investigated. However, the Cer and DHCer that have been used were administered in the form of the product molecule, Cer or DHCer (produced by the catalytic hydrogenation of Cer). In real biological systems, however, the bioactive molecule is produced by action of a sphingomyelinase on the precursor SPM (or DHS) to yield the product Cer (or DHCer). However, very little has been reported regarding the activity of sphingomyelinase enzymes (SMEs) on dihydrosphingomyelin.²⁰

Kuikka *et al.*²⁰, investigated the action of SME on DHS. His results are summarized here:

“When the degradation of 16:0-SM [the acronym ‘SM’ has the same meaning as ‘SPM’ from our work] and 16:0-DHSM by sphingomyelinase are compared, it was clearly observed that 16:0-DHSM was degraded much faster than the 16:0-SM species (10 times less enzyme needed for 16:0-DHSM compared to 16:0-SM). If degradations of 16:0-DHSM and 16:0-SM were performed at a similar enzyme concentration, there was almost no degradation of 16:0-SM during the first hour, whereas 16:0-DHSM was completely degraded in 20 min. Hydrolysis of 18:1-SM and 18:1-DHSM species by bacterial *sphingomyelinase* proceeded with roughly similar kinetics.”²⁰

The results demonstrated that SME is much more active on some molecular species of DHS (16:0-DHS) than it is on SPM, to produce many more molecules of dihydroceramide than ceramide. However, once produced, the dihydroceramide is much less active in cellular signaling than ceramide. This would seem to imply the potential of

DHS to act in a 'down-regulating' capacity, slowing cellular processes and inactivating cellular signaling. Since DHCer has been shown to be inactive in signaling pathways in which Cer is active⁴⁴⁻⁴⁷, one would come to the inevitable conclusion that SME in a cellular system should act on DHS to produce DHCer *in situ*, which would act in a competitive manner with the same targets as Cer. This means that DHS should provide DHCer to act as competitive inhibitor to the Cer activation initiated by enzymatic hydrolysis of SPM.

The results of Kuikka et al.²⁰ demonstrated that dramatic differences in intermolecular packing occur based on differences in i) the nature of the SPL backbone (whether dihydrosphingomyelin or sphingomyelin) and ii) the lengths and amounts of unsaturation of the fatty acyl chains contained within sphingolipid molecular species. Kuikka attributed the faster rate of hydrolysis of DHS by SME to the higher order, or tighter packing (even at elevated temperature), of the macromolecular sheets containing DHS. As mentioned above, the higher order of DHS was reflected in its higher PTT. SME was most effective on the SPLs in an ordered state. And, also as mentioned above, the lengths of and amounts of unsaturation in the fatty amide chains has a large impact on the degree of order of the sphingolipids.

IV. The Mass Spectrometric Analysis of Sphingolipids from Biological Sources

From the discussions above, it is apparent that SPLs play important roles in the proper functioning of cellular systems. They are involved in important signaling pathways such as cell senescence, inflammation and cellular responses to stress, as well as being important structural components of cellular membranes. In fact, the above

discussion shows that the structural features of the SPLs work hand in hand with their signaling properties. These important roles make understanding the molecular composition of membranes vital to the understanding of any cellular system and signaling pathway involving SPLs. Knowing the composition of the SPL classes, the identities and relative composition of their constituent FA chains, and the identities and composition of their constituent LCBs, in cellular membranes, are vital to elucidating the biological and biochemical mechanisms that operate in living systems.

The identification and characterization of DHS¹⁶ and the observation that this SPL class may be present in numerous biological systems raises many questions as to its role in signal transduction and membrane structure. DHS has been identified in bovine milk^{1,9,48}, bovine brain³, chicken egg yolk², the human eye lens² and the porcine eye lens³. The inactivity of DHS in activating cell signaling pathways suggests that its function may be regulatory, modulating the actions of ceramide. Also, its higher PTT and degree of saturation (compared to SPM) suggests that DHS is important for maintaining the integrity, stability and structure of the membrane

All of these discoveries demonstrate the importance of SPLs (and lipids in general) in biological systems and also provide some clues as to the roles of SPLs in the onset of many diseases. Therefore, the main goals of this work were: 1) Determine the difference in the composition of the molecular species of DHS and SPM in normal and cataractous human eye lenses, and 2) develop new and improved chromatographic and mass spectrometric techniques that permit the accurate identification, characterization and quantification of the LCBs and FAs in complex SPL mixtures.

IV.A. CHANGES IN THE COMPOSITION OF THE MOLECULAR SPECIES OF DIHYDROSPHINGOMYELIN AND SPHINGOMYELIN IN HUMAN EYE LENS MEMBRANES, WITH AGE AND THE ONSET OF CATARACTS

Prior to 1991, the major PL component of human lens membranes was accepted to be SPM based on analyses by silica thin-layer chromatography.²⁹⁻³⁶ The amount of SPM in the human lens was reported to be between 60% and 70% of the total PL composition. SPM was believed to be the most abundant PL of the human eye lens from the mid 1960's until the early 1990's.

Then, in 1991, Merchant *et al.*¹⁵ used phosphorus nuclear magnetic resonance (NMR) spectroscopy (³¹P NMR) to observe the chemical shift signals given by the single phosphorus atom in each different class of PLs in a membrane extract. What Merchant *et al.*¹⁵ found was that the most abundant PL in human lens extracts did not give a resonance signal like that of SPM, but instead had a chemical shift at a position in the spectrum that did not correspond to the signal for any available PL standard, or any PL commonly associated with mammalian membranes. At the time, they attributed the largest signal in their spectrum to an 'unknown phospholipid' (UPL). Then, in 1994, Byrdwell *et al.*¹⁶ separated, identified and characterized the UPL. In all reported types of chromatographic analyses, SPM always gave a peak that was not sharp, but rather had a shoulder, and this was never adequately explained. This was even true of commercially available SPM standard that was extracted from bovine brain. Byrdwell *et al.* developed the chromatographic method that allowed the SPLs to be separated.¹⁶

Applying the new separation technique to a human lens extract¹⁶, Byrdwell *et al.* found that 3 peaks eluted where only one peak previously appeared for SPM. Fractions

across these three peaks were collected and submitted to analysis using NMR spectroscopy. Proton (^1H) and ^{31}P NMR spectroscopic data allowed Byrdwell *et al.*¹⁶ to identify the UPL in the human lens for the first time. The structure was determined to be DHS. The difference between DHS and SPM was explained above and is illustrated in Figure 5.

Then, in 1997, liquid chromatography/mass spectrometry (LC/MS) with detection by both atmospheric pressure chemical ionization (APCI) and also electrospray ionization (ESI) MS were used to separate the classes of DHS and SPM chromatographically. Then, the protonated molecules within each class was used to identify the full range of all molecular species having different lengths of fatty chains and different amounts of unsaturation. Thus, 1) the report by Byrdwell *et al.*¹⁶ in 1994 constituted the first report of the identity of the UPL in the human eye lens, and 2) the report by Byrdwell and Borchman² in 1997 was the first time that it was demonstrated that DHS and SPM in a mixture could be identified and differentiated by LC-MS.

Having developed the chromatographic and mass spectrometric techniques to analyze the molecular species of DHS and SPM, the next step was to determine how these compositions change in human eye lens membranes with age and the onset of cataracts. Based on the importance of SPLs in cellular membranes and signal transduction, this investigation is necessary to provide insight into the roles of these lipids in the processes of aging and cataractogenesis. Certainly, the proposed link between 1) SPLs and senescence (Figure 8), and 2) their structural characteristics and membrane structure, suggests the importance of knowing the composition of the SPLs in human lens membranes. In this work, HPLC followed by dual parallel mass spectrometry³ with

detection by both APCI and ESI simultaneously, was used to elucidate the molecular species of SPM and DHS in human eye lens of different ages and degrees of opacity.

We report here for the first time the composition of SPLs in cataracts, we also show that the SPLs increased as a percentage of the total PLs present in cataractous lenses when compared to normal lenses. This was because the PCs and PE plasmalogens disappeared in cataracts, leading to the conclusion that SPLs are the only PLs holding the membrane together in the diseased state. These results suggested that degradation of SPLs by SME is not a major factor associated with cataractogenesis, but that degradation of diacylglycerol-based PLs (such as PCs and PEs) by phospholipase enzymes may be a contributing factor to the disease.

While the degradation of SPLs by SME activity does not seem to be a causative factor associated with cataracts, it appears clear that the role of SPLs in forming extremely stable membrane rafts is a factor in maintaining the partial transparency that remains in the cataractous lens. The fact that the SPLs are the only PLs remaining in cataractous lens membranes, suggested that they play an important role in maintaining membrane structure with the onset of the disease state.

IV.B. THE COMPOSITION OF BOVINE MILK

Because of the structural complexity of SPLs, identification, characterization and quantification has typically been accomplished by analyzing the FA acyl chains and LCB backbones separately, after hydrolysis.^{7,8,49,50} “However, information on the molecular structure of the intact lipid is important when the biological role of the lipid is considered.”¹ Determining the molecular species composition of SPLs will provide

detailed knowledge of the composition of cellular membranes as well as the specific SPLs that are involved in signal transduction.

High performance liquid chromatography (HPLC) with detection by mass spectrometry (MS) is one of the most powerful analytical tools used today, and has been employed to separate and analyze intact SPL molecules from various sources.^{2,3} The lens extracts mentioned above were analyzed using these techniques. However, these methods only provide information about the **SPL groups** (see Scheme 1 of Chapter III) present in the membrane, but do not provide **specific** information about the FAs and LCBs present in the extract. This information can only be acquired by tandem MS. Fragmentation of the protonated SPL molecules using collision induced dissociation (CID) produces structurally useful fragment ions that permit the identification of the **specific** LCBs and FA chains present. Tandem MS therefore, identifies the **individual** SPL molecules that make up the cellular membranes of interest. (For further description please see section **I.A.1** in Chapter III).

SPLs extracted from bovine milk form a very complex mixture due to the numerous LCB/FA combinations present in the sample. Although this complexity is a drawback, it serves as a means to test the capabilities and scope of the mass spectrometric methods developed to determine the LCB/FA composition of SPL mixtures. Several mass spectrometric methods have been employed in the past to analyze intact SPL molecules from bovine milk such as gas-liquid chromatography (GLC) MS^{7,8}, gas chromatography (GC) MS⁶ and HPLC discharge-assisted thermospray (TS) MS^{4,5,9} (also known as plasmaspay (PS) MS). The GLC-MS and GC-MS experiments however, suffered from having to expose the lipids to harsh chemical conditions in order to produce derivitized

LCBs and/or FAs. These procedures involved the use of strong acids and/or bases and high temperatures of about 70°C for extended periods of time (about 18 hours). These methods are therefore undesirable because they can result in: 1) oxidation of unsaturated FA chains, which therefore changes the LCB/FA composition; 2) formation of unwanted artifacts such as esters and aldehydes; 3) loss of sample due to the long and numerous chemical steps necessary to produce these derivatives; and 4) the introduction of contaminants into the analysis.

HPLC with detection by PS-MS was used to analyze the intact SPLs, thereby eliminating many of the problems associated with the GLC-MS and GC-MS methods outlined above. However, the sensitivity of this ionization technique is “not especially good in the case of large compounds such as peptides, saccharides and lipids.”²⁷ The harsh nature of PS (compared to ESI and APCI) results in extensive fragmentation in the ion source making identification of SPLs in complex mixtures, such as bovine milk sphingomyelin (BMS) extract, difficult. This was evidenced by the low signal-to-noise (S/N) ratio observed in these analyses, as well as the small number of LCB/FA combinations that were identified.^{4,9} PS is an older ionization technique, and has been supplanted by the newer more sensitive atmospheric pressure ionization (API) techniques of APCI and ESI MS.²⁷ With the increase in use of these API techniques, a new analytical method needed to be developed that employs these methods to accurately quantify SPLs in complex mixtures (such as BMS). Such an analysis was attempted by Karlsson *et al.* in 1998.¹

In his 1998 paper, Karlsson *et al.* attempted to “describe the complete structural elucidation of intact SPMs by using HPLC/API-MS/MS.” However, poor mass-

spectrometric techniques and incorrect data interpretation resulted in the misidentification of molecular species. In this work, we outline Karlsson *et al.*'s mistakes and present a thorough and accurate quantification of three of the four SPM mixtures that he analyzed (the bovine erythrocytes SPM standard was not analyzed by us). Because of the numerous errors in Karlsson *et al.*'s analysis, our work therefore, represents *the* first accurate and complete structural elucidation of intact SPMs in bovine milk sphingomyelin by APCI-MS and ESI-MS. This work describes a new analytical approach to the analysis of complex SPL mixtures by HPLC with detection by APCI and ESI MS.

BMS is commercially available and of biological significance. Since cow's milk constitutes a common dietary component, the report of the identities of the SPLs in this common dietary staple affects many people. Karlsson *et al.* reported that BMS was composed predominantly of SPM and hydroxy-SPM. Virtually no DHS was reported to be present. However, as will be shown, Karlsson *et al.* misidentified the DHSs as hydroxy-SPMs. This a critical error from both a methodological and biological standpoint, because these two classes of molecules have very different structural features and characteristics in cell signaling pathways. If the class of molecules were 2-hydroxy-SPMs as reported by Karlsson *et al.*, then the action of SME on the molecules would produce 2-hydroxy-ceramide, which would be an active signaling biomolecule. In fact, if the 2-hydroxy-SPM bore any resemblance to phytosphingomyelin, which has an extra hydroxy at the 4-position of the backbone, then 2-N'-hydroxy ceramide produced by SME acting on 2-N'-hydroxy-SPM might be even more active than ceramide. This is because a recent report demonstrated that synthetic phytoceramides (which would come from SME activity on hydroxy-SPMs) induce apoptosis with higher potency than

ceramides.²⁸ Thus, the hydroxy-SPMs reported by Karlsson *et al.* could potentially lead to higher cellular activation than even that given by the normal SPMs in the milk. This is clearly different than if milk contains DHS, which would produce the inactive dihydroceramide.

This work corrects these mistakes, and others, made by Karlsson *et al.* in his 1998 paper and describes the first accurate mass spectrometric method for the identification and quantification of the LCBs and FAs in complex SPL mixtures, using BMS standard as an example. The experimental approaches and results presented in this work, provided detailed information about SPM and DHS molecular structure, and allowed us to develop methods for the determination of the LCB/FA composition of SPL mixtures by APCI and ESI MS.

IV.C. SOLVING THE SODIUM ADDUCT AND DIMER PROBLEM

PLs with phosphocholine HGs (such as SPLs and PCs) have an inherent tendency to form dimers and sodium adducts in ESI-MS (Scheme 2 of Chapter III). Although these ions provide multiple corroborative pieces of information that are useful for the identification of molecular species, they prevented the accurate quantification of GPLs and SPLs using ESI-MS, because they were not formed with equal probability. Also, it was found that dimerization occurred more frequently in the ion trap mass spectrometer than the triple quadrupole mass analyzer, and therefore was a problem specific to these types of mass spectrometers. In this work, we present a new method that eliminates the dimers and sodium adducts by the introduction of additives into the mobile phase via a post-column tee. This method significantly reduced the abundance of dimers and sodium

adducts, resulting in less complex mass spectra in which the protonated molecule was the base peak.

V. Summary

It is apparent from the discussions of SPLs above, that there has been a renewed and intense interest in SPLs over the last decade because of their implication in the signaling and transport mechanisms of numerous cellular systems. However, there is still a gap in the information available about the **specific** SPL molecules that comprise membrane structures and that are key participants in these biochemical mechanisms. As a result, more work needs to be done to develop new analytical methods capable of analyzing the components of the lipid bilayer. Until the composition of the FAs and LCBs of the SPLs in biological systems is determined, a complete understanding of biochemical processes responsible for signal transduction, membrane transport and membrane structure, will remain elusive. This work attempts to fill this gap, by developing novel chromatographic and mass spectrometric methods to unravel the complexity and mystery of the lipid bilayer.

CHAPTER II

EXPERIMENTAL

I. Liquid Chromatography/Mass Spectrometry

I.A. Materials

All solvents were of HPLC quality and were purchased from Sigma-Aldrich Chemical (Milwaukee, WI, USA) and Fisher Scientific (Fair Lawn, NJ, USA) and were used without further purification. Bovine milk, chicken egg yolk and bovine brain sphingomyelin (SPM) commercially available membrane extracts, as well as 1, 2-di-palmitoyl-sn-glycero-3-phosphocholine (DPPC) and bovine brain total lipid extract (25mg/mL) were purchased from Avanti Polar Lipids (Alabaster, AL, USA) and were used without further purification. All other reagents, such as ethylenediaminetetraacetic acid (EDTA), phthalic acid, ammonium formate, glycine etc. were of the highest available quality, were purchased from Sigma-Aldrich Chemical, and were used without further purification. Two types of LC configurations were used throughout this work. The LC1MS1 and LC1MS2 configurations are illustrated in Figure 1 and Figures 2 – 4, respectively. A 10.00 mg/mL solution of each SPM extract in chloroform (CHCl_3) with 0.50 mg/mL DPPC added as an internal standard (IS), were used for the LC1MS2 analyses. LC1MS1 experiments were performed using 10mg/mL solutions without the DPPC IS.

All human lenses were obtained from organ donors post mortem. The monophasic methanol extraction developed by Byrdwell *et al.*⁵³ was used to extract individual young, old and cataractous human eye lenses. These procedures were performed by Douglas

Borchman at the University of Louisville in the Department of Ophthalmology & Visual Sciences. The analytical experiments were performed by Wm. Craig Byrdwell at Florida Atlantic University (Thesis Advisor).

The two mass spectrometers used in this work were the LCQ Deca ion trap (Thermo Finnigan, San Jose CA) and TSQ 700 triple quadrupole (Thermo Finnigan, San Jose CA) mass spectrometers. The operating parameters and LC configurations are illustrated in Figures 1 – 4.

I.B. Liquid Chromatography

The LC1MS1 and LC1MS2 designations **only** refer to the **number** of LC systems and mass spectrometers used, and do not specify the type(s) or location(s) (i.e the mass spectrometer on which a specific ionization method was used) of the ionization method(s) used in the experiment. Figure 2 shows an example of an LC1MS2 setup. The specific LC1MS1 and LC1MS2 experiments that were performed are listed in Tables 1 and 2, respectively. So, for example, the positive APCI tandem mass spectrometric analysis of the SPM extracts is denoted as LC1MS2(a.2), where ‘LC1MS2’ describes the LC configuration, the letter ‘a’ refers to the location of the ionization sources based on Table 1 (in this case APCI was performed on the LCQ and ESI on TSQ) and the last number designates the scan sequences used in the experiment (in this case positive APCI tandem MS). Notice that these references are based on the classification in Tables 1 and 2, so that LC1MS1(b.1) was a different experiment from LC1MS2(b.1), and each referred to the analysis of a different sample. LC1MS1(b.1) was only used to analyze bovine brain total lipid extract (BBTL), while LC1MS2(b.1) was used to analyze only the SPM extracts. All the experiments will be referred to using this classification system as it specifies the

sample(s) being analyzed, the LC configuration(s), ionization source(s) and their location(s) and the scan sequence(s) being performed.

1. SPHINGOMYELIN EXTRACTS

Two normal phase (NP) liquid chromatography configurations were used for the analyses. LC1MS1 (Figure 1) consisted of an AS3000 autosampler, a Constametric 4100MS gradient pump with membrane degasser, a UV 6000LP photodiode array (PDA) detector (Thermo Separation Products, Thermo Finnigan, San Jose, CA) and a CH-430 column heater (Eppendorf, Westbury, NY) set at 57°C. The LC system was controlled by the autosampler, which had its column oven and tray temperatures set at 57°C and 33°C, respectively. The purpose for using the column oven on the autosampler was to preheat the mobile phase before it reached the column. The autosampler was used to make 10 µL injections into the mobile phase, the constitution of which was controlled by a gradient program.

We developed a new gradient program with two solvents. Solvent A was 40% hexane/60% isopropyl alcohol (IPA) and solvent B was 40% H₂O/60% IPA, both with 0.1% NH₄OH. The gradient was as follows: 0 to 60 minutes, 80% A : 20% B; from 60 to 65 minutes, there was a linear change to 50% A : 50% B, which was held for 20 minutes; recycled back to the original conditions from 85 to 90 minutes; which was held for 15 minutes. The purpose of the linear change to 50% A:50% B was to wash any residual PLs off the column before the next experiment. During these sets of experiments, the proportioning valve on the pump failed, so a TSP4000 (Thermo Separation Products, Thermo Finnigan, San Jose, CA) pump was used. As a result, the gradient was changed to account for the inherent operating differences between the instruments. Instead of an

initial composition of 80% A:20% B, a composition of 77% A:23% B for 0 to 60 mins was used. The program continued as follows: from 60 to 65 minutes, there was a linear change to 50% A : 50% B, which was held for 20 minutes; recycled back to the original conditions from 85 to 90 minutes; which was held for 15 minutes. The mobile phase flow rate was 0.8 mL/min throughout the experiment and the entire flow was sent through the photo-diode array detector (PDA) into the mass spectrometer. The sample components were separated using two Adsorbosphere propyl-NH₂ columns (Alltech Associates, Deerfield, IL), connected in series. The shortest possible 0.01" ID stainless steel tubing was used to connect the two columns. The columns were held at 57°C throughout the experiment. The columns were also equilibrated at this temperature for one hour before the first experiment of each day, and 15 mins between sequential separations.

The LC1MS2 (Figures 2 to 4) configuration used the TSP4000 pump and its associated gradient program. The flow rate, columns, temperatures and equilibration times were the same as those used in the LC1MS1 configuration. In LC1MS2 experiments the eluent from the amine columns was split with the aid of tee junctions as follows: a Valco Tee (Valco Instruments, Houston, TX) was attached to the outlet of the column. To the 90° exit of the junction was attached a length of 0.005" I.D. PEEK tubing which went directly to the PDA detector. The outlet from the PDA was connected to a length of 0.005" PEEK tubing which went to the evaporative light scattering detector (ELSD). The ELSD was a model MKII (Varex, Burtonsville, MD, US). The drift tube was set to 140°C, the exhaust temperature was 33°C and the nebulizer gas (UHP nitrogen) pressure was 47 psi. The straight-through side of the first Valco Tee was attached to a second Valco Tee via a short piece of stainless steel of 0.01" internal

diameter (ID) tubing. To each of the two outlets of the second tee, an equal length (3 ft.) of 0.10mm ID deactivated fused silica capillary tubing was attached via an adapting ferrule. One capillary was attached to the ionization source on the LCQ Deca and the other to the ionization source on the TSQ 700.

Three different LC1MS2 experiments were performed: 1) LC1MS2(a), APCI-MS on the LCQ and ESI-MS on the TSQ; 2) LC1MS2(b), APCI-MS on both mass spectrometers (Figure 3); and 3) LC1MS2(c), ESI-MS on the LCQ and APCI-MS on the TSQ (Figure 4). The flow rates to the detectors in each setup were different because of the different sizes of the ion source inlet tubes. The ESI inlet tube had a 100 μ m ID while the APCI had a 150 μ m ID. The flow rates to all detectors are illustrated in Figures 2 to 4. In LC1MS2(a) and LC1MS2(c), 20mM NH_4OCOH in $\text{H}_2\text{O}:\text{ACN}$ (1:4) was delivered at 20 $\mu\text{L}/\text{min}$ from an Applied Biosystems (AB) syringe pump (Foster City, CA, USA) to the ESI source (on the TSQ and LCQ respectively) as the sheath liquid. This was done to provide electrolyte for use in ESI mode. The photodiode array detector (PDA) was interfaced to the LCQ Deca ion trap instrument for data acquisition, while the ELSD was interfaced to the TSQ 700 triple quadrupole instrument.

2. HUMAN EYE LENSES

The NP 3-solvent LC system that was used to separate the lipids in human lens extracts was already previously described.^{2,16} The LC1MS2(c) configuration was used for these analyses. Also, the instruments used in the analysis of the SPM extracts were also used in these experiments (except for the CH-430 column heater), and the autosampler was used to make 40 μL injections into the mobile phase. These experiments were carried out at ambient temperature.

3. ELIMINATION OF DIMERS AND SODIUM ADDUCTS

The NP 3-solvent LC system that was used to separate the lipids in BBTL (25mg/mL) was previously described.³ The LC1MS1(b) (Table 1) configuration, in which ESI-MS was performed on the LCQ, was used for these analyses. The instruments used in the analysis of the SPM extracts were also used in these experiments (except for the CH-430 column heater), and the autosampler was used to make 20 μ L injections into the mobile phase. These experiments were carried out at ambient temperature.

In these experiments various solutions were introduced into the mobile phase post-column via a Valco tee. These solutions were delivered by an AB 140B syringe pump. Another tee was placed just before the ESI source so that the entire 0.8mL/min mobile phase flow (plus the flow rate of the additive from the syringe pump) did not enter the mass spectrometer. In the experiments that required both the sheath liquid and a post-column additive, the AB syringe pump was programmed to deliver both solutions simultaneously. The sheath liquid was always supplied at 20 μ L/min whereas the buffer solutions were supplied at various rates depending on the experiment. In experiments where only the additive was being supplied, then the AB syringe pump was programmed to deliver the desired flow rate. The various buffer solutions that were used and the different experiments that were performed are listed in Table 66 in the ‘**Solving the Sodium Adduct and Dimer Problem**’ section of **Chapter III**.

Figure 1: The LC1MS1a Configuration

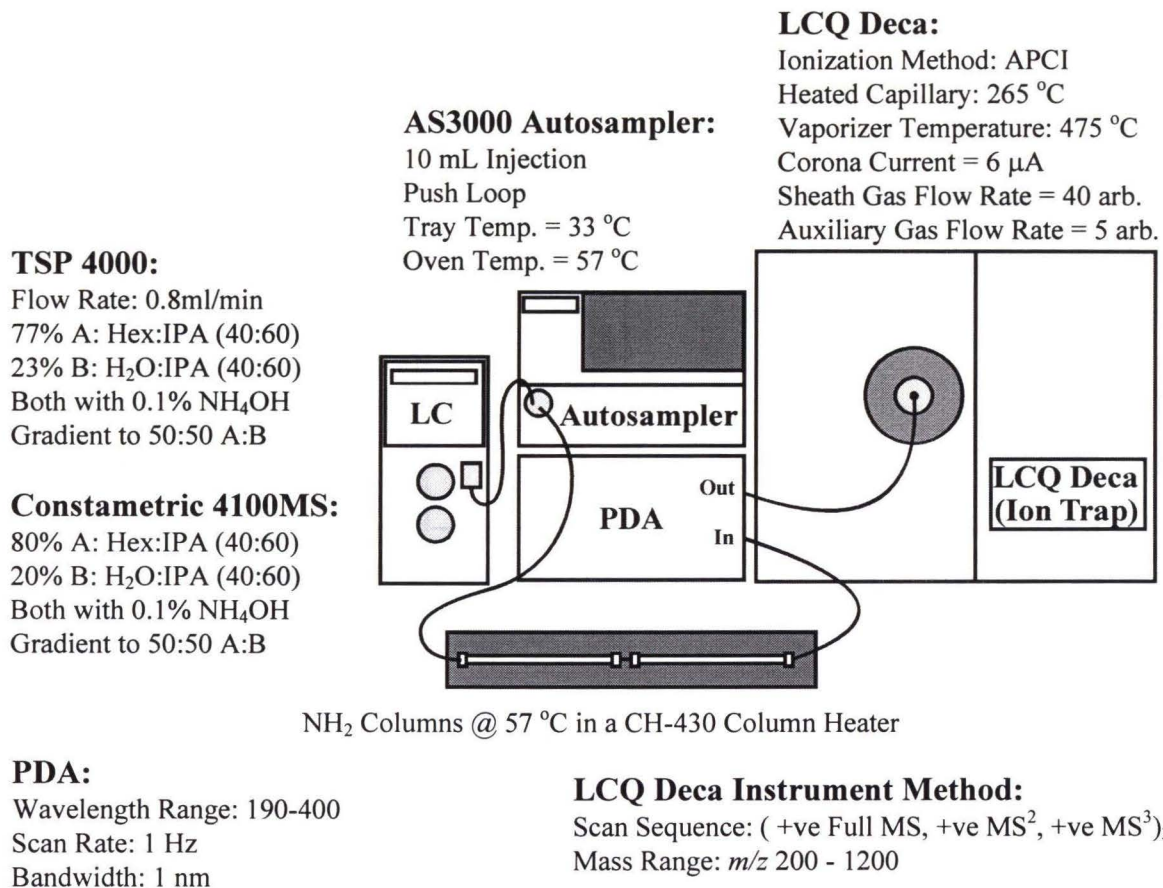


Figure 1. The LC1MS1(a) LC configuration. The specific experimental parameters shown were for the APCI tandem mass spectrometric analysis of the SPM extracts (LC1MS1(a.2) in Table 1). The LC1MS2(b) configuration had the ESI source on the LCQ (instead of the APCI source shown above). [Original picture design was taken from reference 52]

Figure 2: LC1MS2a Configuration Used for the Analysis of the Sphingomyelin Standards

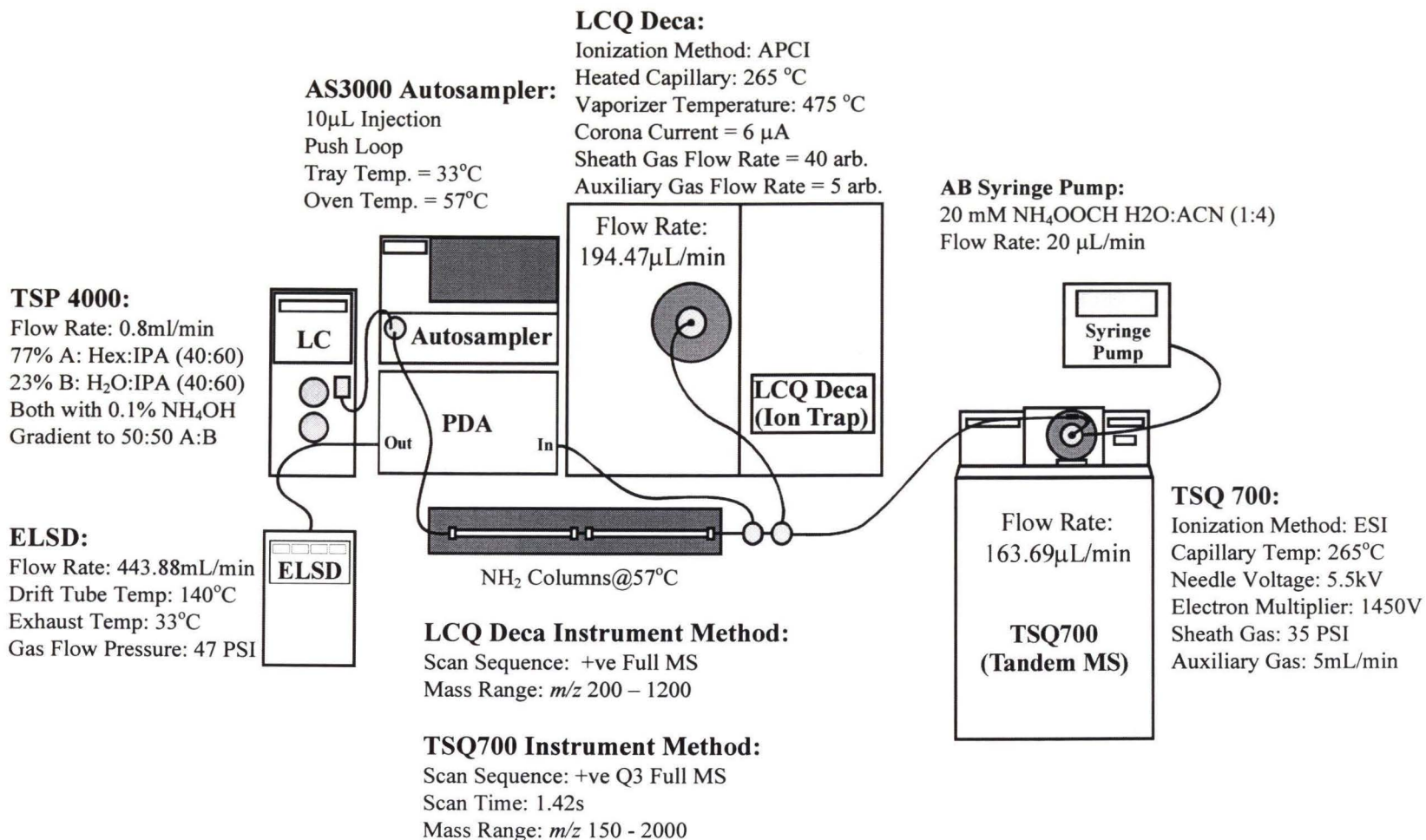


Figure 2. The LC1MS2(a) LC configuration. The specific experimental parameters shown were for the positive full-scan mass spectrometric analysis of the SPM extracts (LC1MS2(a.1) in Table 2). [Original picture design was taken from reference 52]

Figure 4: The LC1MS2c Configuration

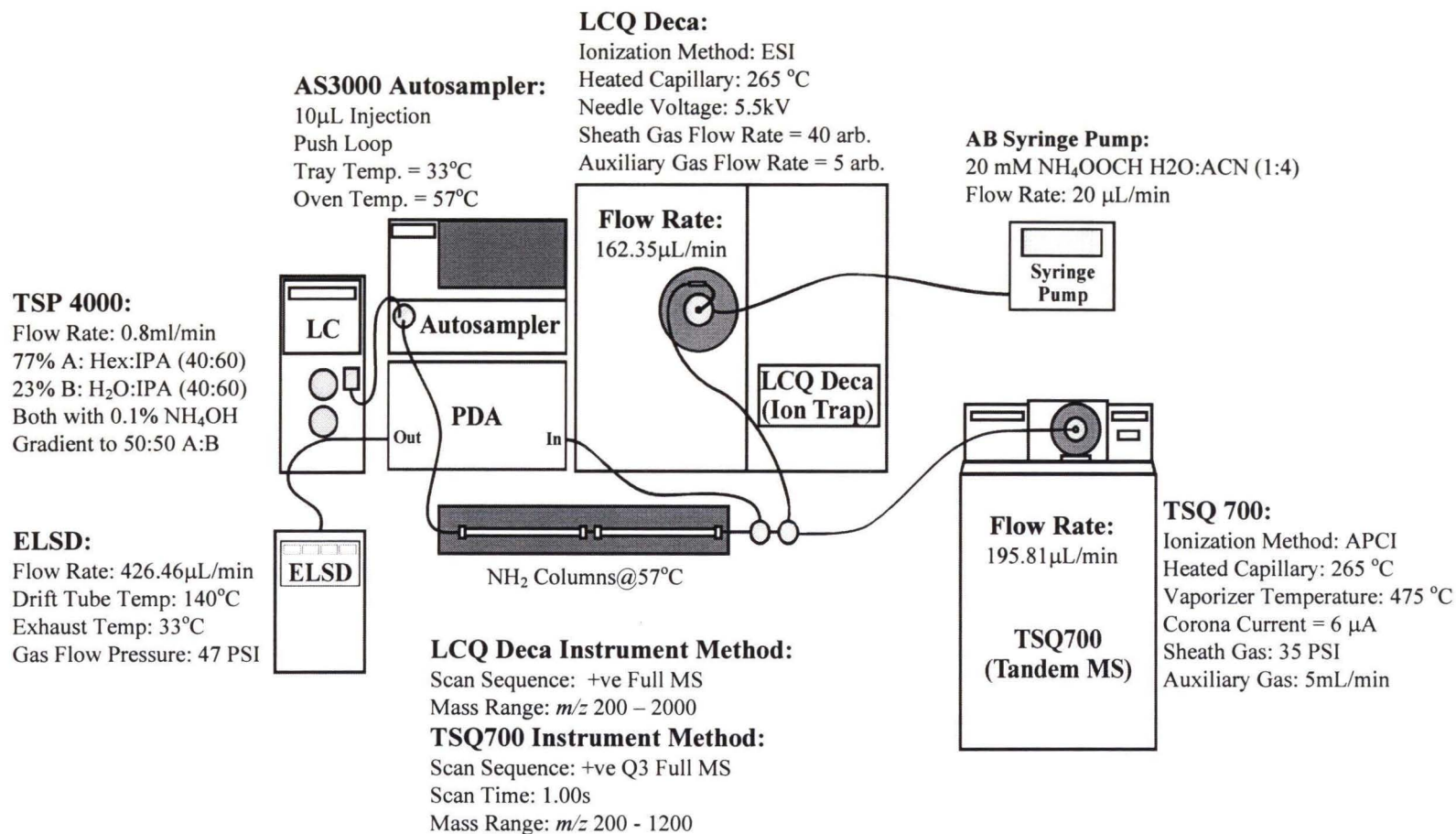


Figure 4. The LC1MS2(c) LC configuration. The specific experimental parameters shown were for the positive full-scan mass spectrometric analysis of the SPM extracts (LC1MS2(c.1) in Table 2). [Original picture design was taken from reference 52]

I.C. Mass Spectrometry

From this point forward, the specific scan sequences will be referred to by the designations listed in Tables 1 and 2. Please refer to this table for details.

1. SPHINGOMYELIN EXTRACTS

1.1 Atmospheric Pressure Chemical Ionization

In the LC1MS1(a), LC1MS2(a) and LC1MS2(b) experiments, APCI was performed on an LCQ Deca (Thermo Finnigan, San Jose CA) ion trap mass spectrometer. The scan sequences for these experiments are shown in Tables 1 and 2. The vaporizer temperature was set to 475°C, the capillary heater was 265°C, the corona current was 6.0μA, and UHP nitrogen was supplied as the sheath gas at 40 arb. (arbitrary units) and the auxiliary gas at 5 arb. The scan range was m/z 200 -1200 for both +APCI and -APCI. The APCI tandem MS used a normalized collision energy of 54%, an activation Q of 0.25 and an activation time of 900ms.

The APCI tandem MS experiments were performed using 9 scan events which are shown in Figure 5. These scan events can be classified into three groups based on the number of full scans, as shown by the shaded regions. So, for example, scan event 5 was the MS/MS of the second most abundant ion in the full-scan mass spectrum from scan event 4. This was designated MS²(2-1), where the 2 represented the order of intensity (from highest to lowest) of the parent ion in the full-scan mass spectrum from scan event 4. Notice that all the MS³ scan events picked the most abundant parent ion from the immediately preceding MS/MS scan. Tandem MS experiments using different parent mass lists were also performed, so as to obtain MSⁿ data for as many ions as possible. If a

parent mass list was used then scan event 5 would be the MS/MS of the second most abundant ion in the parent mass list in the full-scan mass spectrum from scan event 4.

All data acquired on the LCQ was processed using the Xcalibur software package.

Scan Events								
1	2	3	4	5	6	7	8	9
Full MS	MS ² (1-1)	MS ³ (1-2)	Full MS	MS ² (2-4)	MS ³ (1-5)	Full MS	MS ² (3-7)	MS ³ (1-8)

Figure 5. Schematic of the 9 scan events used in the positive APCI tandem MS experiments for the SPM extracts. Example: Scan event 5 was the MS² of the second most abundant ion (or second most abundant ion listed in parent mass list, if one was used) in the full-scan mass spectrum from scan event 4.

In LC1MS2(c) experiments, APCI was performed on a Finnigan MAT TSQ 700 (Thermo Finnigan, San Jose CA) tandem mass spectrometer. The TSQ 700 gave optimal signal in Q3 low mass mode where Q1 was operated in RF-only mode (Q3MS). Using Q3MS, scans were obtained in positive ion mode from m/z 200 – 1200, with a scan time of 1.0s. The vaporizer heater was operated at 475°C, the capillary at 265°C, and the corona current was 6μA. UHP nitrogen was supplied as the sheath gas at 35 psi and auxiliary gas at 5mL/min. Only full-scan +APCI data was acquired on the TSQ. Data obtained on the TSQ 700 were imported into the Xcalibur software on the LCQ using its file conversion tool. This allowed chromatograms and spectra from the two mass spectrometers to be more easily and accurately compared.

1.2. Electrospray Ionization

In the LC1MS2(c) experiments ESI was performed on the LCQ Deca. The spray voltage was set to 5.5kV, the capillary was set at 265°C, 20mM NH₄OCOH at 20μL/min was supplied as the sheath liquid and UHP nitrogen was supplied as the sheath gas at 40

arb. and the auxiliary gas at 5 arb. The scan range was m/z 170 - 2000 for both +ESI and –ESI modes.

In the LC1MS2(a) experiments, ESI was performed on the TSQ 700 in Q3MS mode. Scans were obtained in positive ion mode from m/z 150 – 2000, with a scan time of 1.40s. The spray voltage was set to 5.5kV, the capillary was set at 265°C, 20mM NH_4OCOH at 20 $\mu\text{L}/\text{min}$ was supplied as the sheath liquid and UHP nitrogen was supplied as the sheath gas at 35 psi and the auxiliary gas at 5mL/min. Only full scans were acquired.

A total of 48 unique mass spectrometric experiments were performed, which are listed in Table 3. Each experiment was performed at least twice.

2. HUMAN EYE LENSES

Human eye lenses were analyzed using the LC1MS2(c.3) configuration with APCI and ESI on the TSQ and LCQ, respectively. The ESI-MS parameters were the same as those used in LC1MS2(c.1) and LC1MS2(c.2), except for the following: The scan range was m/z 50 - 2000 for both +ESI and –ESI mode; an upfront collision-induced dissociation (CID) voltage of 20V was used for full-scan analyses and 5V for MS^n analyses; A normalized collision energy of 58% was used for MS/MS analyses.

The APCI-MS experiments were the same as LC1MS2(a.1) except that the scan range was m/z 150 – 1200.

As previously stated, these experiments were performed by Dr. Byrdwell.

3. ELIMINATION OF DIMERS AND SODIUM ADDUCTS

Bovine brain total lipid extract was analyzed using LC1MS1(b.1). The ESI-MS parameters were the same as those used in LC1MS2(c.3) except for the following: An

upfront CID energy of 5V was used for both the full-scan and MSⁿ scans; A normalized collision energy of 50% was used for MSⁿ analyses.

Table 1: Types of LC1MS1 Experiments

Sample	LC1MS1 Config.	Experiment Type	LCQ Scan Sequence
SPM Extracts	a	1	+APCI
		2	(+APCI, +APCI MS ² , +APCI MS ³) ₃
		3	+APCI, -APCI
		4 (BMS only)	+APCI, -APCI, -APCI MS ² , -APCI MS ³
BBTL	b	1	+ESI, +ESI MS ² , +ESI MS ³ , -ESI, -ESI MS ² , -ESI MS ³

Table 1. Different types of LC1MS1 experiments performed on the LCQ.

Table 2: Types of LC1MS2 Experiments

Sample	LC1MS2 Config.	Experiment Type	LCQ Scan Sequence	TSQ Scan Sequence
SPM Extracts	a	1	+APCI	+ESI
		2	(+APCI, +APCI MS ² , +APCI MS ³) ₃	+ESI
	b	1	+APCI	+APCI
	c	1	+ESI	+APCI
		2	+ESI, -ESI	+APCI
Human Eye Lens	c	3	Segment 1: +ESI, +ESI MS ² , -ESI, -ESI MS ² Segment 2: -ESI, +ESI, +ESI MS ² , +ESI MS ³ Segment3: +ESI, +ESI MS ² , -ESI, -ESI MS ²	+APCI

Table 2. LC1MS2 experiments performed on the LCQ and TSQ.

**Table 3: Summary of the Unique Experiments Performed on the
Commercially Available SPM Extracts**

LC Config.	General Exps.	BMS # Unique	BBS # Unique	CES # Unique
LC1MS1	+APCI MS ⁿ	7	7	9
	+APCI	1	1	1
	+/- APCI	1	1	1
	+/- APCI MS ⁿ	1		
LC1MS2 (LCQ:TSQ)	+APCI:+APCI	1	1	1
	+APCI:+ESI	1	1	1
	+APCI-MS ⁿ :+ESI	6		
	+ESI:+APCI	1	1	1
	+/-ESI:+APCI	1	1	1
Total		20	13	15

Table 3: A general listing of the experiments performed on the SPM extracts. By ‘Unique’ we mean that the experiments have different scan sequences or parent mass lists.

II. ^{31}P Nuclear Magnetic Resonance Spectroscopy

II.A. MATERIALS

Solutions of the sphingomyelin extracts in deuterated chloroform were prepared with a concentration of approximately 25mg/mL with 10mg/ml DPPC added as an IS in a 1 mL volumetric flask. 800 μL of each solution was then placed in a 5mm NMR tube along with 400 μL of the Meneses-Glonek reagent (MGR). The MGR was shown to decrease peak widths (increasing the resolution) by preventing aggregation of the PLs in solution. The mixtures were allowed to separate into two phases before beginning the experiments. The MGR was originally described by Meneses and Glonek.¹⁴ Three different samples were prepared per SPM extract. So a total of 9 solutions were analyzed.

II.B. ^{31}P NMR

^{31}P NMR spectra were obtained on a Varian Mercury Plus 400 MHz spectrometer, with a field strength of 9.39 teslas. The operating frequency for ^{31}P NMR was 162.177 MHz. The acquisition parameters were as follows: spectral width, 1012.1Hz; acquisition time, 1.3 seconds; pulse width, 18 μs ; number of transients, 10,000; recycle delay, 2.0 seconds. DPPC, which was known to have a chemical shift of -0.84 δ , was used as the ^{31}P chemical shift reference. All spectra were analyzed using Mestre-C NMR Software version 3.7.9 and were treated using the 'Full FT', 'Automatic Phase APT' and 'Full Auto Baseline Correction' processing options (in that order). Mestre-C was also used to integrate the peaks to produce normalized areas for each SPM extract.

CHAPTER III

RESULTS AND DISCUSSION

I. Commercially Available Sphingomyelin Extracts

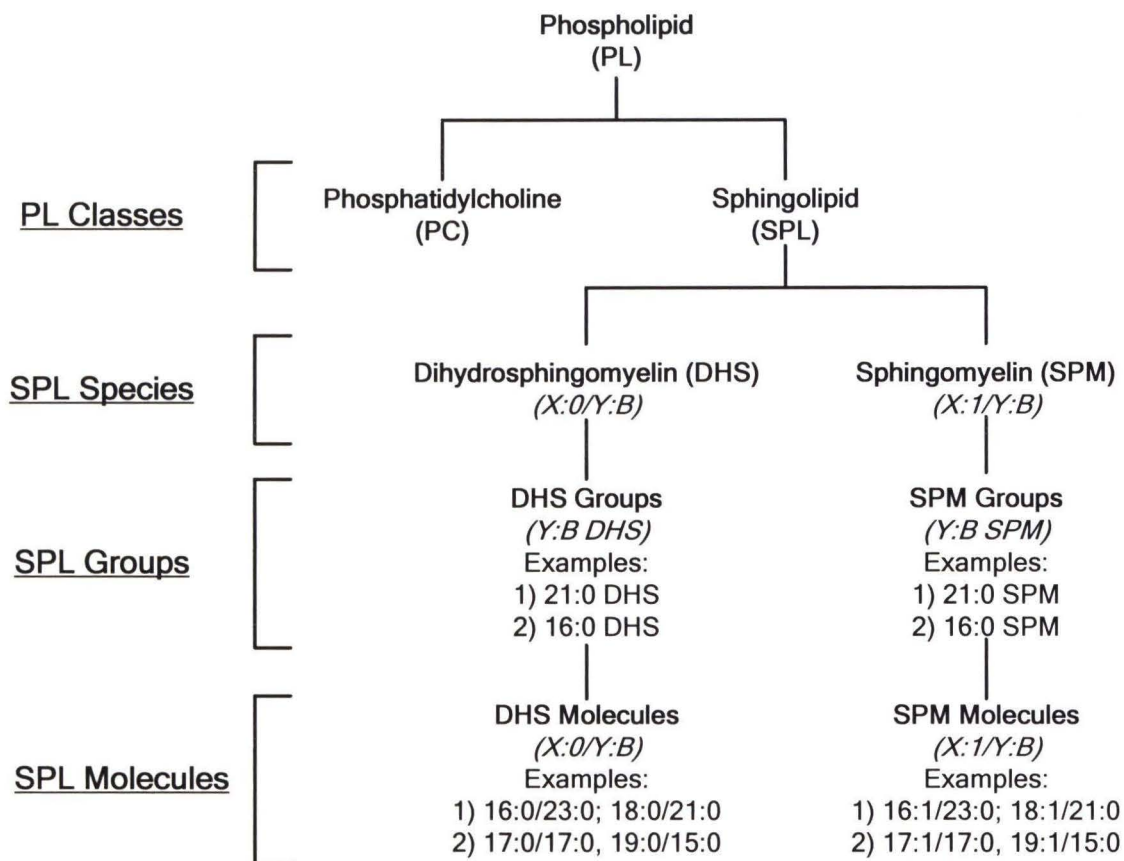
I.A. Liquid Chromatography/Mass Spectrometry

1. MASS SPECTROMETRY

Before beginning the analysis it would be useful to define the terms and concepts that will be referred to throughout this work. The LC1MS2 configuration, in which APCI-MS and ESI-MS were performed on the LCQ and TSQ, respectively (LC1MS2a), will be used to illustrate the principles involved in the analysis of the full-scan APCI and ESI mass spectra (m.s.). The APCI MS, MS² and MS³ results will be described using the qualitative LC1MS1 experiments. Also, since BMS was the most complex SPL mixture, most of the examples will be extracted from this data set. All SPM samples however, were analyzed using 1) +APCI MS, MS² and MS³, -APCI, +ESI and -ESI MS.

SPLs will be referred to using the general formula X:A/Y:B, where X and Y are the number of carbons on the LCB and FA, respectively; and A and B are the number of double bonds on the LCB and FA, respectively. The terms DHS and SPM refer to SPLs that have saturated and unsaturated LCBs respectively. When used in combination with a FA designation, 21:0 DHS (general representation is Y:B DHS) for example, the term refers to a group of DHSs that are isobaric with 18:0/21:0, such as 16:0/23:0, 20:0/19:0 or 14:0/25:0. Scheme 1 shows that the SPL class of PLs is composed of the DHS and SPM species, which in turn contain specific groups of molecules such as 21:0 DHS. These

groups can be subdivided into their component molecules such as the 16:0/23:0 molecule in the 21:0 DHS SPL group.



Scheme 1. Organizational chart showing the subdivisions of the SPL class, and the terms used to refer to each subdivision. The general formulas and acronyms used to refer to the species at each level are also shown.

Typical molecules, and fragment and adduct ions that were observed in the APCI and ESI mass spectra are shown in Schemes 2 and 3, respectively. Throughout this work, these ions will be generally referred to by the labels illustrated in these schemes. References to a fragment ion from a specific molecule will be done by including the molecular designation of the SPL in the formula. For example, the protonated ceramide ion, $[\text{Cer} + \text{H}]^+$, for 1) a single molecule such as 18:1/21:0 will be represented as

[18:1/21:0 Cer + H]⁺, and 2) a SPL group, as [21:0 DHS Cer + H]⁺. The calculated masses for the major fragments of the SPMs (with an 18:1 LCB) and DHSs (with an 18:0 LCB) in the +/-ESI and +/-APCI m.s. are shown in Tables 1 and 2, respectively. Tables 3 and 4 show the masses of the short-chain (S-C) and long-chain (L-C) LCBs, respectively. Tables 5 and 6 shows the LCBs that were identified in the SPM extracts and the FA fragment ions with which they were isobaric. These tables and schemes contain all the information needed to adequately analyze the APCI-MS and ESI-MS m.s.

The main purpose of this project was to determine the LCB/FA composition of bovine milk, chicken egg yolk and bovine brain sphingomyelin extracts by APCI-MS and ESI-MS. To our knowledge, the only other such analysis was attempted by Karlsson *et al.*¹, but poor mass-spectrometric techniques and chromatographic analyses, resulted in the incorrect identification of molecular species. Furthermore, Karlsson *et al.*'s work failed to produce values for the percent composition (mole%) of the SPLs in any of the three samples. Instead, his final compositions (Figure 30) were ambiguous, using asterisks to represent unknown and subjective quantities. Our work corrects these mistakes and provides a more thorough and accurate characterization and quantification of the SPLs in these mixtures. Because our chromatography system was different from previous work²⁻³, and to avoid making the same mistakes that Karlsson *et al.* made in describing the chromatographic characteristics of the SPLs in these samples, the retention characteristics of the SPLs in our chromatographic system will be thoroughly analyzed.

1.1 Bovine Milk

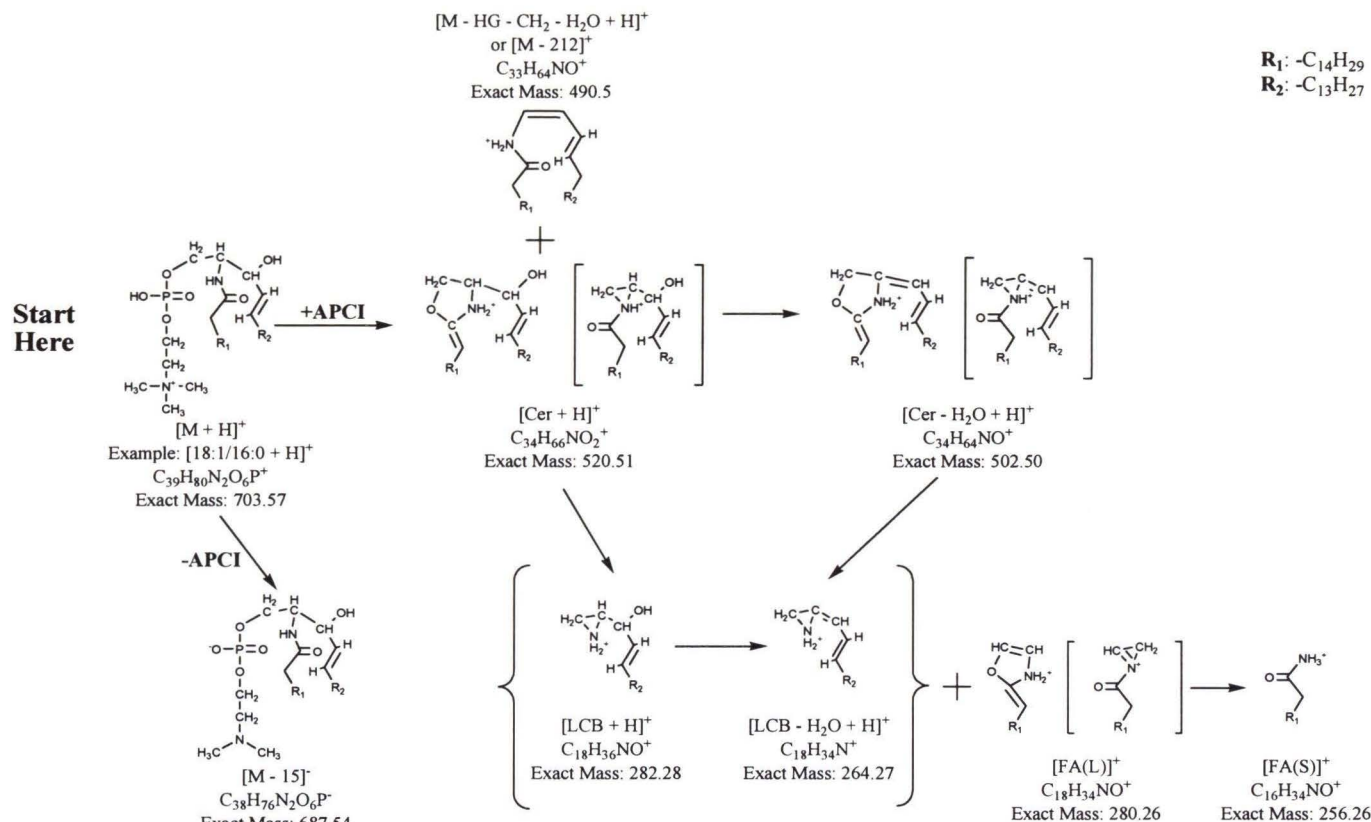
Figure 1 shows ion chromatograms and m.s. from the LC1MS2a analysis of BMS (10.58 mg/mL) with DPPC (0.50 mg/mL) added as an internal standard (IS). **1.1.A** and

1.2.A showed that SPLs from bovine milk eluted during the HPLC separation as three distinct, though not completely resolved, chromatographic peaks denoted as SPL1, SPL2 and SPL3. The average +APCI m.s. across SPL1, SPL2 and SPL3 are shown in **1.1.E**, **1.1.F** and **1.1.G**, respectively. The corresponding average +ESI m.s. across these regions are shown in **1.2.E**, **1.2.F** and **1.2.G**, respectively.

The +APCI m.s. provided more detailed information about molecular structure than +ESI m.s., and can be divided into three general mass regions that were useful for the characterization of molecular species. A low mass region from m/z 200 – 300 showed fragments of individual LCB moieties; a middle mass region from m/z 300 – 450 that contained FA acyl chain fragments; and an upper mass region from m/z 450 – 700, composed of protonated ceramide (Cer) ions and their corresponding dehydrated fragments ($[\text{Cer} - \text{H}_2\text{O} + \text{H}]^+$). The diglyceride (DG) fragment ion (represented as $[\text{DG}]^+$) from DPPC ($[\text{DPPC DG}]^+$) was also observed in the upper mass region. In the +ESI mode the base peak was the protonated molecule. The small amounts of the phosphorylcholine head group (HG) at m/z 184.2 indicated that the SPLs experienced very little fragmentation in the ESI source.

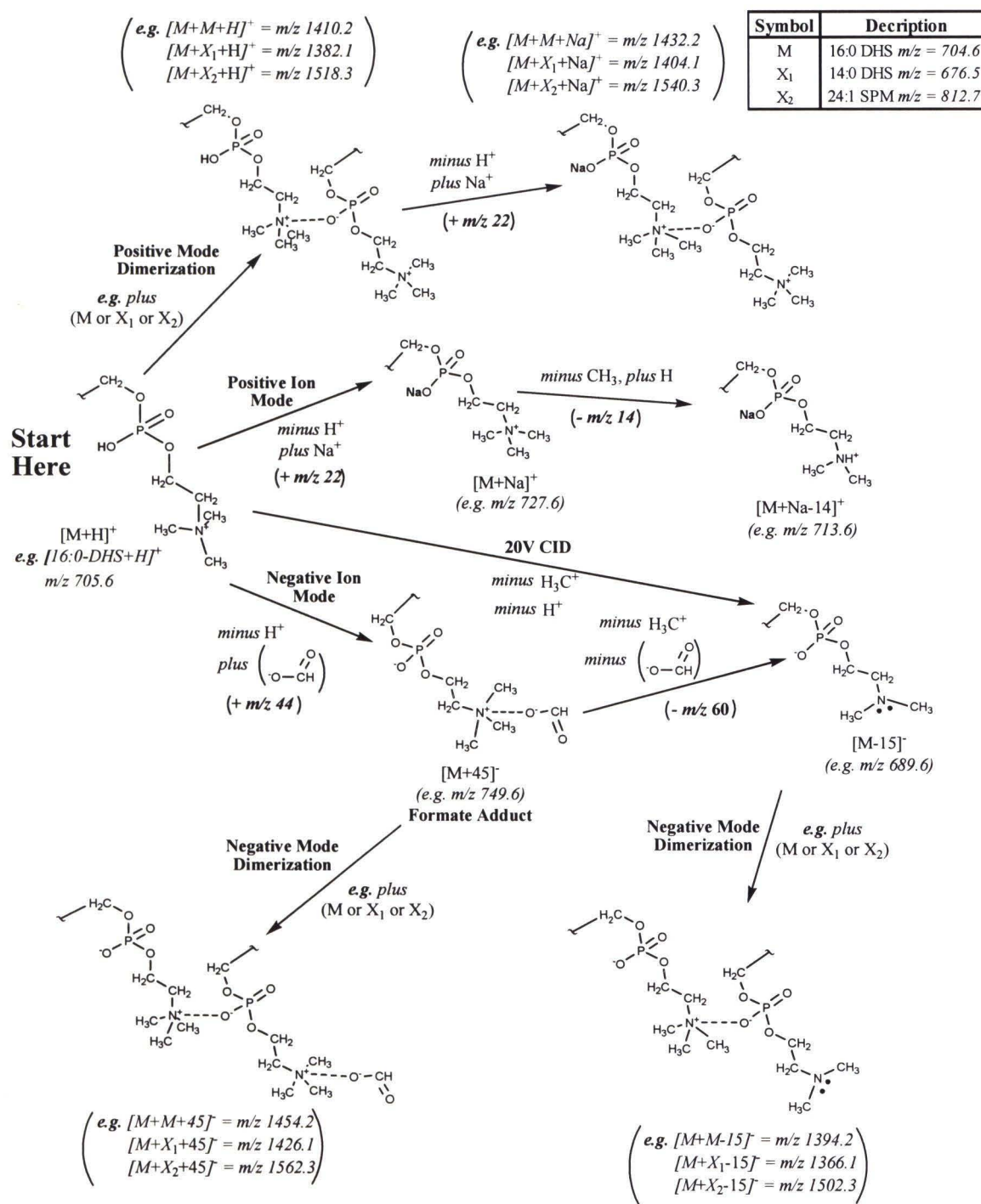
From the +ESI total ion chromatogram (TIC) (**1.2.A**), it was observed that DPPC gave more response per mg of sample under ESI conditions (when compared to the APCI data in **1.1.A**). The $[\text{DPPC DG}]^+$ ion at m/z 551.5 (**2.1.B**) and $[\text{M} + \text{H}]^+$ ion at m/z 734.5 (**2.2.B**) had retention times (RTs) of 26.35 minutes (mins) and 26.26 mins, respectively. Figure 3 shows the structure of the DPPC protonated molecule and the fragments that were produced under APCI-MS conditions.

Scheme 2: Proposed Fragment Ions Formed from Sphingolipids under APCI-MS, MS² and MS³ Conditions



Scheme 2. Proposed fragment ions produced from the sphingolipids under APCI-MS conditions. SPMs and DHSs produced similar fragments; the latter being two mass units heavier due to the absence of the double bond on the LCB backbone. All fragment ions were observed in the MS, MS² and MS³ mass spectra, except for the $[M - 212]^+$ and $[LCB + H]^+$ ions, which were not present in the MS³ m.s. The 3-membered ring structures in square brackets were proposed by Karlsson *et al.*¹, but the 5-membered ring systems are believed to be more stable configurations.

Scheme 3: Proposed Ions Formed from the Sphingolipids in ESI-MS



Scheme 3. Proposed fragment and adduct ions produced from the phosphocholine head group under ESI-MS conditions.

Table 1: Calculated masses for SPMs with an 18:1 LCB

CN:d.b.	18:1 LCB								
	+ESI		-ESI	-ESI/-APCI		+APCI			
	[M+H] ⁺	[M+Na] ⁺	[M+45] ⁻	[M-15] ⁻	[M-HG-CH ₂ -H ₂ O+H] ⁺	[Cer+H] ⁺	[Cer-H ₂ O+H] ⁺	[FA (L)] ⁺	[FA (S)] ⁺
6:0	563.4	585.4	607.4	569.4	350.3	380.4	362.3	140.1	116.1
6:1	561.4	583.4	605.4	567.4	348.3	378.3	360.3	138.1	114.1
8:0	591.5	613.4	635.4	597.4	378.4	408.4	390.4	168.1	144.1
8:1	589.4	611.4	633.4	595.4	376.4	406.4	388.4	166.1	142.1
10:0	619.5	641.5	663.5	625.4	406.4	436.4	418.4	196.2	172.2
10:1	617.5	639.4	661.5	623.4	404.4	434.4	416.4	194.2	170.2
12:0	647.5	669.5	691.5	653.5	434.4	464.4	446.4	224.2	200.2
12:1	645.5	667.5	689.5	651.4	432.4	462.4	444.4	222.2	198.2
12:2	643.5	665.5	687.5	649.4	430.4	460.4	442.4	220.2	196.2
13:0	661.5	683.5	705.5	667.5	448.5	478.5	460.5	238.2	214.2
13:1	659.5	681.5	703.5	665.5	446.4	476.4	458.4	236.2	212.2
13:2	657.5	679.5	701.5	663.4	444.4	474.4	456.4	234.2	210.2
14:0	675.5	697.5	719.5	681.5	462.5	492.5	474.5	252.2	228.2
14:1	673.5	695.5	717.5	679.5	460.5	490.5	472.5	250.2	226.2
14:2	671.5	693.5	715.5	677.5	458.4	488.4	470.4	248.2	224.2
15:0	689.6	711.5	733.5	695.5	476.5	506.5	488.5	266.2	242.2
15:1	687.5	709.5	731.5	693.5	474.5	504.5	486.5	264.2	240.2
15:2	685.5	707.5	729.5	691.5	472.5	502.5	484.5	262.2	238.2
16:0	703.6	725.6	747.6	709.5	490.5	520.5	502.5	280.3	256.3
16:1	701.6	723.5	745.5	707.5	488.5	518.5	500.5	278.2	254.2
16:2	699.5	721.5	743.5	705.5	486.5	516.5	498.5	276.2	252.2
17:0	717.6	739.6	761.6	723.5	504.5	534.5	516.5	294.3	270.3
17:1	715.6	737.6	759.6	721.5	502.5	532.5	514.5	292.3	268.3
17:2	713.6	735.5	757.5	719.5	500.5	530.5	512.5	290.2	266.2
18:0	731.6	753.6	775.6	737.6	518.5	548.5	530.5	308.3	284.3
18:1	729.6	751.6	773.6	735.5	516.5	546.5	528.5	306.3	282.3
18:2	727.6	749.6	771.6	733.5	514.5	544.5	526.5	304.3	280.3
19:0	745.6	767.6	789.6	751.6	532.5	562.6	544.5	322.3	298.3
19:1	743.6	765.6	787.6	749.6	530.5	560.5	542.5	320.3	296.3
19:2	741.6	763.6	785.6	747.5	528.5	558.5	540.5	318.3	294.3
20:0	759.6	781.6	803.6	765.6	546.6	576.6	558.6	336.3	312.3
20:1	757.6	779.6	801.6	763.6	544.5	574.6	556.5	334.3	310.3
20:2	755.6	777.6	799.6	761.6	542.5	572.5	554.5	332.3	308.3
21:0	773.7	795.6	817.6	779.6	560.6	590.6	572.6	350.3	326.3
21:1	771.6	793.6	815.6	777.6	558.6	588.6	570.6	348.3	324.3
21:2	769.6	791.6	813.6	775.6	556.5	586.6	568.5	346.3	322.3
22:0	787.7	809.7	831.7	793.6	574.6	604.6	586.6	364.4	340.4
22:1	785.7	807.6	829.6	791.6	572.6	602.6	584.6	362.3	338.3
22:2	783.6	805.6	827.6	789.6	570.6	600.6	582.6	360.3	336.3
23:0	801.7	823.7	845.7	807.6	588.6	618.6	600.6	378.4	354.4
23:1	799.7	821.7	843.7	805.6	586.6	616.6	598.6	376.4	352.4
23:2	797.7	819.6	841.6	803.6	584.6	614.6	596.6	374.3	350.3
24:0	815.7	837.7	859.7	821.7	602.6	632.6	614.6	392.4	368.4
24:1	813.7	835.7	857.7	819.6	600.6	630.6	612.6	390.4	366.4
24:2	811.7	833.7	855.7	817.6	598.6	628.6	610.6	388.4	364.4
25:0	829.7	851.7	873.7	835.7	616.6	646.7	628.6	406.4	382.4
25:1	827.7	849.7	871.7	833.7	614.6	644.6	626.6	404.4	380.4
25:2	825.7	847.7	869.7	831.6	612.6	642.6	624.6	402.4	378.4
26:0	843.7	865.7	887.7	849.7	630.7	660.7	642.7	420.4	396.4
26:1	841.7	863.7	885.7	847.7	628.6	658.7	640.6	418.4	394.4
26:2	839.7	861.7	883.7	845.7	626.6	656.6	638.6	416.4	392.4

Abbreviations: CN:d.b., Number of carbon atoms: Number of double bonds, on the fatty acid (FA) chain; [M + H]⁺, protonated molecule; [M + Na]⁺, sodium adduct ion; [M + 45]⁻, ammonium adduct ion; [M – 15]⁻, demethylated fragment ion; [M – HG – CH₂ – H₂O + H]⁺, ion formed from the loss of the phosphocholine head group (HG), a molecule of water and a methylene group and then addition of a proton; [Cer + H]⁺, protonated ceramide ion; [Cer – H₂O + H]⁺, dehydrated, protonated ceramide ion; [FA(L)]⁺ and [FA(S)]⁺, FA ‘long’ and FA ‘short’ fragment ions, respectively.

Table 2: Calculated masses for DHSs with an 18:0 LCB

CN:d.b.	18:0 LCB								
	+ESI		-ESI	-ESI/-APCI	+APCI				
	[M+H] ⁺	[M+Na] ⁺	[M+45] ⁺	[M-15] ⁻	[M-HG-CH ₂ -H ₂ O+H] ⁺	[Cer+H] ⁺	[Cer-H ₂ O+H] ⁺	[FA (L)] ⁺	[FA (S)] ⁺
6:0	565.4	587.4	609.4	571.4	352.4	382.4	364.4	140.1	116.1
6:1	563.4	585.4	607.4	569.4	350.3	380.4	362.3	138.1	114.1
8:0	593.5	615.4	637.5	599.4	380.4	410.4	392.4	168.1	144.1
8:1	591.5	613.4	635.4	597.4	378.4	408.4	390.4	166.1	142.1
10:0	621.5	643.5	665.5	627.4	408.4	438.4	420.4	196.2	172.2
10:1	619.5	641.5	663.5	625.4	406.4	436.4	418.4	194.2	170.2
12:0	649.5	671.5	693.5	655.5	436.5	466.5	448.5	224.2	200.2
12:1	647.5	669.5	691.5	653.5	434.4	464.4	446.4	222.2	198.2
12:2	645.5	667.5	689.5	651.4	432.4	462.4	444.4	220.2	196.2
13:0	663.5	685.5	707.5	669.5	450.5	480.5	462.5	238.2	214.2
13:1	661.5	683.5	705.5	667.5	448.5	478.5	460.5	236.2	212.2
13:2	659.5	681.5	703.5	665.5	446.4	476.4	458.4	234.2	210.2
14:0	677.6	699.5	721.5	683.5	464.5	494.5	476.5	252.2	228.2
14:1	675.5	697.5	719.5	681.5	462.5	492.5	474.5	250.2	226.2
14:2	673.5	695.5	717.5	679.5	460.5	490.5	472.5	248.2	224.2
15:0	691.6	713.6	735.6	697.5	478.5	508.5	490.5	266.2	242.2
15:1	689.6	711.5	733.5	695.5	476.5	506.5	488.5	264.2	240.2
15:2	687.5	709.5	731.5	693.5	474.5	504.5	486.5	262.2	238.2
16:0	705.6	727.6	749.6	711.5	492.5	522.5	504.5	280.3	256.3
16:1	703.6	725.6	747.6	709.5	490.5	520.5	502.5	278.2	254.2
16:2	701.6	723.5	745.5	707.5	488.5	518.5	500.5	276.2	252.2
17:0	719.6	741.6	763.6	725.6	506.5	536.5	518.5	294.3	270.3
17:1	717.6	739.6	761.6	723.5	504.5	534.5	516.5	292.3	268.3
17:2	715.6	737.6	759.6	721.5	502.5	532.5	514.5	290.2	266.2
18:0	733.6	755.6	777.6	739.6	520.5	550.6	532.5	308.3	284.3
18:1	731.6	753.6	775.6	737.6	518.5	548.5	530.5	306.3	282.3
18:2	729.6	751.6	773.6	735.5	516.5	546.5	528.5	304.3	280.3
19:0	747.6	769.6	791.6	753.6	534.6	564.6	546.6	322.3	298.3
19:1	745.6	767.6	789.6	751.6	532.5	562.6	544.5	320.3	296.3
19:2	743.6	765.6	787.6	749.6	530.5	560.5	542.5	318.3	294.3
20:0	761.7	783.6	805.6	767.6	548.6	578.6	560.6	336.3	312.3
20:1	759.6	781.6	803.6	765.6	546.6	576.6	558.6	334.3	310.3
20:2	757.6	779.6	801.6	763.6	544.5	574.6	556.5	332.3	308.3
21:0	775.7	797.7	819.7	781.6	562.6	592.6	574.6	350.3	326.3
21:1	773.7	795.6	817.6	779.6	560.6	590.6	572.6	348.3	324.3
21:2	771.6	793.6	815.6	777.6	558.6	588.6	570.6	346.3	322.3
22:0	789.7	811.7	833.7	795.6	576.6	606.6	588.6	364.4	340.4
22:1	787.7	809.7	831.7	793.6	574.6	604.6	586.6	362.3	338.3
22:2	785.7	807.6	829.6	791.6	572.6	602.6	584.6	360.3	336.3
23:0	803.7	825.7	847.7	809.7	590.6	620.6	602.6	378.4	354.4
23:1	801.7	823.7	845.7	807.6	588.6	618.6	600.6	376.4	352.4
23:2	799.7	821.7	843.7	805.6	586.6	616.6	598.6	374.3	350.3
24:0	817.7	839.7	861.7	823.7	604.6	634.7	616.6	392.4	368.4
24:1	815.7	837.7	859.7	821.7	602.6	632.6	614.6	390.4	366.4
24:2	813.7	835.7	857.7	819.6	600.6	630.6	612.6	388.4	364.4
25:0	831.7	853.7	875.7	837.7	618.7	648.7	630.7	406.4	382.4
25:1	829.7	851.7	873.7	835.7	616.6	646.7	628.6	404.4	380.4
25:2	827.7	849.7	871.7	833.7	614.6	644.6	626.6	402.4	378.4
26:0	845.7	867.7	889.7	851.7	632.7	662.7	644.7	420.4	396.4
26:1	843.7	865.7	887.7	849.7	630.7	660.7	642.7	418.4	394.4
26:2	841.7	863.7	885.7	847.7	628.6	658.7	640.6	416.4	392.4

Abbreviations: CN:d.b., Number of carbon atoms: Number of double bonds, on the fatty acid (FA) chain; [M + H]⁺, protonated molecule; [M + Na]⁺, sodium adduct ion; [M + 45]⁺, ammonium adduct ion; [M - 15]⁻, demethylated fragment ion; [M - HG - CH₂ - H₂O + 2H]⁺, ion formed from the loss of the phosphocholine head group (HG), a molecule of water and a methylene group and then addition of a proton; [Cer + H]⁺, protonated ceramide ion; [Cer - H₂O + H]⁺, dehydrated, protonated ceramide ion; [FA(L)]⁺ and [FA(S)]⁺, FA ‘long’ and FA ‘short’ fragment ions, respectively.

Masses of the Long Chain Base (LCB) Fragment Ions under APCI MS Conditions

Table 3: Short Chain (S-C) LCBs

CN:d.b.	[LCB + H] ⁺	[LCB + H - H ₂ O] ⁺
13:0	214.2	196.2
13:1	212.2	194.2
13:2	210.2	192.2
14:0	228.2	210.2
14:1	226.2	208.2
14:2	224.2	206.2
15:0	242.2	224.2
15:1	240.2	222.2
15:2	238.2	220.2
16:0	256.3	238.3
16:1	254.2	236.2
16:2	252.2	234.2
17:0	270.3	252.3
17:1	268.3	250.3
17:2	266.2	248.2
18:0	284.3	266.3
18:1	282.3	264.3
18:2	280.3	262.3
19:0	298.3	280.3
19:1	296.3	278.3
19:2	294.3	276.3

Table 4: Long Chain (L-C) LCBs

CN:d.b.	[LCB + H] ⁺	[LCB + H - H ₂ O] ⁺
20:0	312.3	294.3
20:1	310.3	292.3
20:2	308.3	290.3
21:0	326.3	308.3
21:1	324.3	306.3
21:2	322.3	304.3
22:0	340.4	322.3
22:1	338.3	320.3
22:2	336.3	318.3
23:0	354.4	336.4
23:1	352.4	334.3
23:2	350.3	332.3
24:0	368.4	350.4
24:1	366.4	348.4
24:2	364.4	346.3
25:0	382.4	364.4
25:1	380.4	362.4
25:2	378.4	360.4
26:0	396.4	378.4
26:1	394.4	376.4
26:2	392.4	374.4

Abbreviations: CN:d.b., Number of carbon atoms : Number of double bonds, on the LCB backbone; [LCB + H]⁺, protonated LCB fragment ion; [LCB – H₂O + H]⁺, dehydrated, protonated LCB fragment ion.

Table 5: Isobaric SPM-LCB and FA fragment ions in APCI-MS

LCB	[LCB + H] ⁺	Isobaric with....		[LCB - H ₂ O + H] ⁺	Isobaric with....	
		[FA(S)] ⁺	[FA(L)] ⁺		[FA(S)] ⁺	[FA(L)] ⁺
14:1	226.2	14:1	-	208.2	13:3	11:1
15:1	240.2	15:1	-	222.2	14:3	12:1
16:1	254.2	16:1	-	236.2	15:3	13:1
17:1	268.2	17:1	-	250.2	16:3	14:1
18:1	282.2	18:1	-	264.2	17:3	15:1
19:1	296.3	19:1	-	278.3	18:3	16:1
20:1	310.3	20:1	-	292.3	19:3	17:1

Description: Table 5 shows the unsaturated LCB (SPMs) fragment ions that were identified in the SPM extracts, and the FA fragment ions with which they were isobaric. This information was important for the analysis of the MS² and MS³ +APCI mass spectra.

Table 6: Isobaric DHS-LCB and FA fragment ions in APCI-MS

LCB	[LCB+H] ⁺	Isobaric with....		[LCB-H ₂ O+H] ⁺	Isobaric with....	
		[FA(S)] ⁺	[FA(L)] ⁺		[FA(S)] ⁺	[FA(L)] ⁺
12:0	200.2	12:0	-	182.2	11:2	9:0
13:0	214.2	13:0	-	196.2	12:2	10:0
14:0	228.2	14:0	-	210.2	13:2	11:0
15:0	242.2	15:0	-	224.2	14:2	12:0
16:0	256.2	16:0	-	238.2	15:2	13:0
17:0	270.2	17:0	-	252.2	16:2	14:0
18:0	284.2	18:0	-	266.2	17:2	15:0
19:0	298.3	19:0	-	280.3	18:2	16:0
20:0	312.3	20:0	-	294.3	19:2	17:0

Description: Table 6 shows the saturated LCB (DHSs) fragment ions that were identified and the FA fragment ions with which they were isobaric. This information was important for the analysis of the MS² and MS³ +APCI mass spectra.

LC1MS2a Analysis of Bovine Milk Sphingomyelin

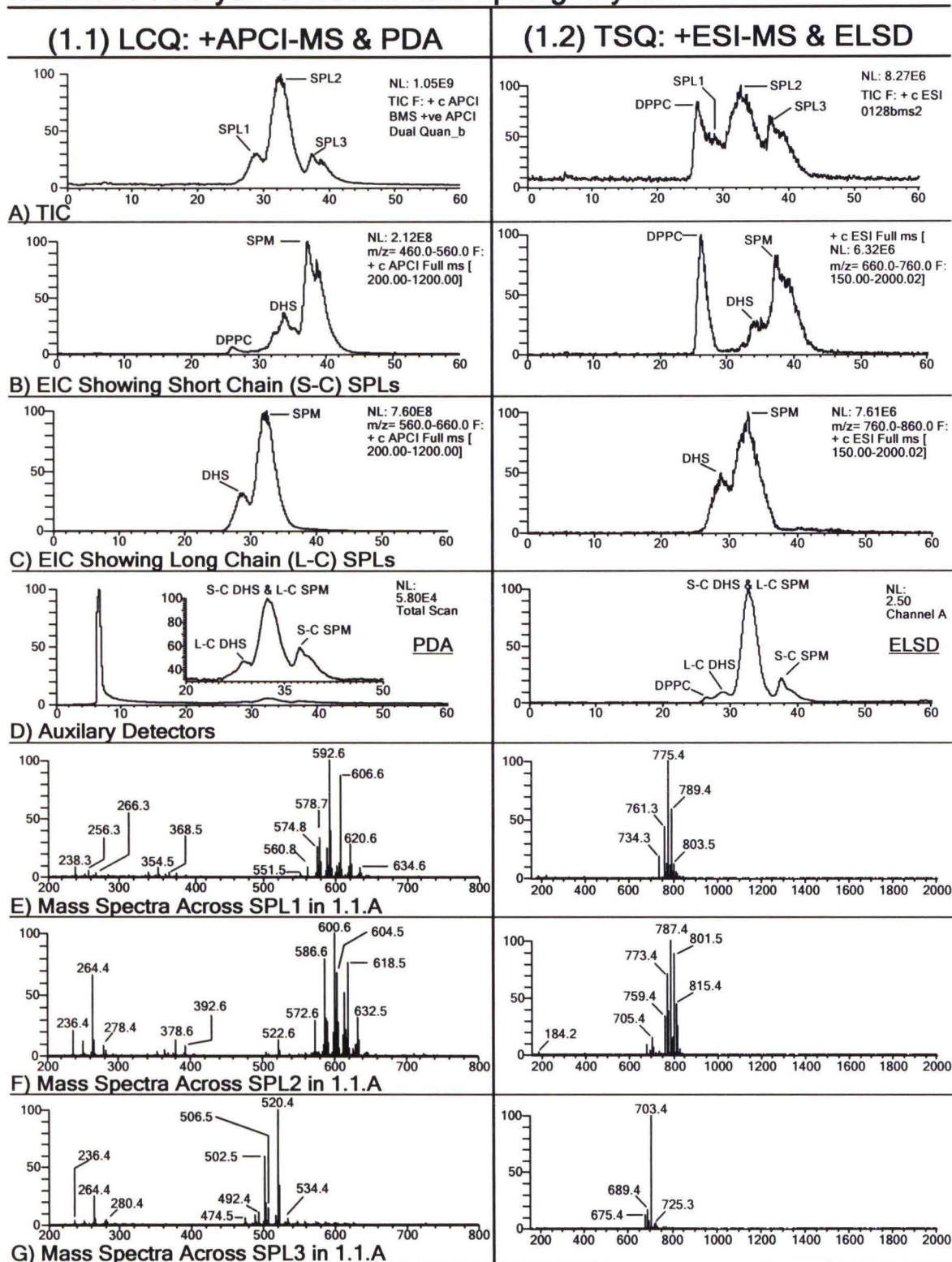


Figure 1. LC1MS2a analysis of BMS. APCI-MS and UV data obtained on the LCQ (column 1.1), and ESI-MS plus ELSD data obtained on the TSQ (column 1.2).

The average +APCI and +ESI m.s. across these regions (**2.1.C** and **2.2.C** respectively), showed that DPPC occurred partially overlapped with SPLs that had primarily 16:0 (m/z 238.3) and 18:0 (m/z 266.4) LCBs with short-chain (S-C) FAs. This was in agreement with previous results, which showed that the first saturated SPL eluted just after the PCs.² The base peak in **2.1.C** had a m/z of 606.6 which corresponded to 22:0 DHS, as shown in Table 2. The DPPC DG ion was also observed in **2.1.C** along with its $[\text{DPPC} + \text{H}]^+$, and $[\text{DPPC} + \text{Na}]^+$ (at m/z 756.4) and $[\text{16:0 FA} + 58]^+$ (at m/z 313.4) ions. The $[\text{16:0 FA} + 58]^+$ ion resulted from single 16:0 FA acyl chains attached to the PL backbone.⁵⁴ The DPPC protonated molecule, sodium adduct ion, and dimer ion (m/z 1467.8), were observed in +ESI mode (**2.2.C**). In contrast to the APCI-MS data, the base peak in the ESI-MS spectra was the $[\text{DPPC} + \text{H}]^+$, which was significantly more abundant than $[\text{22:0 DHS} + \text{H}]^+$ at m/z 789.5. This indicated that the two PL classes (SPLs and PCs) had different responses under APCI and ESI conditions, which affected the use of DPPC as an IS.

The averaged APCI m.s. across SPL1 (**1.1.E**), SPL2 (**1.1.F**) and SPL3 (**1.1.G**) showed a progression from saturated LCB fragment ions such as 16:0 and 18:0 in SPL1, to unsaturated LCBs such as 16:1 (m/z 236.4) and 18:1 (m/z 264.4) in SPL3, with SPL2 containing a mixture primarily composed of 16:1 18:1, 18:0, and 19:1 (m/z 278.4) LCBs. Figures **1.1.E** and **1.2.E** showed that the predominant molecular species had a primary fragment with a m/z of 592.6, and a $[\text{M} + \text{H}]^+$ ion at m/z 775.4, respectively. From Table 2, it may be seen that these masses corresponded to 21:0 DHS. Because SPLs experienced mild fragmentation in the APCI source, the full-scan APCI m.s. contained $[\text{Cer} - \text{H}_2\text{O} + \text{H}]^+$, $[\text{FA(L)}]^+$ (FA ‘long’), and $[\text{FA(S)}]^+$ (FA ‘short’) fragment ions (see

Scheme 1 for the structures of these ions), in addition to the $[\text{Cer} + \text{H}]^+$ ions. As a result of this complexity, extra caution was required when analyzing full-scan APCI spectra, to avoid the inaccurate identification of molecular species. For example, the peak at m/z 574.8 could represent 20:2 DHS or 20:1 SPM, but the absence of an abundant $[\text{M} + \text{H}]^+$ ion peak at m/z 757.6 in the corresponding ESI-MS m.s. indicated that these molecular species probably were not present. In addition, the early RT and fragmentation pattern in the MS^2 and MS^3 m.s (data not shown) indicated that the ion at m/z 574.8 was the

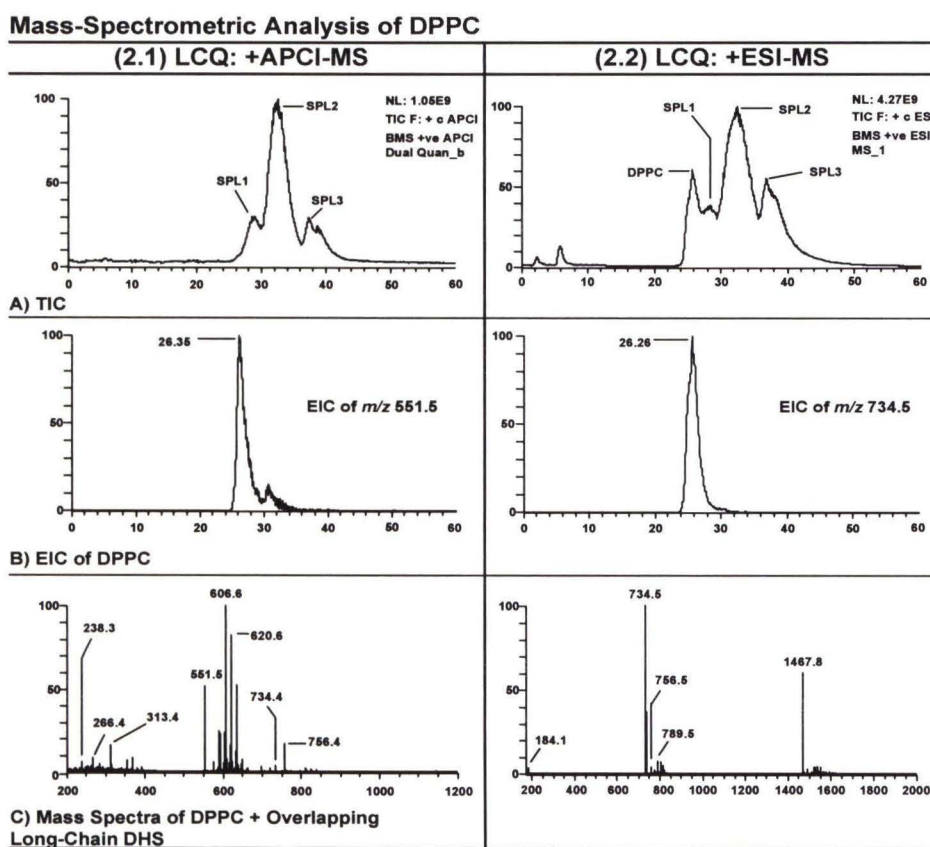


Figure 2. Mass spectrometric analysis of DPPC. A) Total ion +APCI (column 2.1) and +ESI (column 2.2) chromatograms for BMS acquired on the LCQ. B) Extracted ion chromatograms of the DPPC diglyceride ion (2.1.B) and protonated molecule (2.2.B). C) APCI (2.1.C) and ESI (2.2.C) mass spectra across the corresponding DPPC peaks shown in 2.1.B and 2.1.C, respectively. These LC1MS2 runs were acquired sequentially. The LC configuration used in column 2.1 was LC1MS2a (Figure 2). The LC configuration used in column 2.2 was LC1MS2c (Figure 4).

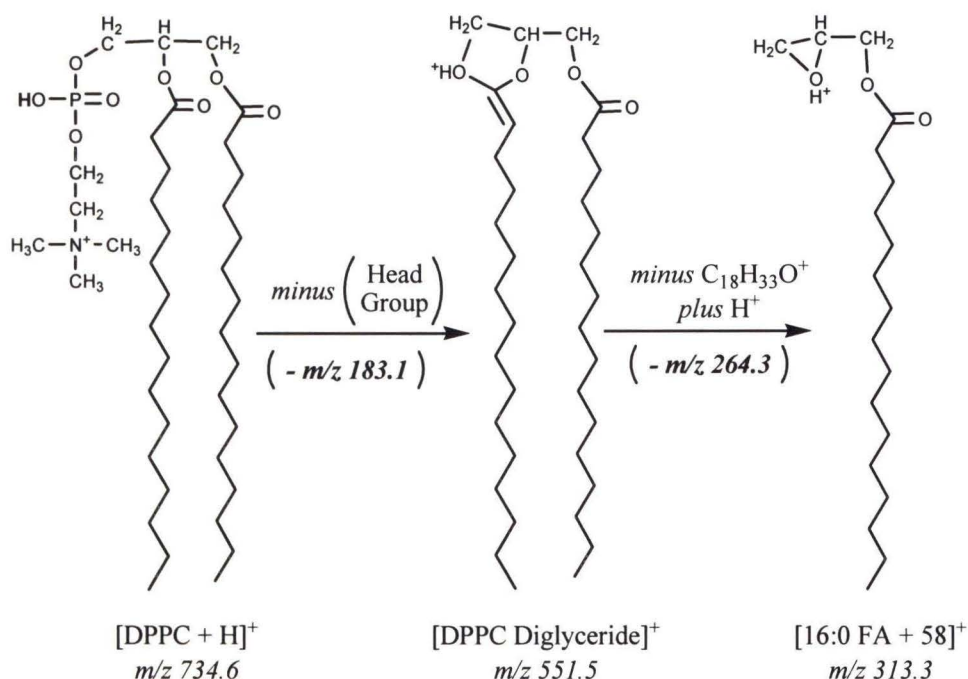


Figure 3. Proposed molecules and fragment ions formed from DPPC under APCI-MS conditions.

dehydrated, protonated ceramide fragment (this fragment will be referred to as the “dehydrated ceramide fragment ion” from this point forward for simplicity) from $[21:0 \text{ DHS Cer} + \text{H}]^+$ (Table 1). Similarly, the peak at m/z 560.8 could be mistakenly identified as 19:2 DHS or 19:1 SPM, but again the ESI m.s. did not show a corresponding peak at m/z 743.6 for the protonated molecule, thereby indicating that neither of these molecular species were present. From the APCI MS² and MS³ m.s. (data not shown), this mass was found to be the $[20:0 \text{ DHS Cer} - \text{H}_2\text{O} + \text{H}]^+$ fragment ion.

The ions at m/z 620.6, 606.6 and 578.7 in the APCI-MS m.s. of SPL1 had corresponding protonated molecules at m/z 803.5, 789.4 and 761.3 in the ESI m.s., respectively. From Table 2 it was seen that these ions represented 23:0 DHS, 22:0 DHS and 20:0 DHS, respectively. The +APCI extracted ion chromatograms (EICs) for these

masses (Figure 4) showed that the SPLs within SPL1 eluted based on the length of the FA chain. SPLs with longer FAs eluted earlier than those with shorter FA chains, resulting in a progressive increase in RT from 23:0 DHS at 27.52 mins. in **4(A)**, to 20:0 DHS at 29.39 mins. in **4(D)**. Therefore, the elution pattern in our chromatographic system was in agreement with previous findings.²⁻³ If the ion at m/z 574.8 was the $[\text{Cer} + \text{H}]^+$ ion of 20:2 DHS or 20:1 SPM, and with the expectation that more non-polar molecules (longer FA) should elute before shorter chains on a NP column, then its RT would be later when compared to 20:0 DHS due to their higher degree of polarity from increased unsaturation. Figure **4(E)** clearly shows however, that this ion eluted earlier than 20:0 DHS and had a RT and chromatographic profile that was similar to 21:0 DHS in **4(C)**. This observation supported the previous conclusion that 574.8 was $[21:0 \text{ DHS Cer} - \text{H}_2\text{O} + \text{H}]^+$, which was generated from $[21:0 \text{ DHS Cer} + \text{H}]^+$ in the ion source. Similarly, Figure **4(F)** confirmed the identity of the ion at m/z 560.8 as the $[20:0 \text{ DHS Cer} - \text{H}_2\text{O} + \text{H}]^+$ fragment ion.

The mass overlap of $[21:0 \text{ DHS Cer} - \text{H}_2\text{O} + \text{H}]^+$ with $[20:2 \text{ DHS Cer} + \text{H}]^+$ had a significant impact on the quantification of these molecules. This will be explained in detail in the “Quantification” section below. In addition, all the other fragment ions shown in Scheme 2 were present in the APCI-MS full-scan m.s. It was important to be aware of this complexity and isobaric ions, in order to accurately identify and quantify the SPLs by APCI-MS.

The ion at m/z 592.6 was initially identified as having a LCB/FA combination of 18:0/21:0 from Table 1. But this molecule was isobaric with 16:0/23:0, 17:0/22:0, 19:0/20:0 etc. The only way to distinguish between them was to identify specific FA and

LCB fragment ions, and to correlate these with the corresponding $[\text{Cer} + \text{H}]^+$ ions. In the middle mass region of **1.1.E**, there were FA moieties at m/z 354.5 and m/z 368.4. As will be demonstrated later, X:0/Y:0 SPLs produced $[\text{FA}(\text{S})]^+$ fragments in higher abundance than the $[\text{FA}(\text{L})]^+$ fragments under APCI-MS conditions. So, if 354.5 was $[\text{23:0 FA}(\text{S})]^+$ (Table 1) and if we assume that it originated from 592.6 (since it was the most abundant FA ion in the middle mass region), then it could be deduced that this SPL had a 16:0 LCB.

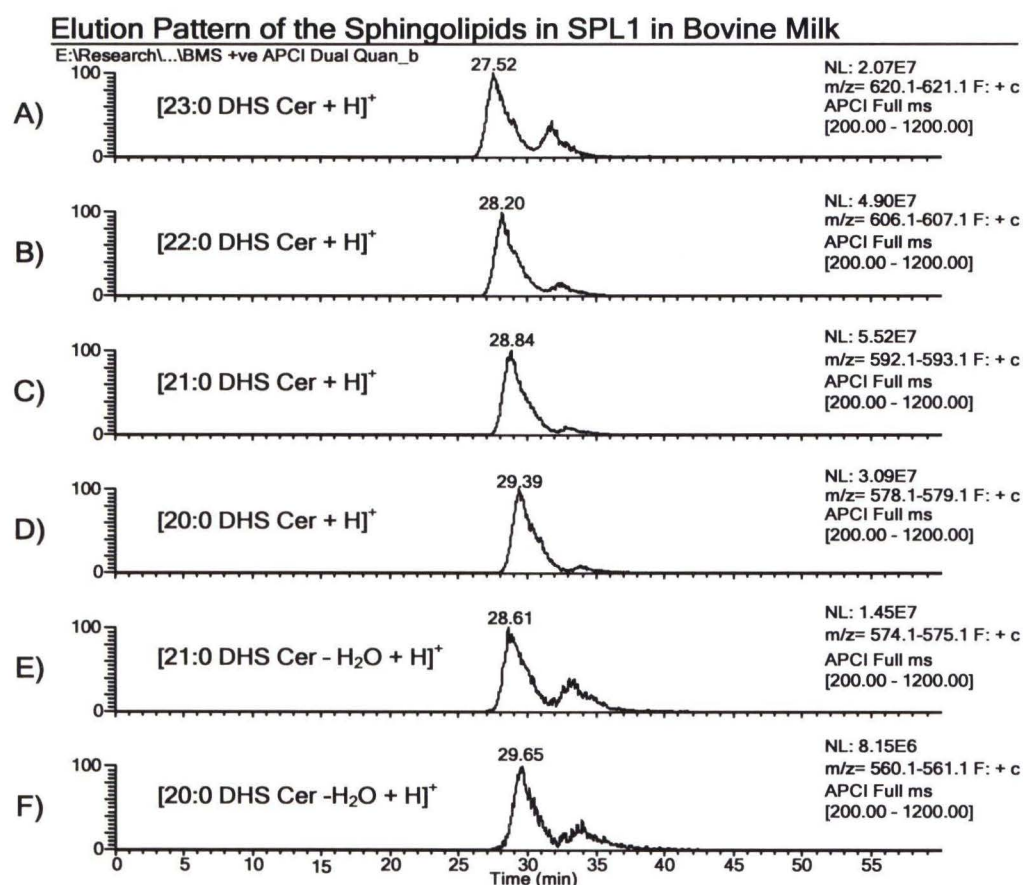


Figure 4. APCI-MS extracted ion chromatograms (EICs) of the protonated ceramide ions of A) 23:0 DHS, B) 22:0 DHS, C) 21:0 DHS and D) 20:0 DHS. E) EIC showing that the ion at m/z 574.6 was the dehydrated ceramide fragment ion from 21:0 DHS. Similarly, F) showed that the ion at m/z 560.6 was $[\text{20:0 DHS Cer} - \text{H}_2\text{O} + \text{H}]^+$.

So the ion at m/z 592.6 could represent 16:0/23:0. The problem arises however, when it was realized that the $[23:0 \text{ FA(S)}]^+$ could also originate from 18:0/23:0 at m/z 620.6. Similarly, the $[24:0 \text{ FA(S)}]^+$ (m/z 368.5) could originate from either 18:0/24:0 at m/z 634.6, 16:0/24:0 at m/z 606.6, or both. So, as the diversity of the LCBs increased so did the number of $[\text{Cer} + \text{H}]^+$ ions from which a particular FA fragment could originate. This meant that it was not possible to unambiguously determine the LCB/FA composition of BMS, CES and BBS, from only the full-scan APCI or ESI m.s.

So, the full-scan ESI and APCI mass spectra were used to determine the groups of SPLs that were present, but additional information was required to identify isobaric species within the group. For example, in SPL1 we saw that 21:0 DHS was present because the $[\text{Cer} + \text{H}]^+$ and $[\text{M} + \text{H}]^+$ ions were observed. But '21:0 DHS' was a group of isobaric SPLs that had saturated LCBs and FAs of varying carbon length. A variety of mass spectrometric techniques have been developed to determine the LCB/FA composition of various SPL mixtures such as, 1) HPLC followed by tandem PSP-MS^{4,5,9}, TSP-MS¹⁰, and API-MS¹, and 2) the mass-spectrometric analysis of trimethylsilyl derivatives⁶ (analyzed by GC-MS) and dinitrophenyl derivatives^{7,8} (analyzed by GC-MS) of the LCB residues. Unfortunately, the API-MS experiments performed by Karlsson *et al.* were poorly designed, resulting in mass spectra that were difficult to interpret. As a result, many of his conclusions were incorrect.

1.1.E and **1.2.E** showed that SPL1 was composed of long-chain (L-C) DHSs that had FA chains ≥ 20 carbon atoms in length. The percent composition of the SPLs within SPL1 is shown in Table 7. The composition by APCI-MS was based on integrating the areas under EICs for the $[\text{Cer} + \text{H}]^+$ and $[\text{Cer} - \text{H}_2\text{O} + \text{H}]^+$ ions, while the composition by

ESI-MS was based on integrating the areas under the EICs for the $[M + H]^+$ ions. The specific methods used to quantify the SPLs are described in the ‘Quantification’ section on page 113. The composition determined by APCI-MS and ESI-MS were in fairly close agreement, indicating that 21:0 DHS was the most abundant at 28.2% (APCI) and 27.3% (ESI). The largest variation between the two methods was observed for 20:0 DHS, which had a mole percent of 15.7% by APCI and 19.5% by ESI, for a difference of 3.8%. From this point forward, the percentages by APCI and ESI will be written as APCI% (ESI%) for simplicity.

Table 7 also shows the SPL molecules that comprise the different DHS groups. For example, the ‘21:0 DHS’ group was composed of the 16:0/23:0, 17:0/22:0 and 18:0/21:0 SPLs, of which 16:0/23:0 was the most abundant accounting for 27.1% (26.3%) of all the SPLs in SPL1. From the LCB/FA composition we see that the most abundant saturated LCB in SPL1 was 16:0 at 59.3% (62.0%) (Table 8). Because 1) the mass spectrometer was programmed to select the 3 most abundant ions (or the 3 most abundant ions from a parent mass list depending on the type of experiment) in the previous full-scan m.s., and 2) 24:1 DHS eluted with other SPLs that always occupied the first three positions in the MS^n queue due to their higher abundance (in comparison to 24:1 DHS), the mass spectrometer never selected 24:1 DHS for MS^n analyses. As a result, the components of this SPL group were not determined. MS^n data for 24:1 DHS could be obtained by programming the mass spectrometer to specifically isolate and fragment this SPL group. However, it would be impractical to perform an entire experiment that was one and a half hours long, to obtain MS^n data for a SPL group that was not one of the most abundant species in BMS. All DHSs and SPMs that were not

resolved (i.e. separated into their constituent molecules) such as 24:1 DHS, were assumed to be composed of only the SPL with an 18:0 or 18:1 LCB, respectively. These LCBs were chosen as the default because they were the most consistently-occurring in all three samples. So the unresolved 24:1 DHS area was assumed to be composed only of 18:0/24:1. All unresolved species were labeled with a '*'.

1.1.F shows an average APCI m.s over the width of SPL2. The major component had a primary fragment with a m/z 600.6. The +ESI m.s. had a base peak at m/z 787.4. From Tables 1 and 2, it was seen that these masses did not correspond to the same SPL. *Mass-to-charge* 787.7 could be either 22:0 SPM or 22:1 DHS while m/z 600.6 could be either 22:1 SPM or 22:2 DHS. The DHS possibilities can be eliminated however, since we already know that L-C DHSs eluted in SPL1. So, m/z 787.4 was most likely 22:0 SPM which had a corresponding $[\text{Cer} + \text{H}]^+$ ion at m/z 604.6, which was observed. The APCI-MS EICs (Figure 5) of the abundant masses in **1.1.F**, showed a similar chromatographic behavior to that described for the DHS species in SPL1. The RTs increased as the length of the FA chain decreased. Also, the early RTs of the ions at m/z 600.6 and m/z 586.6 allowed us to conclude that they were the dehydrated ceramide fragment ions of 23:0 SPM and 22:0 SPM, respectively.

Table 7: Composition of the L-C DHSs (mole%) in the SPL1 Peak of Bovine Milk

DHS	mole% of SPL1		LCB/FA	mole% of SPL1	
	APCI	ESI		APCI	ESI
20:0	15.7	19.5	16:0/22:0	15.5	19.3
			18:0/20:0	0.2	0.2
20:1	1.1	0.5	18:0/20:1*	1.1	0.5
21:0	28.2	27.3	16:0/23:0	27.1	26.3
			17:0/22:0	0.9	0.9
			18:0/21:0	0.2	0.2
21:1	4.1	4.0	18:0/21:1*	4.1	4.0
22:0	23.9	23.6	16:0/24:0	16.7	16.4
			17:0/23:0	2.4	2.4
			18:0/22:0	4.9	4.8
22:1	4.9	3.3	18:1/22:1*	4.9	3.3
23:0	11.0	10.6	17:0/24:0	1.5	1.4
			18:0/23:0	9.5	9.1
23:1	2.8	3.1	18:0/23:1*	2.8	3.1
24:0	5.2	5.0	18:0/24:0	4.9	4.6
			19:0/23:0	0.4	0.4
24:1	1.6	1.4	18:0/24:1*	1.6	1.4
25:0	0.8	0.8	18:0/25:0	0.2	0.3
			19:0/24:0	0.2	0.3
			20:0/23:0	0.3	0.3
25:1	0.4	0.6	18:0/25:1*	0.4	0.6
26:0	0.2	0.2	18:0/26:0	0.1	0.1
			20:0/24:0	0.2	0.1

Table 7: Composition of the long-chain DHSs in SPL1 of bovine milk. The LCB/FA composition of each SPL group is also shown. All unresolved sphingolipid groups are labeled with an asterisk. These species were assumed to be composed of the 18:0 LCB, since it was the most consistently-occurring saturated LCB in all three samples.

Table 8: Composition of the Saturated LCBs (mole%) in SPL1 of Bovine Milk

LCB	APCI (mole%)	ESI (mole%)
16:0	59.3	62.0
17:0	4.9	4.7
18:0	34.8	32.1
19:0	0.6	0.6
20:0	0.5	0.4

Table 8: Composition of the saturated LCBs in the SPL1 peak of bovine milk.

In the middle mass region of the APCI-MS m.s. in Figure 1.1.F, we see fragment ions at m/z 392.6 and m/z 378.6. As will be shown later, SPMs fragment under APCI-MS conditions to yield more abundant $[FA(L)]^+$ than $[FA(S)]^+$ fragment ions. These ions were identified as $[24:0(L)]^+$ and $[23:0(L)]^+$ respectively. The low mass region was composed predominantly of unsaturated LCBs. A small amount of the 18:0 LCB was also observed and the presence of m/z 522.6 in 1.1.F and m/z 705.4 in the ESI-MS m.s. (1.2.F), confirmed the presence of 16:0 DHS. So, SPL2 was composed 1) SPMs with FA chains ≥ 20 carbons in length (L-C SPMs) and 2) DHSs with FA chains with < 20 carbons in length. The latter group was designated short-chain DHSs.

The composition of the SPLs in SPL2 is shown in Tables 9 to 12. Unlike SPL1, the most abundant saturated LCB was 18:0, accounting for 45.4% (40.6%) of the DHSs in SPL2. The most abundant unsaturated LCB was 18:1, which accounted for 56.8% (47.7%) of the SPMs in SPL2. 16:0 DHS was the most abundant DHS and was composed of 16:0/18:0 (4.9% (4.2%)) and 18:0/16:0 (36.3% (31.5%)). 23:0 SPM was the most abundant SPM in SPL2 and was composed of 16:1/25:0 (0.2% (0.2%)), 17:1/24:0 (3.0%

(2.4%)), 18:1/23:0 (20.7% (16.9%)) and 19:0/22:0 (0.4% (0.3%)). So, the LCBs with 16 and 18 carbon atoms were the most abundant in SPL2.

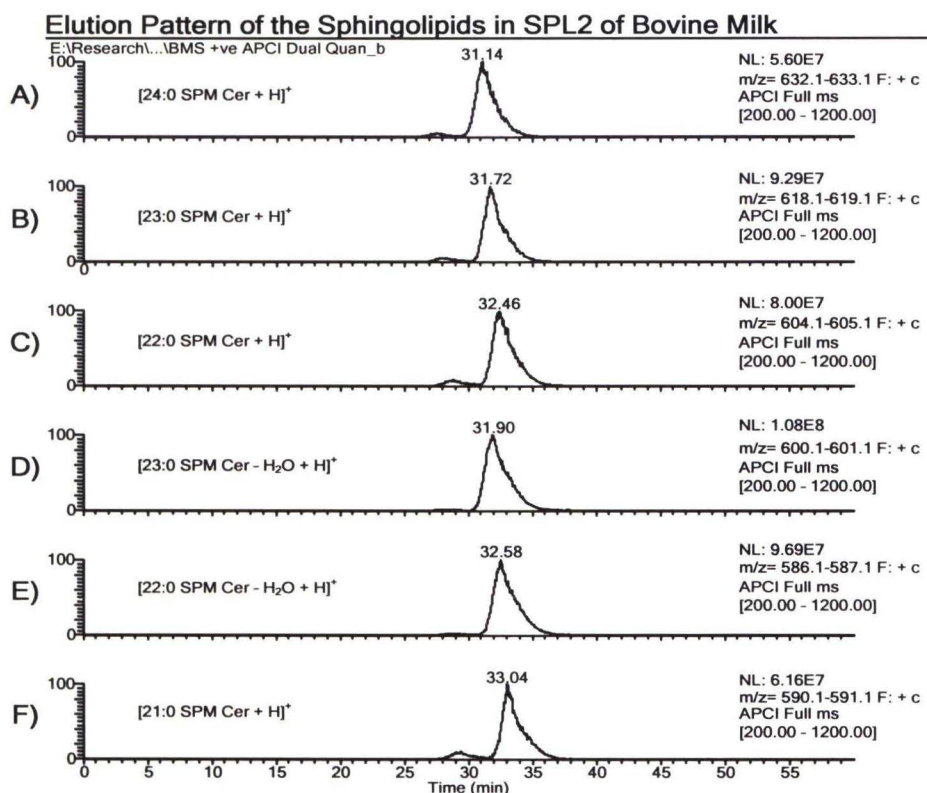


Figure 5. Extracted APCI ion chromatograms (EICs) of the protonated ceramide ion of A) 24:0 SPM, B) 23:0 SPM, C) 22:0 SPM and F) 21:0 SPM. D) EIC showing that the ion at m/z 600.6 was the dehydrated ceramide fragment ion from 23:0 SPM. Similarly, E) showed that the ion at m/z 560.6 was $[22:0 \text{ SPM Cer} - \text{H}_2\text{O} + \text{H}]^+$.

The most abundant SPLs in SPL3 had $[M + H]^+$ ions at *mass-to-charge* ratios of 703.4, 689.4 and 675.4 (**1.2.G**), which had corresponding $[\text{Cer} + \text{H}]^+$ ions at *mass-to-charges* 520.4, 506.5, and 492.4 respectively, according to Table 1. All of these masses were observed in the APCI m.s. (**1.1.G**), which confirmed the presences of 16:0 SPM, 15:0 SPM and 14:0 SPM, respectively. *Mass-to-charge* ratios of 502.5 and 474.5 were the dehydrated ceramide fragments of 16:0 SPM and 14:0 SPM, respectively. These data allowed us to conclude that SPL3 was composed of S-C SPMs. The composition of SPL3

is shown in Table 13. The compositions of SPL3 determined by APCI-MS and ESI-MS were in good agreement. The most abundant SPL group in SPL3 was ‘16:0 SPM’, accounting for 58.7% (59.6%) of all SPMs in SPL3, with 18:1/16:0 being the most abundant species. The LCB composition of SPL3 is shown in Table 14. The most abundant LCB was 18:1, which accounted for 72.0% (71.3%) of all the SPM LCBs in SPL3.

The analysis of the SPL peaks revealed that SPL groups within the same SPL species separated based on the lengths of their FA chains. L-C molecules eluted before S-C molecules within the same class, and saturated LCBs before SPMs. When the APCI-MS m.s. was filtered to show only scans from m/z 460 – 560 (**1.1.B**) that contained masses for the S-C SPLs, and m/z 560 – 660 (**1.1.C**) which contained masses for the L-C species, it could be seen that S-C DHSs overlap with L-C SPMs in SPL2, L-C DHSs eluted just after DPPC in SPL1 and S-C SPMs eluted in SPL3. The same profile was observed in the filtered ESI ion chromatograms (**1.2.B** and **1.2.C**), and chromatograms from the PDA (**1.1.D**) and ELS (**1.2.D**) detectors.

The chromatographic and spectroscopic trends that were observed in BMS may be summarized as follows: 1) The elution pattern of the SPLs was L-C DHSs (SPL1), followed by a mixture of S-C DHSs and L-C SPMs (SPL2), and finally S-C SPMs (SPL3), which was in agreement with previous work²; 2) SPLs were first separated by the number of double bonds in the LCB, then by the length of the FA chain and finally by the number of double bonds on the FA chain; and 3) Protonated ceramide ions of the X:A/Y:2 and X:A/Y:1 SPLs were isobaric with $[X:A/(Y + 1):0 \text{ Cer} - \text{H}_2\text{O} + \text{H}]^+$ ions and their +2 isotopes, respectively.

Composition of the SPLs in the SPL2 Peak of Bovine Milk

Table 9: Composition of the DHSs in SPL2

DHS	% of SPL2		LCB/FA	% of SPL2	
	APCI	ESI		APCI	ESI
12:0	1.7	2.6	14:0/16:0	0.3	0.5
			16:0/14:0	1.2	1.9
			18:0/12:0	0.2	0.3
13:0	0.8	0.6	18:0/13:0*	0.8	0.6
14:0	29.0	38.8	16:0/16:0	26.5	35.6
			17:0/15:0	0.6	0.7
			18:0/14:0	1.9	2.5
15:0	8.7	9.4	16:0/17:0	0.7	0.7
			17:0/16:0	6.3	6.8
			18:0/15:0	1.8	1.9
16:0	41.2	35.7	16:0/18:0	4.9	4.2
			18:0/16:0	36.3	31.5
			12:0/23:0	0.9	0.6
17:0	4.7	3.0	16:0/19:0	0.4	0.3
			17:0/18:0	0.4	0.2
			18:0/17:0	0.2	0.1
18:0	7.0	6.2	19:0/16:0	2.9	1.9
			12:0/24:0	0.7	0.6
			16:0/20:0	1.2	1.1
19:0	6.9	3.6	18:0/18:0	4.1	3.6
			20:0/16:0	1.1	0.9
			14:0/23:0	2.4	1.2
			16:0/21:0	4.3	2.2
			18:0/19:0	0.2	0.1

Table 10: Percent Composition of the SPMs in SPL2

SPM	% of SPL2		LCB/FA	% of SPL2	
	APCI	ESI		APCI	ESI
20:0	6.4	12.3	16:1/22:0	5.9	11.4
			17:1/21:0	0.1	0.3
			18:1/20:0	0.3	0.6
20:1	0.6	0.3	18:1/20:1*	0.6	0.3
21:0	14.3	19.2	16:1/23:0	11.9	16.1
			17:1/22:0	1.9	2.6
			18:1/21:0	0.4	0.6
21:1	1.9	1.9	16:1/23:1	1.7	1.7
			17:1/22:1	0.1	0.1
			18:1/21:1	0.1	0.1
22:0	22.1	22.8	16:1/24:0	6.7	6.9
			17:1/23:0	3.9	4.0
			18:1/22:0	11.5	11.9
22:1	2.5	2.8	16:1/24:1	1.8	2.0
			17:1/23:1	0.6	0.7
			18:1/22:1	0.1	0.1
23:0	24.3	19.9	16:1/25:0	0.2	0.2
			17:1/24:0	3.0	2.4
			18:1/23:0	20.7	16.9
23:1	3.3	3.3	19:1/22:0	0.4	0.3
			16:1/25:1	0.8	0.8
			17:1/24:1	0.4	0.5
24:0	16.0	12.2	18:1/23:1	2.1	2.1
			16:1/26:0	0.4	0.3
			17:1/25:0	0.2	0.2
24:1	3.3	2.1	18:1/24:0	15.0	11.5
			19:1/23:0	0.3	0.2
			18:1/24:1	2.7	1.7
25:0	3.0	1.9	19:1/23:1	0.6	0.4
			18:1/25:0	1.1	0.7
			19:1/24:0	1.5	1.0
25:1	1.5	0.8	20:1/23:0	0.3	0.2
			18:1/25:1	1.1	0.6
			19:1/24:1	0.3	0.2
26:0	0.6	0.4	18:1/26:0*	0.6	0.4
26:1	0.4	0.1	18:1/26:1*	0.4	0.1

Table 11: DHS-LCB Composition in SPL2

DHS-LCB	APCI (%)	ESI (%)
12:0	1.6	1.2
14:0	2.7	1.7
16:0	39.1	45.9
17:0	7.2	7.7
18:0	45.4	40.6
19:0	2.9	1.9
20:0	1.1	0.9

Table 12: SPM-LCB Composition in SPL2

SPM-LCB	APCI (%)	ESI (%)
16:1	29.5	39.4
17:1	10.3	10.7
18:1	56.8	47.7
19:1	3.1	2.1
20:1	0.3	0.2

Tables 9 to 12: Composition of the SPLs in SPL2 of bovine milk. The LCB/FA composition of each SPL group is also shown. All unresolved sphingolipid groups are labeled with an asterisk. These species were assumed to be composed of the 18:0 (DHSs) and 18:1 (SPMs) LCBs, since they were the most consistently-occurring LCBs in all three samples.

Table 13: Percent Composition of the SPLs in SPL3 of Bovine Milk

SPM	% of SPL3		LCB/FA	% of SPL3	
	APCI	ESI		APCI	ESI
10:0	0.1	0.1	16:1/12:0	0.0	0.0
			18:1/10:0	0.1	0.1
12:0	0.7	0.9	16:1/14:0	0.6	0.8
			18:1/12:0	0.1	0.1
13:0	0.6	0.8	17:1/14:0	0.5	0.7
			18:1/13:0	0.0	0.0
14:0	13.8	15.2	16:1/16:0	10.2	11.2
			17:1/15:0	0.0	0.0
			18:1/14:0	3.6	3.9
14:1	0.5	0.2	18:1/14:1*	0.5	0.2
15:0	10.6	11.2	16:1/17:0	0.3	0.3
			17:1/16:0	9.5	10.1
			18:1/15:0	0.8	0.8
15:1	0.6	0.2	18:1/15:1*	0.6	0.2
16:0	58.7	59.6	16:1/18:0	1.7	1.7
			18:1/16:0	57.0	58.0
16:1	1.2	1.7	18:1/16:1	1.2	1.7
17:0	5.3	3.3	17:1/18:0	1.1	0.7
			18:1/17:0	2.1	1.3
			19:1/16:0	2.1	1.3
17:1	0.5	0.3	18:1/17:1*	0.5	0.3
18:0	4.2	4.0	16:1/20:0	0.6	0.5
			18:1/18:0	3.7	3.4
18:1	1.3	1.0	18:1/18:1*	1.3	1.0
19:0	1.8	1.6	16:1/21:0	1.0	0.8
			17:1/20:0	0.2	0.1
			18:1/19:0	0.4	0.3
			19:1/18:0	0.3	0.3

Table 13: Composition of the short chain SPMs in SPL3 of bovine milk. The LCB/FA composition of each SPL group is also shown. All unresolved sphingolipid groups are labeled with an asterisk. These species were assumed to be composed of 18:1 LCBs, since it was the most consistently occurring unsaturated LCB in all three SPM samples.

Table 14: Percent composition of the LCBs in SPL3 of Bovine Milk

LCB	APCI (mole%)	ESI (mole%)
16:1	14.3	15.4
17:1	11.3	11.7
18:1	72.0	71.3
19:1	2.4	1.6

Table 14: Composition of the unsaturated LCBs in the SPL3 peak of bovine milk.

Because of this overlapping of masses and RTs, the accurate identification and quantification of unsaturated SPLs by APCI-MS is not feasible when they are present in a mixture that contains SPLs with both even and odd FA chains. It may be argued that the +2 isotope was not significantly abundant to make an appreciable contribution to the area of the $[X:A/Y:1 \text{ Cer} + H]^+$ ion peaks. There are numerous examples however, in which this comfortable assumption was shown to be false. All these species can, however, be distinguished with tandem MS. This demonstrated that multiple methods of ionization (such as APCI and ESI) and scan modes (positive, negative, MS^2 and MS^3) must be employed in order to unambiguously identify the constituents of a complex SPL mixture, such as BMS.

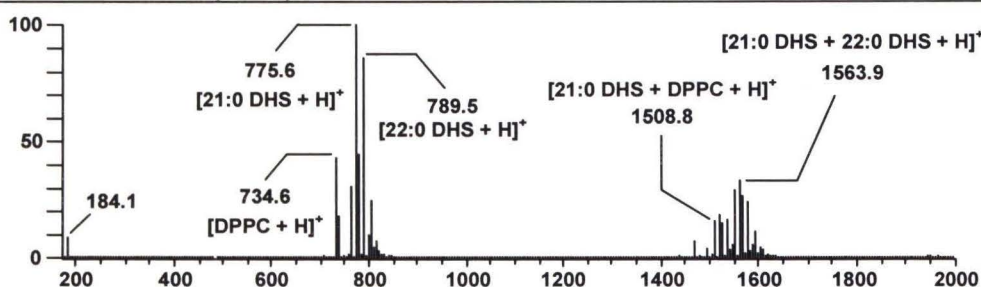
In negative APCI mode, the SPLs formed $[M - 15]^-$ and $[M + 45]^-$ ions (data not shown). The structure of the former ion is shown in Scheme 2 whereas the structure of the latter ion has not yet been elucidated. The sensitivity in -APCI mode was two orders of magnitude less than in +APCI mode. This loss in sensitivity inhibited the identification of the lesser abundant SPLs.

When +ESI-MS data acquired on the LCQ (Figure 6) was compared to the TSQ +ESI-MS data (Figure 1), a relatively large population of high molecular weight masses, in the range m/z 1400 – 1700, was observed in the LCQ data. These masses were PL dimer ions that have the general formula $[M + X + H]^+$, where X can represent any PL molecule that coeluted with M. The general structure of these species, as well as the structures of all adducts and fragment ions observed in the ESI-MS m.s., are illustrated in Scheme 3. **6(A)** and **6(B)** show the formation of three types of heterodimers: 1) ‘Cross-group’ heterodimers such as $[21:0 \text{ DHS} + 22:0 \text{ DHS} + H]^+$ at m/z 1563.9 and $[22:0 \text{ SPM} + 23:0 \text{ SPM} + H]^+$ at m/z 1587.9, formed from the combination of two molecules from different SPL groups within the same species; 2) ‘Cross-species’ heterodimers such as $[22:0 \text{ SPM} + 16:0 \text{ DHS} + H]^+$ at m/z 1491.8, formed from the combination of two molecules from different SPL species; and 3) ‘Cross-class’ heterodimers such as $[21:0 \text{ DHS} + \text{DPPC} + H]^+$ at m/z 1508.8, formed from the combination of two molecules from different PL classes. Homodimers such as $[16:0 \text{ SPM} + 16:0 \text{ SPM} + H]^+$ at m/z 1405.8 in **6(C)**, were formed from the combination of two identical molecules. A comparison of **6(A – C)** with the average ESI m.s. across the SPL2 peak of young eye lenses (YELs) in **6(D)**, showed that the intensity of $[M + Na]^+$ relative to $[M + H]^+$ was significantly greater in YELs than in BMS. As a result of this, the abundance of sodiated homo- and heterodimer adducts (with general formula $[M + X + Na]^+$) were significantly greater in YELs than BMS.

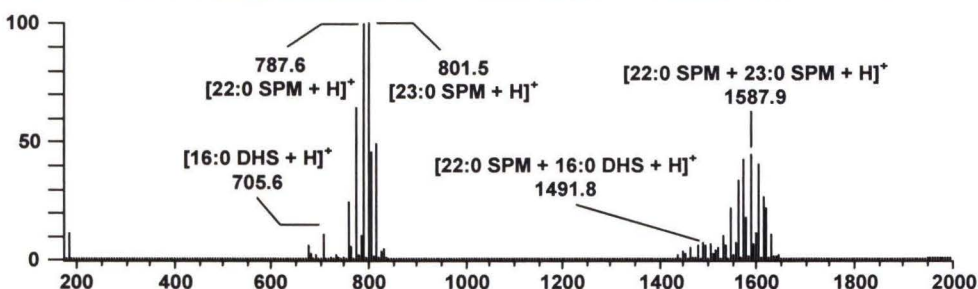
As will be explained later (pages 175 – 176), the higher abundance of the sodium adduct and dimer ions prevented accurate quantitative analysis of the SPLs in human eye lens samples by ESI-MS on the LCQ. As a result, the LC1MS2a configuration was used

Positive ESI-MS (LCQ) of Bovine Milk

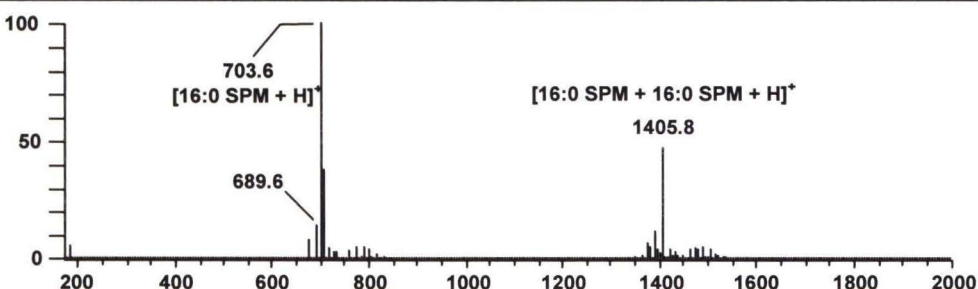
Filename: BMS pos-neg_1



A) SPL1 in BMS

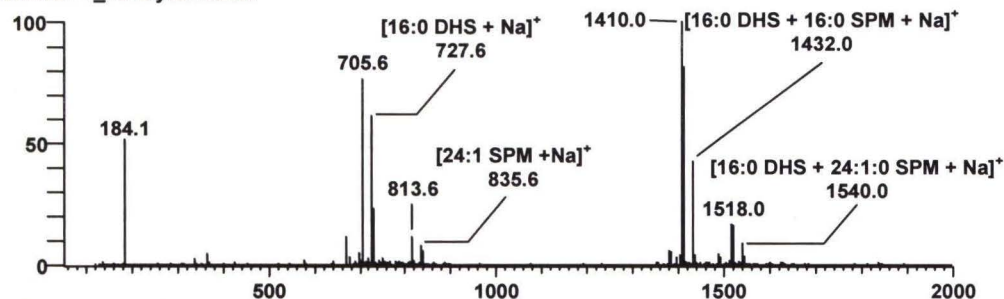


B) SPL2 in BMS



C) SPL3 in BMS

Filename: 6_19YEye01.RAW



D) SPL2 in Young Eye Lens

Figure 6. Positive averaged ESI-MS mass spectra of bovine milk and young eye lens phospholipids, acquired on the LCQ. A) Positive spectrum across the SPL1 peak in BMS; B) positive spectrum across the SPL2 peak in BMS; C) positive spectrum across the SPL3 peak in BMS; and D) positive spectrum across the SPL2 peak in young eye lens samples.

to quantify the SPLs in the SPM extracts. Based on the above observations, the +ESI-MS m.s. can be divided into two primary regions that can aid in molecular species identification. A monomer region from m/z 650 – 850 (TSQ and LCQ ESI-MS data) that contained $[M + H]^+$ ions and their corresponding sodium adducts, and a dimer region from m/z 1300 – 1700 (LCQ ESI-MS data only) composed of PL dimers.

Figure 7 shows some examples of the fragments and adducts that were observed in the LCQ –ESI-MS m.s. Like the LCQ +ESI-MS data, two distinct mass regions were observed. The lower mass region was comprised of $[M + 45]^-$ adduct and $[M - 15]^-$ fragment ions. The abundance of $[M - 15]^-$ ions in BMS (**7(A–C)**) was significantly less when compared to YELs (**7(D)**). For example, the $[16:0 \text{ DHS} - 15]^-$ ion at m/z 689.9 was almost equal in abundance to $[16:0 \text{ DHS} + 45]^-$ at m/z 749.6 in YELs, but was negligible in BMS (**7(B)**). The reason for this difference was that ion source collision induced dissociation (CID) with energy of 20V was used during the analysis of YELs. This facilitated loss of a positive methyl ion from the nitrogen atom of the phosphocholine head group in the ion source, as shown in Scheme 2.

Dimer ions were significantly more abundant in the LCQ ESI-MS data, though small amounts were detected by ESI-MS on the TSQ. This difference suggested that dimers were produced more efficiently in the ion trap mass analyzer, because if they were produced in solution or the ESI source, then the ratio of the intensity of the dimers to the intensities of their corresponding constituent $[M + H]^+$ ions, would be comparable between the two instruments. However, since $[M + X + H]^+ / [M + H]^+$ was significantly larger in the LCQ ESI m.s., it was concluded that confining the ions in a small volume for

a period of approximately 200ms (the trapping time) in the ion trap, permitted dimerizing ion-ion reactions to occur more frequently than in the linear quadrupole mass analyzer.

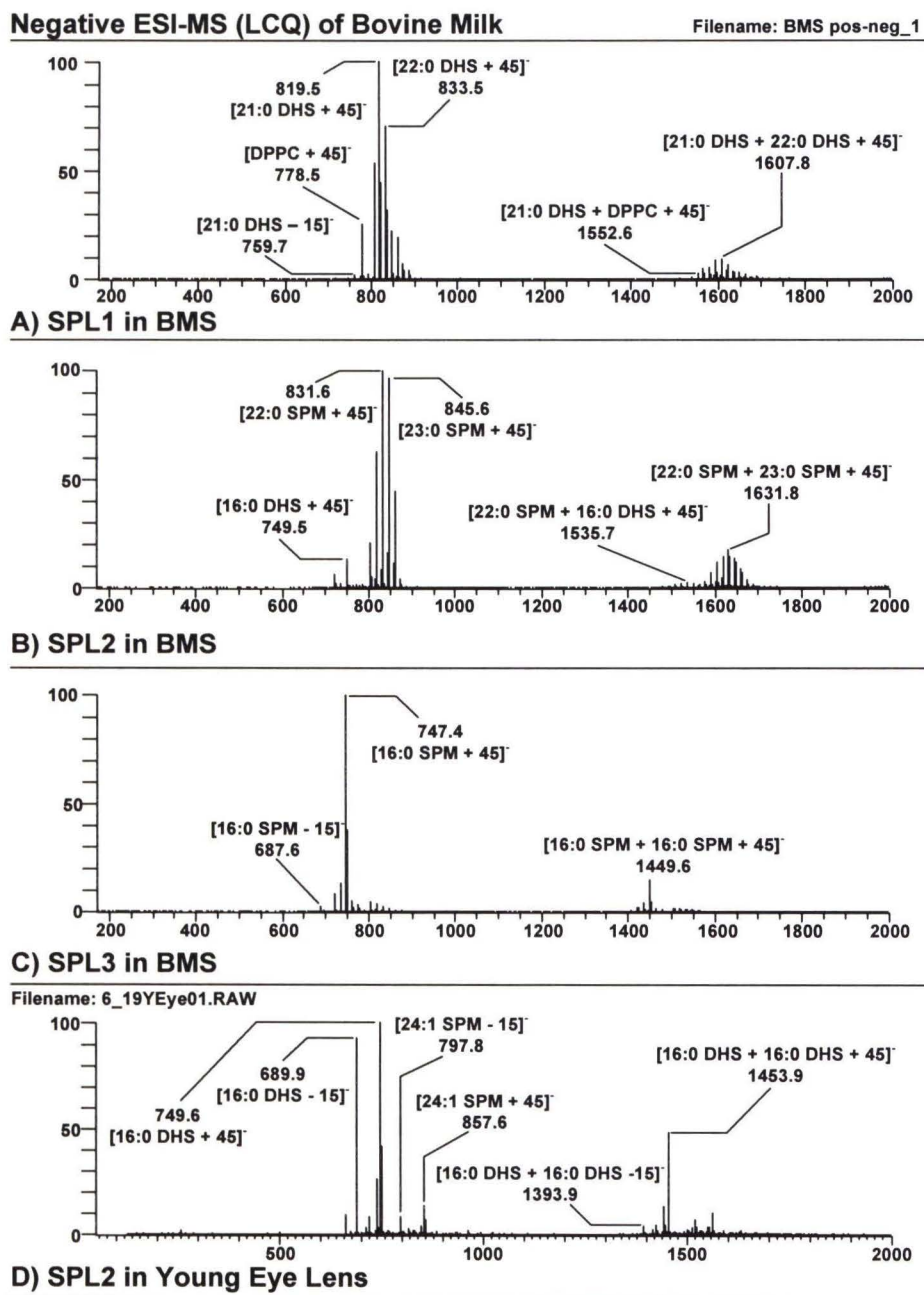


Figure 7. Negative ion averaged ESI-MS mass spectra acquired on the LCQ, of bovine milk and young eye lens phospholipids. A) Negative spectrum across the SPL1 peak in BMS; B) negative spectrum across the SPL2 peak in BMS; C) negative spectrum across the SPL3 peak in BMS; and D) negative spectrum across the SPL2 peak in the young eye lens sample.

The described analysis for the full-scan APCI-MS and ESI-MS m.s. for BMS was also applied to the CES and BBS extracts. Though all the described adduct and fragment ions served to identify specific groups of SPLs, the LCB/FA composition could only be determined from intact SPL molecules using tandem MS, which is described in Section 2.

1.2 Bovine Brain

The APCI and ESI chromatographic profiles for BBS (10.22 mg/mL) with the DPPC (0.50mg/mL) IS (data not shown), were similar to those for BMS. There were three distinct SPL peaks, with SPL1 also overlapping with DPPC in the ESI-MS m.s. The dominant species in SPL1 had a $[\text{Cer} + \text{H}]^+$ at m/z 632.6 and a $[\text{M} + \text{H}]^+$ at m/z 815.7. These ions corresponded to 24:1 DHS from Table 1 and accounted for 29.9% (24.2%) of the DHSs in SPL1 (Table 15). Unlike BMS, the 18:0 LCB accounted for 96.6% (96.0%) of all the saturated LCBs in SPL1, while the 16:0 LCB accounted for only 0.3% (0.2%) (Table 16).

The most abundant species in SPL2 was 24:1 SPM with a $[\text{M} + \text{H}]^+$ ion at m/z 813.5, a $[\text{Cer} + \text{H}]^+$ ion at m/z 630.5 and a $[\text{Cer} - \text{H}_2\text{O} + \text{H}]^+$ ion at m/z 612.6, which accounted for 36.1% (33.0%) of SPMs in SPL2 (Table 18). The S-C DHSs in SPL2 were composed only of SPLs with 18:0 LCBs (Table 17). The SPMs in SPL2, on the other hand, were composed mostly of SPLs with 18:1 (86.8% (82.0%)) and 20:1 (12.8% (17.8%)) LCBs (Table 19). Finally, SPL3 was mostly 18:0 SPM (89.5% (91.4%)), which was composed primarily of 18:1/18:0, with a minor contribution from 16:1/20:0 (Table 20). The 18:1 LCB accounted for 96.9% (98.2%) of all the unsaturated LCBs in SPL3 (Table 21).

Table 15: Composition of the L-C DHSs (mole%) in the SPL1 Peak of Bovine Brain

DHS	mole% of SPL1 in BBS		LCB/FA	mole% of SPL1 in BBS	
	APCI	ESI		APCI	ESI
20:0	10.5	16.6	18:0/20:0	9.4	14.9
			20:0/18:0	1.1	1.8
20:1	1.2	0.8	18:0/20:1*	1.2	0.8
21:0	0.8	0.6	18:0/21:0*	0.8	0.6
22:0	21.9	22.9	18:0/22:0	21.9	22.9
22:1	5.1	6.2	17:0/23:1	1.4	1.7
			18:0/22:1	3.7	4.5
23:0	4.2	3.9	18:0/23:0	4.2	3.9
23:1	0.7	1.5	18:0/23:1	0.7	1.5
24:0	19.6	19.5	18:0/24:0	19.6	19.5
24:1	29.9	24.2	18:0/24:1	29.9	24.2
25:0	1.7	0.9	18:0/25:0	1.6	0.8
			19:0/24:0	0.1	0.0
			20:0/23:0	0.0	0.0
25:1	1.6	0.7	18:0/25:1	1.1	0.5
			19:0/24:1	0.5	0.2
			20:0/23:1	0.0	0.0
26:0	0.8	0.8	16:0/24:0	0.1	0.1
			18:0/26:0	0.7	0.7
26:1	2.1	1.4	16:0/24:1	0.2	0.1
			18:0/26:1	1.9	1.3

Table 16: Composition of the saturated LCBs (mole%) in the SPL1

Peak of Bovine Brain

LCB	APCI (mole%)	ESI (mole%)
16:0	0.3	0.2
17:0	1.4	1.7
18:0	96.6	96.0
19:0	0.5	0.2
20:0	1.2	1.8

Table 17: Composition of the S-C DHSs (mole%) in the SPL2 Peak of
Bovine Brain

DHS-LCB/FA	mole% of SPL2 in BBS	
	APCI	ESI
18:0/16:0 [*]	2.9	4.3
18:0/18:0	89.3	92.1
18:0/18:1 [*]	3.9	1.4
18:0/19:0 [*]	3.8	2.2

Table 18: Composition of the L-C SPMs (mole%) in the SPL2 Peak of
Bovine Brain

SPM	% of SPL2 in BBS		LCB/FA	% of SPL2 in BBS	
	APCI	ESI		APCI	ESI
20:0	18.4	25.9	18:1/20:0	5.9	8.3
			20:1/18:0	12.5	17.5
20:1	1.4	0.3	18:1/20:1 [*]	1.4	0.3
21:0	1.4	0.7	18:1/21:0 [*]	1.4	0.7
22:0	11.7	12.8	18:1/22:0	11.7	12.8
22:1	3.9	3.9	18:1/22:1	3.8	3.9
			20:1/20:1	0.1	0.1
23:0	3.9	3.2	18:1/23:0	3.8	3.1
			19:1/22:0	0.0	0.0
			16:1/25:0	0.0	0.0
23:1	1.3	1.8	18:1/23:1	1.3	1.8
24:0	13.7	13.5	18:1/24:0	13.7	13.5
			16:1/26:0	0.0	0.0
24:1	36.1	33.0	18:1/24:1	36.1	33.0
25:0	1.8	1.1	18:1/25:0	1.7	1.0
			19:1/24:0	0.0	0.0
			20:1/23:0	0.0	0.0
25:1	3.6	1.4	18:1/25:1	3.3	1.2
			19:1/24:1	0.2	0.1
			20:1/23:1	0.1	0.0
26:0	0.6	0.7	18:1/26:0	0.5	0.6
			20:1/24:0	0.1	0.1
			19:1/25:0	0.0	0.0
26:1	2.5	1.9	18:1/26:1	2.3	1.8
			19:1/25:1	0.0	0.0
			20:1/24:1	0.1	0.1

Table 19: Composition of the SPM-LCBs (mole%) in the SPL2 Peak of
Bovine Brain

LCB	APCI (mole%)	ESI (mole%)
16:1	0.0	0.0
18:1	86.8	82.0
19:1	0.3	0.1
20:1	12.8	17.8

Table 20: Composition of the S-C SPMs (mole%) in the SPL3 Peak of
Bovine Brain

SPM	mole% of SPL3 in BBS		LCB/FA	mole% of SPL3 in BBS	
	APCI	ESI		APCI	ESI
14:0	0.1	0.2	18:1/14:0	0.1	0.2
			16:1/16:0	0.0	0.0
15:0	0.0	0.1	18:1/15:0*	0.0	0.1
16:0	3.7	5.9	18:1/16:0	3.2	5.1
			16:1/18:0	0.4	0.7
			20:1/14:0	0.1	0.1
17:0	0.5	0.6	18:1/17:0	0.3	0.3
			17:1/18:0	0.2	0.3
18:0	89.5	91.4	18:1/18:0	89.3	91.2
			16:1/20:0	0.2	0.2
18:1	1.6	0.7	18:1/18:1	1.6	0.7
19:0	4.6	1.0	18:1/19:0	2.4	0.5
			19:1/18:0	2.0	0.4
			17:1/20:0	0.2	0.0
			16:1/21:0	0.1	0.0

Table 21: Composition of the LCBs (mole%) in the SPL3 Peak of

Bovine Brain

LCB	APCI (mole%)	ESI (mole%)
16:1	0.7	0.9
17:1	0.4	0.3
18:1	96.9	98.2
19:1	2.0	0.4
20:1	0.1	0.1

From the above observations, it was observed that BBS was not as complex of a mixture as BMS. BBS was composed almost entirely of SPLs with 18:1 and 18:0 LCBs. In fact from Tables 43, 44, 48 and 49, it was seen that SPLs with 18:1 and 18:0 LCBs accounted for 91.4% (90.6%) and 97.4% (97.1%) of the total DHS and SPM populations, respectively.

1.3 Chicken Egg Yolk

Of the three SPM extracts, CES (10.20 mg/mL with 0.500035 mg/mL DPPC added as an IS) was the least complex because there were very little DHSs (~3% of the total SPL mixture) in this sample. As a result, SPL1 was a very small peak that barely rose above the baseline in the TIC. This indicated that in CES there was predominantly S-C DHSs, L-C SPMs and S-C SPMs, with very little L-C DHSs.

The composition of SPL1 is shown in Table 22. SPL1 was composed only of SPLs with 18:0 LCBs, of which 18:0/22:0 was the most abundant, accounting for 37.5% (47.2%) of SPL1. However, 18:0/22:0 only accounted for 0.93% (1.15%) (Tables 51 and 56 respectively) of the total DHS population. The composition of SPL2 and SPL3 is shown in Tables 23 to 26, and Tables 27 to 28 respectively. SPLs with 18:0 and 18:1

LCBs accounted for 97.6% (97.7%) and 99.0% (99.8%) of the total DHS and SPM populations, respectively (Tables 53, 54, 58 and 59).

So, of the three samples BBS and CES were composed primarily of the 18:1 and 18:0 LCBs. In BMS however, the 16:1, 17:1, 18:1, 16:0, 17:0 and 18:0 LCBs all accounted for more than 5% of their corresponding SPM or DHS populations (Tables 33, 34, 38 and 39). So, the order of complexity (i.e. the order of LCB diversity) of the samples was BMS > BBS > CES.

Table 22: Composition of the L-C DHSs (mole%) in the SPL1 Peak of Chicken Egg Yolk

DHS-LCB/FA	APCI (mole%)	ESI (mole%)
18:0/20:0	19.1	19.8
18:0/22:0	37.5	47.2
18:0/23:0	8.5	3.6
18:0/24:0	21.4	20.5
18:0/24:1	13.6	8.9

Table 23: Composition of the S-C DHSs (mole%) in the SPL2 Peak of
Chicken Egg Yolk

DHS	% of SPL2 in CES		LCB/FA	% of SPL2 in CES	
	APCI	ESI		APCI	ESI
14:0	1.3	1.8	14:0/18:0	0.1	0.1
			16:0/16:0	0.1	0.1
			18:0/14:0	1.2	1.6
15:0	0.5	0.7	18:0/15:0*	0.5	0.7
16:0	85.7	88.8	16:0/18:0	1.9	2.0
			18:0/16:0	83.7	86.8
16:1	5.1	2.9	18:0/16:1*	5.1	2.9
17:0	2.5	1.0	18:0/17:0	2.1	0.8
			19:0/16:0	0.4	0.2
18:0	3.2	3.9	18:0/18:0	3.2	3.9
18:1	1.7	0.9	18:0/18:1*	1.7	0.9

Table 24: Composition of the DHS-LCBs (mole%) in the SPL2 Peak of
Chicken Egg Yolk

LCB	APCI (mole%)	ESI (mole%)
14:0	0.1	0.1
16:0	2.0	2.1
18:0	97.5	97.6
19:0	0.4	0.2

Table 25: Composition of the L-C SPMs (mole%) in the SPL2 Peak of
Chicken Egg Yolk

SPM	% of SPL2 in CES		LCB/FA	% of SPL2 in CES	
	APCI	ESI		APCI	ESI
20:0	11.1	14.8	18:1/20:0	11.1	14.8
20:1	1.9	1.2	18:1/20:1*	1.9	1.2
21:0	2.0	1.6	18:1/21:0	1.7	1.3
			19:1/20:0	0.1	0.1
			20:1/19:0	0.3	0.2
22:0	23.2	25.6	18:1/22:0	23.2	25.6
22:1	3.9	3.6	18:1/22:1	3.9	3.6
22:2	1.9	2.0	18:1/22:2	1.9	2.0
23:0	7.3	6.2	18:1/23:0	7.2	6.0
			19:1/22:0	0.1	0.1
24:0	12.5	14.4	18:1/24:0	12.5	14.4
24:1	25.7	22.8	18:1/24:1	25.7	22.8
24:2	9.4	7.2	18:1/24:2	9.4	7.2
25:0	0.6	0.5	18:1/25:0	0.5	0.5
			19:1/24:0	0.1	0.0
			20:1/23:0	0.0	0.0
26:0	0.1	0.1	18:1/26:0	0.1	0.0
			20:1/24:0	0.0	0.0
26:1	0.3	0.2	18:1/26:1	0.3	0.2

Table 26: Composition of the SPM-LCBs (mole%) in the SPL2 Peak of
Chicken Egg Yolk

LCB	APCI (mole%)	ESI (mole%)
18:1	99.4	99.5
19:1	0.3	0.2
20:1	0.3	0.2

Table 27: Composition of the S-C SPMs (mole%) in the SPL3 Peak of
Chicken Egg Yolk

SPM	% of SPL3 in CES		LCB/FA	% of SPL3 in CES	
	APCI	ESI		APCI	ESI
12:0	0.03	0.06	16:1/14:0	0.00	0.00
			18:1/12:0	0.02	0.06
14:0	0.96	1.60	18:1/14:0	0.96	1.60
15:0	0.27	0.38	18:1/15:0*	0.27	0.38
16:0	85.51	86.30	18:1/16:0	85.51	86.30
16:1	1.79	0.47	18:1/16:1*	1.79	0.47
17:0	4.32	0.61	18:1/17:0	3.37	0.48
			19:1/16:0	0.95	0.13
18:0	5.30	9.47	18:1/18:0	5.30	9.47
18:1	1.22	0.66	18:1/18:1*	1.22	0.66
18:2	0.12	0.20	18:1/18:2	0.12	0.20
19:0	0.47	0.25	18:1/19:0	0.42	0.2104
			19:1/18:0	0.05	0.0367

Table 28: Composition of the SPM-LCBs (mole%) in the SPL3 Peak of
Chicken Egg Yolk

LCB	APCI (mole%)	ESI (mole%)
16:1	0.00	0.00
18:1	99.00	99.82
19:1	1.00	0.17

Note: The description for Tables 15 to 28 was similar to those given for Tables 7 to 14 for bovine milk.

2. TANDEM MASS SPECTROMETRY

The first step in the identification of any SPL was to confirm that the $[\text{Cer} + \text{H}]^+$, $[\text{M} + \text{H}]^+$, $[\text{M} + \text{Na}]^+$, and $[\text{M} + 45]^-$ ions were present and had the correct RTs, by comparing the EICs for each of the relevant ions. All the factors described above (such as retention properties and mass-overlaps) were taken into consideration when identifying these species by full-scan MS. After identifying the SPL group by using the ESI and APCI full-scan m.s., APCI tandem MS was performed to determine the LCB/FA composition. It was found that the SPLs exhibited two distinct fragmentation patterns depending on whether or not there was a double bond in the molecule. The saturated SPLs (X:0/Y:0) had a different fragmentation pattern than all other SPLs. This difference played a significant role in the method used to quantify these species. The methods used to determine the LCB/FA composition of a SPL group (such as 21:0 DHS) were divided into three categories based on the number of double bonds on the FA chain. These analytical procedures are described below.

The LCB/FA composition could not be determined by ESI-MS because it did not cleave the molecule into its FA and LCB ions. This observation was in agreement with previous findings.¹¹ Hsu *et al* however, demonstrated that the lithiated adducts of glycerophosphocholines¹² and SPMs¹³ facilitated their fragmentation by ESI MS/MS. So, the ESI MS/MS of Li-SPLs is an additional experiment which could be performed in addition to those outlined in this work, to obtain more structural information about the SPLs.

2.1. Sphingolipids with Saturated Fatty Acid Chains (X:A/Y:0)

The +APCI and +ESI data for 20:0 SPM and 22:0 SPM from BMS, will be used to illustrate the principles involved in the determination of the LCB/FA composition of SPMs with saturated FAs. The first step was to confirm that the $[\text{Cer} + \text{H}]^+$, $[\text{M} + \text{H}]^+$ $[\text{M} + \text{Na}]^+$ and $[\text{M} + 45]^-$ ions of 20:0 SPM occurred at the correct RTs (in relation to the other L-C SPMs), by examining the +APCI, +ESI and –ESI full-scan EICs. Based on the retention characteristics of the SPLs $[\text{20:0 SPM Cer} + \text{H}]^+$ at m/z 576.6 (**8(B)**) should have a RT that was earlier than $[\text{19:0 SPM Cer} + \text{H}]^+$ at 33.97 mins (**8(F)**) but later than $[\text{21:0 SPM Cer} + \text{H}]^+$ at 32.74 mins (**8(A)**), since the SPLs separated based on the lengths of their FA chains. Figure 8 showed that $[\text{20:0 SPM Cer} + \text{H}]^+$ had the correct RT at 33.20 mins. The EICs for the $[\text{Cer} + \text{H}]^+$, $[\text{M} + \text{H}]^+$ at m/z 759.6 (**8(C)**), $[\text{M} + \text{Na}]^+$ at m/z 781.8 (**8(D)**), and $[\text{M} + 45]^-$ at m/z 803.8 (**8(E)**) ions of 20:0 SPM had similar RTs, which suggested that all these ions originated from the same molecule. All the ions necessary to unambiguously identify the 20:0 SPMs were observed in the average m.s. (**8(G)**, **8(H)** and **8(I)**) across the shaded regions, and were labeled accordingly. All the SPL groups were initially identified in this way. It was important to remember however, that ‘20:0 SPM’ represented a group of isobaric SPLs that had unsaturated LCBs. So, the next step was to identify the constituents of this group (i.e. the LCB/FA composition), by specifically fragmenting the $[\text{20:0 SPM Cer} + \text{H}]^+$ ion and then analyzing the resulting MS^2 and MS^3 m.s.

Determining the LCB/FA composition of SPLs that had no sites of unsaturation on the FA chain was straightforward since the masses of their $[\text{Cer} + \text{H}]^+$ ions did not overlap with the masses of any fragment ions from other species. Figure 9 shows the

average APCI MS² and MS³ m.s. across the shaded region in **8(B)** for 20:0 SPM. Before beginning the analysis however, there were a couple of relevant points to remember: 1) It was important to not only identify relevant fragment ions, but also their patterns in the MSⁿ m.s.; 2) 20:0 SPM was a group of isobaric molecules (such as 18:1/20:0, 19:1/19:0 etc.) that coeluted in this chromatographic system; and 3) Saturated LCB SPLs eluted before unsaturated SPLs, so that although 18:0/20:1 was isobaric with 18:1/20:0, they were chromatographically resolved, with the former eluting in SPL1 and the latter in SPL2 (Figure 1). The structures of the major fragment ions observed in the APCI MS, MS² and MS³ m.s. are illustrated in Scheme 2 and should be consulted during the description of the analysis.

After confirming that 20:0 SPM was present based on the full-scan m.s., the next step was to fragment [20:0 SPM Cer + H]⁺ to produce the MS² m.s., followed by a second fragmentation of [20:0 SPM Cer – H₂O + H]⁺ in the previous MS² m.s., to produce the MS³ m.s. The base peak in the MS² m.s had a *m/z* of 558.4, which from Table 1, was the [20:0 SPM Cer – H₂O + H]⁺ ion. The second most intense peak at *m/z* 364.4 could be either a LCB or FA fragment ion. If it was a LCB fragment then it was either [24:2 LCB + H]⁺ or [25:0 LCB – H₂O + H]⁺ from Table 3, both of which were eliminated as possibilities. The former LCB cannot be combined with any FA so that [24:2/Y:B Cer + H]⁺ had a *m/z* of 576.6. The second possibility, [25:0 LCB – H₂O + H]⁺, suggested a SPL with a 13:1 FA chain. From Table 1, [13:1(L)]⁺ had a *m/z* of 236.4 which was observed in **9(A)** and **9(B)**, but [13:1(S)]⁺ at *m/z* 212.3 was not observed in either spectrum. So this species was not 25:0/13:1. However, even if there was an ion at *m/z* 212.3 in the MS² or MS³ m.s., 25:0/13:1 could still be eliminated because this

molecule belongs to the 20:1 DHS SPL group, which was chromatographically resolved from 20:0 SPM. 25:0/13:1 eluted at the trailing edge of SPL1 whereas 20:0 SPM eluted at the trailing edge of SPL2.

So, the ion at m/z 364.4 must be either a $[FA(S)]^+$ or $[FA(L)]^+$ fragment. If it was the former then it would be a 24:2 FA. But there was no LCB that could be combined with this FA to yield a $[X:1/24:2 \text{ Cer} + H]^+$ that was isobaric with $[20:0 \text{ SPM Cer} + H]^+$. Therefore, by the process of elimination, the second most abundant ion in the MS^2 spectrum must be a $[22:0(L)]^+$ fragment ion, which was combined with a 16:1 LCB to have a m/z of 576.6. The $[16:1 \text{ LCB} + H]^+$ at m/z 254.4, $[16:1 \text{ LCB} - H_2O + H]^+$ at m/z 236.2 and $[22:0 \text{ FA(S)}]^+$ at m/z 340.3, were all observed, which confirmed the presence of 16:1/22:0.

An important point to note was that the $[16:1 \text{ LCB} + H]^+$ ion at m/z 254.4 was not observed in the MS^3 m.s. This ion was produced from the fragmentation of the 20:0 SPM protonated ceramide ion whereas the MS^3 m.s. originated from the isolation and then fragmentation of the $[20:0 \text{ SPM Cer} - H_2O + H]^+$ ion at m/z 558.4, in which the LCB backbone was already dehydrated. This meant therefore, that the mass-overlaps between $[LCB + H]^+$ and $[FA(S)]^+$ ions (Tables 5 and 6) occurred only in the MS^2 m.s., thereby allowing these species to be differentiated in the MS^3 . Table 5 (Table 6 for DHSs) showed that unsaturated LCB fragment ions were not isobaric with any saturated FA fragment ions, so the above analysis for 20:0 SPM was valid. Table 5 (for SPMs) or 6 (for DHSs) was always consulted when analyzing any MS^2 or MS^3 m.s., in order to prevent erroneous SPL identifications.

Full Scan APCI and ESI Mass-Spectrometric Analysis of 20:0 SPM

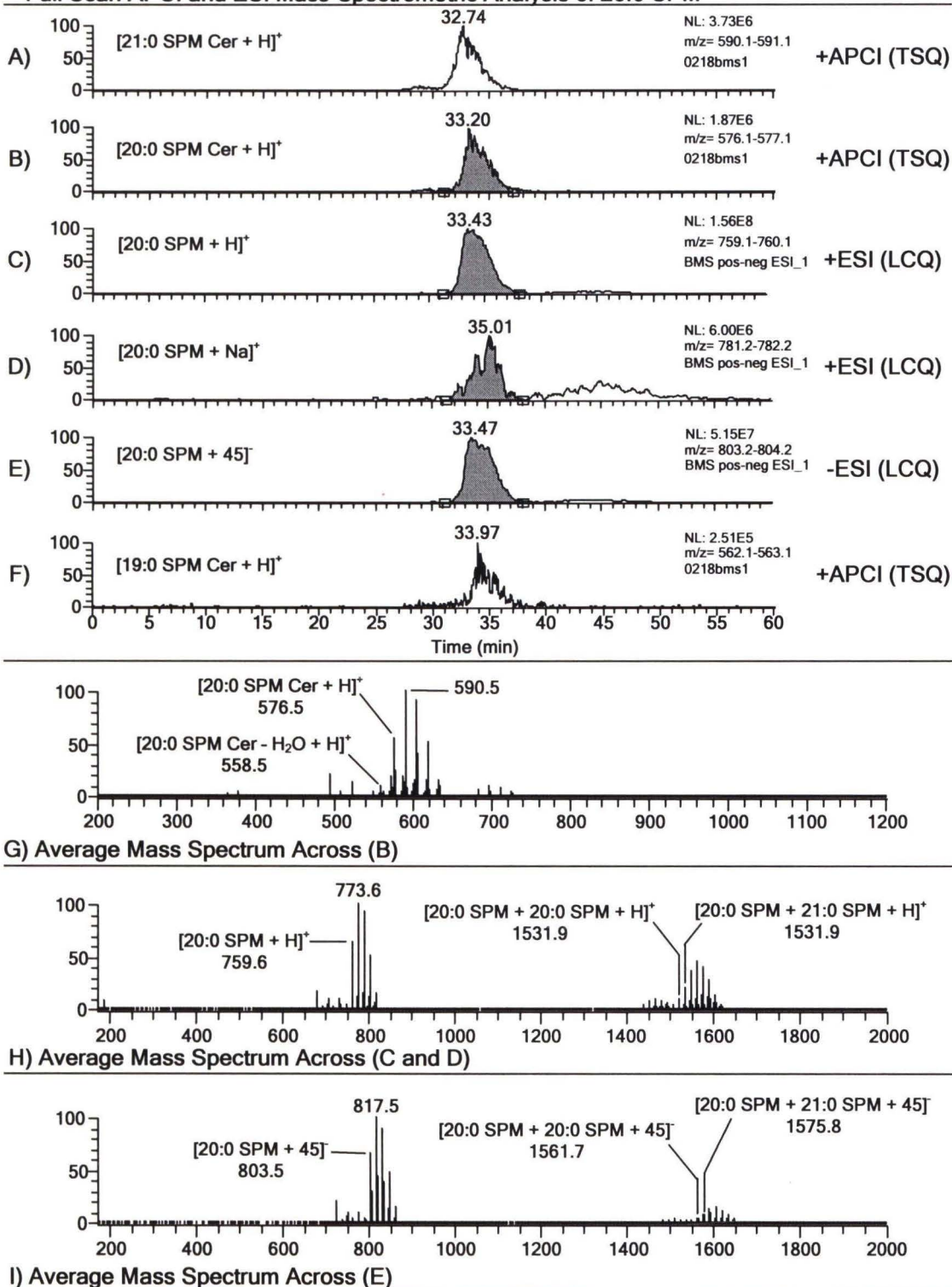


Figure 8. Identification of 20:0 SPM using the full-scan ESI and APCI mass spectra.

From Figure 9, the following fragmentation pattern (FP) was discerned. In the MS² m.s., the three primary ions, in the order of decreasing intensity, were the [Cer – H₂O + H]⁺, [FA(L)]⁺ and [LCB – H₂O + H]⁺ ions. Also, the intensities of the [LCB – H₂O + H]⁺ > [LCB + H]⁺ and the [FA(L)]⁺ > [FA(S)]⁺. [FA(L) + 35]⁺, [M – 212]⁺ and [Cer + H – 46]⁺ fragment ions were also consistently observed in the MS² m.s. Typically, the intensities were: 1) [M – 212]⁺ > [Cer – H₂O + H – 28]⁺ in the MS² and [Cer – H₂O + H – 28]⁺ > [Cer – H₂O + H – 18]⁺ in the MS³; and 2) [FA(L)]⁺ >> [FA(L) + 35]⁺. The major difference between the MS² and MS³ m.s., was that the former had protonated LCB ions. The above fragmentation pattern was designated FP1. All SPLs, except DHSs with saturated FA chains (X:0/Y:0), exhibited FP1 under APCI MS and MS/MS conditions. This implied that FP1 occurred when a double bond was present at any location in the SPL molecule.

The other masses in **9(A)** and **9(B)** were analyzed in a similar way. The ion at *m/z* 336.3 was suspected to be a [FA(L)]⁺ or [LCB – H₂O + H]⁺ based on FP1. Because of differences in retention characteristics, the 23:0 LCB dehydrated fragment ion was eliminated as a possibility. So, this ion was identified as [20:0(L)]⁺ fragment, which had a corresponding [20:0(S)]⁺ fragment at *m/z* 312.3. The [18:1 LCB – H₂O + H]⁺ was observed at *m/z* 264.3 in both the MS² and MS³ spectra, and the [18:1 LCB + H]⁺ at *m/z* 282.3 in the MS² m.s. These ions indicated the presence of 18:1/20:0. The [17:1 LCB – H₂O + H]⁺ was observed at *m/z* 250.3 in **9(B)**. The [21:0(L)]⁺ and [21:0(S)]⁺ fragment ions were also observed and labeled. So, 20:0 SPM was composed of the 18:1/20:0, 16:1/22:0 and 17:1/21:0 SPMs, with 16:1/22:0 being the most abundant.

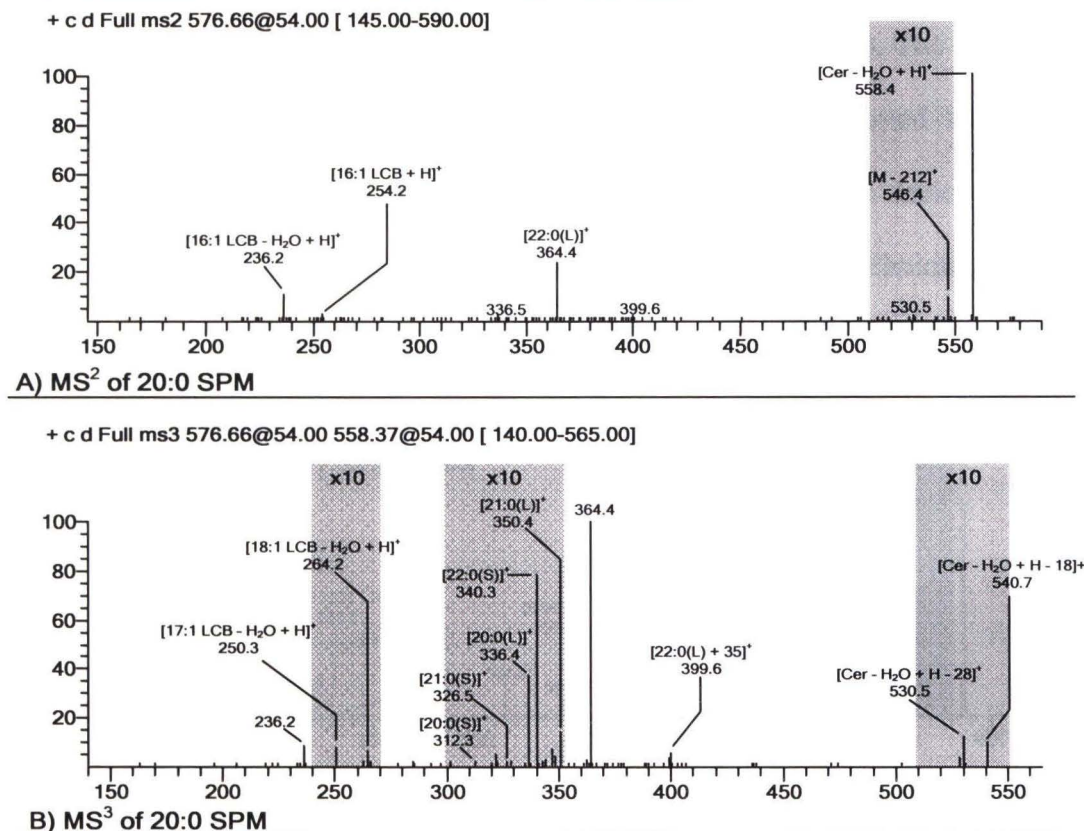


Figure 9. MS² (A) and MS³ (B) mass spectra of 20:0 SPM.

In Figure 9, various sections of the m.s. were magnified by a factor of ten in order to see relevant fragment ions. One may argue that these smaller peaks (such as m/z 312.3) may not be significant. The tandem MS of 22:0 SPM produced fragment ions that could all be observed without magnification, except for the $[M - 212]^+$ ion, which was not important in determining the LCB/FA composition. From Figure 10 it was observed that the fragmentation pattern for 22:0 SPM was FP1, and that this SPL group was composed of 16:1/24:0, 17:1/23:0 and 18:1/22:0. The intensities of the $[FA(S)]^+$ and $[LCB + H]^+$ ions were still significantly less than their corresponding $[FA(L)]^+$ and dehydrated LCB ions, respectively. Even though 22:0 SPM, which represented 17.1% (13.5%) of the total

SPM population in bovine milk (Tables 31 and 36), was 2 to 3 times more abundant than 20:0 SPM (4.9% (7.3%) of the total SPM population in bovine milk). The constancy of FP1 throughout the entire BMS, CES and BBS data sets, supported the proposed identifications of the low intensity ions in **9(B)**. These observations demonstrated that tandem m.s. of the SPLs, was a specific, sensitive and accurate technique, producing similar fragmentation patterns regardless of the intensity of the parent ion.

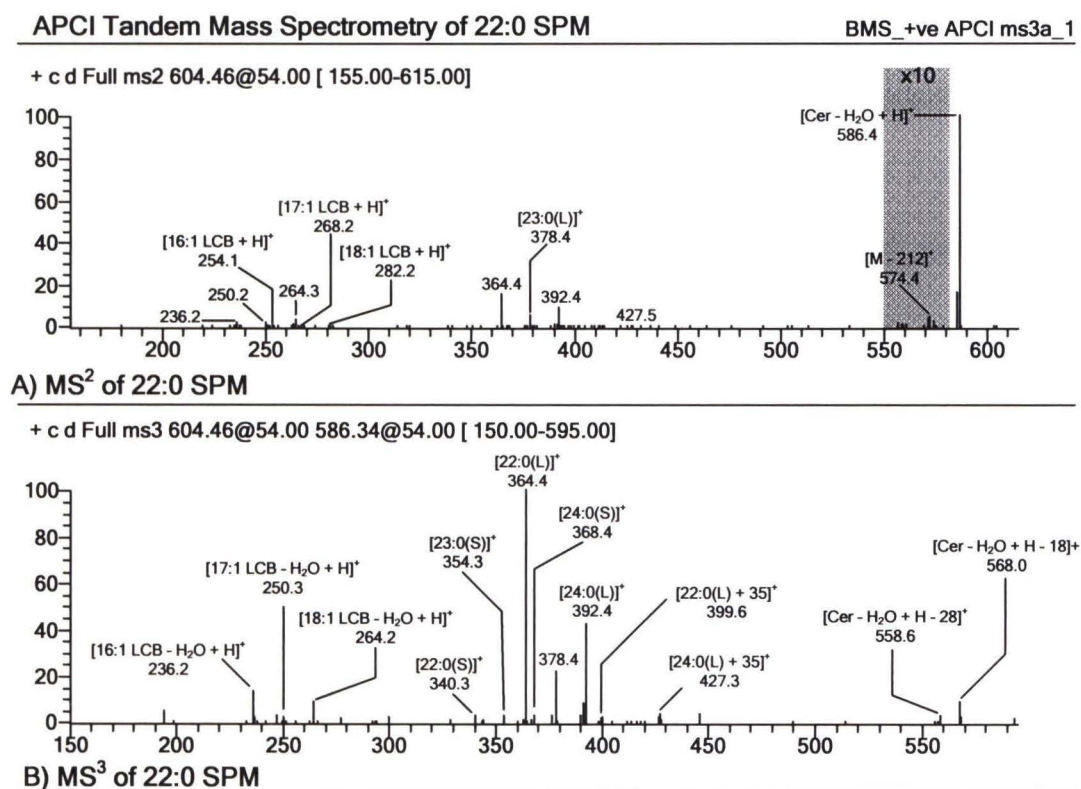


Figure 10. MS² (A) and MS³ (B) mass spectra for 22:0 SPM

22:0 DHS will be used to illustrate the analysis of saturated DHSs. The MS² (**11(A)**) and MS³ (**11(B)**) m.s. of 22:0 DHS was analyzed similarly to 20:0 SPM and 22:0 SPM, described above. For completely saturated SPL systems however, the fragmentation pattern was very different from FP1. The main similarity was that in the

MS² m.s., the base peak was the $[X:0/Y:0 \text{ Cer} - \text{H}_2\text{O} + \text{H}]^+$ ion, as seen for the $[22:0 \text{ DHS Cer} - \text{H}_2\text{O} + \text{H}]^+$ ion at m/z 588.5 in **11(A)**. In contrast to FP1 however, $[22:0(\text{S})]^+$ was more abundant than $[22:0(\text{L})]^+$; $[16:0 \text{ LCB} + \text{H}]^+$ was more abundant than $[16:0 \text{ LCB} - \text{H}_2\text{O} + \text{H}]^+$; $[\text{Cer} - \text{H}_2\text{O} + \text{H} - 28]^+$ and $[\text{Cer} - \text{H}_2\text{O} + \text{H} - 18]^+$ were more abundant than $[\text{M} - 212]^+$ in the MS² m.s.; and the $[\text{FA}(\text{L}) + 35]^+$ was more abundant than $[\text{FA}(\text{L})]^+$. This fragmentation pattern will be referred to as FP2. All completely saturated (X:0/Y:0) SPLs exhibited FP2. From Figure 11 it was seen that 22:0 DHS was composed of 16:0/24:0, 17:0/23:0, and 18:0/22:0, with 16:0/24:0 being the most abundant based on the relative proportions of the FA and LCB fragment ions.

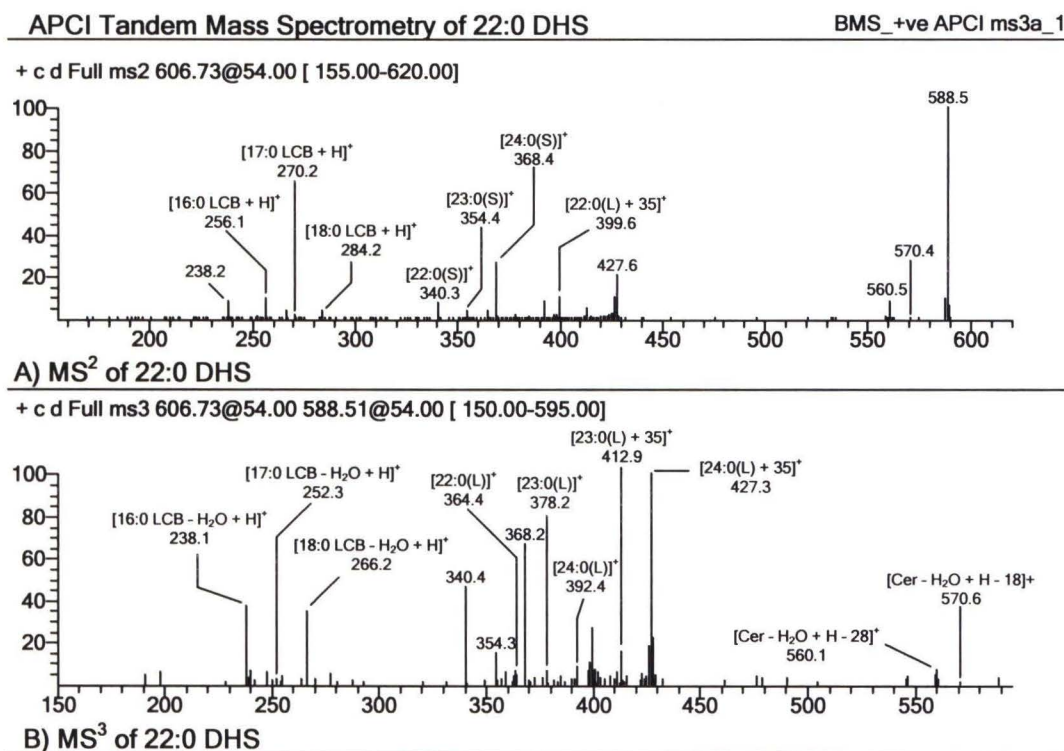


Figure 11. MS² (A) and MS³ (B) APCI mass spectra for 22:0 DHS

Unlike SPMs, the LCBs of DHSs were isobaric with saturated FA fragment ions. From Table 6 for example, it was seen that the $[16:0 \text{ LCB} + \text{H}]^+$ ion was isobaric with

$[16:0(S)]^+$. Since the ion at m/z 256.3 in the MS^2 m.s., was not observed in the MS^3 spectra, then this m/z only represented $[16:0\text{ LCB} + H]^+$. Furthermore, if there was $[16:0(S)]^+$ present then there would be a $[24:0\text{ LCB} + H]^+$ at m/z 368.4 overlapping with $[24:0(S)]^+$. Based on FP2, there should be a relatively abundant dehydrated 24:0 LCB ion at m/z 350.4 in both **11(A)** and **11(B)**. This however, was not observed. So, the absence of $[16:0(S)]^+$ and $[24:0\text{ LCB} - H_2O + H]^+$ fragment ions in the MS^3 m.s. eliminated 24:0/16:0 as a possible constituent of 22:0 DHS. In the second case where the $[16:0\text{ LCB} - H_2O + H]^+$ ion could have overlapped with $[13:0(L)]^+$, then there would be a $[13:0(S)]^+$ at m/z 214.3 in the MS^2 and MS^3 that was more abundant than m/z 238.2, based on FP2. Since this pattern was not observed, it was concluded that m/z 238.3 only represented the dehydrated 16:0 LCB ion. In addition, a 13:0 FA would have a $[25:0\text{ LCB} - H_2O + H]^+$ at m/z 364.3 overlapping with $[22:0(L)]^+$. An ion at m/z 382.3 was observed in both m.s. (Figure 11), but its abundance was inconsistent with FP2. In addition, the absence of a $[13:0(S)]^+$ indicated that 25:0/13:0 was not present. Finally, $[16:0\text{ LCB} - H_2O + H]^+$ could also represent a $[15:2(S)]^+$ from Table 6, but this FA cannot be combined with any LCB to yield a $[Cer + H]^+$ ion isobaric with $[22:0\text{ DHS Cer} + H]^+$.

This example does not represent all of the possible mass-overlaps that occurred in the MS^2 and MS^3 spectra. However, it demonstrated how to analyze and decipher these complex tandem m.s. using knowledge of the retention properties of the SPLs and their fragmentation patterns. All tandem m.s. were generally analyzed as described above.

2.2. Sphingolipids that have Fatty Acids with One Double Bond (X:A/Y:1)

21:1 SPM in CES will be used to illustrate the analysis of SPLs that have one double bond on their FA chain. As before, the first step was to check that 21:1 SPM

eluted at the correct RT. Because of the double bond on the FA chain, it was expected that $[21:1 \text{ SPM Cer} + \text{H}]^+$ (**12(C)**) should elute later than $[21:0 \text{ SPM Cer} + \text{H}]^+$ at 32.36 mins (**12(B)**). However, $[21:1 \text{ SPM} + \text{Cer} + \text{H}]^+$ had an earlier RT at 31.19 mins. This observation, coupled with the absence of the $[21:1 \text{ SPM} + \text{H}]^+$ (**12(D)**) and $[21:1 \text{ SPM} + 45]^-$ (**12(E)**) ions indicated that this group of SPLs was not present. The ion at m/z 588.6 was not $[21:1 \text{ SPM Cer} + \text{H}]^+$ but was the two- C^{13} isotope variant of $[22:0 \text{ SPM Cer} - \text{H}_2\text{O} + \text{H}]^+$. This was confirmed by noting that the peaks in **12(A)** and **12(C)** had similar RTs and chromatographic profiles, which indicated that both ions probably originated from the same molecule. The average MS^2 m.s. across the shaded region in **12(C)** (**12(F)**), showed all of the 22:0 SPM fragment ions along with their +1 and +2 isotope peaks, which confirmed the previous conclusion. Although there were ions at m/z 362.5 ($[22:1(\text{L})]^+$) and m/z 250.0 ($[17:0 \text{ LCB} - \text{H}_2\text{O} + \text{H}]^+$), which suggested the presence of 17:0/22:1, the absence of the $[22:1(\text{S})]^+$ (m/z 338.4), $[17:0 \text{ LCB} + \text{H}]^+$ (m/z 268.3), $[21:1 \text{ SPM} + \text{H}]^+$ and $[21:1 \text{ SPM} + 45]^-$ eliminated this as a possibility. This was yet another example of the importance of considering all pieces of available information.

The fragmentation profile of the MS^2 m.s. in **12(F)**, resembled the profile for the MS^3 m.s. in **10(B)**. This made sense, since **12(F)** was produced from the fragmentation of the + 2 isotope of the $[22:0 \text{ SPM Cer} - \text{H}_2\text{O} + \text{H}]$ ion. In addition, the plus two isotope exhibited FP1. The MS^3 (**12(G)**) did not yield any useful fragments which was typical for all the +2 isotopes. An interesting observation was that the + 2 isotope (**12(C)**) was approximately equal in abundance to $[21:0 \text{ SPM Cer} + \text{H}]^+$ (**12(B)**), which indicated that contributions from isotopes had to be considered when identifying and quantifying the SPLs. Finally, although $[\text{Y}:1 \text{ SPL Cer} + \text{H}]^+$ ions overlapped the +2 isotope of $[(\text{Y} + 1):0$

SPL Cer – H₂O + H]⁺ ions in the +APCI data, the masses and RTs of the [Y:1 SPL + H]⁺ ions were not isobaric with any other species under +ESI conditions. This meant that the EICs for the [M + H]⁺ of X:A/Y:1 SPLs provided definitive evidence of their presence, and this was used as an aid in deciphering the tandem APCI MS data.

The analysis of the ion at *m/z* 588.6 in CES was simple because there was no 21:1 SPM in this sample. In BMS however, the later RT of the [21:1 SPM Cer + H]⁺ ion (compared to [21:0 SPM Cer + H]⁺) at 32.81 min in **13(C)** and the presence of [21:1 SPM + H]⁺ and [21:1 SPM + 45]⁺ (**13(D)** and **13(E)** respectively), confirmed the presence of this group of SPLs. However, there was hump at the front edge of the peak in **13(C)** that started at approximately 30.50 min, which was earlier than 21:0 SPM at 31.00 min. This small peak at 31.31 min was the +2 isotope of [22:0 SPM Cer – H₂O + H]⁺ prior to being overwhelmed by the response from 21:1 SPM. This was a feasible deduction, since the 22:0 SPM eluted from 30.50 to 35.00 min. 21:1 SPM finished eluting by 36.00 min, which was consistent with the peaks for the protonated molecule and ammonium adduct ion. So, there was extensive overlap of these species in the full-scan APCI m.s. and the entire shaded region in Figure 13, represented both ions.

13(F) shows the average MS² m.s across the shaded region in **13(C)**. **13(G)** shows an extracted *m/z* range from 150 to 560, from **13(F)**. The first point to notice was that the profile of the **13(F)** was similar to other SPLs, with the [21:1 SPM Cer – H₂O + H]⁺ ion being the base peak, but different from **12(F)**. This suggested that the ion at *m/z* 588.6 contained [21:1 SPM Cer + H]⁺ ions. Now, 22:0 SPM was shown to be composed of 18:1/22:0, 17:1/23:0 and 16:1/24:0. The fragments from all of these molecules and their +1 and +2 isotopes were observed in the MS² and MS³ spectra. These ions are labeled in

Figure 13, where the curly brackets indicated a group of isotope peaks and their masses are listed in order of abundance. The $[23:1(L)]^+$ at m/z 376.4 and $[16:1 LCB - H_2O + H]^+$ at m/z 236.2 were present in **13(F – H)**, which indicated that 21:1 SPM was composed of 16:1/23:1, 17:1/22:1 and 18:1/21:1.

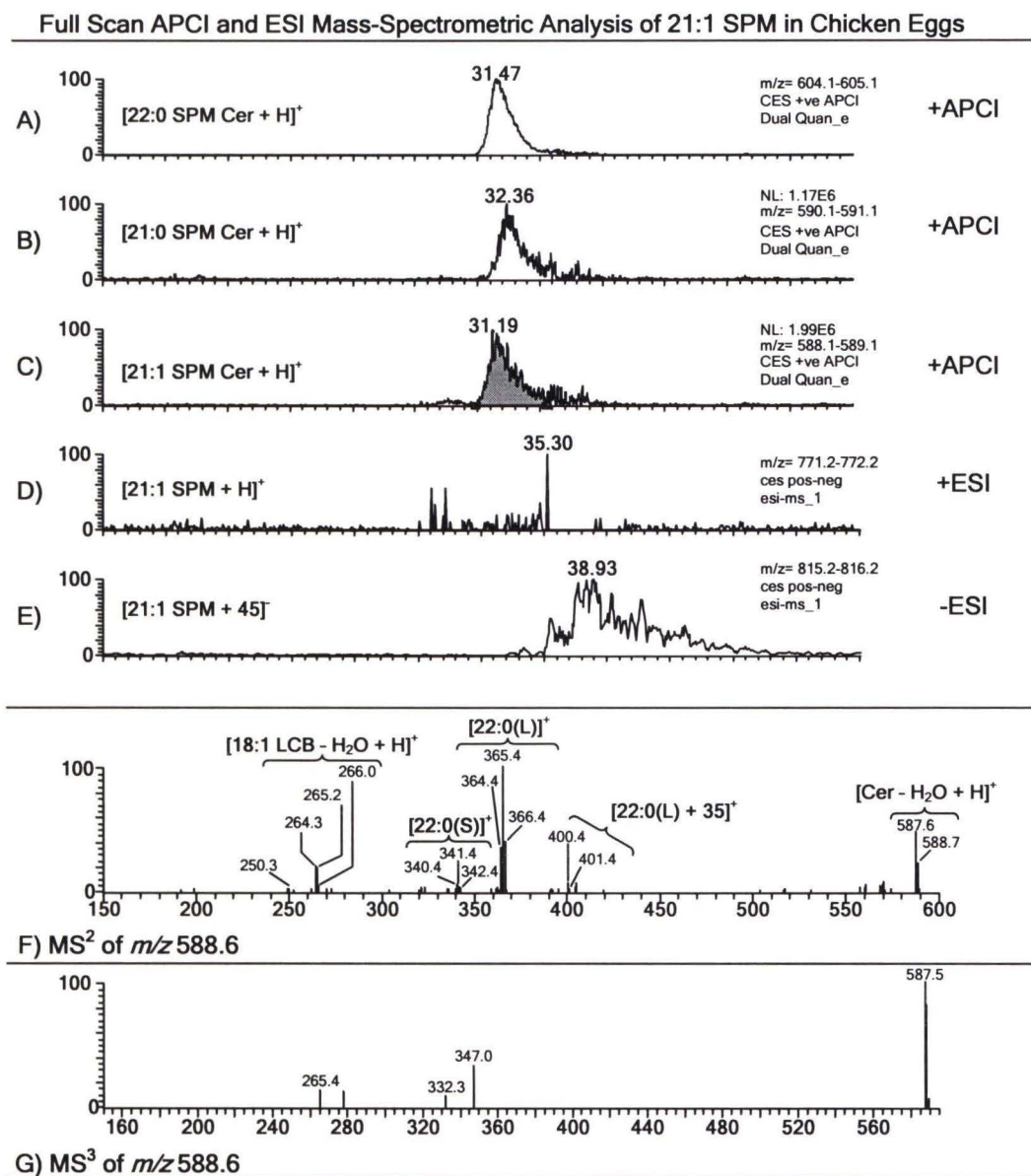


Figure 12. Identification of the ion at m/z 588.6 as the plus two isotope of the 22:0 SPM dehydrated ceramide fragment ion in chicken egg yolk.

The analysis of Y:1 DHSs was similar to that described above. An important point to note was that X:0/Y:1 SPLs exhibited FP1 fragmentation, unlike DHSs with saturated FA chains which exhibited FP2 fragmentation. Also, it was observed that the MS³ fragmentation of Y:1 SPLs that overlapped with the +2 isotope of (Y + 1):0 SPLs produced few recognizable fragment ions, which inhibited the deciphering of the LCB/FA composition. Typically, in this scenario, the [FA(S)]⁺ and [LCB + H]⁺ ions were of very low abundance. A similar observation was made for the Y:2 SPLs. Despite this complexity however, knowledge of the FPs allowed the LCB/FA compositions of the Y:1 and Y:2 SPLs to be elucidated.

2.3. Sphingolipids that have Fatty Acids with Two Double Bonds (X:A/Y:2)

CES contained 18:2 SPM, 22:2 SPM and 24:2 SPM. CES was the only SPM extract that was found to contain X:A/Y:2 SPLs. 22:2 SPM will be used to illustrate the identification of these molecules. [X:A/Y:2 Cer + H]⁺ ions were isobaric with [X:A/(Y + 1):0 Cer – H₂O + H]⁺ ions. Therefore, the analysis of the EICs and m.s. was similar to that described for X:A/Y:1 SPLs.

Points of interest from the analysis were: 1) X:A/Y:2 SPLs exhibited FP1 fragmentation under APCI conditions; 2) the MS² profile for the ion at *m/z* 600.6 in Figure 14 was that expected for a protonated ceramide ion, in which the [Cer – H₂O + H]⁺ ion was the base peak, because 22:2 SPM was present in this sample. In BMS or BBS where there were no Y:2 SPLs however, the MS² m.s. was similar to **12(F)**. The reason for this observation was previously explained for the Y:1 SPLs; and 3) the MS³ m.s. contained few recognizable fragment ions; and 4) The peak for the [X:A/Y:2 + H]⁺

Analysis of 21:1 SPM from Bovine Milk

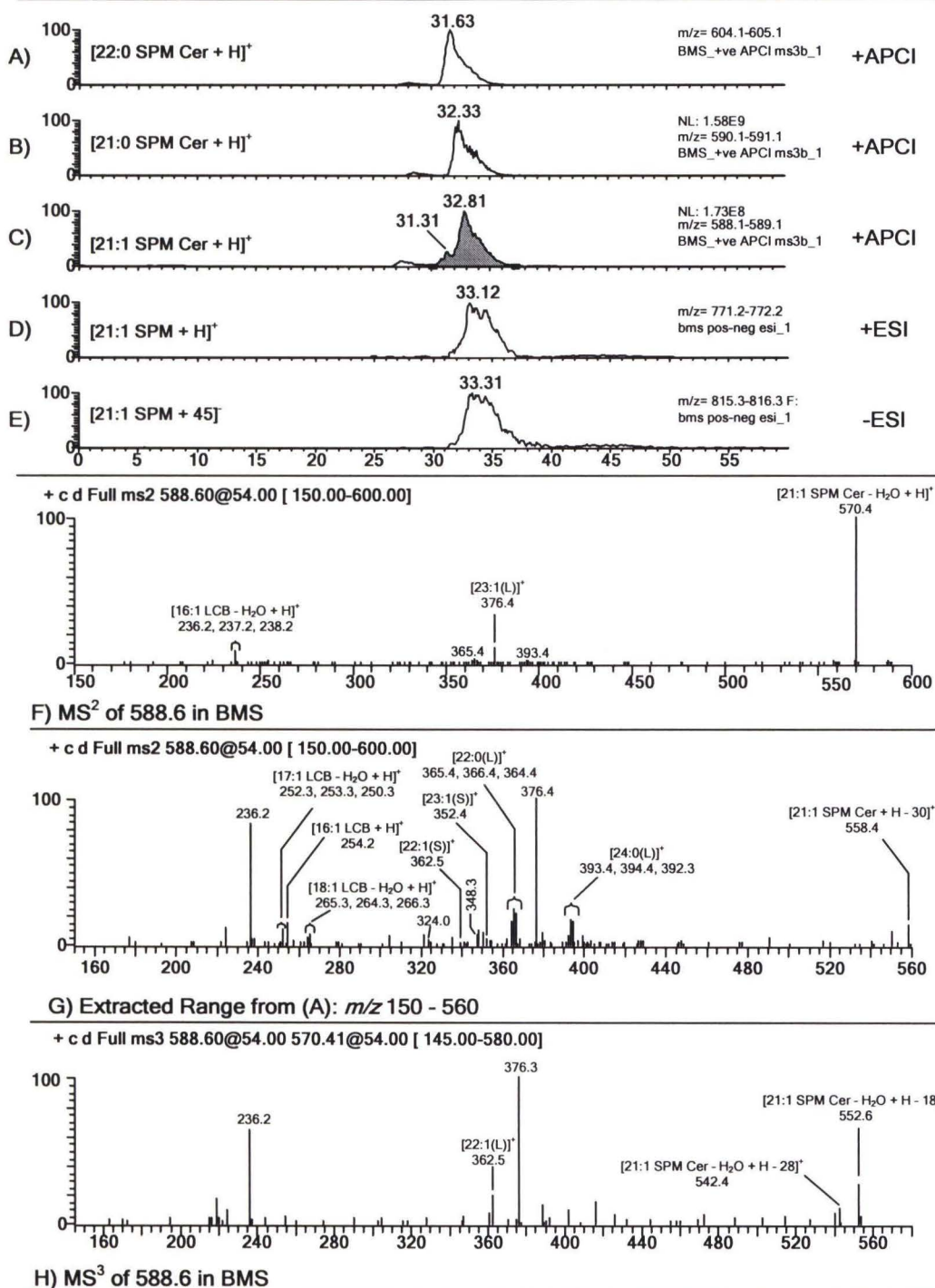


Figure 13. Mass spectrometric analysis of 21:1 SPM in bovine milk. The mass spectra (F – H) and late RT of the species at m/z 588.6 was [21:1 SPM Cer + H]⁺ and the +2 isotope of [22:0 SPM Cer – H₂O + H]⁺. The [21:1(L)]⁺ and [21:1(S)]⁺ ions were present at m/z 348.3 and 324.0 respectively.

Analysis of 22:2 SPM from Chicken Eggs

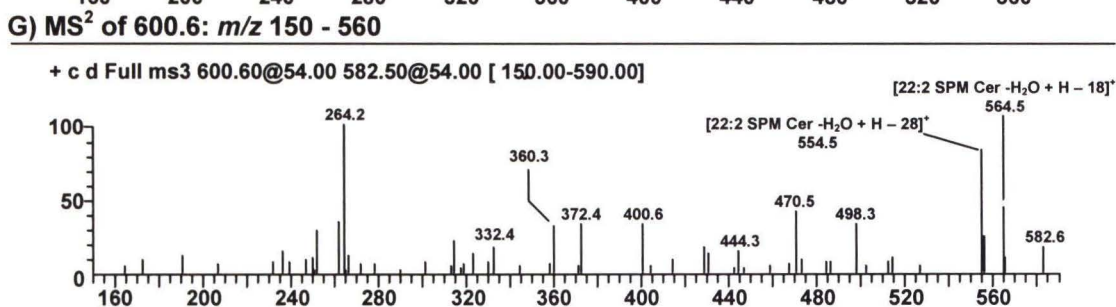
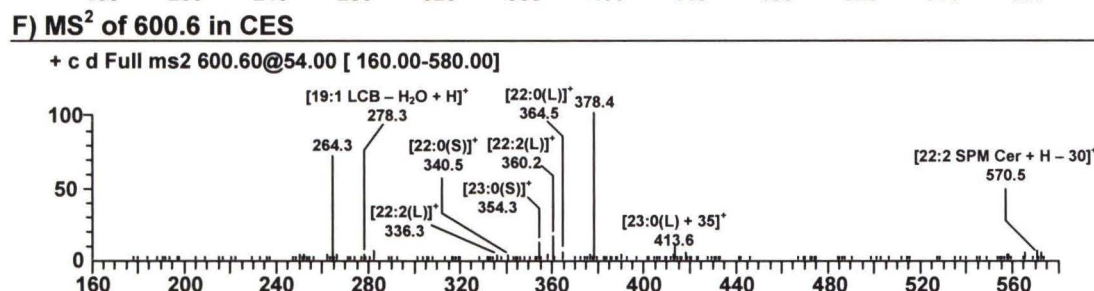
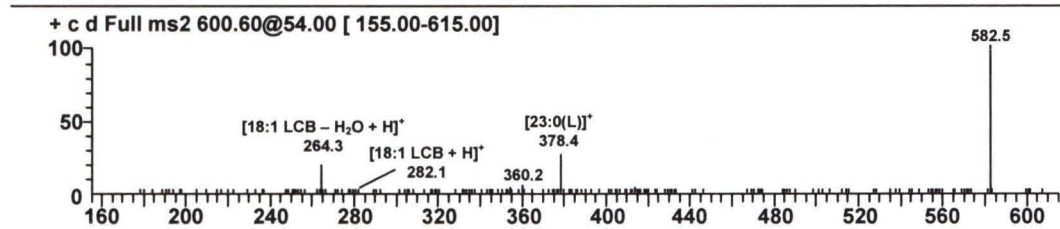
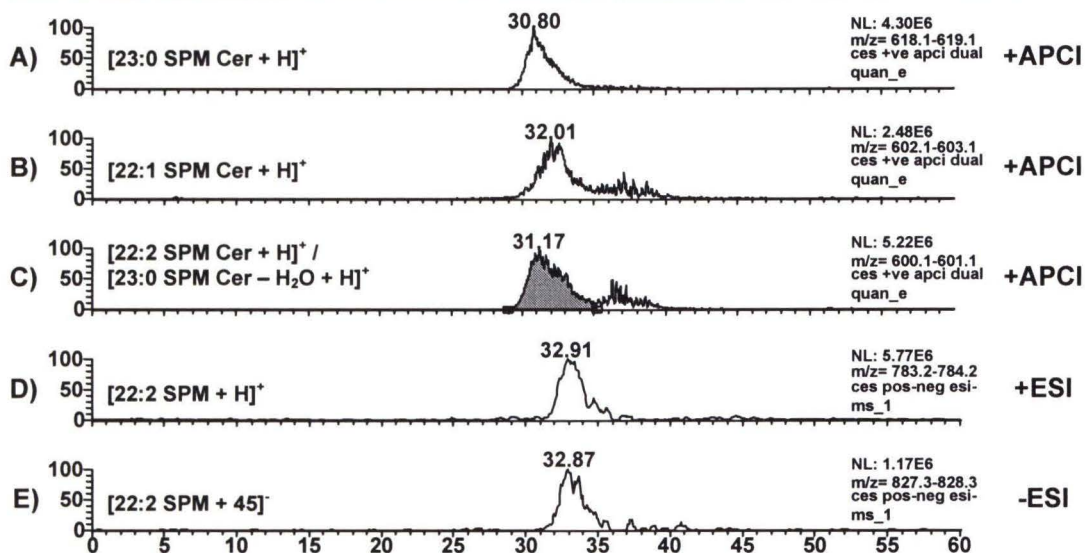


Figure 14. Mass spectrometric analysis of 22:2 SPM in chicken egg yolk. The mass spectra (F – H) and late RT of the species at m/z 600.6 was [22:2 SPM Cer + H]⁺ and [23:0 SPM Cer - H₂O + H]⁺.

ion overlapped with the peak for the $[X:A/(Y - 2) + Na + 2]^+$ ions, when the latter was extremely abundant. This meant therefore, that the $[X:A/Y:2 + 45]^-$ ion was a more definitive indicator of the presence of Y:2 SPLs, since it was not isobaric with any other closely eluting SPL ions.

2.4. Hydroxy-Sphingolipids

The identification of these species will be demonstrated using hydroxy 16:0 SPM (or 16:0 SPMOH) in CES. Hydroxy SPLs should have a later RT than their non-hydroxy counterparts, because of the increase in polarity due to the presence of the hydroxyl group. So, 16:0 SPMOH, which produced the ion at m/z 536.6 should have a later RT than $[16:0 \text{ SPM Cer} + H]^+$. Figure 15 shows that this retention behavior was observed. **15(C)** and **15(D)** show the identification of the 18:1/16:0OH and 18:1OH/16:0 SPLs in CES by tandem MS. Scheme 4 shows the primary fragmentation pathway for 18:1/16:0OH under APCI-MS conditions. All these fragments, except the $[16:0OH(S)]^+$ and $[16:0OH(S) - H_2O^a]^+$ ions which were of very low abundance, were labeled in the MS² and MS³ spectra, thereby confirming the presence of this species. The tandem MS of hydroxy-SPLs was different from that of normal SPLs in that the FA fragment ions were 16 units larger than their non-hydroxyl counterparts. The dehydrated hydroxy-FA fragment ions were also observed.

So, for 18:1/16:0OH, the $[16:0OH(L)]^+$ ion at m/z 296.1 and its dehydrated fragment at $[16:0OH(L) - H_2O]^+$ were observed along with the 18:1 LCB fragment ions. *Mass-to-charge* ratios 254.3 and 272.3 were only observed in the MS² m.s, and were of very low abundance. The ions at m/z 280.1 and 256.3 indicated the presence of $[16:0(L)]^+$ and $[16:0(S)]^+$ respectively. This suggested that 18:1OH/16:0 was coeluting with

18:1/16:0OH. This was confirmed by the ion at m/z 298.3 which corresponded to the $[18:1\text{OH LCB} + \text{H}]^+$. The $[18:0\text{OH LCB} - \text{H}_2\text{O} + \text{H}]^+$ was isobaric with the $[16:0(\text{L})]^+$ ion. Schemes 5 and 6 show two fragmentation pathways for 18:1OH/16:0, with the latter showing the $[18:1\text{OH LCB} + \text{H}]^+$ ion. All these fragments were observed in the MS^2 and MS^3 m.s., thereby confirming the presence of these species.

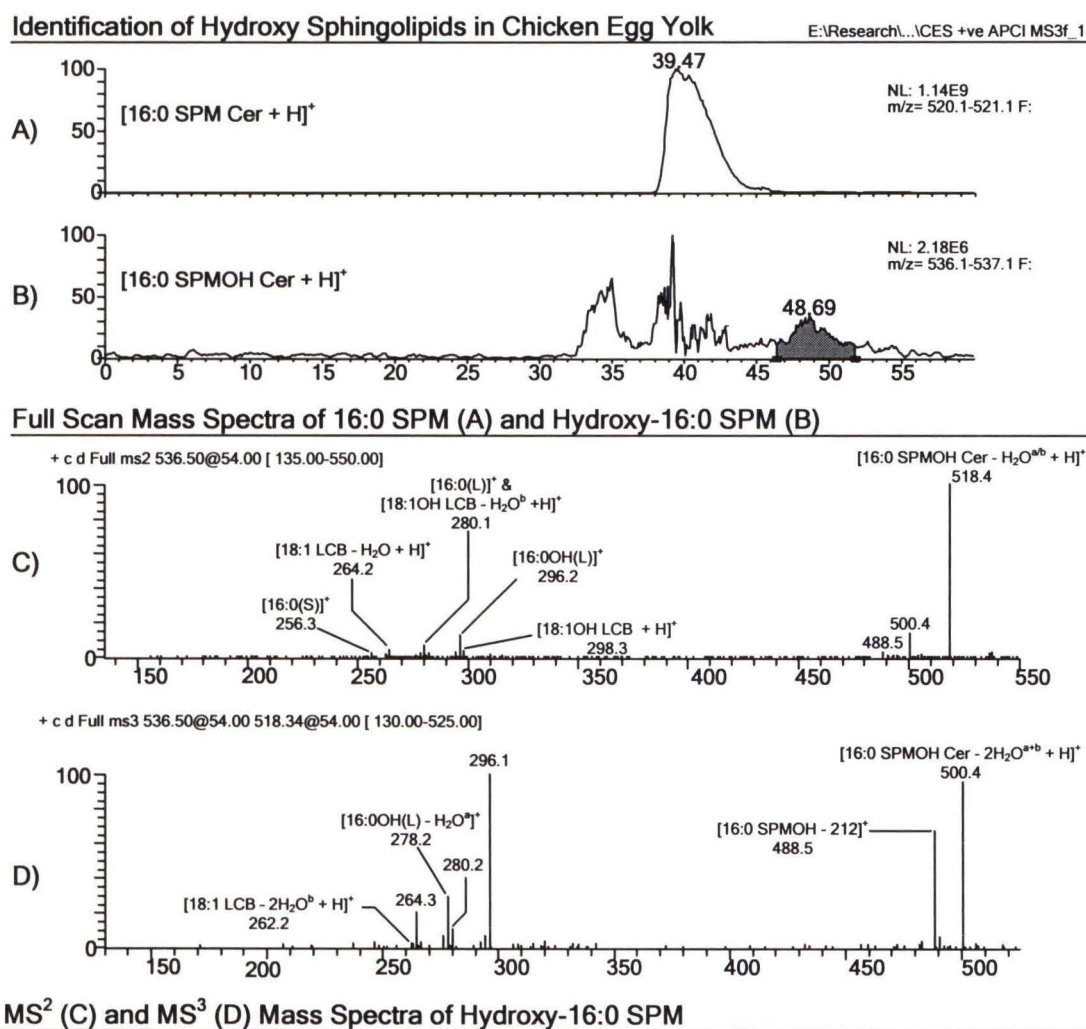


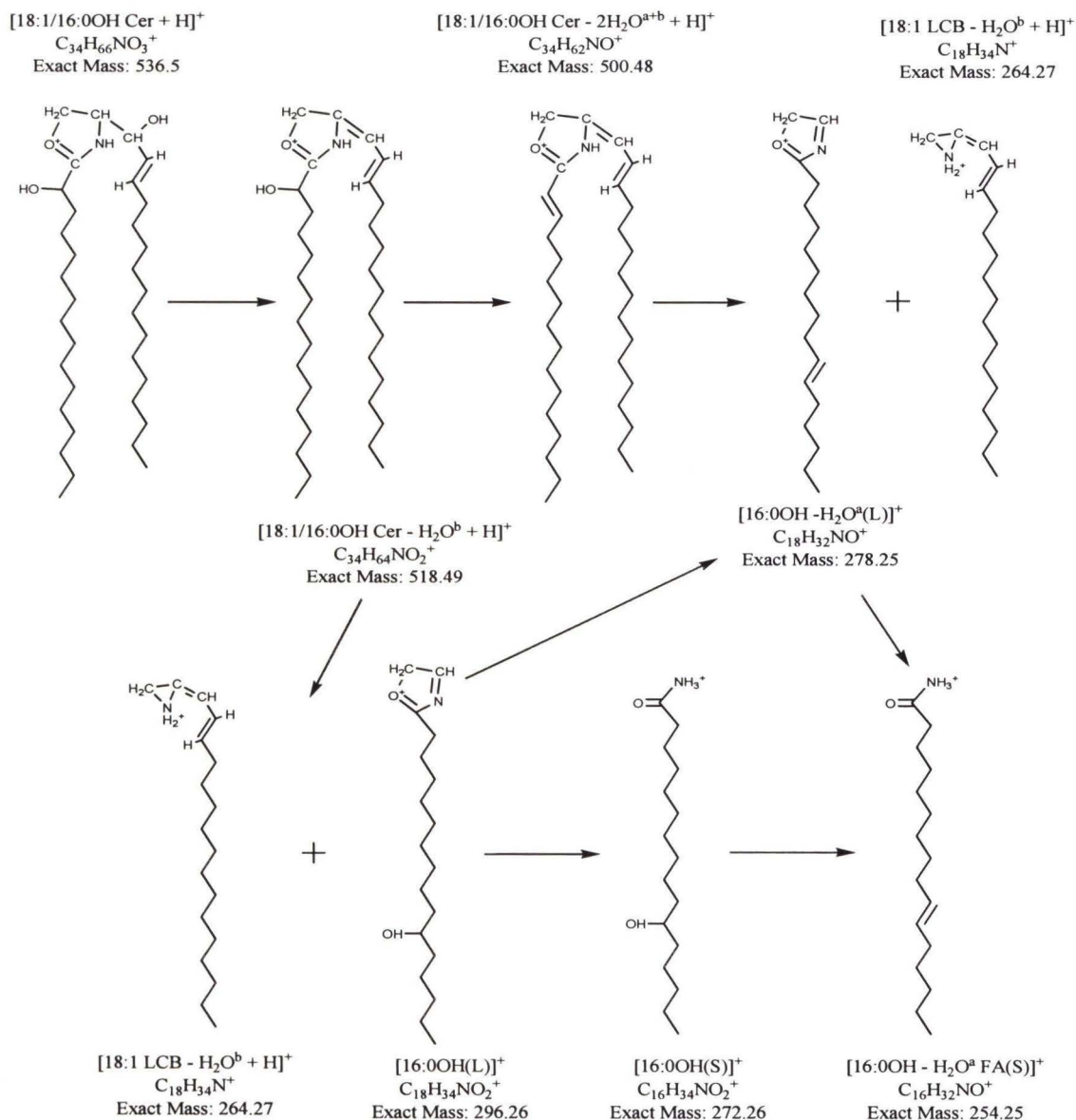
Figure 15. A) EIC for $[16:0 \text{ SPM Cer} + \text{H}]^+$ showing that hydroxy-16:0 SPM (B) had a later RT. The MS^2 (C) and MS^3 (D) mass spectra across the shaded region in (B) showed the fragment ions used to identify this species. The $[16:0\text{OH}(\text{S})]^+$ and its dehydrated fragment ion at m/z 272.3 and 254.3 were present at very low abundances in the MS^2 mass spectra.

Scheme 4: Proposed Fragment Ions formed from 18:1/16:0OH Under

APCI MS, MS² and MS³ Conditions

^a - Additional hydroxyl group

^b - Standard hydroxyl group on the LCB



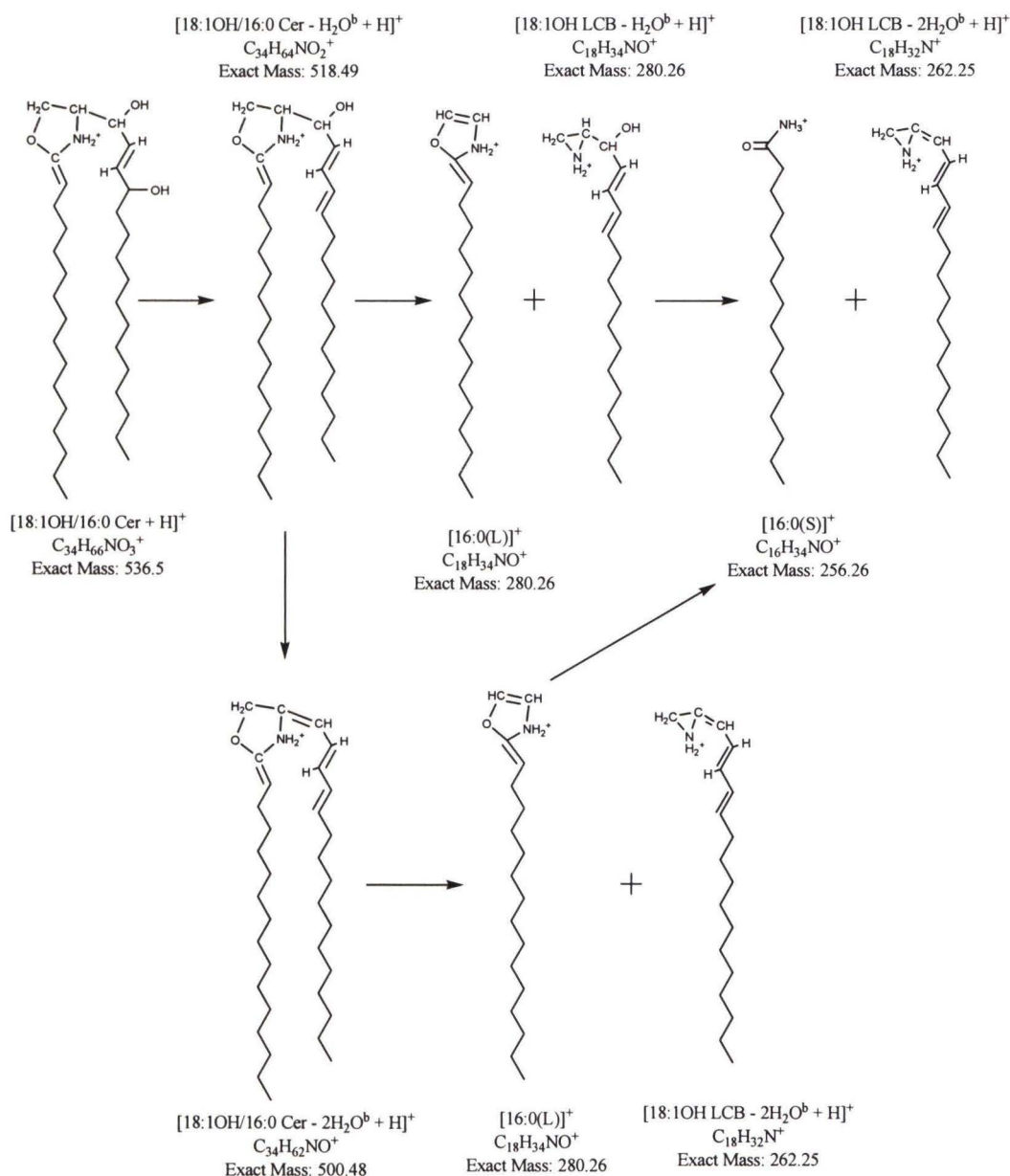
Scheme 4: Proposed fragment ions formed from 18:1/16:0OH under APCI-MS conditions. Superscript ‘a’ is used to represent the additional hydroxyl group in the molecule. The normal –OH on the LCB is denoted by superscripted ‘b’.

Scheme 5: Proposed Fragment Ions formed from 18:1OH/16:0 Under

APCI MS, MS² and MS³ Conditions – Pathway 1

^a - Additional hydroxyl group

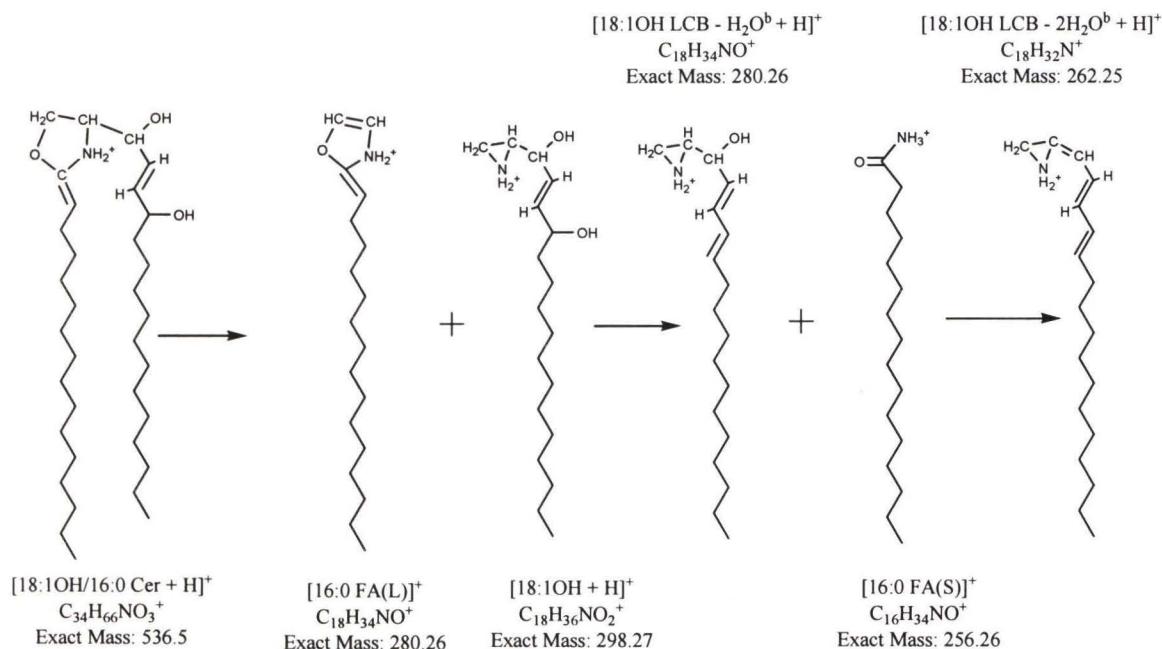
^b - Standard hydroxyl group on the LCB



Scheme 5: Fragmentation of 18:1OH/16:0 under APCI-MS conditions (pathway 1). Superscript ‘a’ is used to represent the additional hydroxyl group on the LCB Backbone. The normal –OH on the LCB is denoted by superscript ‘b’.

Scheme 6: Proposed Fragment Ions formed from 18:1OH/16:0 Under

APCI MS, MS² and MS³ Conditions – Pathway 2



Scheme 6: Fragmentation pathway of 18:1OH/16:0 under APCI-MS conditions (pathway 2). Superscript ‘a’ is used to represent the additional hydroxyl group on the LCB Backbone. The normal –OH on the LCB is denoted by superscript ‘b’.

Tables 61 and 62 show the hydroxy-SPLs that were identified in bovine milk and chicken egg yolk, respectively. All three SPM extracts had very low amounts of these species, which prevented them from being quantified.

2.5 Other Fragment Ions

In addition to the primary fragments illustrated in Scheme 2, Karlsson *et al.* reported 9 other fragments ions, which are shown in Figure 16, using 16:0 SPM as an example. Figure 17 shows the EICs for these ions plus the protonated and dehydrated ceramide ions, for 16:0 SPM. The similar RTs suggested that these ions, except for [16:0

SPM – N(CH₃)₃ – H₂O + Na]⁺, appeared to be present. Of course, their identities can only be proven using tandem MS. The MS² and MS³ m.s. for the ion in **17(F)** are shown in **18(D)** and **18(E)**, respectively. Comparison with the MS, MS² and MS³ m.s. of the [16:0 SPM Cer + H]⁺ ion in **18(A – C)**, confirmed that this ion originated from 16:0 SPM. The same FA, LCB and dehydrated ceramide fragment ions were observed for both species.

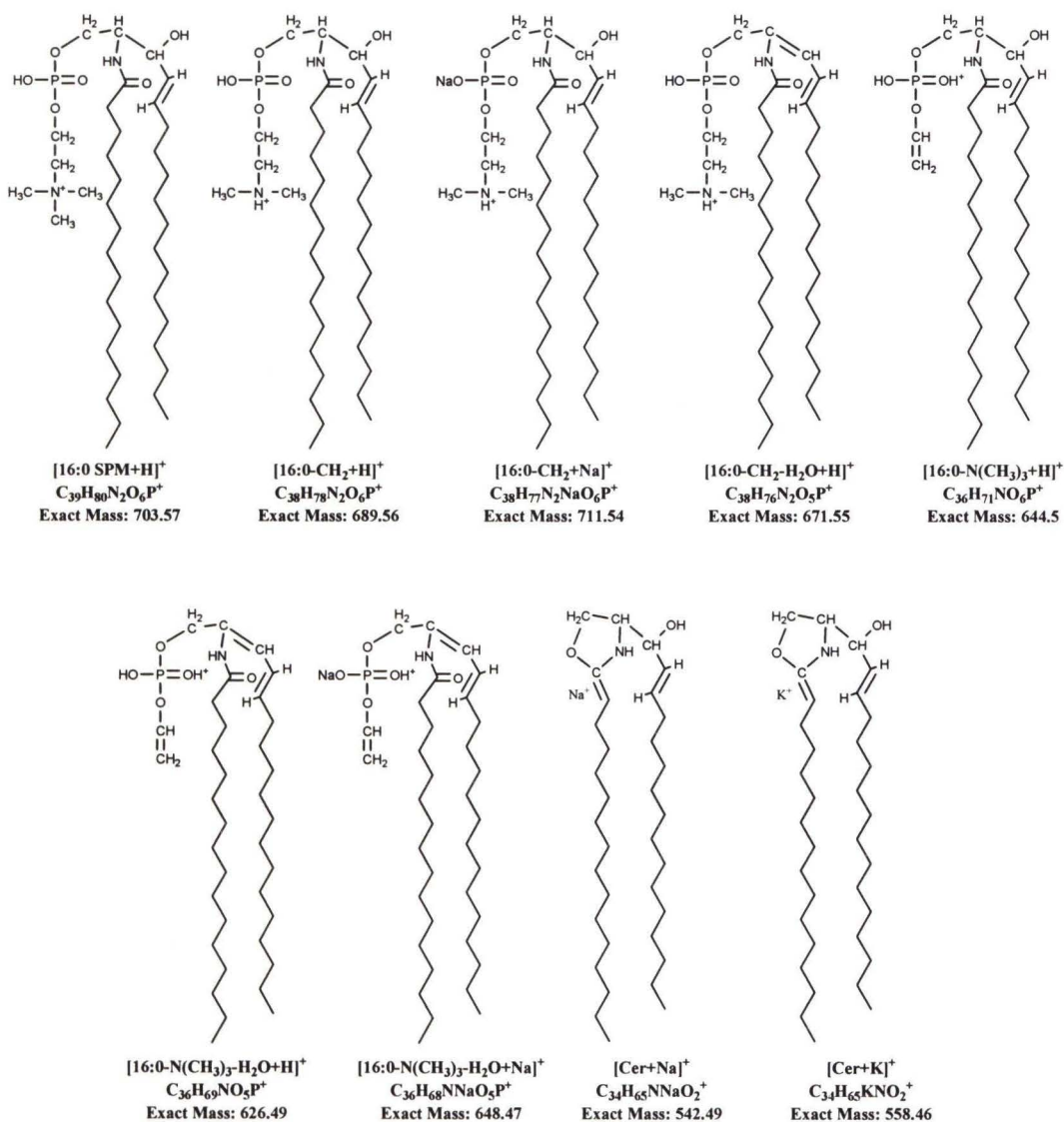


Figure 16. Other fragment ions observed under APCI-MS conditions. These fragments were very abundant in the APCI mass spectra obtained by Karlsson *et al.*¹ However, in our experiments their abundances were much lower in comparison to the protonated ceramide ion.

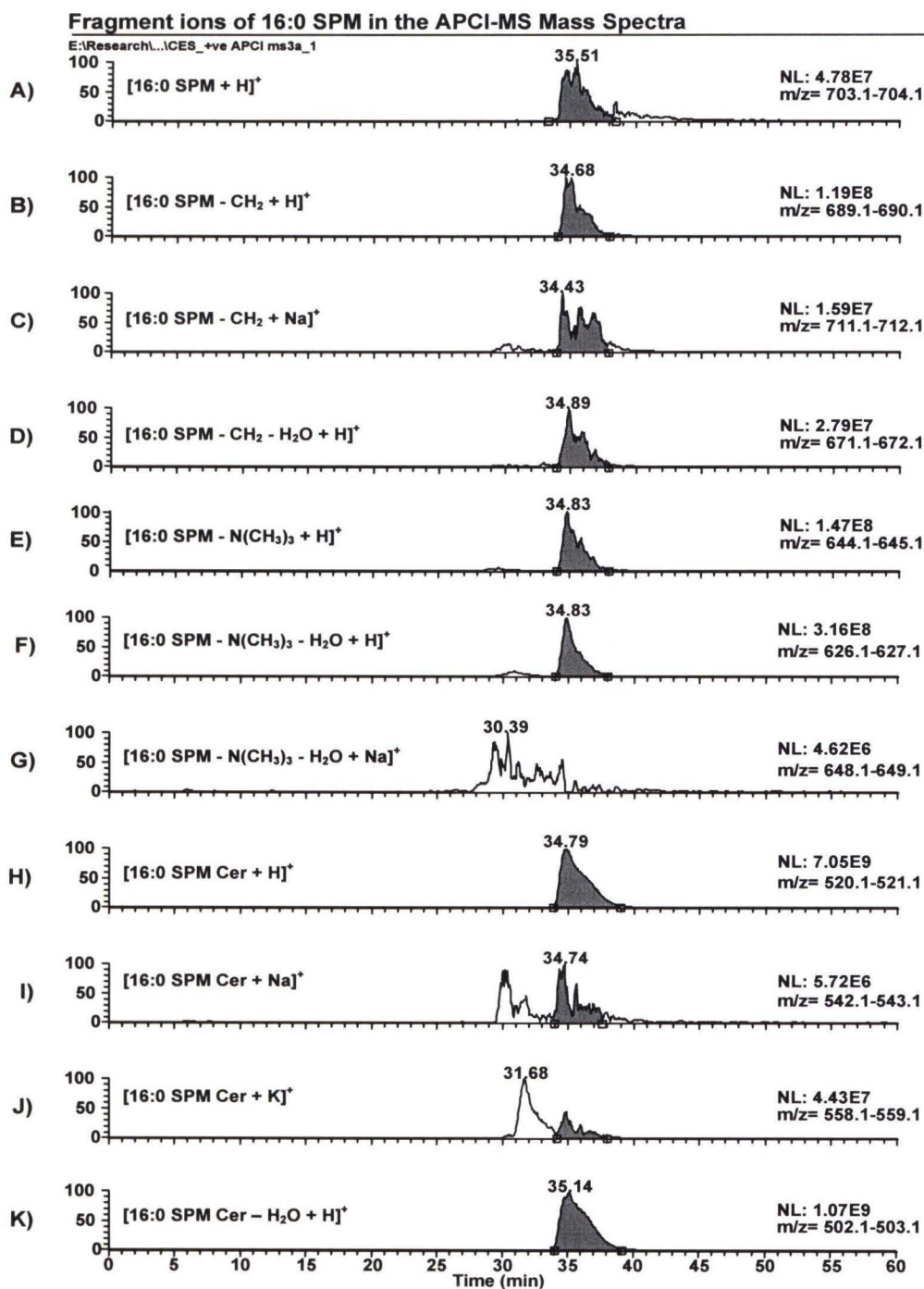


Figure 17. Extracted ion chromatograms showing the fragments from 16:0 SPM under APCI-MS conditions. [16:0 SPM Cer + H]⁺ and its dehydrated ceramide fragment ions were the most abundant. All the other ions were 1 to 2 orders of magnitude less in abundance. Figure 18 shows that all the fragments, except [16:0 SPM Cer - H₂O + H]⁺, had a very low abundances relative to the protonated ceramide ion.

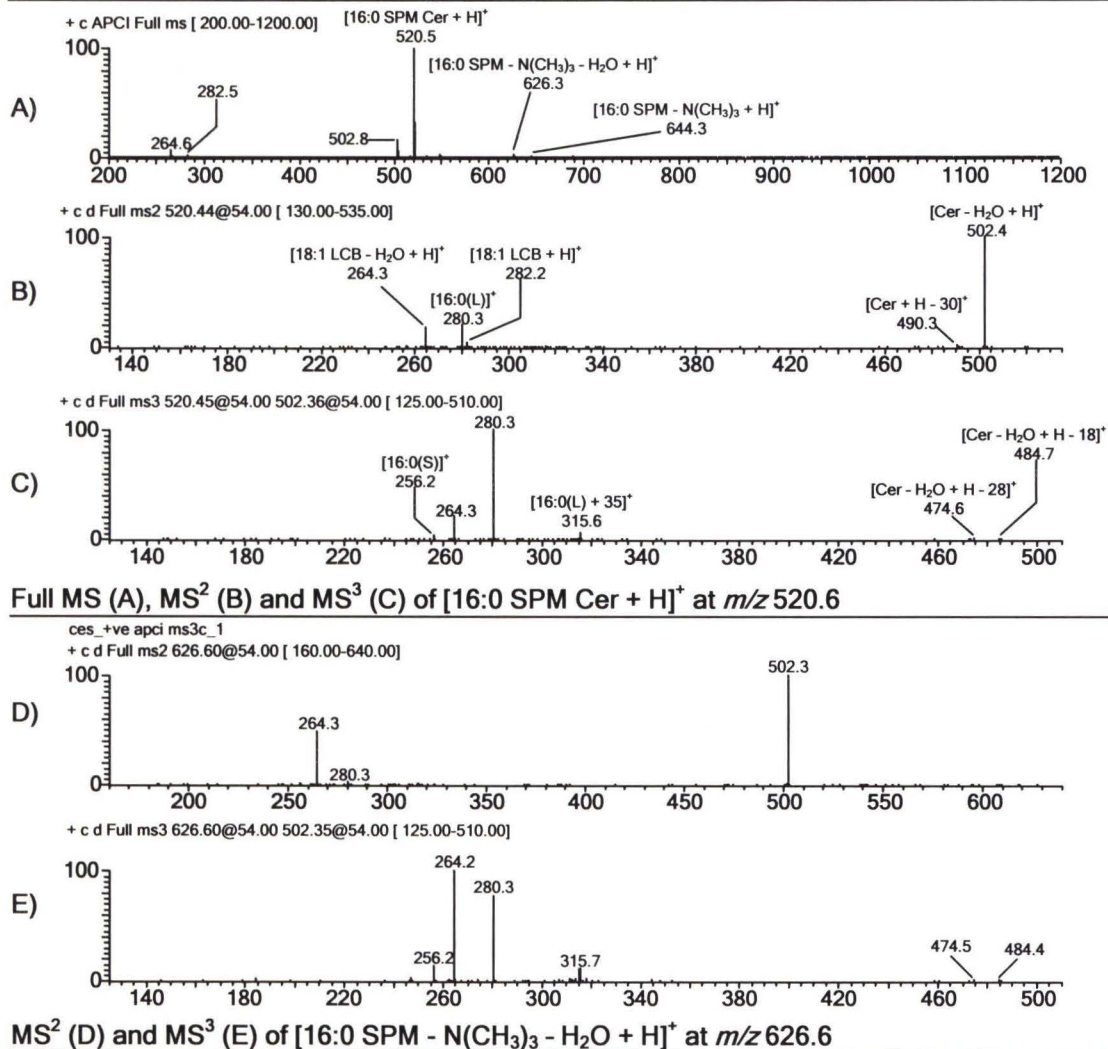


Figure 18. Mass spectra showing that the ion at m/z 626.6 was $[16:0 \text{ SPM} - \text{N}(\text{CH}_3)_3 - \text{H}_2\text{O} + \text{H}]^+$ by comparison with the MS² (B) and MS³ (C) mass spectra for $[16:0 \text{ SPM Cer} + \text{H}]^+$. Both ions had the same LCB and FA fragment ions in the tandem MS data.

The ion at m/z 644.6, $[16:0 \text{ SPM} - \text{N}(\text{CH}_3)_3 + \text{H}]^+$, was also identified by APCI tandem MS. No tandem MS data was obtained for 17(I) and 17(J) because of their low abundances. The ions in 17(A – D) had odd masses and so were not included in the parent mass lists used to specify the ions on which MS/MS experiments were performed. Except for these four fragments, all the other ions had even masses.

From **18(A)** it was observed that the abundances of all of the ions in Figure 16 was very low in relation to $[16:0 \text{ SPM Cer} + \text{H}]^+$. As a result, tandem MS data was not obtained for many of these fragments. Also, since many of these ions had even masses, there was extensive overlapping of the masses of these fragments with other SPL fragment ions. In our work however, the low abundance of these fragments did not pose a serious problem, and the APCI m.s. was easy to decipher. As will be shown later however, these fragments were extremely abundant in the APCI m.s. obtained by Karlsson *et al.*, due to the use of upfront CID. As one can imagine, this complexity would significantly inhibit the accurate analysis and quantification of the SPLs.

3. QUANTIFICATION

As will become clear, the method used to quantify a specific SPL molecule depended on the way in which it was identified. The +APCI MS, MS^2 and MS^3 , +ESI and -ESI data were all used to determine the relative mole percent composition of the SPLs. To quantify the SPLs by APCI-MS it was assumed that all the molecules within the same SPL group had similar ionization efficiencies. If this were true we could, for example, divide the area of the peak for $[20:0 \text{ SPM Cer} + \text{H}]^+$ among its SPL constituents, based on the relative intensities of the $[\text{FA(L)}]^+$ fragments for each SPL in the group. For SPLs with a double bond anywhere in the molecule, the $[\text{FA(L)}]^+$ ions were used to calculate the proportioning factors (PFs), because they were most abundant fragment ions that distinguished between the constituent SPL molecules. Though the dehydrated ceramide ion was the most abundant fragment in the MS^2 m.s., it did not provide definitive information about the LCB/FA composition. For saturated DHSs the $[\text{FA(S)}]^+$ ions were used to divide the area of the protonated ceramide and dehydrated ceramide ions in EICs

among its constituent molecules. This was the general approach used to determine the LCB/FA composition of the SPL mixtures.

Because of the complexity of the methods used to quantify these SPL mixtures, it is best explained using specific examples. It is important to note at this point however, that the methods of quantification described below were dependent on the composition of the SPL mixtures. The scenarios that were encountered during the analysis did by no means exhaust all the possibilities that could occur. For example, in BBS, BMS and CES no Y:2 DHSs were identified. If these were present however, the method used to determine the LCB/FA composition would have to be modified in order to handle any problems associated with the quantification of these species. The analysis illustrated below however, provided a general approach to quantifying SPLs by APCI and ESI MS, and although it does not account for all the possibilities that could occur in any SPL mixture, the principles and methodologies that will be outlined provided a foundation for the analysis of any SPL mixture.

3.1. Quantification of X:A/Y:0 and X:A/Y:2 Sphingolipids

The first step in the quantification of any SPL depended on whether or not the components of the SPL group of interest were identified. The components of 20:0 SPM were identified as 16:1/22:0, 17:1/21:0 and 18:1/22:0. The next step was to check if $[20:0 \text{ SPM Cer} - \text{H}_2\text{O} + \text{H}]^+$ overlapped with $[19:2 \text{ SPM Cer} + \text{H}]^+$. The absence of $[19:2 \text{ SPM} + \text{H}]^+$ and $[19:2 \text{ SPM} + 45]^-$ confirmed that 19:2 SPM was not present. So, the peaks for the $[20:0 \text{ SPM Cer} + \text{H}]^+$ (**19(A)**), $[20:0 \text{ SPM Cer} - \text{H}_2\text{O} + \text{H}]^+$ (**19(B)**) and $[20:0 \text{ SPM} + \text{H}]^+$ (**19(C)**) in EICs were integrated over approximately the same RT range (Figure 19).

Because there was no mass overlap between unsaturated LCBs and saturated FA fragment ions (Table 5), the raw areas of the protonated ceramide, dehydrated ceramide, and protonated molecule of any X:1/Y:0 SPL, were proportioned based on the relative intensities of the $[\text{FA(L)}]^+$ ions in the APCI MS^2 m.s. **20(C)** shows the averaged MS^2 mass spectrum across the $[20:0 \text{ SPM Cer} + \text{H}]^+$ peak in **20(A)**. **20(D)**, **20(E)** and **20(F)** show the intensities of the $[20:0(\text{L})]^+$, $[21:0(\text{L})]^+$ and $[22:0(\text{L})]^+$ ions in **20(C)**, respectively. Assuming that 1) the peak in **20(A)** contained only 20:0 SPM SPLs and 2) the relative intensities of the $[\text{FA(L)}]^+$ ions in the MS^2 m.s. was equal to the relative proportions of the SPL molecules that constituted the 20:0 SPM group, the area of the $[20:0 \text{ SPM Cer} + \text{H}]^+$ peak (**19(A)**) was proportioned based on the intensities of these FA fragment ions.

The area attributable to each component of 20:0 SPM was calculated as follows:

Proportioning factors (PFs) from the $[20:0 \text{ Cer} + \text{H}]^+$ APCI MS^2 m.s. were calculated

$$I[20:0(\text{L})]^+ + I[21:0(\text{L})]^+ + I[22:0(\text{L})]^+ = I_{\text{Total}}$$

$$\frac{I[20:0(\text{L})]^+}{I_{\text{Total}}} = \text{PF}_{18:1/20:0}$$

$$\frac{I[21:0(\text{L})]^+}{I_{\text{Total}}} = \text{PF}_{17:1/21:0}$$

$$\frac{I[22:0(\text{L})]^+}{I_{\text{Total}}} = \text{PF}_{16:1/22:0}$$

Integrated peaks for 20:0 SPM

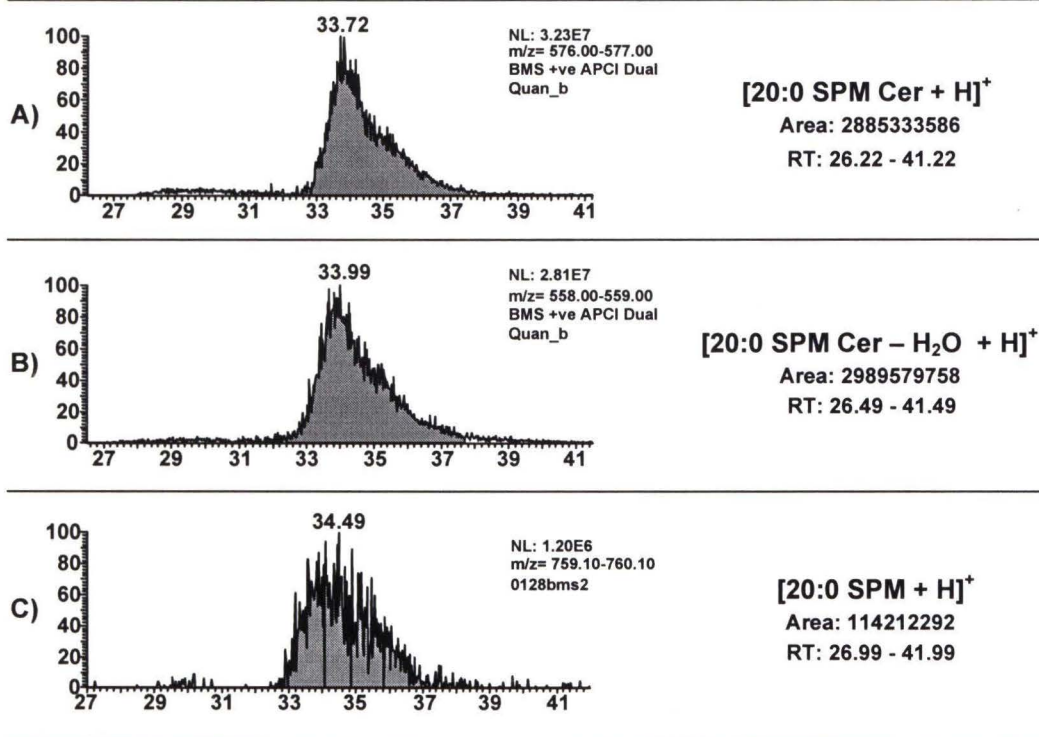


Figure 19. Integration of the peaks for the protonated ceramide ion, dehydrated ceramide ion and protonated molecule of 20:0 SPM in EICs. The area and RT range over which the peak was integrated are shown.

The area for each SPL in 20:0 SPM by APCI-MS was then calculated.

$$A[20:0 \text{ SPM Cer} + H]^+ + A[20:0 \text{ SPM Cer} - H_2O + H]^+ = A_{\text{Total}}$$

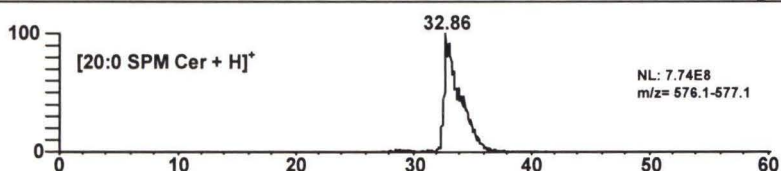
$$PF1_{18:1/20:0} \times A_{\text{Total}} = FAA_{18:1/20:0}$$

$$PF1_{17:1/21:0} \times A_{\text{Total}} = FAA_{17:1/21:0}$$

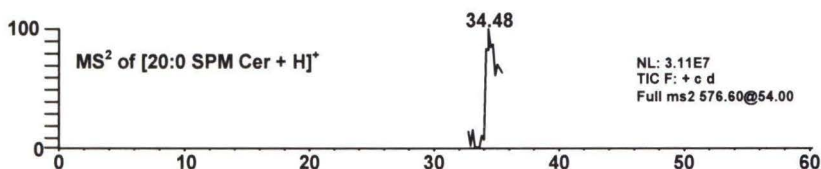
$$PF1_{16:1/22:0} \times A_{\text{Total}} = FAA_{16:1/22:0}$$

Quantification of 20:0 SPM

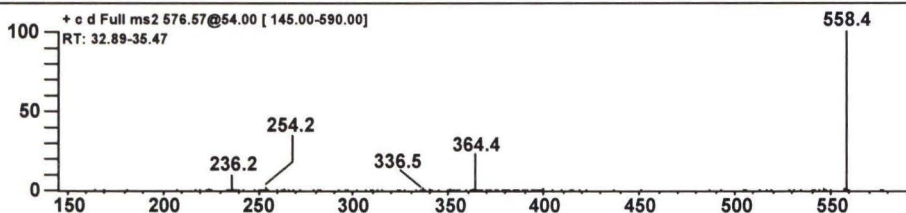
E:\Research\...APCI\BMS_+ve APCI ms3a_1



A) APCI MS EIC for 20:0 SPM



B) APCI MS² TIC for 20:0 SPM



C) Averaged APCI MS² Mass Spectra

+ c d Full ms2 576.60@54.00

RT: 32.89-35.47

m/z	Intensity	Relative
327.0	1668.8	0.02
333.4	1430.2	0.02
335.0	3454.6	0.04
336.5	113389.7	1.29
337.1	3.4	0.00
340.3	52641.1	0.60

D) Spectrum List of (C) Showing [20:0(L)]⁺ Intensity

+ c d Full ms2 576.60@54.00

RT: 32.89-35.47

m/z	Intensity	Relative
341.8	990.1	0.01
345.3	4213.1	0.05
349.2	1897.5	0.02
350.4	47833.5	0.54
352.5	5838.6	0.07
353.3	619.2	0.01

E) Spectrum List of (C) Showing [21:0(L)]⁺ Intensity

+ c d Full ms2 576.60@54.00

RT: 32.89-35.47

m/z	Intensity	Relative
361.1	1420.6	0.02
362.3	54980.3	0.62
363.7	6828.6	0.08
364.4	2017475.4	22.87
365.5	2756.9	0.03
366.3	1064.1	0.01

F) Spectrum List of (C) Showing [22:0(L)]⁺ Intensity

Figure 20. (D), (E) and (F) show the intensities of [20:0(L)]⁺, [21:0(L)]⁺ and [22:0(L)]⁺ in the MS² mass spectra for 20:0 SPM (C). These intensities were used to calculate the proportioning factor necessary to divide the area of the [20:0 SPM Cer + H]⁺ peak (A) among its constituent SPLs.

In the above equations, the superscripted symbols ‘I’, ‘A’, ‘FAA’ and ‘PF’ meant “Intensity”, “Area”, “Final adjusted area” and “Proportioning Factor”, respectively. The number ‘1’ after PF indicated that this proportioning factor was calculated from the MS² m.s. of the protonated ceramide ion. A ‘2’ designated that the PFs were calculated from the MS² m.s. of a dehydrated ceramide ion. The use of PF2 will be illustrated shortly. Also, I_{Total} and A_{Total} represented “Total Intensity” and “Total Area”, respectively. Substituting the values in Figures 19 and 20 into the equations above resulted in areas of 2768351537.06, 65636459.93, 155591761.01, for 16:1/22:0, 17:1/21:0 and 18:1/20:0, and respectively. These areas represented 0.26%, 4.56% and 0.11% of the total SPM population in BMS, respectively. These percentages were calculated using the equations below:

The mole percent of each SPL of the SPM population in BMS from APCI-MS was calculated.

$$\frac{^{FAA}18:1/20:0}{\text{Total Area of the SPMs from APCI-MS}} = \% \text{ of } 18:1/20:0$$

$$\frac{^{FAA}17:1/21:0}{\text{Total Area of the SPMs from APCI-MS}} = \% \text{ of } 17:1/21:0$$

$$\frac{^{FAA}16:1/22:0}{\text{Total Area of the SPMs from APCI-MS}} = \% \text{ of } 16:1/22:0$$

The calculated PFs above were also used to proportion the area for the [20:0 SPM + H]⁺ peak in **19(C)**. The calculation was performed as follows:

The area for each SPL in 20:0 SPM by ESI-MS was calculated.

$$^{PF1}_{18:1/20:0} \times ^A[20:0 \text{ SPM} + H]^+ = ^{FAA}_{18:1/20:0}$$

$$^{PF1}_{17:1/21:0} \times ^A[20:0 \text{ SPM} + H]^+ = ^{FAA}_{17:1/21:0}$$

$$^{PF1}_{16:1/22:0} \times ^A[20:0 \text{ SPM} + H]^+ = ^{FAA}_{16:1/22:0}$$

These areas were then divided by the total SPM area determined by ESI-MS, from which 16:1/22:0, 17:1/21:0 and 18:1/20:0 were found to represent 6.73%, 0.16% and 0.38% of the SPM population, respectively. Though the calculated absolute values for the percentages were different by APCI-MS, the order of abundance was the same with 16:1/22:0 > 18:1/20:0 > 17:1/21:0.

In SPL mixtures where $[X:1/Y:2 \text{ Cer} + H]^+$ overlapped with $[X:1/(Y + 1):0 \text{ Cer} - H_2O + H]^+$, such as $[22:2 \text{ SPM Cer} + H]^+$ and $[23:0 \text{ SPM Cer} - H_2O + H]^+$ in CES, the method of quantification was modified to account for this problem. The peaks for these two SPL groups in EICs were integrated in the following way: 1) The $[23:0 \text{ SPM Cer} + H]^+$ and $[23:0 \text{ SPM} + H]^+$ were integrated over the same RT range; 2) Since $[23:0 \text{ Cer} - H_2O + H]^+$ was isobaric with $[22:2 \text{ SPM Cer} + H]^+$ ion (**14(C)**), one peak was integrated for both ions. The RT range over which this peak was integrated had starting and ending times that coincided with the beginning of the $[23:0 \text{ SPM Cer} + H]^+$ ion peak, and the ending of the $[22:2 \text{ SPM} + H]^+$ ion peak. This ensured that the area represented both species.

From Table 5 it was seen that SPM LCB fragment ions were not isobaric with Y:2 FA fragment ions. The steps in the quantification were as follows: 1) From the MS² m.s. for $[23:0 \text{ SPM Cer} - H_2O + H]^+$ and $[22:2 \text{ SPM Cer} + H]^+$ (**14(F)**), PFs were calculated from the $[FA(L)]^+$ ions as shown above. These were then used to obtain the area

attributable to $[18:1/23:0 \text{ Cer} - \text{H}_2\text{O} + \text{H}]^+$, $[19:1/22:0 \text{ Cer} - \text{H}_2\text{O} + \text{H}]^+$, and $[18:1/22:2 \text{ Cer} + \text{H}]^+$ ions; 2) The $[23:0 \text{ SPM Cer} + \text{H}]^+$ area was proportioned using PFs calculated using the intensities of the $[\text{FA(L)}]^+$ ions in the $[23:0 \text{ SPM Cer} + \text{H}]^+$ MS^2 m.s. This step allowed us to determine the areas of $[18:1/23:0 \text{ Cer} + \text{H}]^+$ and $[19:1/22:0 \text{ Cer} + \text{H}]^+$ ions; 3) Add the areas for the dehydrated and protonated ceramide ions for each molecule to produce the total area attributable to 18:1/23:0 and 19:1/22:0 in CES; 4) It was assumed that the dehydrated ceramide ion of Y:2 SPLs were not isobaric with any species, so the sum of the areas of $[18:1/22:2 \text{ Cer} + \text{H}]^+$ and $[18:1/22:2 \text{ Cer} - \text{H}_2\text{O} + \text{H}]^+$ represented the total area of this species in CES. From these calculations, 18:1/23:0 19:1/22:0 and 18:1/22:2 accounted for 0.66%, 0.01% and 0.17% of the total SPM population by APCI-MS, respectively; and 5) $[18:1/23:0 + \text{H}]^+$ area was distributed using the PFs calculated from the MS^2 m.s. of $[23:0 \text{ SPM Cer} + \text{H}]^+$. So, by ESI-MS 18:1/23:0 and 19:1/22:0 were 0.90% and 0.02% of the SPM population by ESI-MS, respectively.

Since the formate adduct of Y:1 and Y:2 SPLs did not overlap with any other ions in the $-$ ESI EICs, the ratio of $[22:2 \text{ SPM} + 45]^-$ to $[22:1 \text{ SPM} + 45]^-$ was used to proportion the $[22:2 \text{ SPM} + \text{H}]^+$ peak, which overlapped with the + 2 isotope of $[20:0 \text{ SPM} + \text{Na}]^+$. Since 22:2 SPM was only composed of 18:1/22:2 as determined by APCI-MS then the area of $[22:2 \text{ SPM} + 45]^-$ only represented this molecule. This calculation is illustrated below:

$$\frac{^A[22:2 \text{ SPM} + 45]^-}{^A[22:1 \text{ SPM} + 45]^-} \times ^A[22:1 \text{ SPM} + \text{H}]^+ = ^A[22:2 \text{ SPM} + \text{H}]^+ = ^{\text{FAA}}18:1/22:2$$

The other two identified Y:2 SPLs were quantified in this way. 18:1/22:2 was 0.29% of the SPM population by ESI-MS.

To quantify Y:0 SPMs for which there was not sufficient MS² and/or MS³ data to identify its LCB/FA composition, the first step was to determine if $[X:1/(Y - 1):2 \text{ Cer} + \text{H}]^+$ was present by examining the negative and positive ESI m.s. A good example was 18:1/21:0 in BBS. The ESI m.s. confirmed that there was 21:0 SPM, but its low abundance prevented MS/MS data from being obtained. As a result, the LCB/FA composition of 21:0 SPM could not be determined, so it was assumed that the areas for the protonated ceramide, dehydrated ceramide and protonated molecules were only composed of the 18:1/21:0 SPL. Before integrating these peaks however, it had to be confirmed that 20:2 SPM was not present since it was isobaric with $[18:1/21:0 \text{ Cer} - \text{H}_2\text{O} + \text{H}]^+$. Without MS/MS data it would not be possible to proportion that area of the $[18:1/21:0 \text{ SPM Cer} - \text{H}_2\text{O} + \text{H}]^+$ peak between the two species (only CES had Y:2 SPLs but these were all identified using tandem MS). The +ve and -ve ESI-MS m.s. confirmed that there was no 20:2 SPM in BBS, so the area of $[21:0 \text{ SPM Cer} + \text{H}]^+$ was added to the area of $[21:0 \text{ SPM Cer} - \text{H}_2\text{O} + \text{H}]^+$, and the sum represented the 18:1/21:0 SPL. SPLs for which there was no MS/MS data were assumed to be composed only of the 18:0 or 18:1 LCBs, and were labeled with an '*’.

The first step in the quantification of Y:0 DHSs was to determine if there was sufficient MS² and MS³ data to characterize their constituent molecules. If yes, then the peaks for the $[\text{Cer} + \text{H}]^+$, $[\text{Cer} - \text{H}_2\text{O} + \text{H}]^+$, and $[\text{M} + \text{H}]^+$ ions in EICs were integrated over the same RT range. Since there were no Y:2 DHSs in any of the three samples, overlapping of the $[X:0/Y:0 \text{ Cer} - \text{H}_2\text{O} + \text{H}]^+$ and $[X:0/(Y - 1):2 \text{ Cer} + \text{H}]^+$ peaks in EICs was not a problem. A major problem however, was that saturated LCB fragment ions were isobaric with saturated FA fragment ions (Table 6). Since the DHS-LCBs in all

three samples ranged from 12:0 to 20:0 inclusive, then this problem only affected the quantification of S-C DHSs. Since saturated DHSs fragmented by FP2, it was preferable to calculate PFs using the $[\text{FA}(\text{S})]^+$ ions in the MS^2 m.s. The overlap of the masses of these ions in the MS^2 m.s. however, resulted in circumstances where PFs had to be calculated by using either a) $[\text{LCB} - \text{H}_2\text{O} + \text{H}]^+$ in the MS^2 m.s. or b) $[\text{FA}(\text{S})]^+$ in the MS^3 m.s. All DHSs could be quantified by b) only, since the $[\text{LCB} + \text{H}]^+$ ions were not observed in the MS^3 m.s. Doing this however, would have simple tandem instruments from performing similar analyses. In addition, at each stage in MS^n there was a loss of accuracy and sensitivity, which would have introduced more uncertainty in the results. So, where possible it was preferable to calculate PFs using ions from the MS^2 m.s. Table 5, Table 6 and Scheme 7 were used in conjunction to determine the best ions from which to calculate the PFs.

Quantification of Y:0 DHSs will be explained using 14:0 DHS in BMS, which was composed of 16:0/16:0, 17:0/15:0 and 18:0/14:0. The procedure was as follows: 1) The first step was to determine if there were any overlapping $[\text{LCB} + \text{H}]^+$ and $[\text{FA}(\text{S})]^+$ ions in the MS^2 m.s. So, from Table 6 it was seen that the mass of the protonated 16:0 LCB was isobaric with the $[\text{16:0}(\text{S})]^+$. Remember that under FP2 the intensity of $[\text{LCB} + \text{H}]^+$ was approximately equal to $[\text{LCB} - \text{H}_2\text{O} + \text{H}]^+$, both of which were relatively abundant in the MS^2 m.s. So, PFs for 14:0 DHS were not calculated using the $[\text{FA}(\text{S})]^+$ ions because the intensity of the peak at m/z 256.3 represented two fragment ions; 2) Next, we determined if the dehydrated LCB ion could be used to calculate the PFs. From Table 6 however, it was seen that the masses of the 17:0 and 18:0 dehydrated LCB fragment ions were isobaric with $[\text{14:0}(\text{L})]^+$ and $[\text{15:0}(\text{L})]^+$ respectively. Therefore, PFs

could not be calculated from these ions; 3) Once it was demonstrated that PFs could not be calculated using the $[\text{FA}(\text{S})]^+$ or $[\text{LCB} - \text{H}_2\text{O} + \text{H}]^+$ ions in the MS^2 m.s., the intensities of the $[\text{FA}(\text{S})]^+$ ions in the MS^3 m.s were used to calculate the PFs for 14:0 DHS; 4) The PFs were used to divide the areas under the peaks of the $[\text{14:0 DHS} + \text{H}]^+$, $[\text{14:0 DHS Cer} + \text{H}]^+$ and $[\text{14:0 DHS Cer} - \text{H}_2\text{O} + \text{H}]^+$ ions in EICs, as previously described for Y:0 SPMs whose dehydrated ceramide ion did not overlap with $[\text{Y:2 SPM Cer} + \text{H}]^+$ ions; 5) Finally, the areas for the 16:0/16:0, 17:0/15:0 and 18:0/14:0 were divided by the area for the total DHS population to determine their percentages by APCI-MS and ESI-MS.

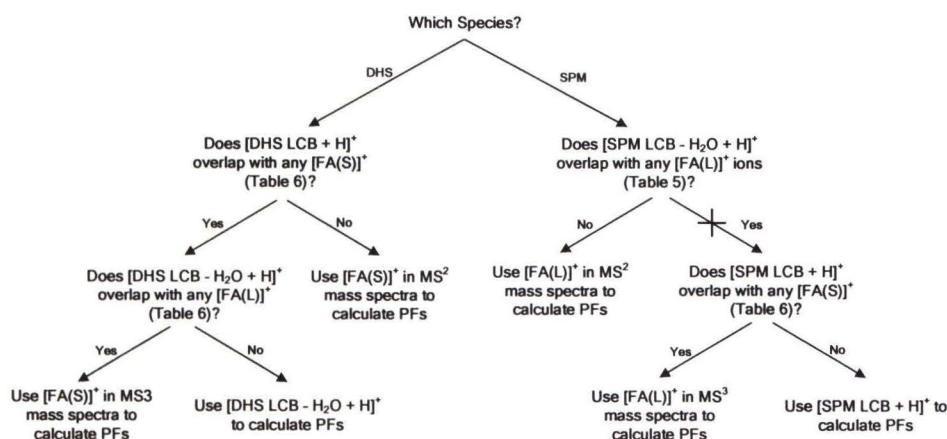
Since there were no Y:2 DHSs in any of the three samples, in situations where there was not sufficient MS/MS data the Y:0 DHSs were quantified by same the method (for APCI and ESI) used to quantify the Y:0 SPMs. The quantification of the X:1/Y:0, X:1/Y:2 and X:0/Y:0 SPLs in BBS, BMS, and CES is summarized in Scheme 8.

3.2 Quantification of X:A/Y:1 Sphingolipids

The integration and quantification of SPMs with one site of unsaturation on the FA chain was similar to the methods used for X:1/Y:2 SPLs with a few minor differences. The analysis proceeded as follows. If the SPM LCBs and Y:1 FA fragment ions did not overlap, then quantification was the same as described above for Y:2 SPMs except that the PFs were calculated using the $[\text{FA}(\text{L})]^+$ from the Y:1 SPL and the ^{13}C -free, ^{13}C and 2-times- ^{13}C isotope variants of the $[\text{FA}(\text{L})]^+$ for the $(\text{Y} + 1):0$ SPL. For example $[\text{21:1 SPM Cer} + \text{H}]^+$, which was composed of 16:1/23:1, 17:1/22:1 and 18:1/21:1, was isobaric with the +2 isotope of $[\text{22:0 SPM Cer} - \text{H}_2\text{O} + \text{H}]^+$, which constituted of 16:1/24:0, 17:1/23:0 and 18:1/22:0. Figure 21 shows the intensities of the

FA(L) fragment ions in the average MS² m.s. of 21:1 SPM. The PFs were calculated using the intensities of the highlighted ions. As before, the intensities of the [FA(L)]⁺ ions of 21:1 SPM were assumed to represent the abundances of each molecule in the SPL group. Unlike previous calculations however, the intensities of the ¹³C-free [FA(L)]⁺ ion and the +1 and +2 [FA(L)]⁺ isotopes of 22:0 SPM, were used to calculate the PFs for the 18:1/22:0, 17:1/23:0 and 16:1/24:0 SPLs in 22:0 SPM. The calculated PFs are shown in Table 29. From the table it was seen that the 16:1/23:1, 17:1/22:1 and 18:1/21:1 SPLs were 44.8%, 1.9% and 2.4% of the area of [21:1 SPM Cer + H]⁺ ion peak. From these percentages the FAA for each SPL was calculated as described in detail above. An important observation, was that the +2 isotope of [22:0 SPM Cer – H₂O + H]⁺ accounted for 50.9% of the area of the peak. This showed that the +2 isotope of the SPL ions had to be considered when quantifying SPLs by APCI-MS.

Scheme 7: Flow Diagram for Deciding which Ions to use to Calculate Proportioning Factors



Scheme 7: This scheme serves a guide to aid in deciding which ions are most suitable to calculate PFs. The arrow with a cross indicates a scenario that was not observed in our analyses.

Scheme 8: Quantification of X:1/Y:0, X:1/Y:2 and X:0/Y:0 SPLs

Quantification of:

A. Isobaric $[X:1/Y:0 \text{ Cer} - \text{H}_2\text{O} + \text{H}]^+$ and $[X:1/(Y-1):2 \text{ Cer} + \text{H}]^+$

1) Y:0 SPM composed of

X:1/Y:0 and $(X+1):1/(Y-1):0$

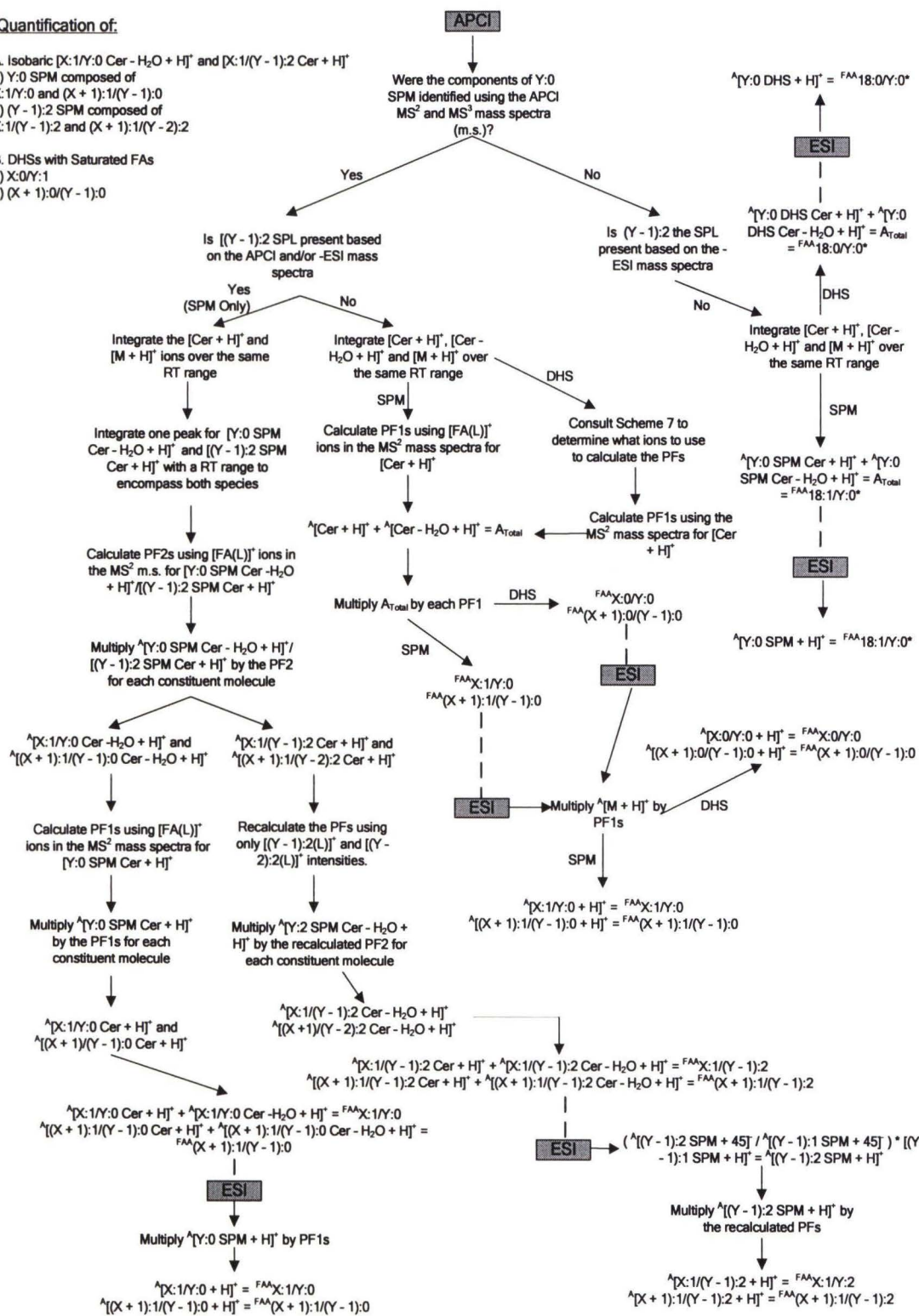
2) (Y-1):2 SPM composed of

X:1/(Y-1):2 and $(X+1):1/(Y-2):2$

B. DHSs with Saturated FAs

1) X:0/Y:1

2) $(X+1):0/(Y-1):0$



Scheme 8: The methods used to calculate the final adjusted area (FAA) for the Y:0 and Y:2 sphingolipids by APCI and ESI MS. The mole% for each SPL was calculated by dividing the FAA by the total area of the SPM or DHS populations, multiplied by 100%. Abbreviations: Superscripted 'A', represented "Area of"; PF1 and PF2, are the proportioning factors calculated from the MS² m.s. of protonated ceramide and dehydrated ceramide fragment ions respectively.

For quantification by ESI-MS, the [21:1 SPM + H]⁺ ion was proportioned using the PFs in Table 30, because the ESI area only represented the three constituent SPLs. So, their relation to each other was calculated and used to proportion the [M + H]⁺ area.

When there wasn't sufficient MS/MS data to proportion the peak, the area was assumed to only represent the SPL with an 18:1 LCB. But since the Y:0 SPLs were always more abundant than Y:1 SPLs then there was always overlap between the [Y:1 SPL Cer + H]⁺ and the +2 isotope of [(Y + 1):0 Cer - H₂O + H]⁺, ions. So, the [Y:1 Cer + H]⁺ peak area represented these two overlapping species. This had to be considered in our analysis. Since only three Y:2 SPLs were identified (found in CES) by ESI-MS and APCI tandem MS, then the other [X:1/Y:0 Cer - H₂O + H]⁺ ions were not isobaric with any other ions. Based on these observations, the FAA for the Y:1 SPLs that have no MS/MS data, was calculated as follows:

$$\frac{^A[X:1/Y:1 \text{ Cer} - \text{H}_2\text{O} + \text{H}]^+}{^A[X:1/Y:0 \text{ Cer} - \text{H}_2\text{O} + \text{H}]^+} \times ^A[X:1/Y:0 \text{ Cer} + \text{H}]^+ = ^A[X:1/Y:1 \text{ Cer} + \text{H}]^+$$

$$^A[X:1/Y:1 \text{ Cer} + \text{H}]^+ + ^A[X:1/Y:1 \text{ Cer} - \text{H}_2\text{O} + \text{H}]^+ = ^{\text{FAA}} 18:1/Y:1^*$$

By ESI-MS the area of the [M + H]⁺ ion peak was assumed to represent the FAA for 18:1/Y:1^{*}, since these ions were not isobaric with any other coeluting SPL ion.

Spectrum List for 21:1 SPM			BMS_+ve APCI ms3b_1
+ c d Full ms2 588.60@54.00			
RT: 32.83-35.87			
m/z	Intensity	Relative	
348.3	8997.8	0.54	[21:1(L)] ⁺
350.3	14407.6	0.86	
352.3	6548.0	0.39	
354.0	4347.3	0.26	
354.7	4392.3	0.26	
357.3	1037.9	0.06	
359.9	1459.4	0.09	
361.3	1282.4	0.08	
362.2	7113.3	0.43	[22:1(L)] ⁺
364.4	26192.5	1.57	
365.4	42449.5	2.54	[22:0(L)] ⁺
366.4	35948.8	2.15	
+ c d Full ms2 588.60@54.00			
RT: 32.83-35.87			
m/z	Intensity	Relative	
376.4	169154.9	10.11	[23:1(L)] ⁺
377.3	560.8	0.03	
378.1	2191.0	0.13	[23:0(L)] ⁺
379.4	14567.6	0.87	
380.7	3745.4	0.22	
383.5	1964.8	0.12	
384.3	1369.6	0.08	
389.5	2231.9	0.13	
391.2	3250.4	0.19	
392.4	9933.4	0.59	[24:0(L)] ⁺
393.4	29579.3	1.77	
394.3	27370.4	1.64	

Figure 21. Spectrum list showing the intensities of the $[\text{FA}(\text{L})]^+$ ions used to calculate the proportioning factors for the isobaric species $[\text{21:1 SPM Cer} + \text{H}]^+$ and the + 2 isotope of $[\text{22:0 SPM Cer} - \text{H}_2\text{O} + \text{H}]^+$. The $[\text{FA}(\text{L})]^+$ intensities that were used are highlighted.

Only BBS had MS/MS data for Y:1 DHSs. Quantification for these SPLs however, was problematic because the Y:1 DHSs fragmented by FP1 whereas the overlapping (Y + 1):0 DHSs fragmented by FP2. Since the species which we are interested in (Y:1 DHSs) however, fragmented by FP1, quantification was performed using the $[\text{FA}(\text{L})]^+$ ions. Fortunately, the identified Y:1 DHSs had FA chains longer than 20 carbon atoms in length, so that there were no isobaric LCB and FA fragments in the MS^2 m.s. Therefore, the APCI and ESI areas were proportioned using the $[\text{FA}(\text{L})]^+$ ions as previously described above for the overlap of $[\text{Y:1 SPMs Cer} + \text{H}]^+$ with the +2 isotope of $[(\text{Y} + 1):0 \text{ SPMs Cer} - \text{H}_2\text{O} + \text{H}]^+$. By ESI-MS, the area of the $[\text{M} + \text{H}]^+$ ion peak was assumed

to represent the FAA for 18:0/Y:1^{*}, since these ions were not isobaric with any other coeluting SPL ion.

The quantification of SPLs with one double bond on the FA chain is summarized in Scheme 9.

Table 29: Calculation of the Proportioning Factors (PFs) for

[21:1 SPM Cer + H]⁺ in APCI-MS

Molecule	[FA(L)] ⁺	Intensity (from MS ²)	PF (Intensity/Total Intensity)	%
16:1/23:1	[23:1(L)] ⁺	169154.9	0.45	44.8
17:1/22:1	[22:1(L)] ⁺	7113.3	0.02	1.9
18:1/21:1	[21:1(L)] ⁺	8997.8	0.02	2.4
[18:1/22:0 Cer- H ₂ O+H] ⁺ (+2)	[22:0(L)] ⁺	26192.5	0.07	6.9
	[22:0(L)] ⁺ (+1)	42449.5	0.11	11.3
	[22:0(L)] ⁺ (+2)	35948.8	0.10	9.5
[17:1/23:0 Cer- H ₂ O+H] ⁺ (+2)	[23:0(L)] ⁺	2191.0	0.01	0.6
	[23:0(L)] ⁺ (+1)	14567.6	0.04	3.9
	[23:0(L)] ⁺ (+2)	3745.4	0.01	1.0
[16:1/24:0 Cer- H ₂ O+H] ⁺ (+2)	[24:0(L)] ⁺	9933.4	0.03	2.6
	[24:0(L)] ⁺ (+1)	29579.3	0.08	7.8
	[24:0(L)] ⁺ (+2)	27370.4	0.07	7.3
Totals		377243.9	1.00	100.00

Table 29: The intensity of the ions in the MS² mass spectrum for [21:1 SPM Cer + H]⁺ that were used to calculate the proportioning factors. The intensities were summed, and the each was divided by the total intensity to produce a PF for that constituent lipid. The ions with one ¹³C and two ¹³Cs are represented as (+1) and (+2), respectively. The listed PFs were used to divide the area of the protonated ceramide ion peak among its constituent SPL molecules.

Table 30: Calculation of the Proportioning Factors (PFs) for

[21:1 SPM + H]⁺ in ESI-MS

Molecules	Intensity	PF for ESI-MS (Intensity/ Total Intensity)
18:1/21:1	8997.80	0.05
16:1/23:1	169154.90	0.91
17:1/22:1	7113.30	0.04
Totals	185266.00	1.00

Table 30: The [21:1 SPM + H]⁺ ion was not isobaric with any other SPL ion. So, its area only represented its three constituent molecules. Therefore, the PFs in Table 29 cannot be used to divide the area among these molecules. So, new PFs are calculated based only on the intensities of the FA(L) ions for 21:1 SPM in the APCI MS² mass spectrum.

The final composition of bovine milk, chicken egg yolk and bovine brain SPM extracts by APCI-MS and ESI-MS is shown in Tables 31 to 60. 10:0 SPM in BMS was the least abundant SPL group with a mole percentage of 0.1% (0.1%). Its chromatographic S/N was automatically calculated to be 5.65 by the Xcalibur Software. The mass spectrometric S/N for 10:0 SPM was calculated to be 4.63, by dividing the intensity of the [10:0 SPM Cer + H]⁺ peak in an EIC by the standard deviation of the intensities of the noise peaks in the range *m/z* 400-700. Since both were greater than a S/N of 3, it was concluded that all the calculated percentages were above the detection limit of the instruments. Similar calculations were performed for all samples, and all the reported percentages were above the detection limit. This work represents the first accurate determination of the LCB/FA composition of SPL mixtures by APCI-MS and ESI-MS.

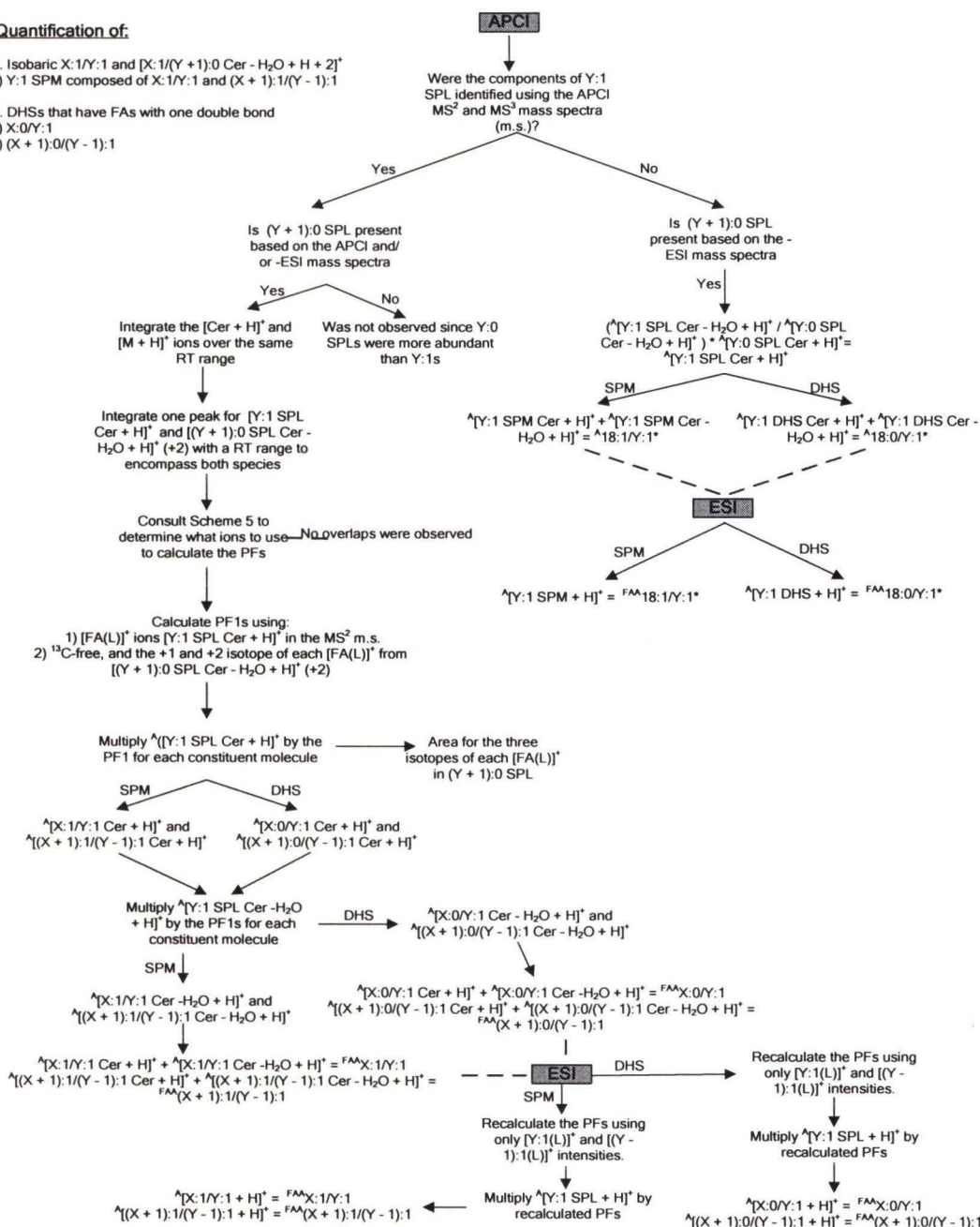
Scheme 9: Quantification of X:1/Y:1 and X:0/Y:1 SPLs

Quantification of:

A. Isobaric X:1/Y:1 and [X:1/(Y+1):0 Cer - H₂O + H + 2]⁺
 1) Y:1 SPM composed of X:1/Y:1 and (X+1):1/(Y-1):1

B. DHSs that have FAs with one double bond

- 1) X:0/Y:1
 2) (X+1):0/(Y-1):1



Scheme 9: Scheme 9 shows the methods used to calculate the final adjusted area (FAA) for the Y:1 sphingolipids by APCI and ESI MS. The mole% for each SPL was then calculated by dividing the FAA by the total area of the SPM or DHS populations multiplied by 100%. The scheme shows the method in general terms where superscripted 'A' represented "Area". PF1 and PF2 are the proportioning factors calculated from the MS² m.s. of the protonated ceramide and dehydrated ceramide fragment ions respectively. The +1 and +2 isotope ions are represented by placing '(+1)' and '(+2)', respectively, after the general formula for the ion.

**4. COMPOSITION OF THE LONG-CHAIN BASE/FATTY
ACID COMBINATIONS IN BOVINE MILK, BOVINE
BRAIN AND CHICKEN EGG YOLK SPHINGOMYELIN
EXTRACTS BY ON-LINE HIGH PERFORMANCE LIQUID
CHROMATOGRAPHY WITH DETECTION BY
ATMOSPHERIC PRESSURE CHEMICAL IONIZATION
AND ELECTROSPRAY IONIZATION MASS
SPECTROMETRY**

4.1. Composition of Bovine Milk by APCI-MS

Table 31: Composition (mole%) of the LCB/FA Combinations

FA	DHS							SPM				
	12:0	14:0	16:0	17:0	18:0	19:0	20:0	16:1	17:1	18:1	19:1	20:1
10:0										0.02		
12:0					0.03			0.00		0.02		
13:0					0.13*					0.01		
14:0	0.12		0.19		0.30			0.14	0.12	0.80		
14:1										0.12*		
15:0				0.09	0.28				0.01	0.17		
15:1										0.15*		
16:0		0.05	4.19	1.00	5.74	0.45	0.17	2.30	2.15	12.88	0.48	
16:1										0.28		
17:0			0.10		0.03			0.06		0.48		
17:1										0.11*		
18:0			0.77	0.06	0.64			0.38	0.24	0.83	0.07	
18:1										0.30*		
19:0			0.07		0.04					0.08		
20:0			0.19		0.14			0.13	0.04	0.26		
20:1					0.96*					0.47*		
21:0			0.67		0.14			0.22	0.11	0.33		
21:1					3.47*					0.07		
22:0			13.04	0.78	4.09			4.56	1.48	8.94	0.30	
22:1					4.11*				0.06	0.07		
23:0	0.14	0.37	22.84	2.05	8.02	0.32	0.24	9.22	2.98	16.02	0.21	0.24
23:1					2.38*			1.33	0.49	1.61	0.46	
24:0			14.02	1.27	4.08	0.20	0.14	5.15	2.31	11.62	1.19	
24:1					1.33*			1.40	0.35	2.06	0.26	
25:0					0.19			0.19	0.19	0.88		
25:1					0.32*			0.61		0.87		
26:0					0.06			0.33		0.48*		
26:1										0.32*		
Total DHS =100%								Total SPM = 100%				

4.1. Composition of Bovine Milk by APCI-MS (continued)

Table 32
Fatty Acid (FA) Composition

Fatty Acid	Mole %
10:0	0.0
12:0	0.0
13:0	0.0
14:0	1.0
14:1	0.1
15:0	0.2
15:1	0.1
16:0	16.5
16:1	0.2
17:0	0.5
17:1	0.1
18:0	1.5
18:1	0.2
19:0	0.1
20:0	0.4
20:1	0.6
21:0	0.7
21:1	0.8
22:0	15.8
22:1	1.0
23:0	29.8
23:1	3.6
24:0	20.2
24:1	3.5
25:0	1.0
25:1	1.2
26:0	0.7
26:1	0.3
Total Saturated	88.4

Table 33
Saturated LCB Composition

DHS-LCB	Mole %
12:0	0.3
14:0	0.4
16:0	56.1
17:0	5.2
18:0	36.5
19:0	1.0
20:0	0.6

Table 34
Unsaturated LCB Composition

SPM-LCB	Mole %
16:1	26.0
17:1	10.5
18:1	60.2
19:1	3.0
20:1	0.2

Table 35
Sphingolipid Composition

SPL	Mole %
DHS	20.8
SPM	79.2

4.2. Composition of Bovine Milk by ESI-MS

Table 36: Composition (Mole%) of the LCB/FA Combinations

FA	DHS							SPM				
	12:0	14:0	16:0	17:0	18:0	19:0	20:0	16:1	17:1	18:1	19:1	20:1
10:0										0.03		
12:0					0.06			0.00		0.05		
13:0					0.15*					0.01		
14:0	0.15		0.43		0.58			0.34	0.30	1.60		
14:1										0.07*		
15:0				0.17	0.43				0.02	0.33		
15:1										0.09*		
16:0		0.11	8.05	1.53	7.12	0.42	0.21	4.60	4.12	23.70	0.54	
16:1										0.70		
17:0			0.16		0.02			0.12		0.54		
17:1										0.11*		
18:0			0.95	0.06	0.81			0.69	0.27	1.40	0.11	
18:1										0.40*		
19:0			0.06		0.03					0.13		
20:0			0.24		0.17			0.22	0.06	0.38		
20:1					0.37*					0.18*		
21:0			0.51		0.13			0.34	0.16	0.34		
21:1					3.13*					0.05		
22:0			14.96	0.69	3.71			6.73	1.53	7.05	0.19	
22:1					2.54*				0.04	0.06		
23:0	0.13	0.28	20.32	1.86	7.05	0.28	0.25	9.50	2.35	9.99	0.12	0.11
23:1					2.37*			1.02	0.42	1.24	0.22	
24:0			12.71	1.12	3.58	0.21	0.09	4.06	1.44	6.78	0.57	
24:1					1.10*			1.20	0.27	1.00	0.11	
25:0					0.19			0.12	0.11	0.42		
25:1					0.49*			0.47		0.37		
26:0					0.04			0.19		0.24*		
26:1										0.07*		

Total DHS = 100%

Total SPM = 100%

4.2. Composition of Bovine Milk by ESI-MS (continued)

Table 37
Fatty Acid (FA) Composition

FA	Mole %
10:0	0.0
12:0	0.1
13:0	0.0
14:0	2.0
14:1	0.1
15:0	0.4
15:1	0.1
16:0	29.9
16:1	0.6
17:0	0.6
17:1	0.1
18:0	2.3
18:1	0.3
19:0	0.1
20:0	0.6
20:1	0.2
21:0	0.8
21:1	0.7
22:0	16.3
22:1	0.6
23:0	23.7
23:1	2.8
24:0	13.8
24:1	2.3
25:0	0.6
25:1	0.8
26:0	0.4
26:1	0.1
Total Saturated	91.5

Table 38
Saturated LCB Composition

DHS-LCB	Mole %
12:0	0.3
14:0	0.4
16:0	58.4
17:0	5.4
18:0	34.1
19:0	0.9
20:0	0.6

Table 39
Unsaturated LCB Composition

SPM-LCB	Mole %
16:1	29.6
17:1	11.1
18:1	57.3
19:1	1.9
20:1	0.1

Table 40
Sphingolipid Composition

SPL	Mole %
DHS	19.8
SPM	80.2

4.3. Composition of Bovine Brain by APCI-MS

Table 41: Composition (mole%) of the LCB/FA Combinations

FA	DHS					SPM				
	16:0	17:0	18:0	19:0	20:0	16:1	17:1	18:1	19:1	20:1
14:0								0.04		0.04
15:0								0.02*		
16:0			0.65*			0.00		1.44		
17:0								0.12		
18:0			19.60		0.88	0.19	0.10	40.35	0.89	6.83
18:1			0.86*					0.73		
19:0			0.84*					1.07		
20:0			7.31			0.09	0.08	3.24		
20:1			0.94*					0.76*		0.04
21:0			0.64*			0.02		0.76*		
22:0			17.11					6.40	0.02	
22:1			2.92					2.07		
23:0			3.24		0.03			2.11		0.02
23:1		1.09	0.56		0.03			0.69		0.04
24:0	0.08		15.28	0.06				7.49	0.02	0.04
24:1	0.13		23.30	0.35				19.78	0.11	0.06
25:0			1.23			0.02		0.92	0.00	
25:1			0.88					1.81	0.01	
26:0			0.51			0.00		0.28		
26:1			1.48					1.28		

Total DHS = 100%

Total SPM = 100%

4.3. Composition of Bovine Brain by APCI-MS (continued)

Table 42
Fatty Acid (FA) Composition

FA	%
14:0	0.1
15:0	0.0
16:0	1.3
17:0	0.1
18:0	43.4
18:1	0.8
19:0	1.0
20:0	4.1
20:1	0.8
21:0	0.8
22:0	8.3
22:1	2.2
23:0	2.3
23:1	0.9
24:0	8.9
24:1	20.6
25:0	1.0
25:1	1.7
26:0	0.3
26:1	1.3
Total Saturated	71.7

Table 43
Saturated LCB Composition

DHS-LCB	%
16:0	0.2
17:0	1.1
18:0	97.4
19:0	0.4
20:0	0.9

Table 44
Unsaturated LCB Composition

SPM-LCB	%
16:1	0.3
17:1	0.2
18:1	91.4
19:1	1.1
20:1	7.1

Table 45
Sphingolipid Composition

SPL	%
DHS	17.7
SPM	82.3

4.4. Composition of Bovine Brain by ESI-MS

Table 46: Composition (mole%) of the LCB/FA Combinations

FA	DHS					SPM				
	16:0	17:0	18:0	19:0	20:0	16:1	17:1	18:1	19:1	20:1
14:0								0.11		0.07
15:0								0.04*		
16:0			1.16*			0.01		2.71		
17:0								0.17		
18:0			24.55		1.31	0.36	0.15	48.31	0.22	8.25
18:1			0.36*					0.39		
19:0			0.59*					0.26		
20:0			10.90			0.11	0.02	3.92		
20:1			0.56*					0.15*		0.04
21:0			0.45*			0.01		0.31*		
22:0			16.79					6.02	0.01	
22:1			3.29					1.82		
23:0			2.87		0.02			1.47		0.01
23:1		1.23	1.07		0.01			0.84		0.01
24:0	0.08		14.28	0.03				6.35	0.01	0.04
24:1	0.08		17.77	0.15				15.51	0.04	0.04
25:0			0.58			0.02		0.47	0.00	
25:1			0.38					0.59	0.01	
26:0			0.54			0.00		0.30		
26:1			0.94					0.84		

Total DHS = 100%

Total SPM = 100%

4.4. Composition of Bovine Brain by ESI-MS (continued)

Table 47
Fatty Acid (FA) Composition

FA	Mole %
14:0	0.1
15:0	0.0
16:0	2.4
17:0	0.1
18:0	51.8
18:1	0.4
19:0	0.3
20:0	5.3
20:1	0.3
21:0	0.3
22:0	7.9
22:1	2.1
23:0	1.7
23:1	1.1
24:0	7.8
24:1	16.0
25:0	0.5
25:1	0.6
26:0	0.3
26:1	0.9
Saturated	78.8

Table 48
Saturated LCB Composition

DHS-LCB	Mole %
16:0	0.2
17:0	1.2
18:0	97.1
19:0	0.2
20:0	1.3

Table 49
Unsaturated LCB Composition

SPM-LCB	Mole %
16:1	0.5
17:1	0.2
18:1	90.6
19:1	0.3
20:1	8.5

Table 50
Sphingolipid Composition

SPL	Mole %
DHS	17.5
SPM	82.5

4.5. Composition of Chicken Egg Yolk by APCI-MS

Table 51: Composition (mole%) of the LCB/FA Combinations

FA	DHS				SPM			
	14:0	16:0	18:0	19:0	16:1	18:1	19:1	20:1
12:0						0.02		
14:0			1.14		0.00	0.87		
15:0			0.53*			0.25*		
16:0		0.05	81.66	0.38		77.64	0.87	
16:1			4.94*			1.63*		
17:0			2.03			3.06		
18:0	0.10	1.88	3.13			4.81	0.04	
18:1			1.66*			1.11*		
18:2						0.11		
19:0						0.39		0.02
20:0			0.47			1.03	0.01	
20:1						0.17*		
21:0						0.15		
22:0			0.93			2.14	0.01	
22:1						0.36		
22:2						0.17		
23:0			0.21			0.66		0.00
24:0			0.53			1.15	0.01	0.00
24:1			0.34			2.36		
24:2						0.86		
25:0						0.05		
26:0						0.01		
26:1						0.03		

Total DHS = 100%

Total SPM = 100%

4.5. Composition of Chicken Egg Yolk by APCI-MS (Continued)

Table 52
Fatty Acid (FA) Composition

FA	Mole %
12:0	0.0
14:0	0.9
15:0	0.3
16:0	78.6
16:1	1.7
17:0	3.0
18:0	4.9
18:1	1.1
18:2	0.1
19:0	0.4
20:0	1.0
20:1	0.2
21:0	0.1
22:0	2.1
22:1	0.4
22:2	0.2
23:0	0.7
24:0	1.1
24:1	2.3
24:2	0.8
25:0	0.0
26:0	0.0
26:1	0.0
Saturated	93.2

Table 53
Saturated LCB Composition

DHS-LCB	Mole %
14:0	0.1
16:0	1.9
18:0	97.6
19:0	0.4

Table 54
Unsaturated LCB Composition

SPM	Mole %
16:1	0.0
18:1	99.0
19:1	0.9
20:1	0.0

Table 55
Sphingolipid Composition

SPL	Mole %
DHS	3.1
SPM	96.9

4.6. Composition of Chicken Egg Yolk by ESI-MS

Table 56: Composition (mole%) of the LCB/FA Combinations

FA	DHS				SPM			
	14:0	16:0	18:0	19:0	16:1	18:1	19:1	20:1
12:0						0.05		
14:0			1.58		0.00	1.36		
15:0			0.67*			0.32*		
16:0		0.07	84.65	0.15		73.45	0.11	
16:1			2.86*			0.40*		
17:0			0.78			0.41		
18:0	0.14	1.95	3.79			8.06	0.03	
18:1			0.92*			0.56*		
18:2						0.17		
19:0						0.18		0.03
20:0			0.48			2.20	0.01	
20:1						0.17*		
21:0						0.20		
22:0			1.15			3.81	0.02	
22:1						0.54		
22:2						0.29		
23:0			0.09			0.90		0.00
24:0			0.50			2.14	0.00	0.00
24:1			0.22			3.39		
24:2						1.07		
25:0						0.07		
26:0						0.01		
26:1						0.03		

Total DHS = 100%

Total SPM = 100%

4.6. Composition of Chicken Egg Yolk by ESI-MS (continued)

Table 57
Fatty Acid (FA) Composition

FA	Mole %
12:0	0.0
14:0	1.4
15:0	0.3
16:0	74.3
16:1	0.6
17:0	0.4
18:0	7.9
18:1	0.6
18:2	0.2
19:0	0.2
20:0	2.1
20:1	0.2
21:0	0.2
22:0	3.6
22:1	0.5
22:2	0.3
23:0	0.9
24:0	2.0
24:1	3.2
24:2	1.0
25:0	0.1
26:0	0.0
26:1	0.0
Saturated	93.5

Table 58
Saturated LCB Composition

DHS-LCB	Mole %
14:0	0.1
16:0	2.0
18:0	97.7
19:0	0.1

Table 59
Unsaturated LCB Composition

SPM-LCB	Mole %
16:1	0.0
18:1	99.8
19:1	0.2
20:1	0.0

Table 60
Sphingolipid Composition

SPL	Mole %
DHS	6.7
SPM	93.3

Table 61: Hydroxy-Sphingolipids Identified in Bovine Milk from APCI**Tandem Mass Spectrometry**

FA-OH	16:1	17:1	18:1
19:0-OH			*
20:0-OH			*
21:0-OH	*	*	*
22:0-OH	*	*	*
23:0-OH	*	*	*
24:0-OH	*	*	
25:0-OH	*		

Table 61: Hydroxy-sphingolipids in bovine milk identified from APCI tandem mass spectrometry. The asterisks indicate the LCB/FA-OHs that were identified, and are not an indication of relative amounts present. The abundance of the hydroxy-SPLs were too low to be quantified by LC-MS. This was in agreement with previous reports that estimated that FA-OHs were less than 1% of the total FAs in bovine milk.⁷

Table 62: Hydroxy-Sphingolipids Identified in Chicken Egg Yolk from**APCI Tandem Mass Spectrometry**

FA	18:1	18:1-OH
16:0		*
16:0-OH	*	
18:0-OH	*	

Table 62: Hydroxy-sphingolipids in bovine milk identified from APCI tandem mass spectrometry. The asterisks indicate the hydroxy-SPLs that were identified, and are not an indication of relative amounts present. The abundance of the hydroxy-SPLs were too low to be quantified by LC-MS.

I.C. ^{31}P Nuclear Magnetic Resonance

Figure 22 shows the ^{31}P NMR spectra of BMS, CES and BBS. The resonance signals from downfield to upfield are as follows: DHS at 0.13 δ , SPM at -0.08δ , and DPPC at -0.84δ . The chemical shifts of SPM, DPPC and especially the unknown phospholipid (DHS), were in agreement with previous reports.^{15,16,17} The normalized area was shown beneath each peak.

1. QUANTIFICATION BY ^{31}P NMR

Table 63 shows the composition of bovine milk, chicken egg yolk and bovine brain by ^{31}P NMR. It was seen that the NMR results were very reproducible, differing by only $\sim 0.1\%$ between samples of the same SPM extract. It was also observed that BMS had the highest percentage of DHS at 16.2% followed by BBS at 12.8% then CES at 2.6%. By LC-MS BMS contained 20.8% (19.8%) DHS. For CES, DHS account for 3.1% (6.7%) of the total SPL population. For BBS, DHS was 17.7% (APCI) and 17.5% (ESI) of the total SPL population. So it can be concluded that BMS contained the most DHS, followed by BBS then CES, by LC-MS. So, although the raw values were different between the two methods the trends were the same.

There was relatively close agreement between the ^{31}P NMR and LC-MS results. Both APCI MS and ESI MS overestimated the DHS percentage, by + 3% and + 4% (averaged), respectively. Quantification by ^{31}P NMR was considered to be more accurate than quantification by LC-MS also. So, a deviation of only 3% – 4% by LC-MS suggested that our method of quantification was accurate in determining the percentage of DHS and SPM in the sample. Determination of the LCB/FA composition however,

cannot be accomplished by ^{31}P NMR, so to verify the results by LC-MS, GC-MS experiments will have to be performed.

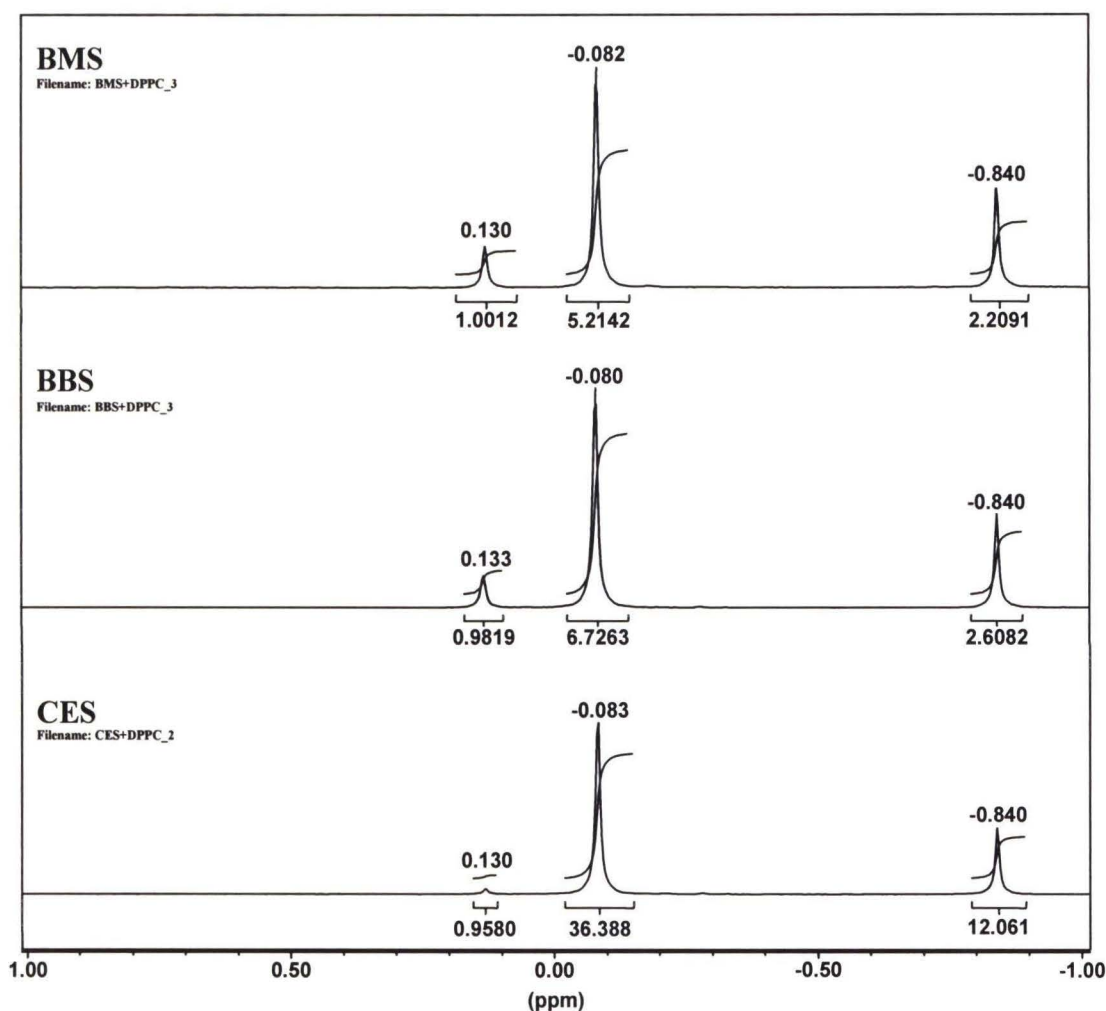


Figure 22. ^{31}P NMR spectra of BMS, BBS and CES. The resonance signals from downfield to upfield are as follows: DHS at 0.13 δ , SPM at -0.08 δ and DPPC at -0.84 δ . Each peak is integrated and the normalized areas are shown below each peak. DPPC was used to calibrate the scale.

2. COMPOSITION OF BOVINE MILK, BOVINE BRAIN AND CHICKEN EGG YOLK SPHINGOMYELIN EXTRACTS BY ^{31}P NUCLEAR MAGNETIC RESONANCE SPECTROSCOPY

Table 63: Composition of Bovine Milk, Bovine Brain and Chicken Egg

Yolk Sphingomyelin by ^{31}P NMR

Extract	Species	Sample 1 (mole%)	Sample 2 (mole%)	Sample 3 (mole%)	Average (mole%)
BMS	DHS	16.2	16.3	16.1	16.2
	SPM	83.8	83.7	83.9	83.8
BBS	DHS	12.8	12.7	12.7	12.8
	SPM	87.2	87.3	87.3	87.2
CES	DHS	2.7	2.6	2.6	2.6
	SPM	97.3	97.4	97.4	97.4

Table 63: Composition of bovine milk, bovine brain and chicken egg yolk sphingomyelin extracts. Three different samples were analyzed for each SPM extract. The peaks were integrated using Mestre-C NMR software.

I.E. KARLSSON'S MISTAKES

1. FULL-SCAN AND TANDEM MASS SPECTROMETRY

Having determined the LCB/FA composition for all three SPM samples by APCI-MS and ESI-MS, the work of Karlsson *et al.* can now be effectively analyzed. Their chromatographic system also resulted in three SPL peaks which they denoted as SM1, SM2 and SM3 (Figure 23). Figure 24 shows the corresponding average m.s. across these regions from their report. When **24(A – C)** was compared to our results in **1.1(E – G)** it was observed that the ions and their corresponding abundances, were the same. Based on the extensive analysis above and on previous findings²⁻³, it was proven that SPL1 was composed of L-C DHSs, SPL2 of L-C SPMs and S-C DHSs, and SPL3 of S-C SPMs. Karlsson *et al.* however, characterized the SPL peaks as follows: “SM1, saturated LCBs with hydroxy-FAs, saturated and/or unsaturated; SM2, unsaturated LCBs with long-chain FAs, saturated and/or unsaturated; and SM3, unsaturated LCBs with short-chain FAs, saturated and/or unsaturated.”

There was no mention of L-C non-hydroxy-DHSs in SM1 or S-C DHSs in SM2, which contradicted our analysis. Karlsson *et al.* identified L-C DHSs (Figure 31) in bovine milk, but did not describe their retention characteristics. So, we do not know if Karlsson *et al.* knew if they eluted in SM1, SM2 or SM3. A comparison of the ESI m.s. in Figure 24 to those in Figure 1 clearly supports this assumption. In addition our tandem MS data unambiguously confirmed that these ions were not hydroxy-SPLs. Also, Karlsson *et al.* did not identify any S-C DHSs in bovine milk. But, as will be shown later, because Karlsson *et al.* used upfront CID for the analysis, there was extensive

fragmentation in the APCI ion source, which produced complex m.s. that made it difficult, if not impossible, to accurately identify these species present at low abundances.

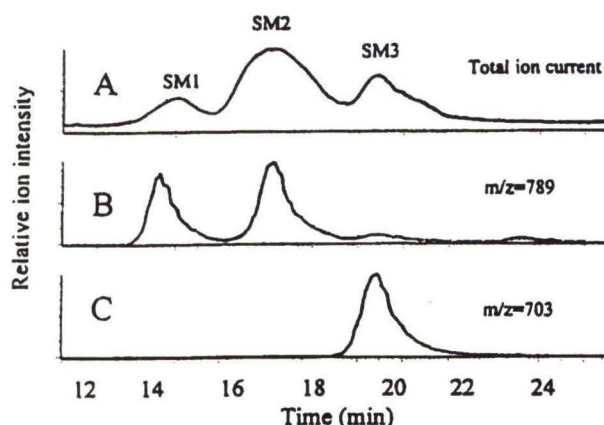


Figure 5. Mass chromatograms of sphingomyelin from bovine milk obtained in ESI: (A) reconstructed total ion current; (B) reconstructed ion chromatogram at $m/z = 789$; and (C) reconstructed ion chromatogram at m/z 703.

Figure 23. Figure 5 from Karlsson *et al.*'s paper showing the chromatographic profile of the SPLs in bovine milk.

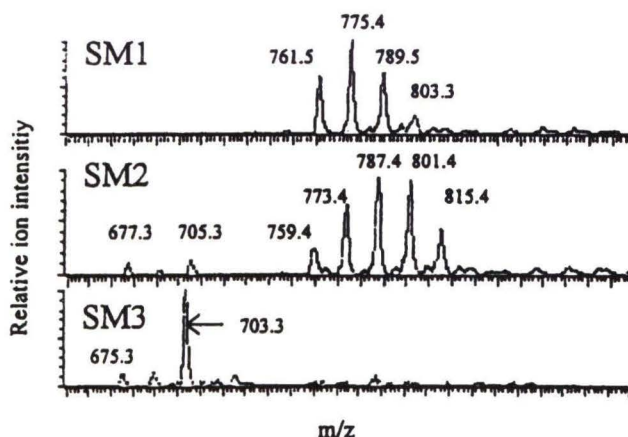


Figure 6. ESI mass spectra of SM1, SM2 and SM3 in Fig. 5(A) (poor printing resolution). Approximately 5 ng of bovine milk sphingomyelin sample were injected.

Figure 24. Figure 6 from Karlsson *et al.*'s paper showing the ESI mass spectra across SM1, SM2 and SM3, in Figure 23.

If the ions in SM1 were hydroxy-SPLs with saturated LCBs then the *mass-to-charge* ratios of 761.5, 775.4, 789.5 and 803.3 in Figure 24, were DHSs with 19:1-OH, 20:1-OH, 21:1-OH and 22:1-OH FA chains, respectively. But from our analysis of the SPL1 peak (pages 52 - 68) and the tandem MS data for the ion at m/z 789.7 (pages 96 - 98), it was unambiguously proven that this ion was $[22:0 \text{ DHS} + \text{H}]^+$. The $[22:0 \text{ DHS} + \text{H}]^+$ ion (**1.2.E**), $[22:0 \text{ DHS} + 45]^-$ ion at m/z 833.5 (**7(A)**), protonated ceramide ion at m/z 606.6 (**1.1.E**) were all observed. In addition, the MS^n m.s. shown in Figure 11 proved that 22:0 DHS was present and composed of the 16:0/24:0, 17:0/23:0 and 18:0/22:0 SPLs. The analysis of the MS^2 and MS^3 m.s. was described in detail. All of the masses indicated in Figure 24, were identified in the same way as 22:0 DHS. So, the *mass-to-charge* ratios from left to right in SM1 of Figure 23 were proven to be 20:0 DHS, 21:0 DHS, 22:0 DHS and 23:0 DHS, respectively. Also, since the hydroxy-SPLs were shown to elute later than their non-hydroxy SPL counterparts (pages 105 – 109), the OH-DHSs cannot possible elute in SM1. This meant therefore, that Karlsson *et al.*'s interpretation of the data was incorrect.

From our analysis, it was clear that Karlsson *et al.*'s characterization of the ions in SM1 was incorrect. However, to be certain, we needed to demonstrate where the error was made. Figure 25 shows how Karlsson *et al.* identified the hydroxy-SPLs from the APCI tandem m.s. According to the caption, the figure showed the “product ion spectra of the Cer^+ ion (m/z 606) from the m/z 789 protonated molecule in SM1 (upper) and SM2 (lower).” The upper m.s. will be designated as **25(A)** and the lower as **25(B)** for this discussion. Karlsson *et al.* stated that SM1 was composed of hydroxy-SPLs with saturated LCBs, but in **25(A)**, the labeled ions at m/z 236.4 and m/z 264.3 were the 16:1

and 18:1 dehydrated LCB fragment ions. This contradicted his own conclusion. If **25(A)** was the MS/MS of an ion that had a saturated LCB, then one would expect to observe saturated LCB fragment ions in the tandem m.s. In addition, the identification of the ions at m/z 365.4 and m/z 393.4 as the 21:0-OH and 23:0-OH FAs respectively, when considered along with the ions at m/z 236.4 and 264.3, suggested the presence of 18:1/21:0-OH and 16:1/23:0-OH. In their final table of results (Figure 31) Karlsson *et al.* reported that these identified unsaturated hydroxy-SPLs (OH-SPMs) had a relatively low abundance in bovine milk. So, clearly his conclusion that SM1 was composed of hydroxy-SPLs with saturated LCBs (OH-DHSs), was not in agreement with his analysis of the tandem mass spectrum illustrated in **25(A)**, and his final reported results.

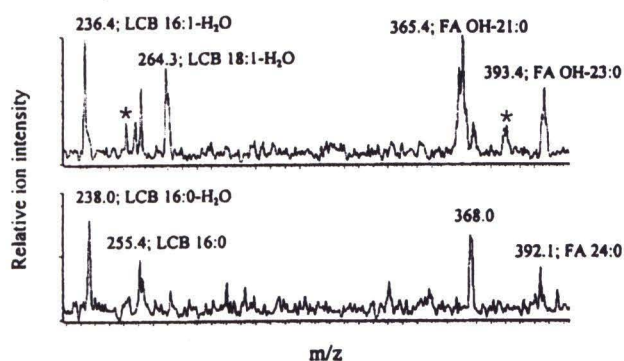


Figure 7. Product ion spectra (CID, APCI) of the Cer⁺ fragment ion (m/z 606) from the m/z 789 protonated molecule in peak SM1 (upper) and SM2 (lower) [see Fig. 5(B) and (C)] showing fatty acid and long-chain base ions. Ions of m/z 368 and 392 are both derived from a 24:0 FA (see Fig. 3). Approximately 5000 ng of bovine milk sphingomyelin sample were injected.

Figure 25. Figure 7 from Karlsson *et al.*'s paper showing the APCI MS/MS of the ion at m/z 606.6. The asterisks indicated ions which were not labeled. These peaks, from left to right, were probably the $[17:1 \text{ LCB} - \text{H}_2\text{O} + \text{H} + 1]^+$ at m/z 251.2 and $[23:0(\text{L}) + 1]^+$ at m/z 379.4.

Now one could suggest that Karlsson *et al.* meant to state that SM1 was composed of OH-SPMs. However, this conclusion would also be incorrect. The

calculated masses for $[21:0\text{OH(L)}]^+$ and $[23:0\text{OH(L)}]^+$ are 366.4 and 394.4, respectively. In **25(A)** however, the suggested masses, were both one *mass-to-charge* unit less than the calculated values, which suggested that these were not the indicated hydroxy-FAs. This was confirmed by the absence of the $[21:0\text{OH(L)} - \text{H}_2\text{O}]^+$ and $[23:0\text{OH(L)} - \text{H}_2\text{O}]^+$ ions, which from our analysis of 16:0 SPMOH above, were relatively abundant in the tandem m.s. So it appears that **25(A)** was not the MS/MS of the proposed hydroxy-SPLs.

Furthermore, the conclusion that SM1 were OH-SPMs was contradictory to the retention properties of the SPLs. The chromatographic properties of the SPLs were described in detail above, and it was shown that on a propyl-amine stationary phase (or, from a theoretical standpoint, on any polar stationary phase), the higher polarity of the hydroxy-SPLs caused them to have later RTs than their non-hydroxy counterpart. This was proven by comparing the RTs of 16:0 SPM and 16:0 SPM-OH (pages 105 – 109) in CES. This chromatographic behavior was expected, based on results from previous work and the fundamental principles of chromatography, which dictate that more polar molecules are retained longer than less polar molecules on a polar column. Karlsson *et al.* used a polar DIOL column for the LC separation. Therefore, it would be inaccurate to conclude that the first molecules to elute (SM1) were hydroxy-SPMs. It is highly improbable that, for example, 21:0 SPMOH eluted earlier than 21:0 SPM (in SM2) on a DIOL column. Even though his conclusions contradicted the fundamental principles of chromatography, Karlsson *et al.* offered no explanation for this deviation. One can only conclude therefore, that they were unaware of this error and that the mass spectrum shown in **25(A)** was not of a OH-SPL. This was confirmed by comparing **25(A)** with the MS² and MS³ m.s. of the +2 isotope of 22:0 SPM (Figure 26) from our work.

The most abundant ion in SM2 had a m/z of 787.4, which we identified as 22:0 SPM using tandem APCI-MS (pages 95 – 96). This suggested that the ion at m/z 789 in SM2 was probably the +2 isotope of $[22:0 \text{ SPM Cer} + \text{H}]^+$. From Figure 10, we see that the major components of 22:0 SPM were 18:1/22:0, 17:1/23:0 and 16:1/24:0, which had $[\text{FA}(\text{L})]^+$ fragment ions at m/z 364.4, m/z 378.4 and m/z 392.4, respectively. So, the MS^n m.s. of the +2 isotope of $[22:0 \text{ SPM Cer} + \text{H}]^+$ at m/z 606.6, should contain the +1 and +2 isotopes of the $[22:0(\text{L})]^+$, $[23:0(\text{L})]^+$ and $[24:0(\text{L})]^+$ ions at m/z 365.4, m/z 379.4 and m/z 393.4, respectively. Figure 26 shows the MS^2 (**26(A)**) and MS^3 (**26(B)**) m.s. of 606.6 from SPL2 of our work, in which the FA fragment ions are labeled, along with their corresponding +1 and +2 isotope peaks. Comparing Figure 26 to **25(A)** proved that the ions at m/z 365.4 and m/z 393.4 were the +1 isotopes of $[22:0(\text{L})]^+$ and $[24:0(\text{L})]^+$, respectively, and that **25(A)** was not the MS/MS of 606 from SM1. Therefore, the reason that the FA fragment ions in **25(A)** were one *mass-to-charge* unit less than the calculated masses for $[21:0\text{OH}(\text{L})]^+$ and $[23:0\text{OH}(\text{L})]^+$ was because these ions were incorrectly identified by Karlsson *et al.*

Since no scale was shown in **25(A)**, it was difficult to determine the m/z values of the unlabelled peaks, which we marked with asterisks. However, the peak approximately midway between the $[22:0(\text{L})]^+$ and $[24:0(\text{L})]^+$ isotope fragment ions, was probably the +1 isotope of $[23:0(\text{L})]^+$ at m/z 379.4, by comparison with Figure 26. Similarly, the unidentified ion midway between the 16:1 and 18:1 dehydrated LCB fragment ions was probably the +1 isotope of $[17:1 \text{ LCB} - \text{H}_2\text{O} + \text{H}]^+$ at m/z 251.2. So, **25(A)** was the MS/MS of the +2 isotope of $[22:0 \text{ SPM Cer} + \text{H}]^+$ from SM2, which agreed with all the available information. All the pieces of information obtained in our analysis supported

the conclusion that SM2 was composed of L-C SPMs and S-C DHSs, and so perhaps **25(A)** was actually the MS/MS mass spectrum for 606.6 from SM2.

25(B) shows saturated 16:0 LCB fragment ions, which contradicted Karlsson *et al.*'s conclusion that SM2 was composed of SPLs with unsaturated LCBs. Now we could argue that, Karlsson *et al.*'s characterization of SM2 was also incorrect and that he meant to say that SM2 was composed of DHSs. But, the results in Figure 31 showed that they reported that DHSs had a low abundance in bovine milk, whereas **23(A)** showed that SM2 was the largest SPL peak. In addition the results from ^{31}P NMR above clearly indicated that DHSs were significantly less abundant in bovine milk than SPMs. This meant therefore, that **25(B)** was not the MS/MS of 606.6 from SM2. Based on the above observations and by comparing **25(B)** with Figure 11, we concluded that perhaps **25(B)** was actually the MS/MS of 606.6 from SM1. So, comparing **25(B)** to Figure 11, the 16:0 LCB fragment ions and the $[24:0(\text{L})]^+$ and $[24:0(\text{S})]^+$ ions at *mass-to-charges* 368.4 and 392.1 respectively were observed, confirming the presence of 16:0/24:0. Also, the observed fragmentation pattern in **25(B)** was FP2, which was exhibited only by saturated DHSs (pages 96 – 98). From Table 7 we see that 16:0/24:0 was the most abundant SPL in 22:0 DHS, and accounted for 16.7% (16.4%) of all the SPLs in SPL1. 16:0/24:0 was the second most abundant SPL in SPL1 which was in agreement with **24(A)**. So, all the pieces of information obtained in our analysis supported the conclusion that SM1 was composed of L-C DHSs, and so perhaps **25(B)** was actually the MS/MS mass spectrum for 606.6 from SM1.

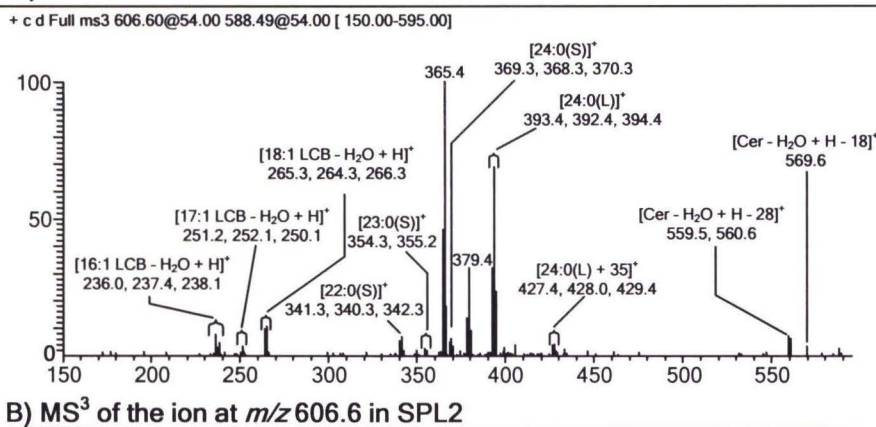
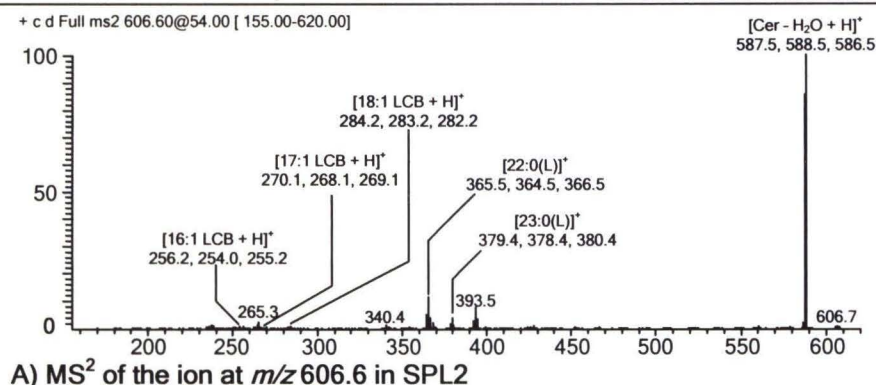


Figure 26. The MS² (A) and MS³ (B) of the ion at m/z 606.6 in SPL2. This figure clearly shows that this ion was the +2 isotope of [22:0 SPM Cer + H]⁺, which proved that mass spectra in Figure 25 were incorrectly labeled by Karlsson *et al.*. The upper was the MS/MS of 606.6 in SM2 and the lower was the MS/MS of 606.6 in SM1.

The above analysis proved that Karlsson *et al.* incorrectly interpreted the mass spectra in **25(A)** and **25(B)**, which implied that their identification of hydroxy-SPLs in SM1 was inaccurate. Based on the data Karlsson *et al.* presented in his paper, there was no indication of any hydroxy-SPLs in bovine milk since the m.s. he used to prove this conclusion was inaccurately characterized. As we have shown above however, OH-SPMs were present in bovine milk (Table 61), but their abundance was so low that they were difficult to identify and could not be quantified. The OH-SPLs were shown to elute later than their non-hydroxy SPL counterparts and were identified using APCI tandem MS.

Other observations in Karlsson *et al.*'s paper suggested that his identification of OH-SPLs in bovine milk was not in agreement with the data he acquired. For example, Karlsson *et al.* stated that "the estimated relative amounts of hydroxy-FAs [in our Figure 31] were in agreement with previous findings" that were found in reference 8. In that reference, Morrison and Hay stated that "the proportion of hydroxy fatty acids in the total fatty acids" in bovine milk, "was always very small (estimated < 1%), and could not be determined accurately." In agreement with this paper, Karlsson *et al.* reported that OH-SPLs had a very low abundance in his final tabulated results. However from **23(A)**, it can be seen that SM1 certainly accounted for more than 1% of the total SPL population. Therefore, his statement that SM1 was composed of OH-DHSs contradicted his own conclusion that they were relatively low in abundance (< 1% based on Morrison and Hay's paper). So, it appears that in his desire to find OH-SPLs in bovine milk, Karlsson *et al.* misinterpreted the data.

In addition, Karlsson *et al.* did not identify any OH-SPLs in bovine milk when using HPLC plasmaspay (PSP)⁴ MS (Figure 32), and he offered no explanation for this difference between the analyses, even though the m.s. obtained using APCI MS/MS were very similar to those obtained by PSP MS/MS (Figure 27). Based on the marginal quality his analysis by HPLC APCI MS/MS however, all of Karlsson *et al.*'s previous papers that describe the HPLC tandem MS of SPLs are questionable, since they may contain similar analytical errors. The fact that no OH-SPLs were observed by PSP MS/MS should have raised red flags in the researchers' minds that should have prompted them to investigate this inconsistency.

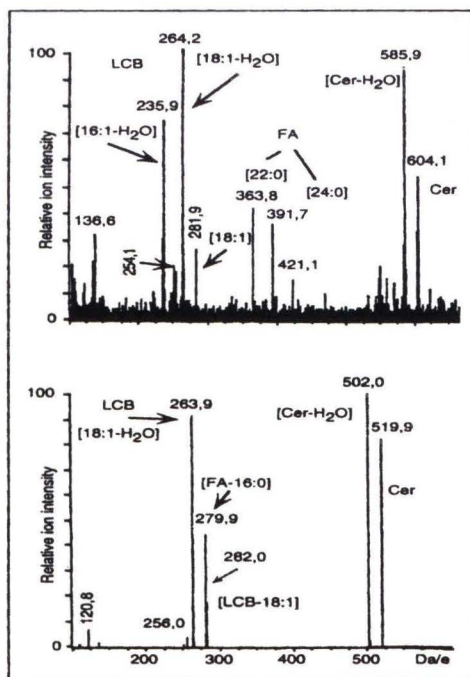


Fig. 5: MS/MS-CID spectra of the ceramide units of Da/e 604.8 (upper) and 520.7 (lower) showing ions of long-chain base (LCB) and fatty acid (FA) origin

Figure 27. Figure 5 from reference 4 showing the PSP MS/MS-CID spectra of protonated ceramides. The mass spectra were similar to that obtained by APCI MSⁿ. This data was obtained by Karlsson *et al.*

From the above observations it was proven that Karlsson *et al.*'s, characterization of SM1 as hydroxy-SPLs was incorrect, and that our description of the retention characteristics of the SPLs was accurate, where SM1 was composed of L-C DHSs. This is in agreement with Morrison and Hay, who reported that there was 17.8% (wt%) of DHS in bovine milk. In fact, Tables 31 to 40 indicate that our results by APCI and ESI MS are in very good agreement with Morrison and Hay.⁸ Finally, Tables 61 and 62 show that OH-SPMs were present in BMS and CES, respectively. No OH-SPLs were identified in BBS.

Figure 28 shows a diagram from Karlsson *et al.*'s paper, which illustrated the +ESI (28(A)) and +APCI (28(B)) m.s. for 18:1/18:0. Unlike the ESI m.s. of 18:1/18:0

from our data (Figure 29), the m.s. in Figure 28 showed extensive fragmentation in both the APCI and ESI ion sources. This was expected, since Karlsson *et al.* used upfront CID for the analyses. Although no upfront CID was used in our experiments, the inherent gentle fragmentation characteristic of APCI (versus ESI for example) resulted in mild fragmentation of the SPLs in the ion source. As previously described (pages 109 – 113), all the ions shown in Scheme 2 and Figure 16 (except for $[M - N(CH_3)_3 - H_2O + Na]^+$) were present in the full-scan APCI m.s. This complexity was a significant problem in the APCI data which was addressed in our analysis, and it should be obvious that Karlsson *et al.*'s use of upfront CID exacerbated the problem (see **28(B)**).

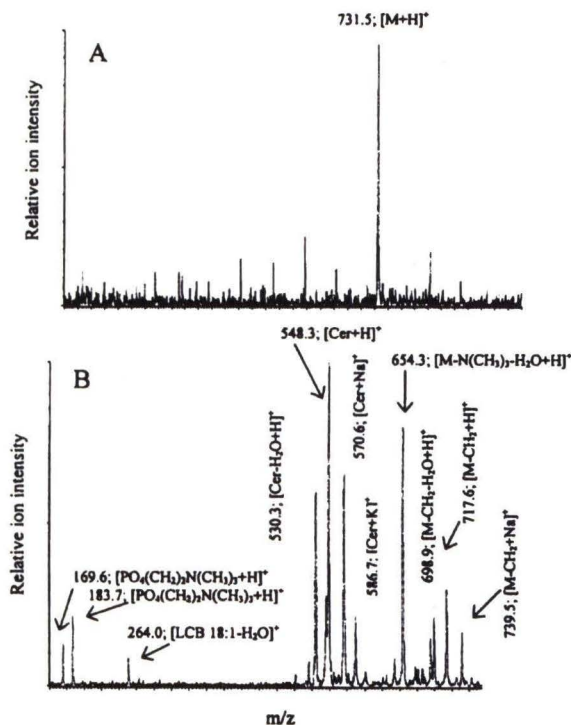


Figure 2. Mass spectrum of *d*-18:1/18:0-sphingomyelin obtained by (A) electrospray ionization and (B) atmospheric pressure chemical ionization. See Experimental section for additional mass spectrometry.

Figure 28. Diagram from Karlsson *et al.*'s paper illustrating the +ESI and +APCI MS of *d*-18:1/18:0. The use of upfront CID in these experiments resulted in extensive fragmentation in the APCI source. The +ESI and +APCI m.s. acquired in our analyses are shown in Figure 29.

From a single molecule of 18:1/18:0, Karlsson *et al.* indicated 8 unique primary fragment ions in the full-scan APCI-MS m.s., whereas in our data, the primary ions were $[18:0 \text{ SPM Cer} + \text{H}]^+$ at m/z 548.6, and its dehydrated fragment ion at m/z 530.8 (**29(B)**). By ‘unique’ we mean those SPL ions that contain the single combination of LCB and FA. The $[\text{Phosphoryl Choline} + \text{H}]^+$ and $[\text{Phosphoryl Choline} - \text{CH}_2 + \text{H}]^+$ ions were not observed in our analysis because the scan range used by us was from m/z 200 - 1200. The fragments in **28(B)** were of significant abundance, some of which accounted for more than 50% of the $[\text{Cer} + \text{H}]^+$ ion peak (for example, $[\text{Cer} + \text{Na}]^+$ at m/z 570.6). Although these fragments were also observed in our data their abundances were significantly lower than the $[\text{Cer} + \text{H}]^+$ (only the dehydrated ceramide fragment ions had an appreciable abundance in our data), which allowed for the unambiguous identification of each molecular species

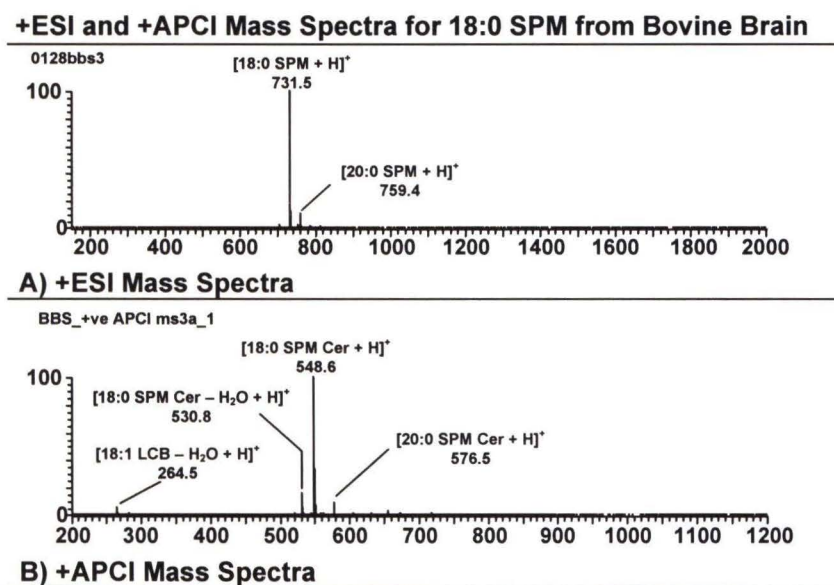


Figure 29. The positive ESI (**A**) and positive APCI (**B**) mass spectra of 18:0 SPM in bovine brain. Comparison with Karlsson *et al.*'s data in Figure 28 showed that there was extensive fragmentation in their data that made it difficult to decipher the mass spectra.

It is important to note that Karlsson *et al.* only showed the full-scan APCI m.s. in which 18:1/18:0 was the predominant SPL molecule. Showing this example however, was a bit misleading because it did not fully communicate to the reader the extreme complexity of the m.s. The m.s in Figure 28 was probably from bovine brain, since in this sample 18:0 SPM accounted for 89.5% (91.4%) of the SPLs in the SPL3 peak (Table 20). But what would Karlsson *et al.*'s average mass spectrum. across SM2 in BMS look like? In SPL2 of BMS there were a larger number of SPL species (more than in SPL3 of BBS) and there was extensive overlap between the L-C SPMs and S-C DHSs. We found that there were 8 distinct DHS groups and 14 SPM groups in SPL2 (Tables 9 and 10 respectively), which implied that Karlsson *et al.*'s average mass spectrum across SM2 should contain a minimum of 176 fragment ions (since there were 8 fragments per SPL group), many of which were isobaric. In our data for BMS however, the minimum number of fragments that were observed in the mass spectrum across SPL2, was 44 (2 primary fragments per SPL group).

As illustrated in the “Identification” and “Quantification” sections above, it was still difficult and laborious to determine the LCB/FA composition, even though our APCI-MS data was 4 times less complex. It should be obvious therefore, that with 176 fragment ions in the APCI m.s., it would be extremely difficult, if not impossible, to unambiguously identify and quantify the SPLs in bovine milk using their technique. This, of course, would explain why Karlsson *et al.*'s reported “composition” of these extracts was so ambiguous; using asterisks to represent an unknown and subjective quantity (see Figure 31).

Also, the extensive fragmentation in Karlsson *et al.*'s APCI data probably contributed to their misinterpretation of the results. With so many molecular species and isobaric fragment ions, it was more than likely that numerous errors were made in the identification process. Evidence of these errors was obvious in his reported identification of hydroxy-SPLs in SM1 of BMS. Karlsson *et al.*'s use of upfront CID resulted in the nonspecific and extensive fragmentation of all the molecules eluting from the column, which drastically increased the complexity of the APCI m.s. In such a chaotic "ion soup", identification and quantification of the SPLs was a daunting task, bordering on the impossible. This was a poor mass-spectrometric analysis.

A similar case can be made against the results obtained by both positive and negative ESI-MS. Although the fragments produced from CID in the ESI source (compared to the protonated molecule) were not as intense as those in APCI m.s. (compared to $[\text{Cer} + \text{H}]^+$), the increased complexity and reduction in the signal to noise ratio provided no direct benefit to the analyses. Comparing **28(A)** to **29(A)** it was observed that in the latter mass spectrum, the $[\text{18:0 SPM} + \text{H}]^+$ ion was the base peak with little to no fragmentation in the ion source, thereby reducing ambiguity to a minimum. Though Karlsson *et al.* did not show the results for -APCI and -ESI experiments, the same criticisms will apply, since upfront CID was also used in these experiments.

Figure 30 shows the main mass spectral ions that Karlsson *et al.* identified in +ESI, and +APCI MS, and tandem MS, with the primary ions enclosed in square brackets. The 3-membered ring structures for the protonated ceramide and $[\text{FA(L)}]^+$ ions are believed to be less stable than the proposed 5-membered ring structures in Scheme 2.

In our analysis, like that of Karlsson *et al.*, the ESI MS/MS of the protonated molecules only produced the phosphorylcholine HG fragment at m/z 184.1, and was therefore not useful in determining the LCB/FA composition. The APCI MS/MS spectra in Karlsson *et al.*'s work (Figure 25) had a very poor S/N in comparison to our data (Figure 26), but their general description of their analysis was accurate. He did account for the overlapping of the masses of the LCB and FA fragment ions in the MS/MS spectra. In addition, he was aware that the $[\text{LCB} + \text{H}]^+$ and $[\text{LCB} - \text{H}_2\text{O} + \text{H}]^+$ ions, both had to be observed in order to prove the identity of a specific LCB. Similarly, the $[\text{FA}(\text{L})]^+$ and $[\text{FA}(\text{S})]^+$ ions both had to be present in the tandem m.s. in order to prove the identity of a specific FA.

ESI:

$[\text{M} + \text{H}]^+$, $[\text{phosphoryl choline} + \text{H}]^+$

APCI:

$[\text{M} - \text{CH}_3 + \text{H}]^+$, $[\text{M} - \text{CH}_2 - \text{H}_2\text{O} + \text{H}]^+$, $[\text{M} - \text{CH}_2 + \text{Na}]^+$, $[\text{M} - \text{CH}_2 - \text{H}_2\text{O} + \text{H}]^+$, $[\text{M} - \text{N}(\text{CH}_3)_3 - \text{H}_2\text{O} + \text{H}]^+$, $[\text{M} - \text{N}(\text{CH}_3)_3 - \text{H}_2\text{O} + \text{Na}]^+$, ***$[\text{Cer} + \text{H}]^+$*** , $[\text{Cer} + \text{Na}]^+$, $[\text{Cer} + \text{K}]^+$, $[\text{Cer} - \text{H}_2\text{O} + \text{H}]^+$, ***$[\text{LCB} - \text{H}_2\text{O}]^+$*** , $[\text{phosphoryl choline} + \text{H}]^+$, $[\text{phosphoryl choline} - \text{CH}_2 + \text{H}]^+$

Tandem mass spectrometry (CID-APCI):

$[\text{LCB}]^+$, $[\text{LCB} - \text{H}_2\text{O}]^+$, $[\text{FA long}]^+$, $[\text{FA short}]^+$

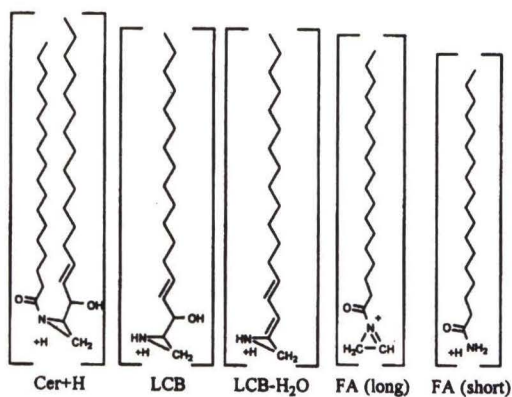


Figure 3. Some mass spectral ions obtained in electrospray ionization, atmospheric pressure chemical ionization and tandem mass spectrometry. The proposed/suggested structures refer to those written in bold italics above.

Figure 30: Figure 3 from Karlsson *et al.*'s paper showing the structures of the primary fragment ions observed in the APCI MS and MS/MS mass spectra.

Since his description of the MS/MS analysis was accurate, his misidentification of OH-SPLs was probably influenced by the results of Morrison and Hay. So, the main problems with his work were: 1) The incorrect identification of SM1 as hydroxy-SPLs; 2) The use of upfront CID in the analysis, which resulted in extremely complex APCI and ESI m.s.; and 3) Because of (2) identification and quantification of the SPLs could not be accurately performed and so the final “composition” was questionable and ambiguous.

2. THE RESULTS

Karlsson *et al.* only reported the composition of these samples by APCI-MS. Using the dual parallel methods developed in this work however, the composition by both APCI-MS and ESI-MS was determined (Tables 31 – 60). From these results, it was observed that the number of LCB/FA combinations were greater in BMS than in any other sample. 49 protonated molecules of intact SPM were identified in BMS by ESI-MS (Tables 7, 9, 10 and 13), which was 13 more than reported by Karlsson *et al.*. In addition, 97 LCB/FA combinations altogether were found in comparison to 28 from Karlsson *et al.*'s work. According to Karlsson *et al.*, “of the 36 protonated molecules detected in ESI, 12 were present at levels above the limit of detection for MS/MS analyses in APCI.” Hence there were more LCB-FA combinations in BMS than shown.” So, Karlsson *et al.* was only able to determine the LCB/FA composition of 33.3% of the SPL groups detected by ESI-MS. In contrast, of our 49 protonated molecules, MSⁿ data was obtained for 35. Therefore, the LCB/FA compositions of 71.4% of the SPL groups detected by ESI-MS were determined. So, our analysis of BMS was 38.1% more sensitive, when compared to Karlsson *et al.*'s results. This was a significant improvement in the sensitivity, and ultimately, the accuracy of the analysis. The remaining 14 minor

molecular species, for which MSⁿ data was not acquired in our work, were labeled with asterisks.

For bovine brain and chicken egg yolk, at least, 37 (Tables 15, 17, 18 and 20) and 35 (Tables 22, 23, 25 and 27) protonated molecules were found, respectively (compared to 20 and 30, respectively, from Karlsson *et al.*'s results). In bovine brain and chicken egg yolk SPM, 58 and 41 LCB/FA combinations were found (same tables as show above for the protonated molecules), respectively, compared to 16 and 11 combinations, respectively, from Karlsson *et al.*'s results. In all samples, since several protonated molecules were present at levels below the limit of detection for MSⁿ analyses, some other LCB/FA combinations were present. However, the analysis presented in this work far surpassed all previous attempts to determine the LCB/FA composition of bovine milk, chicken egg yolk, and bovine brain SPM extracts by APCI and ESI MS.

Table 1. LCB-FA combinations in sphingomyelin as obtained by APCI-MS/MS from bovine milk, bovine brain, bovine erythrocytes and chicken egg yolk.^a

Bovine milk		LCB						Bovine erythrocytes		LCB					
FA	16:1	16:0	17:1	17:0	18:1	18:0		FA	17:1	18:2	18:1	18:0	19:1		
14:0					*			16:0	***		***		*		
16:0	*		**		***			17:0			***				
18:0	***							18:0	**		**				
21:0					***			20:0			*				
22:0	***	*	***	*	**	***		22:0			***	*	*		
23:1		*						23:1					***		
23:0	***	*	**		***	***		23:0			**		*		
24:0	**	*	***		***			24:1			***				
25:0	**							24:0	*	***	***		**		
OH-21:0	*				*			25:0			**				
OH-22:0			*		*			26:1		**					
OH-23:0	*							26:0			**				
Bovine brain		LCB						Chicken egg yolk		LCB					
FA	16:1	18:1	18:0	19:1	20:1			FA	18:2	18:1	19:1				
16:0		*						16:1		*					
18:0		***	*					16:0	*	***	**				
20:0		**						17:0			**				
21:0		*						18:0		**					
22:0		**						20:0		**	*				
24:1		***		**	*			22:0		**					
24:0	**	***						23:1			**				
25:1		**		*				24:1		***					
26:1		**													
27:1	*	*													

^a *, ** and *** denotes low, medium and high relative amounts, respectively.

Figure 31. Karlsson *et al.*'s final table of results showing the LCB/FA compositions of bovine milk, bovine brain and chicken egg yolk sphingomyelin extracts. The composition was denoted using asterisks to represent ambiguous quantities. Our compositions in Tables 31 to 60 significantly improve upon Karlsson *et al.*'s results.

Table 2. LCB-FA combinations in sphingomyelin from bovine milk as obtained by PSP-MS/MS^a

FA	LCB				
	16:0	16:1	17:0	17:1	18:1
14:0					**
16:0		**		**	***
16:1			*	*	
17:1	*				
18:0					*
18:1	**				
20:0		*			
20:1	*				
22:0	**	***	**	***	
23:0		***		**	***
23:1			**		*
24:0		***		**	***
24:1	**				

^a*, ** and *** denote low, medium and high relative amounts, respectively.

Figure 32. A table from Karlsson *et al.*'s paper showing the LCB/FA composition of bovine milk by plasmaspray tandem mass spectrometry.

I.F. Conclusions

In his 1998 paper, Karlsson *et al.* attempted to “describe the complete structural elucidation of intact SPMs by using HPLC/API-MS/MS.” However, poor mass spectrometric techniques and data interpretation resulted in the misidentification of molecular species. His use of upfront CID caused extensive fragmentation in the ion source, producing 8 unique fragments per SPL molecule, many of which were isobaric with the protonated ceramide and fragment ions from other molecules. This resulted in very complex APCI and ESI m.s. that made it difficult, if not impossible, to accurately identify and quantify the SPLs in these mixtures. This difficulty probably contributed to their misidentification of the hydroxy-SPLs in SM1 of bovine milk. All these problems indicated that their reported compositions of bovine milk, bovine erythrocytes, bovine brain and chicken egg yolk SPM extracts, were dubious. In our work, we outlined

Karlsson *et al.*'s mistakes and presented a thorough and accurate quantification of three of the four SPM extracts that they analyzed (a bovine erythrocytes SPM extract was not analyzed here). Because of the numerous errors in Karlsson *et al.*'s analysis, our work therefore, is the first accurate and complete structural elucidation of intact SPMs in bovine milk, bovine brain, and chicken egg yolk sphingomyelin extracts by APCI-MS and ESI-MS. This work lays the foundation for the analysis of any SPL mixture by HPLC with detection by dual parallel mass spectrometry using APCI and ESI.

It was found in our analysis that quantification of the SPLs using only full-scan APCI m.s. was not possible in mixtures that contained 1) SPLs with one (i.e. Y:1 SPLs) or two sites (i.e. Y:2 SPLs) of unsaturation on the FA chain, and 2) SPLs with both even and odd FA chain lengths. This was because Y:2 and Y:1 SPLs were isobaric with $[(Y + 1):0 \text{ SPL Cer} - \text{H}_2\text{O} + \text{H}]^+$ and its plus 2 isotope, respectively. These ions also had overlapping RTs and therefore, could only be quantified using APCI MSⁿ data. Also, it was found that Y:2 SPLs were isobaric with the +2 isotope of the sodium adducts of saturated SPLs in ESI mass spectra, and they also had overlapping RTs. Therefore, these species could not be quantified by ESI-MS unless negative-ion ESI-MS data was available, from which the relative proportions of these species could be determined. These were just some of the many mass and RT overlaps that were observed in the full-scan m.s., and it should be obvious that if the m.s. was more complicated (such as in Karlsson *et al.*'s analysis, which was 4 times more complex) then both identification and quantification of the SPLs would be impractical.

The general steps in our analysis were as follows. First, protonated ceramide ions in full-scan APCI-MS m.s., and the protonated molecules and formate adduct ions in the

ESI full-scan m.s., for each SPL group were identified. Second, the protonated ceramide ions obtained by APCI-MS, were submitted to MS² and MS³ analysis in order to identify the LCB/FA combinations present in each SPL group. Finally, after identification, the composition of the LCB/FA combinations (mole%) was determined from the peak areas in extracted ion chromatograms. The methods used to quantify the LCBs and FAs in this work provide a starting point for the analysis of any SPL mixture.

To improve the accuracy of the results, APCI:APCI (LCQ:TSQ) and ESI:APCI (LCQ:TSQ) LC1MS2 experiments were also performed. Unfortunately, because of a lack of time, the quantification of the SPLs in these data sets was not performed. Also, an ESI:ESI (LCQ:TSQ) experiment should be performed, so as to have mass spectral data for the three SPM samples using all possible dual parallel mass-spectrometric configurations. Quantification of the SPLs from the complete set of experiments outlined above, will allow response factors (RFs) that account for the differences between the two instruments and ionization techniques to be calculated. Applying these RFs to the raw areas from EICs will produce a more consistent and accurate composition of the SPLs in these samples. These experiments would also determine if the formation of dimer and sodium adduct ions in the LCQ ion trap affects the quantification of the SPLs. Also, we have developed a method to eliminate the formation of dimers and sodium adducts in the LCQ, by introducing a solution of 50mM glycine in 1M NH₄OCOH at a pH of 8.5, post-column. Additional LC1MS2 experiments would help to determine what effect this solution has on the accuracy of the quantification. Finally, the LCB/FA composition of these samples should also be determined by GC-MS, so that the results can be compared to those obtained by LC-MS. RFs could then be calculated from the GC-MS data, and

combined with those from the LC1MS2 experiments, to further improve the accuracy of the analysis.

The experimental approaches and results presented in this work provided detailed information about SPM and DHS molecular structure, and developed methods that allowed the determination of the LCB/FA composition of SPL mixtures by APCI and ESI MS in parallel, simultaneously. These procedures almost certainly prove useful in elucidating the role that SPM and DHS plays in intracellular signaling and the structure of cell membranes.

II. Human Eye Lenses

II.A. Liquid Chromatography/Mass Spectrometry

1. MASS SPECTROMETRY

An HPLC APCI-MS (Figure 33.1) and ESI-MS (Figure 33.2) separation of the lipids in young human eye lens (YELs) samples is shown in Figure 33. It was observed that the SPLs had the same retention properties as those described for the commercially available SPM extracts (the SPM extracts were CES, BBS, and BMS). In addition, the analysis of the SPL peaks by APCI and ESI full-scan MS, was similar. The differences between the two analyses were as follows: 1) APCI was performed on the TSQ and ESI on the LCQ, which resulted in a high abundance of PL dimer ions, and sodium adduct ions in the ESI-MS data (see pages 76 – 80); 2) Upfront CID of energy 20V was used in the analysis by ESI-MS. This produced mild fragmentation of the SPLs in the ESI source; and 3) there was a very abundant contaminant at m/z 705.4 in both the ESI and APCI data.

This contaminant had the same mass as $[16:0 \text{ DHS} + \text{H}]^+$ and $[16:1 \text{ SPM} + \text{H}]^+$, which significantly affected the quantification by ESI-MS, since 16:0 DHS was the most abundant SPL group in human lenses.² The quantification by APCI-MS however, was not affected by the presence of this contaminant. This was because the SPLs were quantified using the areas of the protonated ceramide ions in EICs. Since the $[\text{Cer} + \text{H}]^+$ ions had even masses, and were all 183 *mass-to-charge* units less than their corresponding protonated molecules, then the mass of the contaminant was not isobaric with any protonated ceramide ions. As a result, the APCI-MS data was used to determine the SPL

composition of these samples. All the terms and concepts described on pages 50 – 52 will also be used to explain the analysis of these samples.

Young Human Lens Extract, Dual Parallel, LC/LCQ

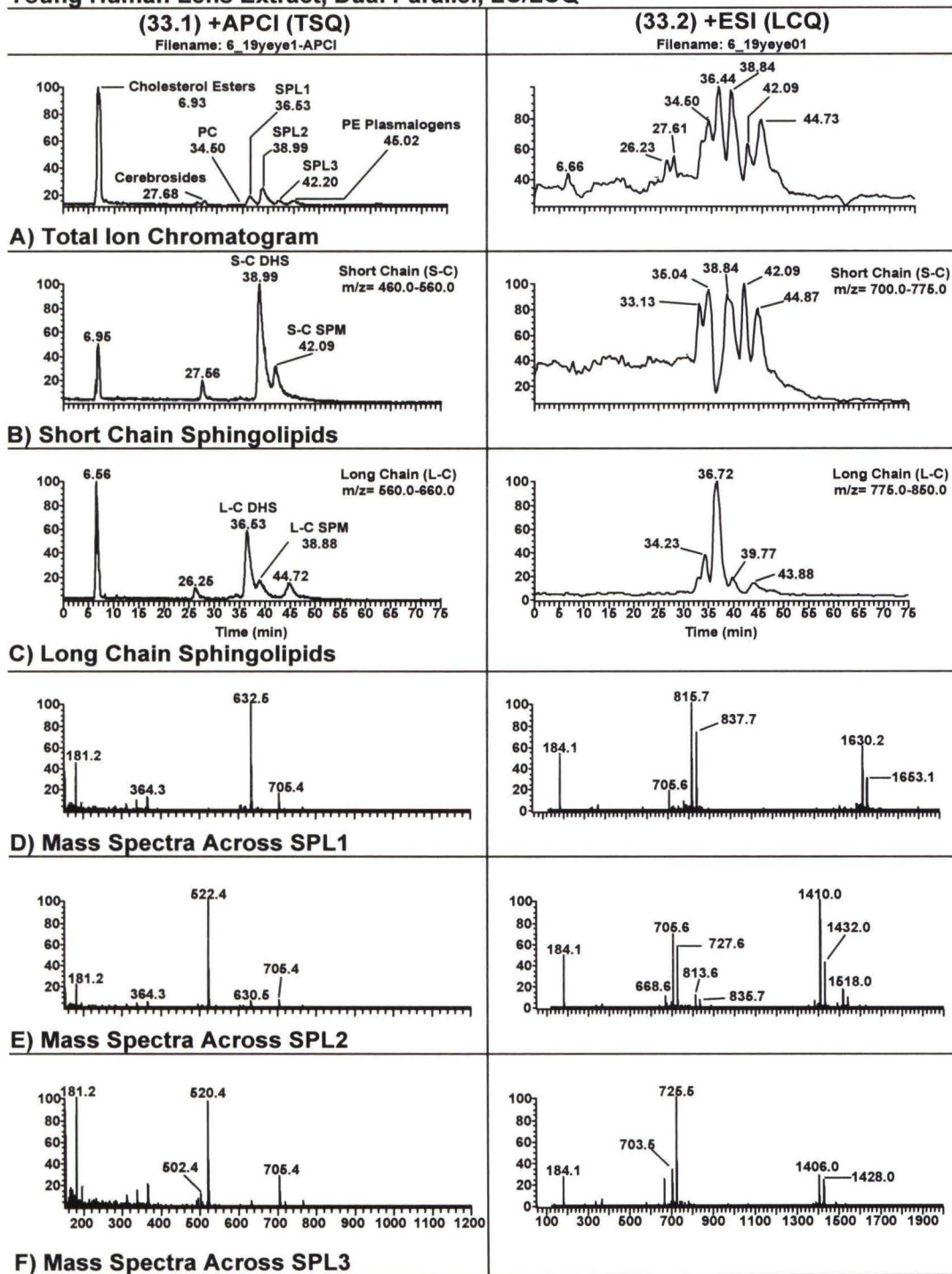


Figure 33. Positive APCI (column 33.1) and positive ESI (column 33.2) extracted ion chromatograms (A – C) of young eye lens extracts.

From Figure 33 it was observed that human eye lenses contained cholesterol, cholesterol esters, cerebrosides, phosphatidyl cholines, sphingolipids (DHS and SPM) and phosphatidyl ethanolamine plasmalogens, in order of RT (**33.1.A** and **33.2.A**). The +APCI m.s. (**33.1.D** – **33.1.F**) showed that the protonated ceramide ion was the base peak, and that there was very little fragmentation in the ion source. The most abundant species in SPL1, SPL2 and SPL3 were 24:1 DHS, 16:0 DHS and 16:0 SPM respectively. The corresponding protonated molecules for these species were observed in the +ESI m.s. (**33.2.D** – **33.2.E**) in addition to their dimer and sodium adducts.

The 705.4 contaminant was observed in all m.s. However, the high background in **33.2.B** produced from the contaminant ended at approximately 55 minutes, which indicated that it was present in the solvent bottle that contained hexane/IPA (see the solvent program in Figure 7 in Chapter II.) When a new batch of this solvent was made using fresh hexane, the contaminant disappeared. Unfortunately, the experiments above were performed using the only available lens samples and so the analysis could not be redone. Negative ESI-MS data across SPL2 for young eye lenses was shown in Figure 7, and its analysis was similar to that described for the commercially available SPM extracts.

2. TANDEM MASS SPECTROMETRY

The LCQ was set up to perform MS^2 and MS^3 on the most abundant ions, in both positive and negative ESI mode. However, most of the MS^n analyses were performed on the contaminant, since it was very abundant in the m.s. As a result no useful tandem MS data was obtained for the eye lens SPLs. As previously explained however, tandem ESI

MS of the SPLs does not produce LCB or FA fragment ions, and so would not be useful in the determination of the LCB/FA composition.

No APCI tandem MS data was acquired for these analyses. As described in detail for the SPM extracts, quantification by full-scan APCI-MS was not possible due to the extensive mass-overlap of fragment ions in the m.s. This was a problem for the SPM extracts because there were SPLs with both even and odd FA chains. Only SPLs with even FAs were present in human lens samples however, so that there were no mass-overlaps between 1) $[Y:2 \text{ SPL Cer} + \text{H}]^+$ and $[(Y + 1):0 \text{ SPL Cer} - \text{H}_2\text{O} + \text{H}]^+$; and 2) $[Y:1 \text{ SPL Cer} + \text{H}]^+$ and the +2 isotope of $[(Y + 1):0 \text{ SPL Cer} - \text{H}_2\text{O} + \text{H}]^+$. So, the SPLs were quantified by determining the areas of the peaks of the protonated ceramide ions in EICs. Since the dehydrated ceramide fragment ions were not as abundant as in the LCQ data for the SPM extracts, they were not used for quantification. Other lipids, such as cholesterol, cholesterol esters, phosphatidyl cholines, phosphatidyl ethanolamine plasmalogens, and cerebroside, were also present in the eye lens, but they were not quantified.

II.B. Results

The results were obtained from individual lenses of specific ages, and allowed us to determine how the composition of the molecular species of DHS, SPM and PC changed with the age and with the onset of cataracts. It was observed that, in all human eye lens samples, the predominant DHSs were 16:0, 24:1, 14:0 and 24:0, from highest to lowest abundance. The predominant SPMs were 16:0, 24:1, 24:0 and 14:0, in order of decreasing abundance. Also, the compositions of PC were the same in young and old

eye lenses(OELs). But in cataractous eye lenses (CELs), the abundance of the PCs was so low as to be unobservable in this sample.

Figures 34 to 36 show the compositions of the sphingolipid populations obtained by APCI-MS in young, old and cataractous eye lenses. The DHS molecular species represented 82.2%, 80.5% and 81.1% of the SPLs in YELs, OEL, and CELs respectively. The sum of all the percentages in Figures 34 to 36 was 100%. From these figures (which represents the data in Table 64) it was observed that DHS was the most abundant species for every identified SPL group. The ratio of DHS to SPM was different for different acyl chains. For example, the ratio of 24:1 DHS to 24:1 SPM was equal to 6.3:1, while the 24:0 DHS: 24:0 SPM was equal to 1.8:1. The ratio of 1.8:1 indicated that there was a preference for the monounsaturated molecule. So, for example, there was a preference for 24:1 DHS versus 24:1 SPM since the former had 1 double bond in the molecule, whereas the latter had two double bonds; one on the LCB backbone and the other on the FA chain. The same pattern was observed in all three lens samples, as shown in Figures 34 to 36.

Figures 37 to 39 show the compositions of the molecular groups in each SPL species. In these figures, the total DHS and SPM populations were each normalized to 100%. From these figures it was observed that DHS contained more 16:0 than SPM, but that SPM contained more 14:0 than DHS, in all three samples. In addition, the preference for the monounsaturated species was also observed in all eye lens samples. This information provided detailed knowledge of the composition of the human eye lens membrane, which is essential for developing an understanding of membrane stability, fluidity, transparency and structure.

The DHS and SPM populations exhibited small differences between the young and old eye lenses. Previous results by ^{31}P NMR^{15, 19} showed that as a class, DHS did not increase significantly with age. However, since MS was capable of distinguishing between the molecular species of SPL classes, we were also able to show how the molecular species within a SPL class changed with age and the onset of cataracts. From Figure 37 it was observed that there was an increase in the 24:0 and 24:1 DHS molecular species, and a decrease in 16:0 DHS in old lenses. The increases and decreases of the DHS molecular species offset each other to produce no net change in the amount of the class present, as shown by ^{31}P NMR. The case for SPM was slightly different. SPM was shown by ^{31}P NMR to increase with age^{15, 19}, as a class. The APCI-MS data in Figure 35 showed that the 16:0, 24:0 and 24:1 increased slightly with age, but only 14:0 showed a decrease. This determination of the molecular species composition was crucial to gaining a complete understanding of the structure of the lens membrane and may help to elucidate the role that SPLs play in the processes of aging and cataractogenesis. This information on individual molecular species cannot be obtained from ^{31}P NMR.

When Figures 37 and 38 were compared, there was a noticeable change in the molecular species (SPM and DHS) between the ‘normal’ (young and old) lenses and the cataractous lenses. The amount of 24:1 decreased in cataractous lenses, while the amounts of 16:0 increased. It was interesting to note that both DHS and SPM exhibited similar changes. Both DHS and SPM gained 16:0 at the expense of 24:1. These data represent the first time that the composition of the DHS molecular species in cataractous lenses has been shown.

Quantification using the $[M + H]^+$ ion of the SPLs in ESI m.s., was also attempted. However, it was found that the results by ESI-MS on the LCQ did not agree with those obtained using APCI on the TSQ. In previous papers in which different LC/MS machines were used² however, both APCI-MS and ESI-MS techniques gave similar results for the composition of the SPLs. In addition, the analysis of the SPM extracts in Section I. above produced results that were consistent between the two ionization techniques. These observations implied therefore, that the disagreement between the APCI and ESI results obtained for the eye lens samples was caused by a difference between the two mass spectrometers used for the different analyses.

Unlike the commercially available SPM extracts, the eye lens samples were analyzed using APCI on the TSQ and ESI on the LCQ. It was shown in Section I (pages 76 - 80) that when ESI-MS was performed on the LCQ (versus the TSQ), a large abundance of dimer and sodiated adduct ions were present in the ESI data. Mass spectra showing these undesirable ions are shown in Figures 6, 7 and 33. A detailed description of the types of dimers that were observed and their relative intensities was previously explained, and all those principles can also be applied here.

From one SPL molecule, ESI on the LCQ produced 1) the $[M + H]^+$ ion 2) the sodium adduct ion and 3) dimer ions that had the general formula $[M + X + H]^+$, where X could represent ANY SPL that coeluted with M. For example, if there were 20 other SPL molecules eluting at the same time as M, then there would be 21 different dimer ions produced from M (20 heterodimers and 1 homodimer). In addition, all of these dimers also had a corresponding sodium adduct ion with general formula $[M + X + Na]^+$, bringing the total number of ions produced from each of the hypothetical SPL molecules

to approximately 42 in ESI mode. These undesirable dimer ions, in addition to the 705.4 contaminant, had a significant impact on the quantitative analysis of the SPLs using the ESI data acquired on the LCQ. To overcome this problem, the areas of the $[M + H]^+$, $[M + Na]^+$ and $[M + M + H]^+$ and $[M + M + Na]^+$ ions were added together in an attempt to account for all the molecules of a particular molecular species. Unfortunately, this method failed because the dimers and/or sodium adducts were not formed with equal probability.

Despite the difficulties encountered with performing ESI-MS on the LCQ, reliable quantification was still possible using the APCI-MS data from the TSQ. The data shown in Figures 34 to 39 and Tables 64 and 65, demonstrated that changes did occur in the composition of the molecular species of the DHS and SPM classes with aging and the onset of cataracts.

Table 64: Composition of the Sphingolipids (mole%) in Young, Old and Cataractous Eye Lenses

Species	Young		Old		Cataracts	
	DHS (%)	SPM (%)	DHS (%)	SPM (%)	DHS (%)	SPM (%)
14:0	3.6	1.2	3.6	1.2	3.9	1.3
16:0	50.2	9.3	48.7	10.2	51.6	10.5
16:1	0.6	0.4	0.6	0.5	0.8	0.5
18:0	0.4	0.1	0.4	0.1	0.4	0.1
18:1	0.1	0.0	0.1	0.0	0.1	0.0
18:2	0.0	0.0	0.0	0.0	0.0	0.0
20:0	0.2	0.1	0.2	0.1	0.2	0.1
20:1	0.1	0.0	0.1	0.0	0.1	0.0
20:2	0.0	0.0	0.0	0.0	0.0	0.0
22:0	1.5	0.7	1.5	0.8	1.3	0.7
22:1	2.5	0.4	2.3	0.4	2.4	0.4
22:2	0.1	0.3	0.1	0.3	0.1	0.3
24:0	3.6	2.0	3.8	2.2	3.2	2.1
24:1	17.9	2.8	18.0	3.2	15.8	2.6
24:2	1.0	0.2	0.8	0.3	0.8	0.2
26:0	0.0	0.0	0.1	0.0	0.0	0.1
26:1	0.3	0.1	0.3	0.1	0.2	0.1
26:2	0.0	0.0	0.0	0.0	0.0	0.0

Table 64. Composition of the sphingolipids in young, old and cataractous eye lenses determined by APCI-MS

Figure 34: Composition of the Sphingolipids in Young Eye Lens Extract

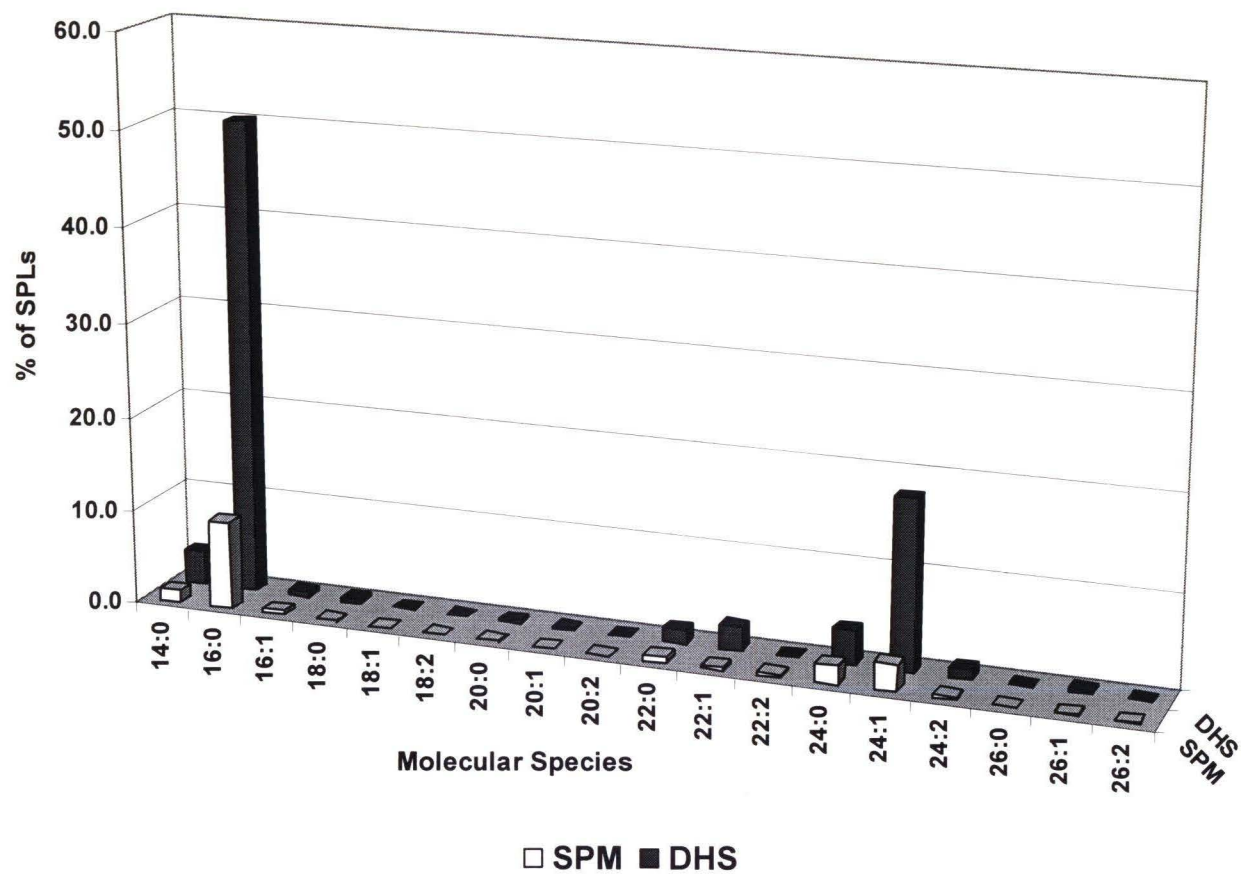


Figure 34. The chart shows the data for young eye lenses from Table 64. The sum of all percentages is equal to 100%.

Figure 35: Composition of the Sphingolipids in Old Eye Lens Extract

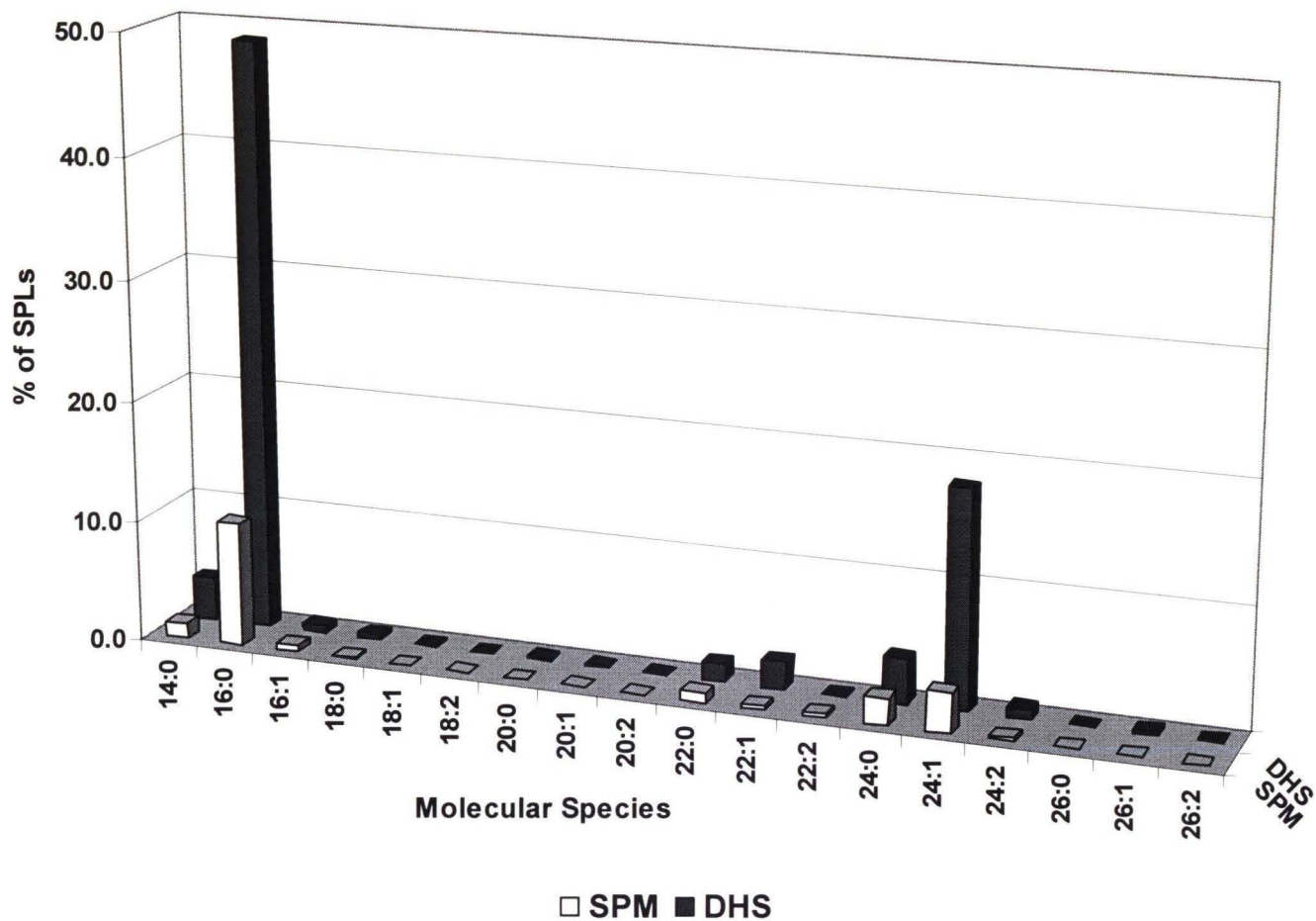


Figure 35. The chart shows the data for old eye lenses from Table 64. The sum of all percentages is equal to 100%.

Figure 36: Composition of the Sphingolipids in Cataractous Eye Lens Extract

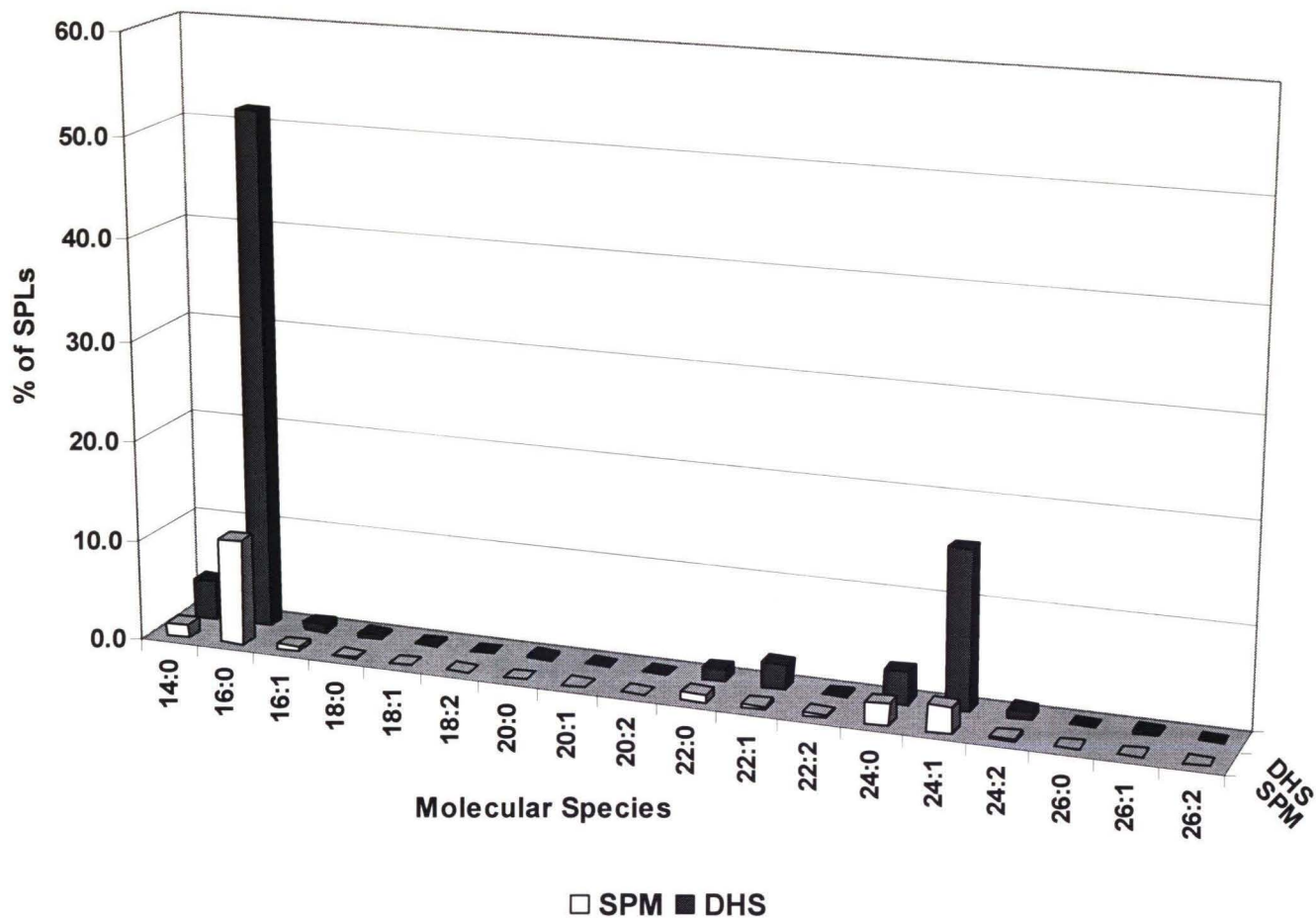
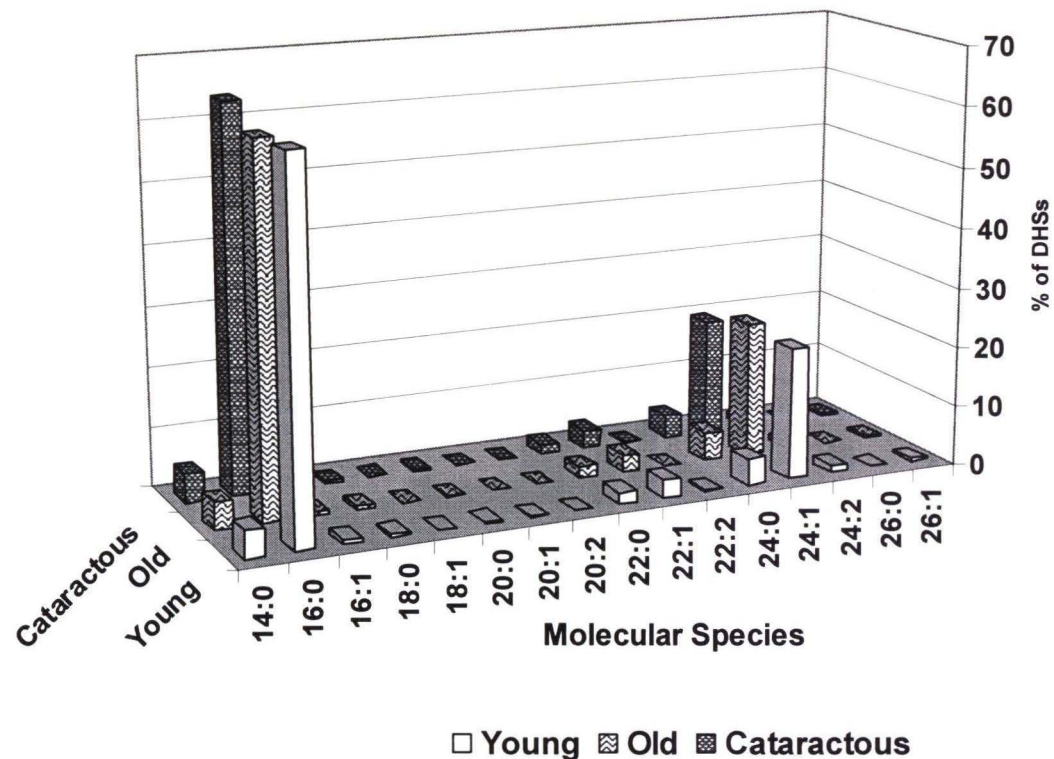


Figure 36. The chart shows the data for cataractous lenses from Table 64. The sum of all percentages is equal to 100%.

Figure 37: Compositions of the DHSs (mole%) in Human Lenses by APCI-MS



DHS	Young (%)	Old (%)	Cataractous (%)
14:0	4.4	4.4	4.8
16:0	61.1	60.5	63.7
16:1	0.7	0.7	1.0
18:0	0.5	0.5	0.5
18:1	0.1	0.1	0.2
20:0	0.3	0.2	0.2
20:1	0.1	0.1	0.1
20:2	0.0	0.0	0.0
22:0	1.8	1.9	1.6
22:1	3.0	2.8	3.0
22:2	0.1	0.1	0.1
24:0	4.4	4.7	3.9
24:1	21.8	22.4	19.5
24:2	1.2	1.0	1.0
26:0	0.0	0.1	0.1
26:1	0.4	0.3	0.3

Figure 38: Compositions of the SPMs (mole%) in Human Lenses by APCI-MS

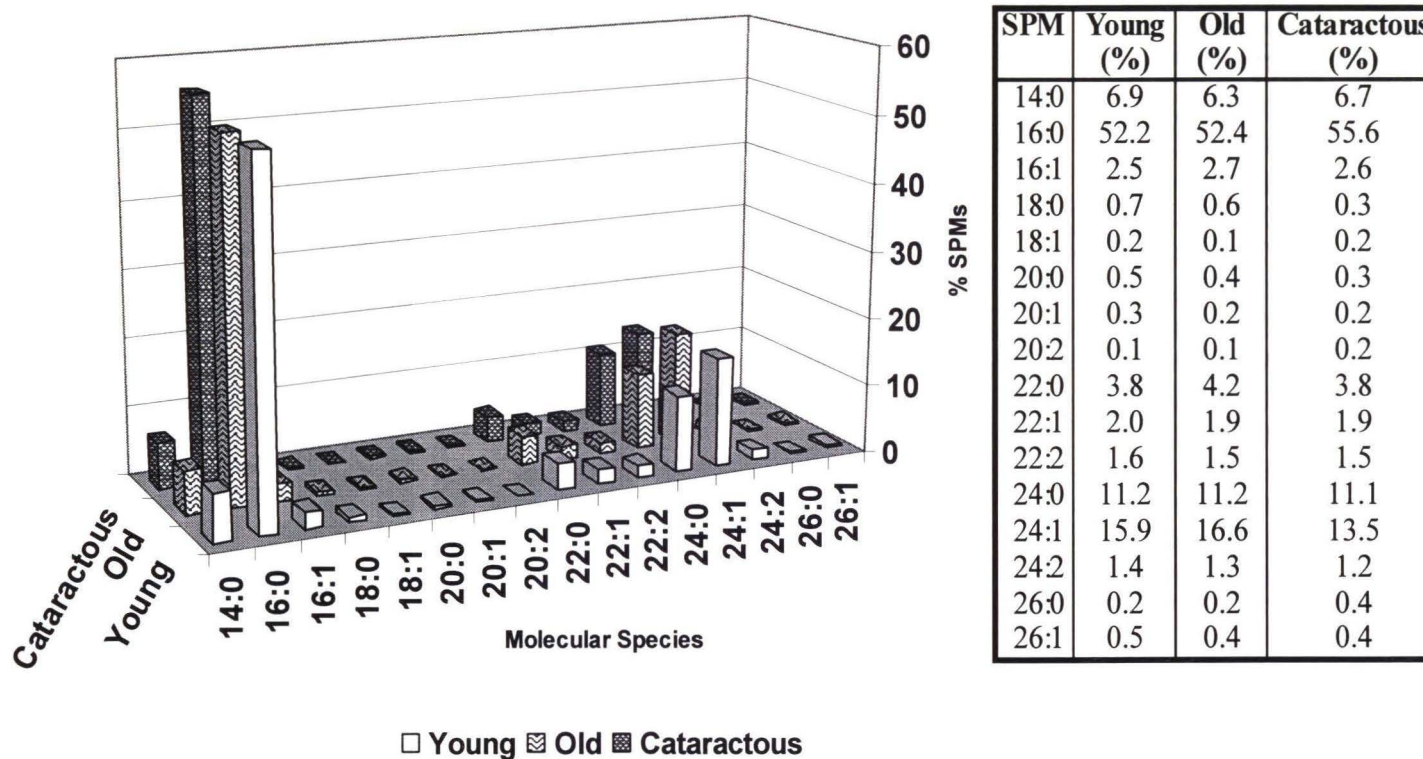


Figure 39: Compositions of the PCs (mole%) in Human Lenses by APCI-MS

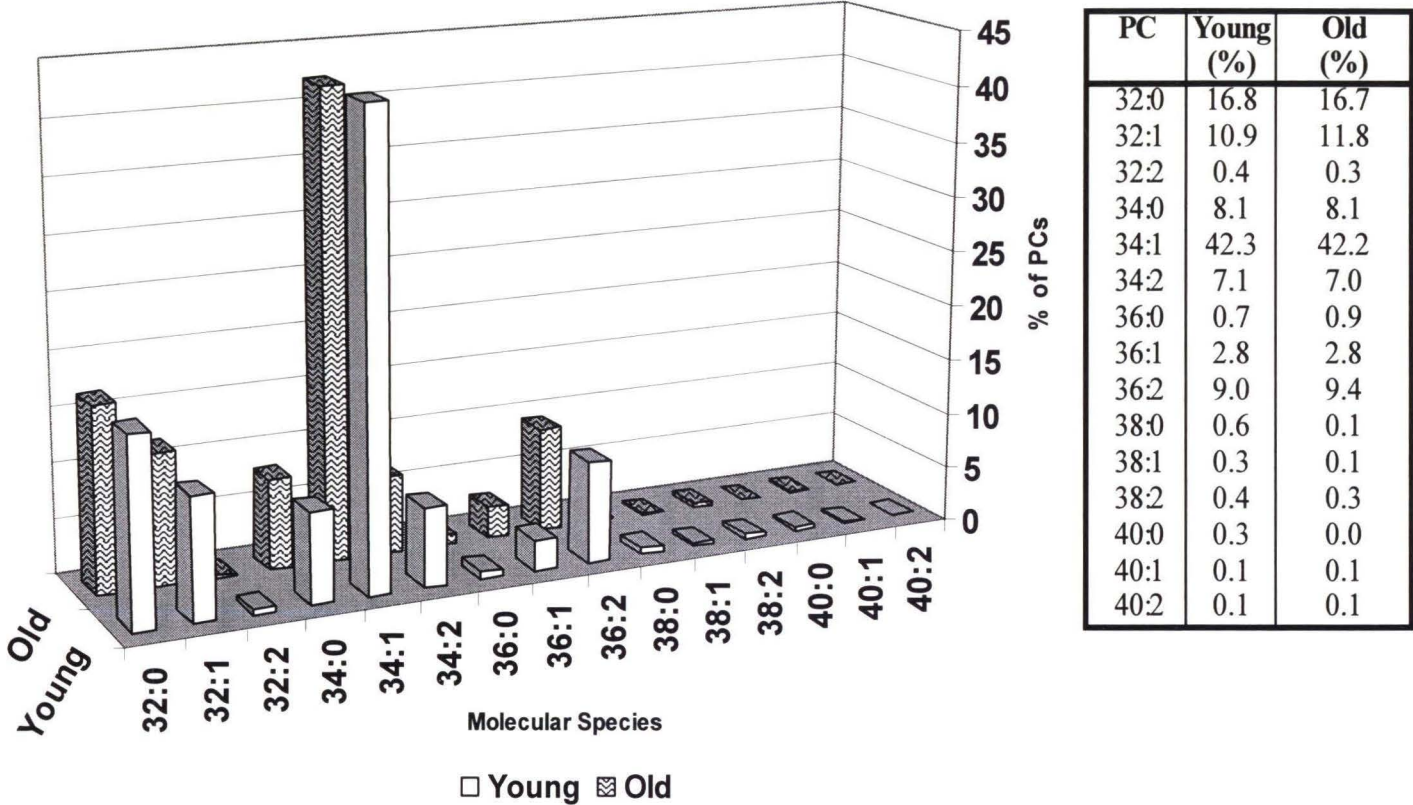


Table 65: Composition of the SPLs (mole%) in Human Lenses by APCI-MS

SPLs	Young (%)	Old (%)	Cataractous (%)
DHS	82.2	80.5	81.1
SPM	17.8	19.5	18.9

Table 65: Composition of the sphingolipids in young, old and cataractous human eye lens extracts. The data showed that the DHS and SPM species remained unchanged in old and cataractous lenses.

II.C. Conclusions

1. METHODOLOGY

The data presented above constitute the first report of how the molecular species of DHS and SPM change with age and with the onset of cataracts. The next step in our investigation would be to determine if the observed changes were statistically significant. This of course can only be accomplished by analyzing a larger number of lenses, using different LC/MS configurations. Nevertheless, the fact that the changes with age and cataract formation were similar for DHS and SPM indicated that these trends are likely to be an accurate reflection of changes that occur with age and cataractogenesis.

In order to improve the quantitative analysis of the PLs by ESI-MS, new methods needed to be developed to minimize the formation of the dimer and sodium adduct ions in the ion trap of the LCQ. Of course, sequential APCI and ESI analyses could be performed on the TSQ, but the higher sensitivity and the MSⁿ capabilities of the LCQ made it desirable to use it as an analytical tool for SPL analysis. Furthermore, eliminating the LCQ from the experimental analysis would also eliminate the advantages of

analyzing these samples by dual parallel mass spectrometry. After much experimentation, it was found that introducing a mixture of 50mM glycine/1M NH_4COOH at a pH of 8.5 via a post-column tee, eliminated the sodium adduct and dimer ions. However, further experiments need to be done to determine what effect this additive will have on the quantification of the SPLs.

The results shown above provided useful information about how specific SPM and DHS groups changed within the lens. However, it would be even more advantageous to know how the LCB/FA composition of the eye lens membrane changes with age and cataract formation. This analysis would be very similar to that described above for the commercially available SPM extracts, and would therefore provide a complete composition of the lens membrane SPLs. This could be accomplished by performing APCI tandem MS on the LCQ and ESI MS on the TSQ in parallel, as was done for the SPM extracts above. Furthermore, the improvements that were suggested for the analysis of the LCB/FA composition of the SPM extracts (such as analyzing derivatives of the LCBs by GC-MS and using different LC configurations, etc.) also apply to the analysis of the lens samples. Of course, the dimer and sodium adduct problem needs to be solved before quantification can be performed using the LCQ ESI-MS data. Also, since eye lens samples are difficult to obtain, these method development experiments can be performed using the SPM extracts that are commercially available.

2. BIOLOGICAL IMPLICATIONS

The results above showed that 1) there was a preference for monounsaturated SPLs in the eye lens and 2) the amounts of 16:0-DHS and 16:0-SPM increased in old and cataractous lenses, even though the amount of DHS did not decrease as a class. These

molecular species play an important role in maintaining the transparency and stability of the lens membrane. It is known that sphingomyelinase enzymes (SMEs) are present in the human lens, and Kuikka *et al.*²⁰ reported that SME showed a dramatic preference for 16:0-DHS compared to 16:0-SPM. Therefore, the observed increase in 16:0 DHS in old and cataractous lenses implied that degradation of the SPLs by SME is probably not a major factor associated with aging and cataractogenesis. These data provided information regarding the physiological basis of lens transparency on the cellular and molecular levels, contribute to determining the causes and mechanisms of cataract formation, and helping to understand the defects in lens development.

From Figures 37 and 38 it was observed that the SPLs do not diminish with age or cataract formation. Figure 39 shows however, that the PCs disappeared with the formation of cataracts. In addition, **40(C)** shows there was a substantial decrease in the abundance of PE plasmalogens in cataractous lenses. This implied that there was a general decrease in diacylglycerol-based PLs, which suggested that degradation by phospholipase enzymes may be a contributing factor to the onset of cataractogenesis. From Figure 40, it was observed that the SPLs were the only phospholipids that remained intact in cataractous eye lens membranes. This observation provided invaluable insight into the mechanisms that may be involved in cataract formation.

While the degradation of SPLs caused by their roles in signaling brought about by sphingomyelinase activity, does not seem to be a causative factor associated with the disease state, it appears clear that the role of sphingolipids in forming extremely stable membrane rafts is a factor in maintaining the partial transparency that remains in the cataractous lens. The fact that the SPLs are the primary PLs remaining in cataractous

lens membranes suggested that they play an important role in maintaining membrane structure with the onset of the disease state. The fact that the percentage composition of the molecular species changes with cataract formation, and that the different molecular species have been shown to have different phase transition temperatures (indicating differing degrees of membrane stabilization), indicate that the molecular species of DHS play a role in determining the characteristics of the membrane of the cataractous lens. The changes in molecular species composition can only be determined by MS, and this work presents the first such analysis of cataractous lenses. Unfortunately, to date, very little work has been reported on the relationship between the structure of DHSs and their function in cell membranes .

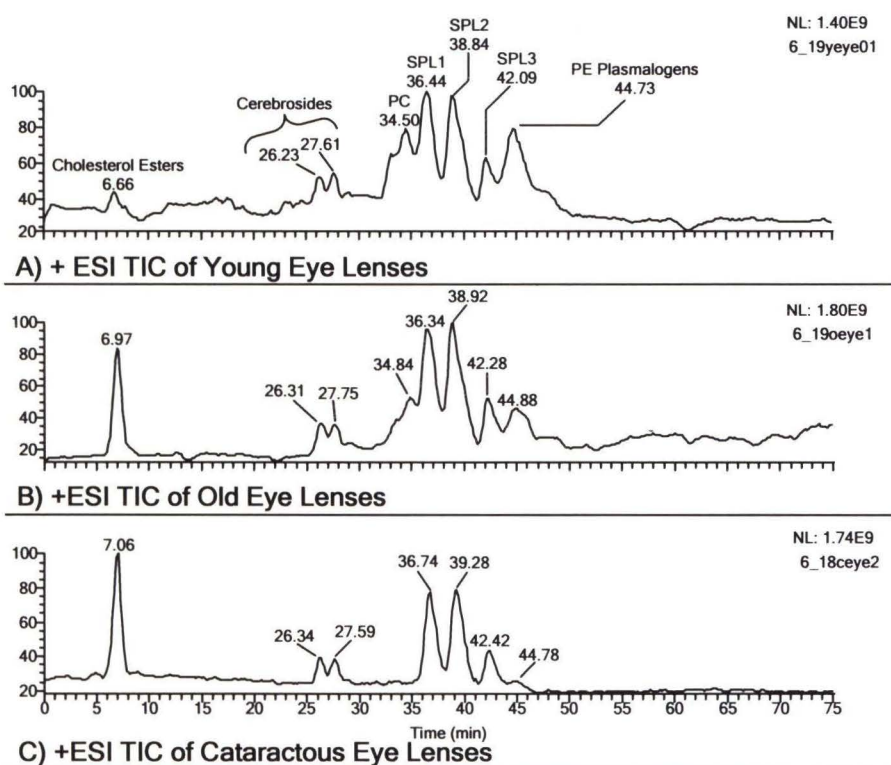


Figure 40. Total ion chromatograms showing the lipids present in young (A), old (B) and cataractous (C) human eye lenses. The disappearance of the PC peak and substantial reduction in the PE plasmalogen peak in (C), implied that these PLs were degraded during the onset of cataracts.

Although the other identified PLs were not quantified, their molecular species compositions would also provide additional information about membrane structure. Such knowledge can provide justification for a lack of a role of certain components (sphingomyelinases), or a possible role for other components (phospholipases). So, based on our preliminary observations we can see that determining the molecular species composition of lens membranes in young, old and cataractous samples can provide invaluable information about the mechanisms involved in cataractogenesis and aging. To develop a complete model of the human lens membrane however, the LCB/FA compositions of SPLs in these samples need to be determined. The current results indicated, however, that there are changes in the SPL molecular species composition that may be relevant to an understanding of the processes involved in aging and cataractogenesis.

III. Solving the “Sodium Adduct and Dimer Problem” in

ESI-MS

As described in the analysis of human lens extracts and commercially available SPM extracts above, when ESI-MS was performed on the LCQ, a large abundance of dimer and sodium adduct ions populated the m.s. (Figures 6 and 7). These ions complicated the analysis by ESI-MS and prevented accurate quantification of the PLs on the ion trap instrument. The reasons for these observations were extensively described above (pages 76 – 80). By changing the chromatographic and mass spectrometric conditions, the problem was eventually solved. Bovine brain total lipid extract (BBTL) (25 mg/mL) was used to carry out the experiments. In a typical BBTL ESI-MS analysis on the LCQ it was found that the PCs formed dimer ions more efficiently than sodium adducts, while the reverse was true for the SPLs (Figure 41). So, for PCs, the order of the abundances of the primary ions was $[M + H]^+ > \text{Dimer} > [M + Na]^+$. For the SPLs, the order was $[M + Na]^+ > [M + H]^+ > \text{Dimer}$. These observations are illustrated in **41(A)** and **41(B)** for palmitoyl-oleoyl-PC (POPC) and 18:0 SPM, respectively. The sections below describe, generally, the approaches that were attempted to eliminate the formation of dimers and sodium adducts (DSAs) in ion trap ESI-MS. See Table 66 for experimental details.

III.A. Modified Heated Capillary

It was originally thought that the larger bore of the heated capillary on the LCQ was the cause of the dimer formation. So, a TSQ heated capillary, which had a smaller bore diameter than the LCQ capillary, was modified and fitted on the LCQ to test this

hypothesis. However, the ESI m.s. still contained PL DSAs, indicating that this hypothesis was not correct. In addition, there was a decrease in overall sensitivity due to the lower flow of molecules into the mass analyzer, caused by the smaller bore. **(Filename: 0619Bov1)**

III.B. Ethylenediaminetetraacetic Acid

It was postulated that adding a chelating agent to the system could both compete for the Na^+ ions and interact with the nitrogen atom of the phosphocholine HG, thereby preventing both dimerization and sodium adduct formation. The phosphocholine HG was critical to the dimerization process (see Scheme 3). Ethylenediaminetetraacetic acid (EDTA) was tested because 1) it is known to be a good chelater of metal ions, and 2) it was one of the components of the MGR, which was used for the ^{31}P NMR analysis of PLs¹⁴. If the EDTA in the MGR was successful in eliminating the DSAs then it had the advantage of serving dual roles (i.e. a role in both the ^{31}P NMR and HPLC-ESI-MS of PLs) in the analysis, so that one sample could be analyzed by both techniques. Therefore, a solution of MGR + BBTL in CDCl_3 was analyzed by HPLC-ESI-MS, and the results indicated that this approach was not a solution to the problem as the DSAs were still abundant. **(Filename: 060702Brain1)**. With the failure of adding the EDTA to the sample (via the MGR), adding it to the mobile phase solvents was also tried. 200mM of EDTA was added to each of the solvents in the chromatographic system. This experiment was also unsuccessful **(Filename: 0620Bov1)**.

Different EDTA mixtures were then added post-column from a syringe pump to the flow stream. Numerous mixtures, flow rates and concentrations were tried (Table 66), and it was found that a mixture of 40mM EDTA/ H_2O (or MeOH) introduced into the

flow stream, substantially reduced the formation of DSAs. Figure 41 shows an ESI-MS m.s. of BBTL without any additives (**41(A–B)**) and with 40mM EDTA/MeOH (1:4) introduced into the flow stream post-column at 50 μ L/min (**41 (C–E)**). Comparing these m.s. showed that the EDTA protonated ion at m/z 293.1 was the base peak. [EDTA + Na]⁺ (m/z 315.2), [EDTA – 45]⁺ (m/z 247.1), [EDTA – 132]⁺ (m/z 160.0) and [EDTA – 160]⁺ (m/z 132.0) were also observed and labeled correspondingly. **42(B)** shows the cleavages that resulted in these fragment ions. In addition to these fragments, the EDTA also produced dimers, trimers and tetramers, along with their corresponding SAs, and also combined with the PLs to yield [EDTA + PL]⁺ adducts. [EDTA + POPC]⁺ at m/z 1051.8 and [EDTA + 18:0 SPM]⁺ at m/z 1023.6 are shown as examples in Figure 41. In the designation for these ions, ‘EDTA’ represents the EDTA configuration in which there is no charge on any of the atoms (i.e. the H₄Y form of EDTA⁵¹).

From the above analysis of the m.s., it was obvious that while EDTA eliminated the PL DSAs, it also produced many adducts and fragments of its own which complicated the m.s., decreased the S/N and reduced the overall sensitivity. The occurrence of these EDTA adducts and fragments was undesirable. Another problem was that the EDTA precipitated in the ESI source and clogged the heated capillary when flow rates were greater than 100 μ L/min to the source. Therefore, in order to use this mixture low flow rates to the ESI source were required. So, EDTA got rid of the DSAs but had the following disadvantages: 1) The EDTA protonated ion was the base peak in all m.s.; 2) EDTA polymerization and adduct formation complicated the m.s. and decreased the S/N; and 3) EDTA clogged the heated capillary if the flow rate to the source exceeded 100 μ L/min. It may be argued, that the ‘clogging problem’ could be diminished by

reducing the concentration or flow rate of EDTA introduced into the system per minute. However, from experiments 1 – 17 in Table 66, it was shown that the minimum flow rate and [EDTA] required to eliminate the dimers and sodium adducts were 40mM EDTA and 50 μ L/min, respectively. Reducing the concentration or flow rate below these values resulted in the observation of DSAs.

Experiments 13 and 14 also showed that the distance between the end of the column and the ionization source affected the efficiency of the EDTA in reducing the DSAs. This implied that time was needed for the EDTA to effectively compete for the Na⁺ ions and form stable electrostatic interactions with the phosphocholine HG of the PLs. It's important to note also, that although PL-EDTA adducts were observed, their abundances were low in comparison to the PL protonated molecule, indicating that the association between the two molecules was just enough to prevent PL-PL dimerization in the ion trap, but not strong enough to result in high abundances of PL-EDTA adducts in the m.s. In negative ESI mode, the [EDTA – H]⁻ ion and its associated ‘polymers’ dominated the -ESI m.s. The undesirable EDTA adducts and ‘polymers’ prompted the search for a better solution to the DSA problem.

III.C. 18-Crown-6

When the chelating agent 18-Crown-6 ether (18C6) (**43(A)**) was tried, the [18C6 + NH₄]⁺ ion (**43(B)**) at *m/z* 282.3 was the base peak in all ESI m.s. NH₄⁺ came from the 20mM NH₄OCOH that was used as the sheath liquid. This suggested that 18C6 interacted with NH₄⁺ more efficiently than Na⁺ under these conditions. Another interesting observation was that the [PC + Na]⁺ ions were significantly more abundant than [PC + H]⁺ ions, which was different from the pattern observed in **41(A)**. This suggested that

NH_4^+ competes with Na^+ for the phosphate oxygen atom on the HG. Unlike Na^+ however, NH_4^+ doesn't interact as strongly with the oxygen and so dissociates rapidly before detection so that no $[\text{M} + \text{NH}_4]^+$ ions were observed in the m.s. These results suggested however, that NH_4OCOH helped to reduce SAs.

Another interesting observation was that the 18C6 chelated Na^+ while it was bonded to the PLs (**43(C)**), producing ions such as $[\text{18C6} + \text{18:0 SPM} + \text{Na}]^+$ (m/z 1017.8) and $[\text{18C6} + \text{POPC} + \text{Na}]^+$ (m/z 1046.3), which were greater in intensity than their corresponding $[\text{M} + \text{Na}]^+$ and $[\text{M} + \text{H}]^+$ ions. Also, the positive ESI m.s. had a noisy background due to the presence of a large amount of adduct and fragment ions. The negative ESI spectra did not yield any useful information. So, since the DSAs were still a problem, the 18C6 was not a solution.

III.D. Ammonium Formate

Based on the observation that NH_4^+ helped reduce the SAs, 20mM NH_4OCOH in $\text{H}_2\text{O}/\text{ACN}$ (1:4) was introduced into the mobile phase at 50 $\mu\text{L}/\text{min}$ via a post-column tee. There was no reduction in the abundances of the DSAs in comparison to **41(A)** and **41(B)**.

III.E. Diethylenetriaminetetraacetic Acid

All the problems described for EDTA were also observed for diethylenetriaminetetraacetic Acid (DTPA), except that in the latter the problems were more pronounced. The sensitivity was less than that observed for EDTA. DTPA appeared to ionize much more easily under ESI conditions producing a very abundant protonated ion at m/z 394.2 (**44(A)**) that overwhelmed all the other ions in the mass spectra. Similar

fragment ions were observed for both EDTA (**42(B)**) and DTPA (**43(B)**), except DTPA produced an extra fragment at m/z 261.2.

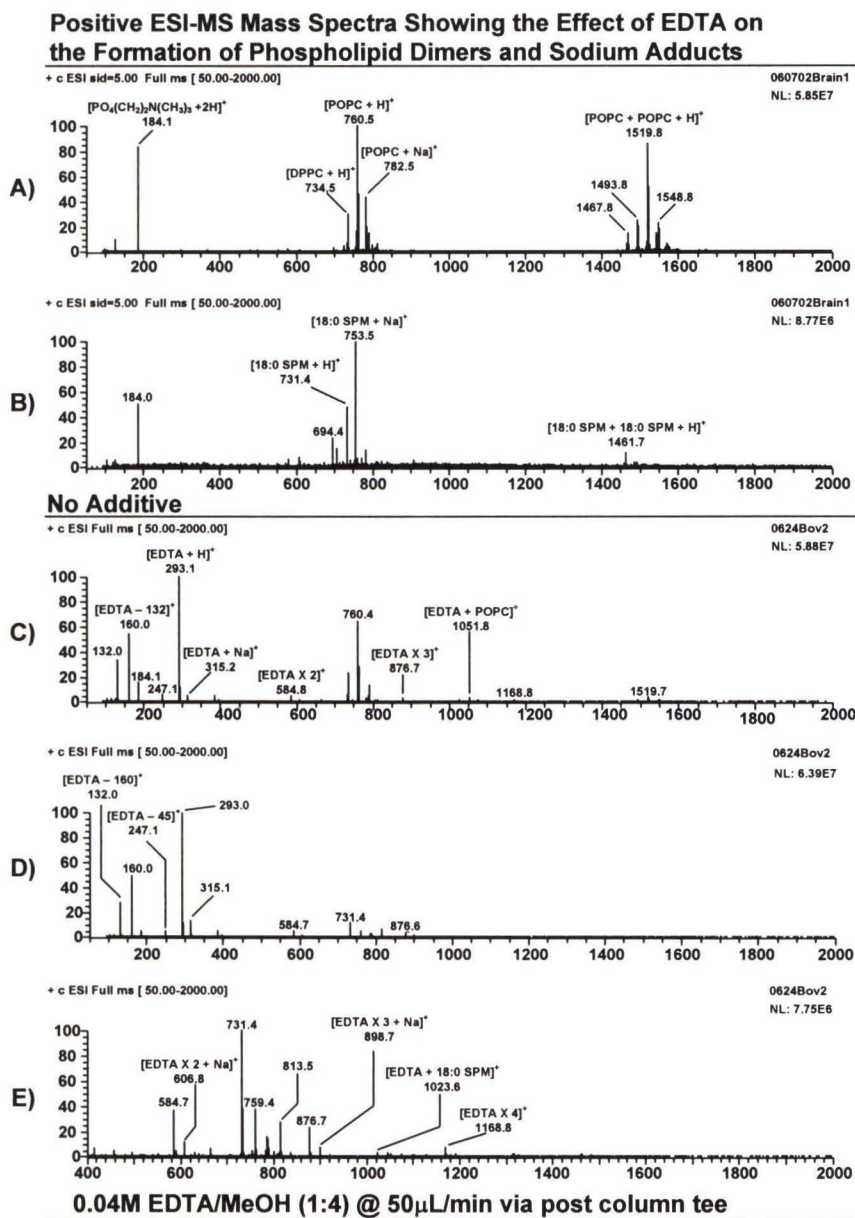


Figure 41. Positive ESI-MS mass spectra of bovine brain total lipid extract. (A) and (B) show the mass spectra of a ‘normal’ analysis in which no additive was introduced into the system. (C) to (D) show the mass spectra when 40mM EDTA in MeOH @ 50μL/min was introduced into the mobile phase via a post-column tee. (C) shows the full-scan mass spectrum of the phosphatidylcholines, (D) of the short-chain sphingomyelins and (E) was an extracted m/z range from (D).

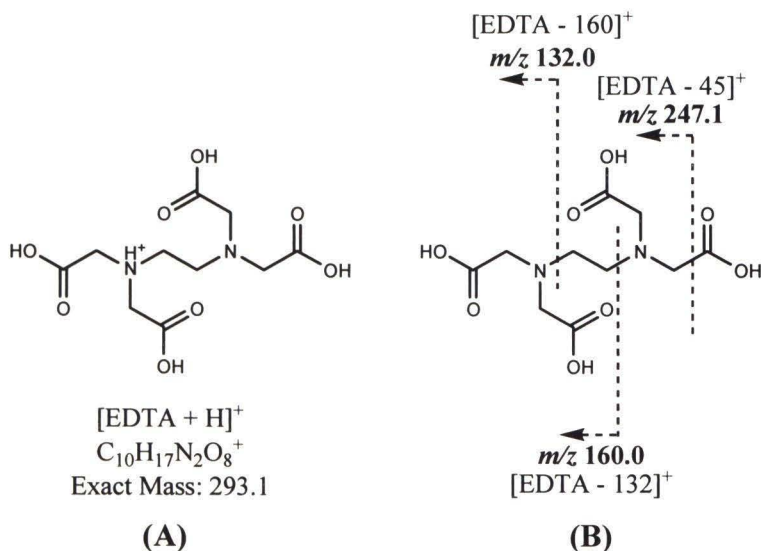


Figure 42. (A) The protonated H_4Y configuration of EDTA. (B) The cleavages that produce the primary fragment ions observed in the ESI-MS m.s.

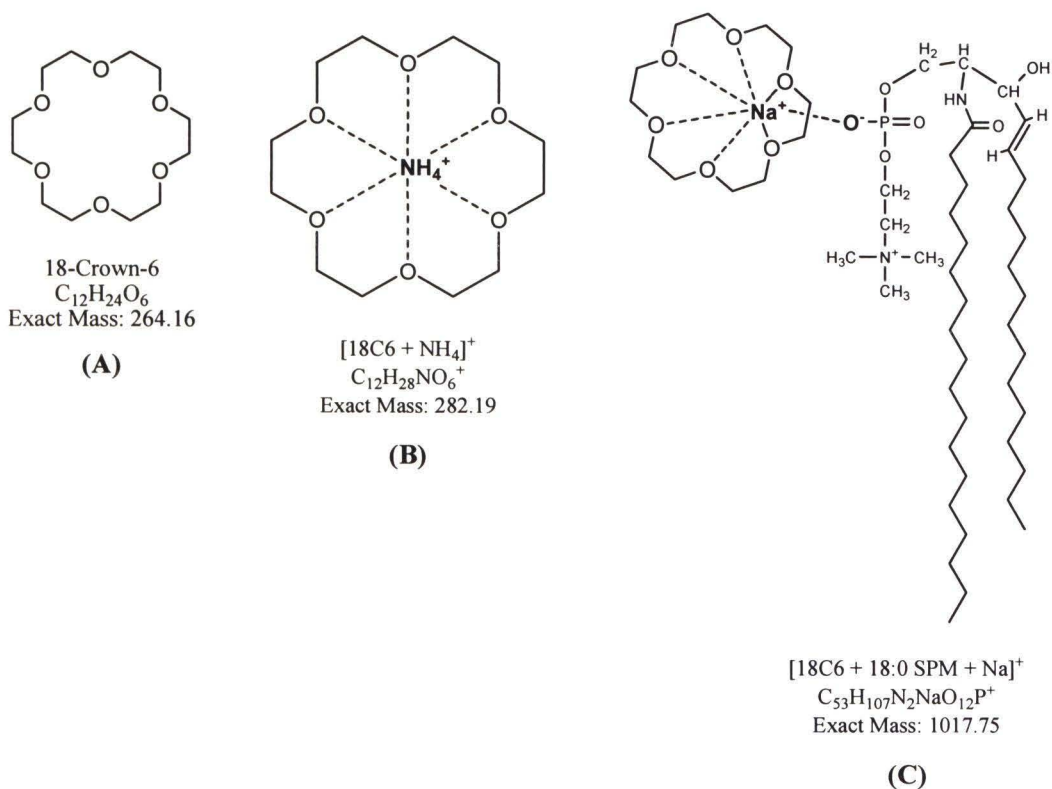


Figure 43. The ions of the 18-Crown-6 (18C6) ether molecule (A) that were observed in the ESI mass spectra. (B) The chelation of NH_4^+ by 18C6. (C) The $[\text{18C6} + \text{PL} + \text{Na}]^+$ complex observed in the ESI-MS m.s.

DTPA also formed more abundant ‘polymers’ compared to EDTA. DTPA dimers (m/z 787.0), trimers (m/z 1180.0), tetramers (m/z 1574.0) and pentamers (m/z 1967.0) were observed in the m.s. In addition, DTPA clogged the heated capillary much more frequently than EDTA, even at a lower concentration of 5mM. Like EDTA, the DTPA negative ions dominated the negative ESI-MS mass spectra. Based on all of these disadvantages, DTPA was determined to be an inadequate solution to the problem, even though it effectively eliminated the PL DSAs.

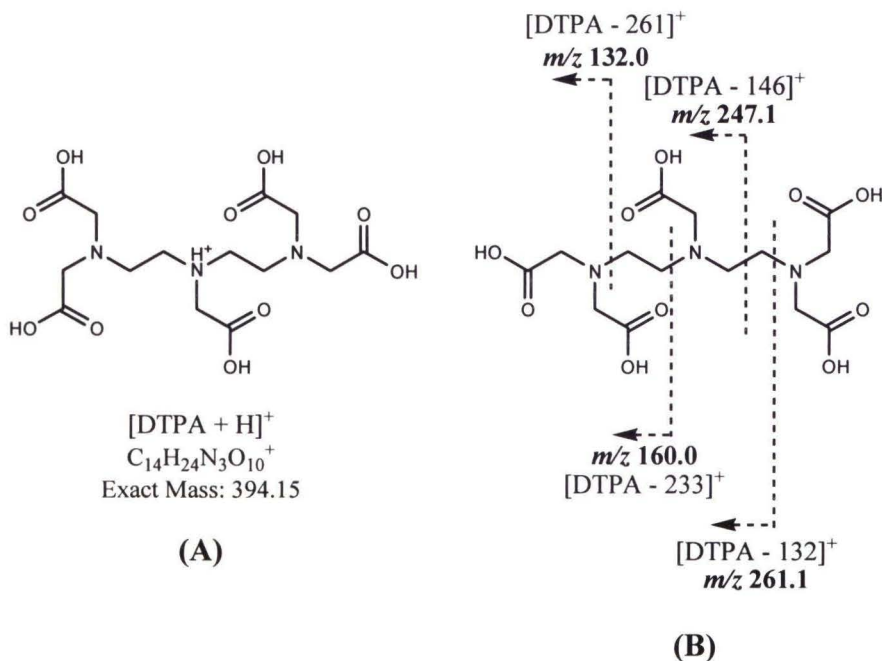


Figure 44. (A) the $[H_5Y + H]^+$ configuration of DTPA. (B) The cleavages that produce the primary fragment ions observed in the ESI m.s

III.F. Ammonium Acetate Solutions

Solutions of ammonium acetate (experiments 27 – 30 in Table 66), reduced the PC dimers substantially but had no effect on the SPM sodium adducts. This formulation

was therefore eliminated as a possibility, but it suggested that combining ammonium acetate or formate solution with a chelating agent, or perhaps another molecule with carboxylic acid functional groups, may provide a solution. This was exactly the case, as amino acids such as glycine and alanine combined with ammonium acetate or formate, eliminated the DSAs.

III.G. Amino Acids

The structures of the standard 20 amino acids (AAs) are shown in Figure 45. The asterisks indicate the AAs that were tested.

1. GLUTAMIC ACID (Glu)

Glu cause clogging of the heated capillary. Also, there was a very noisy background due to the high abundance of the polymeric ions of Glu. The DSAs were significantly reduced but the noisy background eliminated this AA as a usable solution to the problem. Glu also formed adducts with the PLs. The Glu ions were very abundant in the $-ESI$ m.s., overwhelming the response from all other species.

2. ASPARTIC ACID (Asp)

The behavior of Asp was similar to that observed for Glu. This of course made sense, since their structures were similar. However, it was observed that Asp was a little bit more effective at reducing the DSAs than Glu. This was probably due to the smaller size of Asp, which allowed it to approach the phosphocholine HG more easily, and interact with it more strongly. These observations suggested that: 1) Smaller AAs were more effective at eliminating DSAs for the reason just mentioned and 2) the presence of the additional carboxylic acid group in Asp and Glu resulted in an increase in the

abundance of polymeric AA ions as well as PL-AA adducts. So, smaller AAs with one COOH group were tested.

3. SERINE (Ser)

Serine was not effective in any way because the DSAs still populated the mass spectra and there was very poor S/N..

4. ALANINE (Ala)

From the experiments with 18C6 it was decided to include the ammonium ion in the additive since it appeared to help reduce the DSA abundances. A solution of 50mM Alanine in 1M $\text{NH}_4\text{OOCCH}_3$ at a pH of 9.60 was introduced into the mobile phase at 50 $\mu\text{L}/\text{min}$ post-column. The results showed that the DSAs were effectively reduced. In addition, the S/N was high and there were very few undesired fragment and adduct ions of Ala in the m.s. (those that were produced were of very low abundance in comparison to the PL protonated molecules). In the low mass region (m/z 50 – 300), however, the ammonium acetate produced a lot of fragments. These however, did not pose a problem in the analysis, since their mass-to-charge ratios were significantly less than the protonated PL molecules. Comparing experiment 38 with 37 (Table 66), it was observed that the ammonium acetate significantly increased the response from the SPLs. However, the PL-acetate adduct ions were observed in the –ESI mass spectra.

Since Ala was successful in eliminating the DSAs, it was postulated that Gly should be even more effective due to its smaller size. These were the next experiments that were performed.

5. GLYCINE (Gly)

Comparison of experiment 41 with experiment 38 showed that Gly was more effective in eliminating the DSAs. Also, using Gly with NH_4OCOH resulted in fewer undesirable ions in the low mass region (m/z 50 – 300) in both the positive and negative ESI mass spectra. From Figure 46, it was seen that the DSAs were effectively eliminated in both the positive (**45(C-D)**) and negative (**45(E-F)**) ESI-MS m.s. by supplying 50mM Glycine in 1M NH_4OCOH at a pH of 8.80 at 50 $\mu\text{L}/\text{min}$ from a syringe pump via a post-column tee (compare 45 (**C-D**) with 41(**C-E**)). The PL formate adducts were observed in –ESI mode. Numerous experiments were also performed to determine the optimal sample injection volume (experiments 51 – 61) and NH_4OCOH concentration (experiments 43 – 50), and it was found that an injection of 5 μL and a concentration of 1M NH_4OCOH worked best.

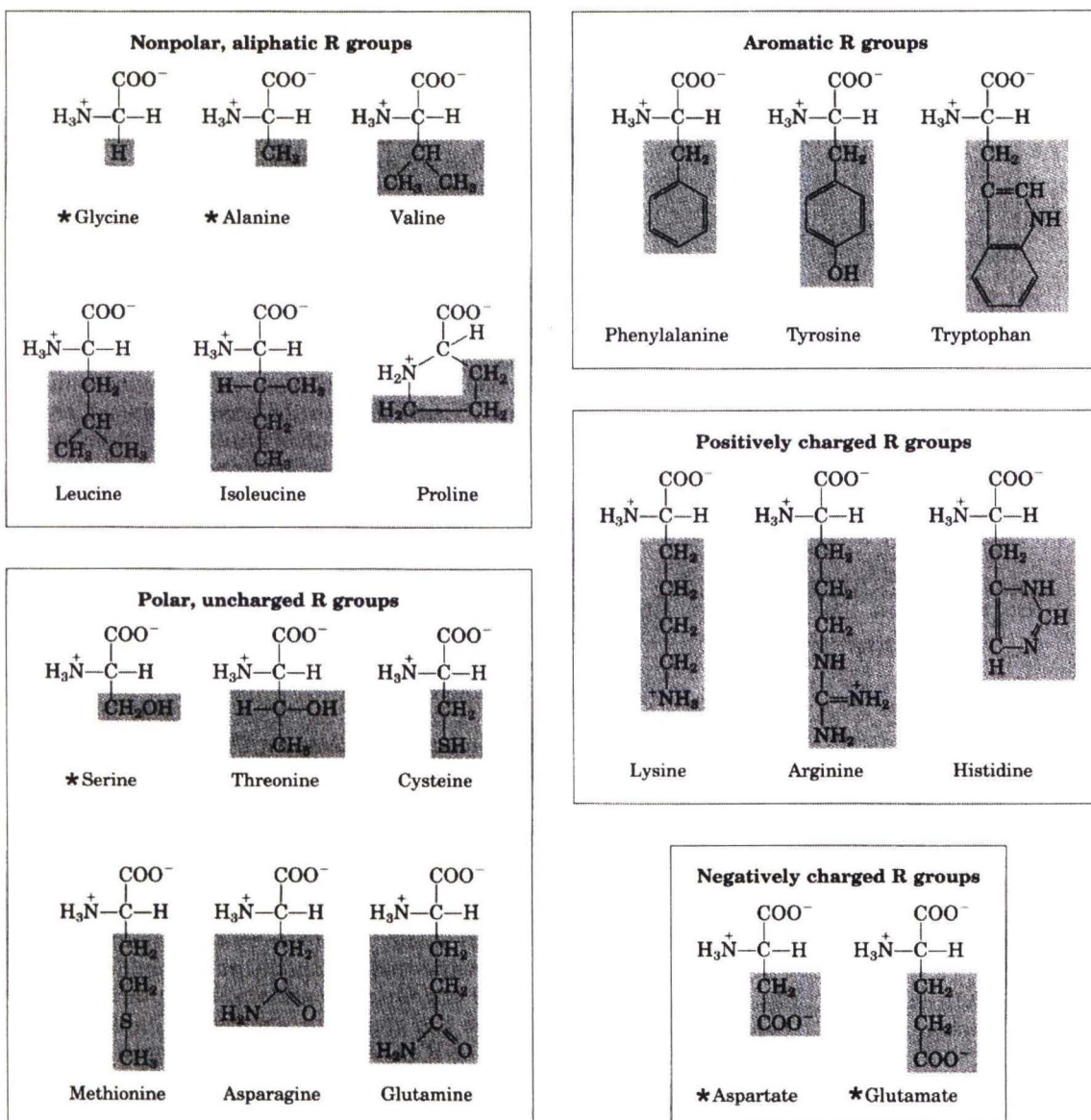


Figure 45. “The 20 standard amino acids of proteins. They are shown with their amino and carboxylic groups ionized, as they would occur at a pH of 7.0.”²⁶ The unshaded portions are those groups unique to each amino acid. The asterisks indicate the amino acids that were tested.

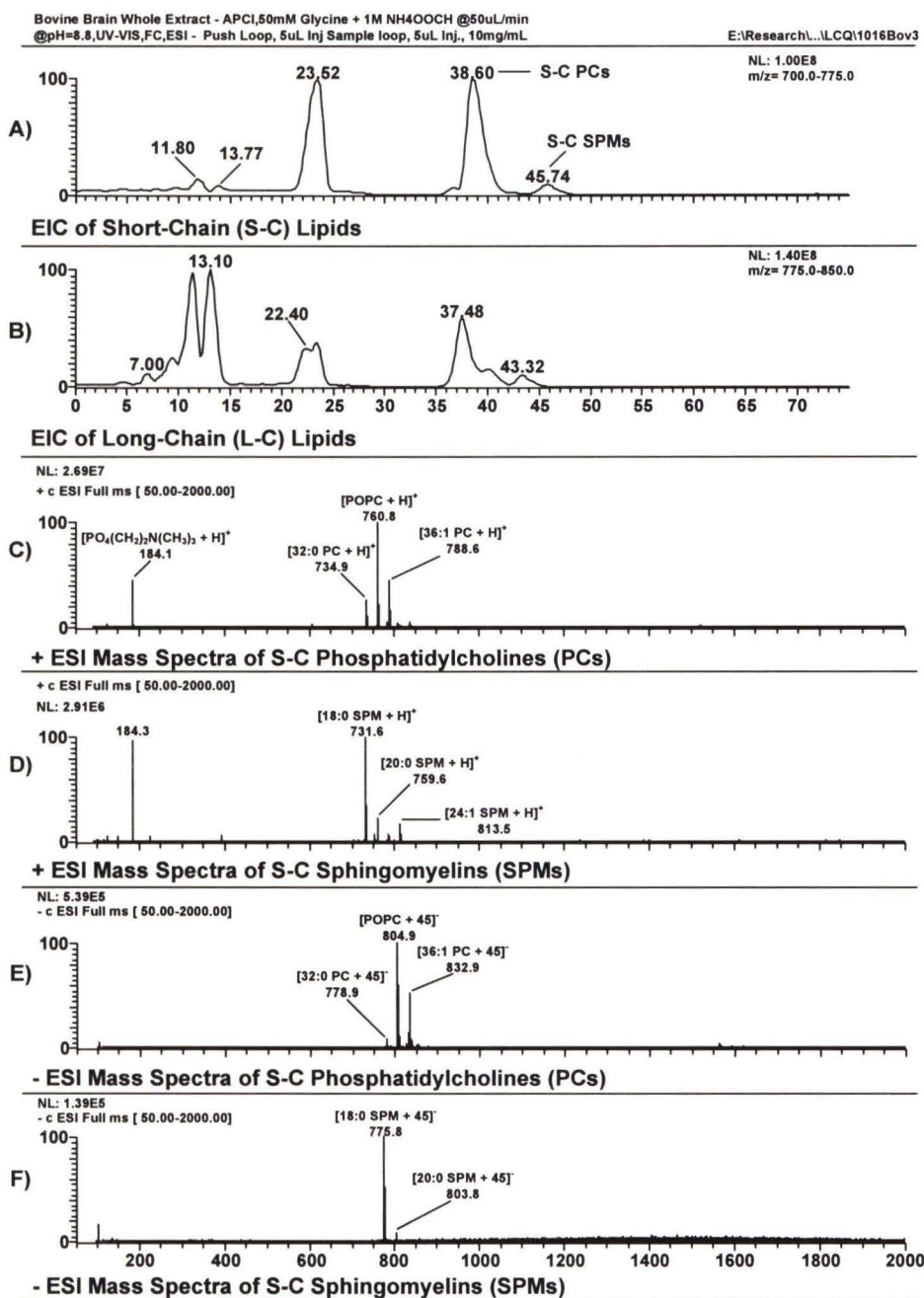


Figure 46. (A) and (B) are extracted ion chromatograms (EICs) showing the short-chain (S-C) and long-chain (L-C) lipids respectively, in bovine brain total lipid extract (BBTL). (C) and (D) show the positive ESI mass spectra for the S-C phosphatidylcholines (PCs) and S-C sphingomyelins (SPMs) respectively. (E) and (F) show the negative ESI mass spectra for the S-C PCs and S-C SPMs respectively. These chromatograms show that introducing 40mM glycine/1M NH₄OOCH with a pH of 8.80 into the flow stream via a post-column tee eliminated the phospholipid dimers and sodium adducts. Compare the mass spectra in this figure with those in Figure 45.

III.H. Conclusions

So, after trying numerous mixtures, introduction of 50mM glycine in 1M NH_4OCOH with a pH of 8.80 at 50 $\mu\text{L}/\text{min}$ from a syringe pump into the mobile phase via a post-column tee, effectively eliminated the DSAs without any immediately observable disadvantages. To carry this project forward the next step would be to determine how this additive affects the quantification of the PLs by ESI-MS. This could be done by comparing the results from a normal BBTL run with one in which the additive was used.

The main findings of the present work were as follows: 1) A good chelating agent such as EDTA and DTPA can be used to prevent the formation of PL metal ion adducts (such as sodium ion adducts) in ESI-MS. The caveat however, is that these chelating agents precipitate very easily in the ion source resulting in clogging of the heated capillary. So they can only be used with low sample concentrations and low flow rates. 2) AAs can be used to effectively compete with the PLs for sodium ions, thereby preventing the formation of sodium adducts. The AAs also prevented PL dimerization. These properties work best under basic conditions where the carboxylic acid groups were stripped of their hydrogen atoms at pHs greater than 7.0. Also, AAs with more than one COOH group (Asp and Glu) formed dimers, trimers, tetramers, etc. very easily in the ion source and also produced PL-AA adducts more easily than other AAs 3) Ammonium acetate and formate were both found to increase the response from the PLs in ESI-MS with the latter producing fewer ions in the low mass region (m/z 50 – 300). In addition, the ammonium ion was found to aid in the reduction of the abundance of SAs.

All these observations culminated in a satisfactory answer to the Dimer and Sodium Adduct Problem in ESI-MS, which was addition of 50mM glycine in 1M NH_4COOH with a pH of 8.80 introduced into the mobile phase at 50 $\mu\text{L}/\text{min}$ post-column.

Table 66: The Main Experiments Performed to Eliminate the Dimers and Sodium Adducts (DSAs)

<u>Ethylenediaminetetraacetic Acid (EDTA)</u>			
#	Experiment/LC Config.	Filename	Results/Comments
1	0.02M NaOH/0.2M EDTA @ 50 μ L/min via post-column tee	0619Bov2	All ions sodiated; PC dimers were eliminated; Clogging of the heated capillary; EDTA got rid of dimers.
2	0.02M NaOH/0.2M EDTA @ 40 μ L/min via post-column tee	0621Bov1	No clogging; All ions sodiated; PC dimers returned; 50 μ L/min was minimum flow required.
3	0.02M NH ₄ OH/0.2M EDTA @ 50 μ L/min via post-column tee	0621Bov1_02 0621171118	No clogging; PC dimers reduced; SAs still a problem; EDTA got rid of dimers but SAs were still present.
4-5	Tee 1: 0.02M NH ₄ OH/0.2M EDTA; Tee 2: 1% NH ₄ OH/MeOH; Both @ 50 μ L/min	0622Bov1, 0622Bov2	Decrease in S/N because of the abundant EDTA protonated molecule at m/z 293.0 and its associated dimers, trimers and tetramers; Decreased sensitivity up to 2 orders of magnitude; PL dimers and SAs were greatly minimized;
6	Tee 1: 0.02M NH ₄ OH/0.2M EDTA; Tee 2: 5% NH ₄ OH/MeOH; Both @ 50 μ L/min	0622Bov3	Reduced DSAs but S/N was poor and EDTA formed dimers/trimers and tetramers.
7	0.04M EDTA/MeOH (1:4) Sparger	0624Bov1	Dimers were extremely abundant but Na adducts were eliminated.
8	0.04M EDTA/MeOH (1:4) @ 50 μ L/min via post-column tee	0624Bov2	DSAs were eliminated; High abundance of the EDTA protonated molecule; Some EDTA 'polymers'.

9	0.02M EDTA/MeOH (1:4) @ 50 μ L/min via post-column tee	0624Bov3	Dimers returned; But Na adducts were still at a minimum; The EDTA protonated molecule was no longer the base peak in the mass spectra.
10	0.03M EDTA/MeOH @ 50 μ L/min via post-column tee	0624Bov4	DSAs eliminated but the EDTA protonated molecule and its associated 'polymers' returned. The EDTA protonated molecule was the base peak.
11	0.03M EDTA/MeOH @ 50 μ L/min via post-column tee; 2% NH ₄ OH in MeOH sparger	0624Bov5	Decrease in sensitivity; EDTA protonated molecule was the base peak; EDTA 'polymers' were present; DSAs were eliminated.
12	0.03M EDTA/MeOH @ 50 μ L/min via post-column tee; 20mM NH ₄ COOH in H ₂ O/ACN (1:4) @ 20 μ L/min sheath liquid	0625Bov5_020625165656	Decrease in sensitivity; EDTA protonated molecule was the base peak; EDTA 'polymers' were present; DSAs were eliminated.
13	0.03M EDTA/MeOH @ 50 μ L/min via post-column tee; 20mM NH ₄ COOH in H ₂ O/ACN (1:4) @ 20 μ L/min sheath liquid; Distance between column and ESI source was reduced.	0628Bov2	The DSAs were not as effectively eliminated as in previous experiments. This indicated that time is needed for the EDTA to associate with the phosphocholine HG and Na ions.
14	0.03M EDTA/MeOH @ 50 μ L/min via post-column tee; 20mM NH ₄ COOH in H ₂ O/ACN (1:4) @ 20 μ L/min sheath liquid; Distance between column and ESI source was increased relative to 0628Bov3.	0628Bov3	Decrease in sensitivity; EDTA protonated molecule was the base peak; EDTA 'polymers' were present; DSAs were eliminated.

15	0.04M EDTA/MeOH @ 50μL/min via post-column tee; 20mM NH ₄ OCOH in H ₂ O/ACN (1:4) @ 20μL/min sheath liquid;	0904Bov2_0209 41053;	Decrease in sensitivity; EDTA protonated molecule was the base peak; EDTA ‘polymers’ were present; DSAs were eliminated
16 -17	0.04M EDTA/MeOH @ 50μL/min via post-column tee; 20mM NH ₄ OCOH in H ₂ O/ACN (1:4) @ 20μL/min sheath liquid	0904Bov3; 0904Bov4	
<u>18-Crown-6 Ether (18-C-6)</u>			
#	Experiment/LC Config.	Filename	Results/Comments
18	30mM 18-C-6 in Hex @ 20μL/min via a post-column tee; 20mM NH ₄ OCOH in H ₂ O/ACN (1:4) @ 20μL/min sheath liquid	060902Brain1	Sodium adducts and PL dimers dominate the mass spectra; There was very little protonated molecules.
19	100mM 18-C-6 in Hexane (Hex) @ 50μL/min via a post-column tee; 20mM NH ₄ OCOH in H ₂ O/ACN (1:4) @ 20μL/min sheath liquid	0831Bov2	DSAs still very abundant; [18-C-6 + NH ₄] ⁺ was the base peak; Formation of [18-C-6 + PL + Na] ⁺ ; Poor S/N; Lower sensitivity; Negative ESI m.s. did not have any useful identifiable ions – mostly noise.

20	200mM 18-C-6 in MeOH @ 50μL/min via a post-column tee; 20mM NH ₄ OCOH in H ₂ O/ACN (1:4) @ 20μL/min sheath liquid	0831Bov3	Same as Experiment 19
21	200mM 18-C-6 in MeOH @ added to sample; 20mM NH ₄ OCOH in H ₂ O/ACN (1:4) @ 20μL/min sheath liquid	0831Bov4	Same as Experiment 19
22	200mM 18-C-6 in Hex @ 50μL/min via a post-column tee; 20mM NH ₄ OCOH in H ₂ O/ACN (1:4) @ 20μL/min sheath liquid	0831Bov5	Same as Experiment 19
<u>Ammonium Formate</u>			
#	Experiment/LC Config.	Filename	Results/Comments
23	20mM NH ₄ OCOH in H ₂ O/ACN (1:4) @ 50μL/min via post-column tee.	072402Bov1_020724190903	No change in DSA abundances.
<u>Diethylenetriaminetetraacetic Acid (DTPA)</u>			
#	Experiment/LC Config.	Filename	Results/Comments

24-26	(X)mM DTPA/H ₂ O @ 50μL/min via post-column tee, where ‘X’ represents different concentrations.	0820B0v1 (30mM); 0907Bov1 (10mM); 0907Bov2 (5mM)	Decrease in sensitivity; DTPA protonated molecule was the base peak; DTPA ‘polymers’ were present; DSAs were eliminated. Extensive clogging of heated capillary even at 5mM.
<u>Ammonium Acetate Solutions</u>			
#	Experiment/LC Config.	Filename	Results/Comments
27	200mM NH ₄ ⁺ CH ₃ COO ⁻ /H ₂ O @ 20μL/min via a post-column tee	0821Bov1	Reduced PC dimers but not the SPM sodium adducts; PC dimers were still relatively abundant.
28	200mM NH ₄ ⁺ CH ₃ COO ⁻ /H ₂ O @ 50μL/min via a post-column tee	0821Bov2	
29	2M NH ₄ ⁺ CH ₃ COO ⁻ /H ₂ O @ 5μL/min via a post-column tee	0907Bov3	
30	100mM NH ₄ ⁺ CH ₃ COO ⁻ /H ₂ O @ pH = 8.00 @ 50μL/min via a post-column tee	0909Bov2	
<u>Phthalic Acid</u>			
#	Experiment/LC Config.	Filename	Results/Comments

31	100mM Phthalic Acid/H ₂ O @ 50μL/min via a post-column tee	0823Bov1	Poor S/N; High abundance of phthalic acid 'polymers'.
<u>Amino Acids</u>			
#	Experiment/LC Config.	Filename	Results/Comments
32	50mM Glutamic Acid/H ₂ O @ pH= 10 @ 20μL/min via post-column tee.	0823Bov4	Clogging of the heated capillary; Very noisy background due to the polymeric ions of glutamic acid; The DSAs were significantly reduced but, the noisy background eliminated this amino acid from being a good solution to the problem; Glutamic acid also formed adducts with the PLs; The -ESI data was dominated by the glutamate ions.
33	25mM Glutamic Acid/H ₂ O @ pH= 10 @ 20μL/min via post-column tee.	0826Bov3	
34	50mM Aspartic Acid/MeOH @ pH= 10 @ 20μL/min via post-column tee	0828Bov2_020828170219	DSAs eliminated but there was a very high background due to the polymeric ions of aspartic acid; The PLs formed adducts with aspartic acid; -ESI mass spectra were dominated by the aspartate ions.
35	50mM Aspartic Acid/MeOH @ pH= 8 @ 20μL/min via post-column tee	0909Bov3	
36	50mM Serine in 1M NH ₄ OCOH/H ₂ O @ pH= 8.8 @ 50μL/min via post-column tee	0916Bov1	Poor S/N; Large amount of fragment and adduct ions produced; DSAs were still a problem.
37	50mM Alanine/ H ₂ O @ 50μL/min via post-column tee	0904Bov5	The DSAs were significantly reduced; There were no PL-Ala adducts; But S/N was mediocre.

38	50mM Alanine in 1M NH₄OOCCH₃ @ 50μL/min via post-column tee @ pH = 9.60	0910Bov1	Addition of the 1M NH₄OOCCH₃ significantly improved the S/N, and helped to lower the DSA abundances. This was a successful experiment as the DSAs were eliminated, there was a low background and high S/N. The low end of m/z region from 50 – 300 was populated by a lot of fragment ions. However, these did not pose a problem.
39- 40	The additive in Exp. 38 was retried using different pH levels.	0910Bov2; 0910Bov3	It was found that a pH of about 8.5 worked the best.
41	50mM Glycine in 1M NH ₄ OOCCH ₃ @ 50μL/min via post-column tee @ pH = 8.75	0910Bov4	Similar results to those in Exp 38 were obtained, except that the DSAs had an even lower abundance using Gly.
42	50mM Glycine in 1M NH₄OCOH @ 50μL/min via post-column tee @ pH = 8.80	1014Bov6	Similar results to those in Exp 40 were obtained, except that low mass region did not contain as many fragments as the Ala mass spectra.
43-50	Tested various concentrations of NH ₄ OCOH	See log book	A concentration of 1M NH ₄ OCOH was required for best results.
51-61	Tested various injection volumes	See log book	An injection of 5μL of BBTL extract was best.

Table 66. Some of the experiments that were performed to solve the Sodium Adduct and Dimer Problem, in ESI-MS.

IV. Concluding Remarks

We report here for the first time the change in composition of the molecular species of dihydrosphingomyelin (DHS) and sphingomyelin (SPM) in young, old and cataractous human eye lens membranes. Also, this work is the first report of the composition of these sphingolipids (SPLs) in cataractous lenses. The observation that SPMs and DHSs were not degraded with the onset of the diseased state, but that the diacylglycerol based PLs (such as phosphatidylcholines and phosphatidylethanolamine plasmalogens), were degraded, indicated the following: 1) Degradation of the SPLs due to sphingomyelinase enzyme activity was not a major contributor to the onset of the diseased state; 2) The fact the SPLs were the only phospholipids (PLs) present in cataractous lens membrane extracts suggested that their ability to form stable membrane rafts in the lipid bilayer was responsible for maintaining the structure and integrity of the membrane in cataractous lenses; and 3) Degradation of diacylglycerol based PLs may be a major contributor to the onset of the disease.

Although these results provided invaluable insight into the mechanisms involved in cataractogenesis, the strongest achievements of this work were the development of novel methods to analyze and quantify SPLs in complex mixtures, by dual parallel atmospheric pressure chemical ionization (APCI) and electrospray ionization (ESI) mass spectrometry (MS), simultaneously. Specifically, we described the first accurate mass spectrometric method to determine the long-chain base (LCB) and fatty acid (FA) compositions of complex SPL mixtures by APCI and ESI MS. Although this analysis was previously attempted by Karlsson *et al.*¹, misidentification of molecular species, poor mass-spectrometric techniques and inconsistencies between their conclusions, data and

reported results rendered that work spurious. Also, the compositions of the LCBs and FAs reported by Karlsson *et al.*¹ were dubious, since asterisks were used to represent unknown and ambiguous quantities. In our work, we corrected these mistakes, and then developed a new method to determine the compositions of bovine milk, bovine brain and chicken egg yolk sphingomyelin extrates. Finally, the fact that our results were in agreement with previous reports⁸ illustrated the efficacy and accuracy of our analytical approach.

Finally, the formation of PL dimers and sodium adducts has been a major problem preventing our ability to perform quantitative analysis of PLs by ion trap ESI mass spectrometry. This problem was solved in this work by introducing an additive into the mobile phase post-column. The method which we developed almost completely eliminated the formation of PL dimers and sodium adducts. This greatly simplified the mass spectra and will hopefully produce percentage compositions on the LCQ that are comparable to compositions determined from APCI MS.

The results and methods presented in this work are milestones in the fields of biological and analytical mass spectrometry. Further work may be done in order to further apply and improve upon these methods. However, we now have all of the necessary tools in place to use to increase our understanding of the roles SPLs play in cataractogenesis, signal transduction and membrane structure.

LITERATURE CITED

1. Anders A. Karlsson, P. Michelsen and G. Odham, *J. Mass Spectrom.* **33**, 1192-1198 (1998)
2. Wm. Craig Byrdwell, Doug Borchman, *Ophthalmic Res.*, **29**, 191-206 (1997)
3. Wm. Craig Byrdwell, *Rapid Commun. Mass Spectrom.* **12**, 256-272 (1998)
4. Anders A. Karlsson, Kristina C. Arnoldsson, Gunilla Westerdahl and Goran Odham, *Milchwissenschaft*, **52**, 554 (1997)
5. L. Nyberg, Sphingomyelin from Bovine Milk. Pages 120 -125 in Phospholipids: Characterization, Metabolism, and Novel Biological Applications. G. Cevc and F. Paltauf, *J. Am. Oil Chem. Soc. Press*, Champaign, IL. (1995)
6. Nils U. Olsson, Peter Kaufmann, Susanna Dzeletovic, *J. of Chromatogr. B*, **698**, 1 – 8 (1997)
7. W. R. Morrison, *Biochim. Biophys. Acta*, **176**, 537 – 546 (1969)
8. W. R. Morrison and J. D. Hay, *Biochim. Biophys. Acta*, **202**, 460 - 467 (1970)
9. Anders Valeur, N. Urban Olsson, Peter Kaufmann, Shun Wada, Carl-Gunnar Kroon, Gunilla Westerdahl and Goran Odham, *Biol. Mass Spectrom.*, **23**, 313 (1994)
10. Hee-Yong Kim and Norman Salem, Jr., *Anal. Chem.*, **59**, 722-726 (1987)
11. J. L. Kerwin, A. R. Tuininga and L. H. Ericsson, *J. Lipid Res.*, **35**, 1102 (1994)
12. Fong-Fu Hsu, Alan Bohrer, and John Turk, *J. Am. Soc. Mass Spectrom.*, **9**, 516-526 (1998)
13. Fong-Fu Hsu and John Turk, *J. Am. Soc. Mass Spectrom.*, **11**, 437-449 (2000)
14. Patricio Meneses and Thomas Glonek, *J. Lipid. Res.*, **29**, 679 – 689 (1988)

15. Thomas E. Merchant, Jonathan H. Lass, Patricio Meneses, Jack V. Greiner, and Thomas Glonek, *Invest. Ophthalm. Vis. Sci.*, **32(3)**, 549 – 555 (1991)
16. W. Craig Byrdwell, Douglas Borchman, Richard A. Porter, K. Grant Taylor, and M. Cecilia Yappert, *Invest. Ophthalm. Vis. Sci.*, **35(13)**, 4333 – 4343 (1994)
17. Jan Lei Iwata, Lidia G. Bardygula-Nonn, Thomas Glonek and Jack Greiner, *Curr. Eye Res.*, **14(10)**, 937 – 941 (1995)
18. Nikolaos Sotirhos, Bengt Herslof, and Lennar Kenne, *J. Lipid Res.* **27**, 386 - 392 (1986)
19. Douglas Borchman, W. Craig Byrdwell, and M. Cecilia Yappert, *Invest. Ophthalm. Vis. Sci.*, **35**, 3938 – 3942 (1994)
20. Miia Kuikka, Bodil Ramstedt, Henna Ohvo-Rekila, Jessica Tuuf, and J. Peter Slotte, *Biophys. J.*, **80**, 2327-2337 (2001)
21. Hannun, Y. A., **Sphingomyelin-Mediated Signal Transduction**, R.G. Landes, Co., Texas (1997)
22. T. Okazaki, R. M. Bell, Y. A. Hannun, *J. Biol. Chem.*, **264**, 19076-19080 (1989)
23. Hannun, Y. A., Ceramide: A Stress Response Mediator Involved in Growth Suppression in **Sphingomyelin-Mediated Signal Transduction**, R.G. Landes, Co., Texas (1997)
24. P.R. Cullis, D. B. Fenske, M. J. Hope, Physical Properties and Functional Roles of Lipids in Membranes, in **Biochemistry of Lipids, Lipoproteins and Membranes**, D. E. Vance and J. Vance (Eds.), Elsevier, Amsterdam (1996)

25. A. H. Merrill, C. C. Sweeley, "Sphingolipids: Metabolism and Cell Signaling", in **Advances in Lipid Research**, R. M. Bell, A. H. Merrill, Y. A. Hannun, Eds., Academic Press, Inc., San Diego, CA (1993)
26. Albert L. Lehninger, David L. Nelson, Michael M. Cox, **Principles of Biochemistry**, Worth Publishers, New York, NY (1993)
27. J. Abian, *J. Mass Spectrom.*, **34**, 157 – 168 (1999)
28. O. Hwang, G. Kim, Y.J. Jang, S.W. Kim, G. Choi, and H.J. Jeon, *Mol. Pharm.*, **59** (5), 1249-1255 (2001)
29. J.S. Andrews, and T. Leonard-Martin, *Invest. Ophthalmol. Vis. Sci.*, **1**, 39-45 (1981)
30. G.L. Feldman, L.S. Feldman, and G. Rouser, *Lipids*, **1**, 161 (1966)
31. G.L. Feldman, *Surv. Ophthalmol.*, **12**, 207-243 (1967)
32. R.M. Broekhuysse, *Biochim. Biophys. Acta*, **187**, 354-365 (1969)
33. R.M. Broekhuysse, *Biochim. Biophys. Acta*, **218**, 546-548 (1970)
34. E. Cotlier, Y. Obara, and B. Toftness, *Biochim. Biophys. Acta*, **530**, 267-278 (1978)
35. L. Rosenfeld, and A. Spector, *Exp. Eye Res.*, **33**, 641-650 (1981)
36. S. Zigman, T. Paxhia, G. Marinetti, and S. Girsch, *Curr. Eye Res.*, **3**, 887-896 (1984)
37. Y.A. Hannun, C.R. Loomis, A.H. Merrill, and R.M. Bell, *J. Biol. Chem.*, **262**(67), 12604-12609 (1986)
38. Y.A. Hannun, *J. Biol. Chem.*, **269**, 3125 – 3128
39. Y. Barenholz, T.E. Thompson, *Chem. Phys. Lipids*, **102**, 29-34 (1999)

40. X.M. Li, J.M. Smaby, M.M. Momsen, H.L. Brockman, and R.E. Brown, *Biophys. J.*, **78**, 1921-1931 (2000)
41. L.K. Bar, Y. Barenholz, and T.E. Thompson, *Biochemistry*, **36**, 2507-2516
42. D. Borchman, W.C. Byrdwell, and M.C. Yappert, *Ophthalmic Rec.*, **28**, 81-85 (1996)
43. E.E. Prieschl, and T. Baumruker, *Immunol. Today*, **21**, 555-560 (2000)
44. G.S. Dbaiibo, M.Y. Pushkareva, S. Jayadev, J.K. Schwarz, J.M. Horowitz, L.M. Obeid, and Y.A. Hannun, *Proc. Natl. Acad. Sci. USA*, **92**, 1347-1351 (1995)
45. A. Gomez-Munoz, A. Martin, L. Obrien, and D.N. Brindley, *J. Biol. Chem.*, **269**, 8937-8943 (1994)
46. Y.J. Chun, S. Lee, S.A. Yang, S. Park, and M.Y. Kim, *Biochem. Biophys. Res. Commun.*, **298**, 687-692 (2002)
47. K. Shikata, H. Niiro, H. Azuma, T. Tachibana, and K. Ogino, *Bioorg. Med. Chem. Lett.*, **13**, 613-616 (2003)
48. Robert G. Jensen, *J. Dairy Sci.*, **85**, 295-350 (2002)
49. C.C. Sweeley, *J. Lipid Res.*, **4**, 402 (1963)
50. K. A. Karlsson and G. A. L. Holm, *Acta Chem. Scand.*, **19**, 2423 (1965)
51. Daniel C. Harris, **Exploring Chemical Analysis**, W. H. Freeman and Company, New York, NY (2001)
52. Wm. Craig Byrdwell, *J. Liq. Chromatogr. R. T.*, **26 (19)**, 3147-3181 (2003)
53. Wm. Craig Byrdwell, H. Sato, A. K. Schwarz, D. Borchman, M. C. Yappert, and D. X. Tang, *Lipids*, **37 (11)**, 1087-1092 (2002)
54. C. G. Crawford and R. D. Plattner, *J. Lipid Res.*, **24**, 456-460 (1983)

